

Photobiological Studies of Ross Sea Phytoplankton

A Dissertation

Presented to

The Faculty of the School of Marine Science

The College of William and Mary in Virginia

In Partial Fulfillment

Of the Requirements for the Degree of

Doctor of Philosophy

by

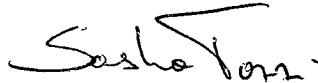
Sasha Tozzi

2010

APPROVAL SHEET

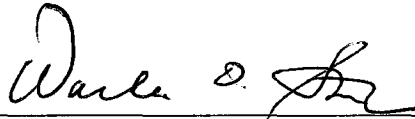
This dissertation is submitted in partial fulfillment of
the requirements for the degree of

Doctor of Philosophy

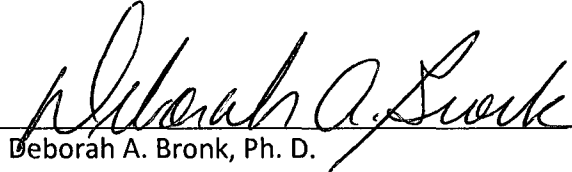


Sasha Tozzi

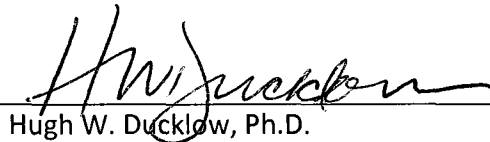
Approved, 22 May 2009



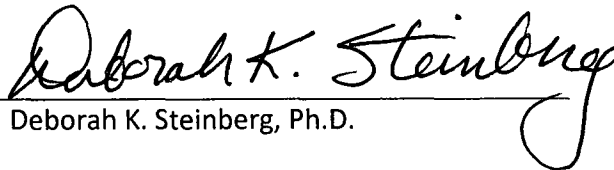
Walker O. Smith, Jr., Ph.D.
Committee Chair/Advisor



Deborah A. Bronk, Ph. D.



Hugh W. Ducklow, Ph.D.



Deborah K. Steinberg, Ph.D.



Richard T. Barber, Ph. D.
Duke University
Beaufort, NC

TABLE OF CONTENTS

	Page
ACKNOWLEDGEMENTS	viii
LIST OF TABLES	ix
LIST OF FIGURES	x
ABSTRACT	xiii
SECTION I. Project Introduction	2
Research background and motivation	3
<i>The Ross Sea, Antarctica</i>	4
<i>Ross Sea phytoplankton</i>	7
<i>Chlorophyll fluorescence and photosynthetic characteristics</i>	9
<i>Differences between FRR and PAM fluorometry</i>	13
<i>Fluorescence in the Ross Sea</i>	14
<i>Iron and light variability in the Ross Sea</i>	15
<i>Aims and motivation of this research</i>	16
<i>Scientific relevance</i>	17
Literature Cited	19
SECTION II. The photo-physiological differences among Ross Sea diatoms, <i>Phaeocystis antarctica</i> , and natural assemblages and their photosynthetic responses to light, temperature, micronutrients, and pCO ₂ variations	26
Abstract	27
Introduction	27
Material and Methods	30
<i>Variable Chl a fluorescence measurements</i>	30
<i>Phytoplankton cultures and natural assemblages</i>	31

<i>Photorecovery (PR) experiments</i>	32
<i>Ross Sea iron, light and CO₂ experiments 1 and 2 (RSC1 and RSC2)</i>	34
<i>Ross Sea temperature and iron experiment 1 (RST1)</i>	34
<i>Ross Sea light and temperature experiment 2 (RST2)</i>	35
<i>Fe, Zn, Co, and Vitamin B₁₂ experiment (WHOI 1, 2 and 3)</i>	35
<i>Statistical analysis</i>	36
Results	36
<i>Photorecovery (PR) experiments</i>	36
<i>Iron and temperature (RST1)</i>	38
<i>Light and temperature (RST2)</i>	38
<i>Iron, light and CO₂ (RSC1 & RSC2)</i>	39
<i>Fe, Zn, Co, and vitamin B₁₂ (WHOI 1, 2 and 3)</i>	39
Discussion	40
Literature Cited	69

SECTION III. Large scale variations in phytoplankton photosynthetic activity in the Ross Sea (Antarctica)

polynyas related to environmental parameters and bloom dynamics.....	74
Abstract	75
Introduction	76
<i>The Ross Sea</i>	76
<i>Ecophysiology and photobiology of high-latitude phytoplankton functional groups</i>	76
<i>Role of iron</i>	78
<i>Fluorescence, fluorescence induction, and variable fluorescence</i>	79
Material and Methods	81
<i>Study Area</i>	81
<i>Hydrography</i>	82
<i>Irradiance</i>	82

<i>Nutrient analysis</i>	82
<i>Chlorophyll</i>	83
<i>HPLC pigments</i>	83
<i>Variable Chl a fluorescence measurements</i>	84
<i>Seawater blanks</i>	85
<i>Light calculations</i>	86
Results	87
<i>Physical features of surface waters (0-200 m)</i>	87
<i>Chlorophyll a standing stocks, pigment and nutrient concentrations</i>	88
<i>FRRF and PAM</i>	89
Discussion	91
Literature Cited	109

SECTION IV. Phytoplankton photophysiology and primary productivity derived from variable fluorescence measurements in the Ross Sea, Antarctica 118

Abstract	119
Introduction	120
<i>The Ross Sea, Antarctica</i>	120
<i>Fast repetition rate fluorometry</i>	121
Material and Methods	125
<i>Study site</i>	125
<i>Radiometry and optical environment</i>	125
<i>Chlorophyll</i>	126
<i>Primary productivity and P vs. E determinations</i>	126
<i>Variable fluorescence</i>	128
<i>Variable fluorescence based primary productivity models</i>	129
<i>Rapid light curves</i>	131

Results	132
Discussion	134
Literature Cited	148
SECTION V. Summary	153
Appendix 1.....	157
Appendix 2.....	167
Appendix 3.....	172
VITA	183

Dedicated to my entire family and to the loving memory of the ones I have lost.

ACKNOWLEDGEMENTS

I would like to thank my major advisor Walker O. Smith, Jr. and my committee members Deborah A. Bronk, Hugh W. Ducklow, Deborah K. Steinberg and Richard T. Barber for their support, guidance and patience throughout my degree. Additionally I would like to thank Zbigniew S. Kolber for being a great mentor and for providing me with the instrumentation that allowed me to collect the majority of the data presented in this dissertation. Many other people contributed in several different ways and made my research possible; the long list includes my lab mates Jill Peloquin, Amy Shields, Jennifer Dreyer and Scott Polk as well Joe Cope and Dave Gillett for helping me with part of the statistical analysis and Denis Klimov for technical assistance with instrumentation. Special thanks go to the captains and crews of the RVIB N. B. Palmer and USCGC Polar Star as well to all the collaborators at sea and in McMurdo station.

Important collaborators at sea have been Vernon Asper, Giacomo DiTullio, Mak Saito, Erin Bertrand, Dave Hutchins, Yuanyuan Feng, Julie Rose and all the other participants of the IVARS and CORSACS programs. My experience at VIMS was enriched and my work was facilitated by all the amazing people I had the fortune to encounter here, starting with Iris Anderson, Gina Burrell, Maxine Butler, Sue Presson, Fonda Powell, the entire ITNS department that came to my rescue in many occasions with Bob Poley, Chris Palmer and Kevin Kiley. I would like also to thank Mike Newman and Jeff Shield for giving me the opportunity to be their teaching assistant.

This project would not ever become successful without the love and support of my family in Italy and South Africa and without the constant and unconditional support of many of my friends as Rob and Beth Condon, Debra Parthree, Jens and Nettan Carlsson, Steve Litvin and Stacy De Matteo and very importantly John Boon and the Salsa Verde's crew that allowed to keep me sane by sailing Spring thru Fall at least once a week. Special thanks to Amy DiCarlantonio for her unparalleled support and love.

This project was generously funded by the Virginia Institute of Marine Science and the National Science Foundation (Grants OPP- 0338157 and OPP-0087401).

LIST OF TABLES

Table	Page
SECTION II	
1	Synthesis of photorecovery experiments results..... 46
2	Synthesis of other experimental conditions used during CORSACS I and II..... 47
SECTION III	
3	Cruises number of stations and available variable fluorescence measurements..... 97
4	Physical, chemical and biological water properties for cruises NPB0601 and NBP0608..... 98
5	Correlations between F_v/F_m , dissolved macronutrients and temperature for NBP0601..... 99
6	Correlations between F_v/F_m , dissolved macronutrients and temperature for NBP0608..... 100
SECTION IV	
7	Summary of studies comparing active fluorescence and carbon and oxygen based estimates of oceanic photosynthetic production.....141
8	T-test comparison of diatom and <i>P. antarctica</i> dominated stations.....142
9	List of parameters used, their definitions and units.....143

LIST OF FIGURES

Figure		Page
	SECTION I	
1	Map of the Ross Sea.....	5
	SECTION II	
2	PR#1 Potential photochemical efficiency of PSII vs. time comparison between <i>P. antarctica</i> and <i>Pseudo-nitzschia</i>	48
3	PR# 2 (a)Potential photochemical efficiency of PSII vs. time, (b)percent recovery of F_v/F_m over time.....	49
4	PR# 3 (a)Potential photochemical efficiency of PSII vs. time, (b)percent recovery of F_v/F_m over time.....	50
5	PR# 4 (a)Potential photochemical efficiency of PSII vs. time, (b)percent recovery of F_v/F_m over time.....	51
6	PR# 5 (a)Potential photochemical efficiency of PSII vs. time, (b)percent recovery of F_v/F_m over time.....	52
7	PR# 7 (a)Potential photochemical efficiency of PSII vs. time, (b)percent recovery of F_v/F_m over time.....	53
8	PR# 8 (a)Potential photochemical efficiency of PSII vs. time, (b)percent recovery of F_v/F_m over time.....	54
9	RST1 experiment potential photochemical efficiency of PSII vs. time.....	55
10	RST1 experiment absorption cross section (σ_{PSII}) vs. time.....	56
11	RST2 potential photochemical efficiency of PSII vs. time.....	57
12	RST2 experiment absorption cross section (σ_{PSII}) vs. time.....	58
13	RSC1 potential photochemical efficiency of PSII vs. time.....	59
14	RSC1 absorption cross section (σ_{PSII}) vs. time.....	60
15	RSC2 potential photochemical efficiency of PSII vs. time.....	61
16	RSC2 absorption cross section (σ_{PSII}) vs. time.....	62
17	WHOI experiment 1 potential photochemical efficiency of PSII vs. time.....	63

18	WHOI experiment 1 in growth chamber at $\pm 1^\circ\text{C}$ and $150 \mu\text{mol photons m}^{-2} \text{s}^{-1}$, absorption cross section (σ_{PII}) vs. time.....	64
19	WHOI experiment 2 potential photochemical efficiency of PSII vs. time.....	65
20	WHOI experiment 2 absorption cross section (σ_{PII}) vs. time.....	66
21	WHOI experiment 3 potential photochemical efficiency of PSII vs. time.....	67
22	WHOI experiment 3 absorption cross section (σ_{PII}) vs. time.....	68
SECTION III		
23	Map showing bathymetry of the study area and station locations of R/V N.B. Palmer cruise NBPO601 sampled between December 27, 2005 and January 23, 2006.....	101
24	Map showing bathymetry of the study area and station locations of R/V N.B. Palmer cruise NBPO601 sampled between November 6 and December 6, 2006.	102
25	Scatter plot showing relationship between chlorophyll <i>a</i> concentration and MBARI F_m (a) and ship underway Turner AU 10 Fluorometer fluorescence (b) for cruise NBPO601.....	103
26	Scatter plot of chlorophyll <i>a</i> concentration versus MBARI F_m (a), versus ship underway Turner AU 10 Fluorometer fluorescence (b) and PAM F_m (c) for cruise NBPO608.....	104
27	3D Scatter plot of filtered sea water blanks F_m % signal of corresponding CTD F_m samples vs. depth and chlorophyll <i>a</i> concentration.....	105
28	Scatter plots of water column temperature versus depth (a), nitrate (b), phosphate (c), silicate (d), salinity (e), and fluorescence quantum yields (f) for NBPO601(•) and NBPO608 (•).....	106
29	Scatter plots of water column fluorescence quantum yields versus depth (a), nitrate (b), phosphate (c), silicate (d), salinity (e), and fluorescence quantum yields (f) for NBPO601(•) and NBPO608 (•). Regression fit for NBPO601 (red line) and NBPO608 (black line).....	107
30	Distribution in water column of absorption cross section for NBPO601 (•), and for NBPO608 (•).....	108
31	Scatter plots of dissolved iron vs. fluorescence quantum yields for NBPO601 (•) and NBPO608 (•).....	109

SECTION IV

32	Map showing bathymetry of the study area and station locations of R/V N.B. Palmer cruise NBP0601 sampled between December 27, 2005 and January 23, 2006.....	144
33	Distributions of (a) attenuation coefficients (K_d , m^{-1}); (b) euphotic zone depths (Z_{eu} , m); (c) mixed layer depths (Z_{mix} , m); (d) Fuco: 19'hexanoyloxyfucoxanthin ratio at 20 m (<0.2 were considered to be dominated by <i>Phaeocystis antarctica</i>).....	145
34	Correlations between electron transport rates calculated (a) from fitting rapid light curves (RLC) with rectangular hyperbolic function (ETR_r) and multiplied by the maximum fluorescence (F_m) and ^{14}C -primary productivity (PP); (b) ETR_r and productivity normalized to chlorophyll <i>a</i> (P_B); (c) relative electron transport (rETR) multiplied by F_m and PP; (d) rETR and P_B ; (e) ETR calculated from exponential fitting (ETR_e) multiplied by F_m and PP; (f) ETR_e and P_B	146
35	Correlation between relative electron transport rates (rETR) multiplied by the maximum fluorescence (F_m) and ^{14}C -primary productivity (PP) displayed on a \log_{10} scale and fitted with power function); (b) rETR and productivity normalized to chlorophyll <i>a</i> (P_B).....	147
36	Averaged profiles of stations dominated by <i>P. antarctica</i> (red line, averaged CTD casts 36, 37, 39, 40) and by diatoms (green line, averaged CTD cast 88, 89, 91, 97). (a)Temperature; (b)water density; (c) N:P ratio; (d)Silicate concentration; (e) total chlorophyll <i>a</i> concentration; (f) greater than 20 μm chlorophyll <i>a</i> concentration; (g) Fuco:Hex ratio; (h) F_v/F_m ; (i) absorption cross section; (j) RLC derived α ; (k) RLC derived P_{max} ; (l) RLC derived E_k	148

ABSTRACT

The Ross Sea polynya is characterized by high spatial and temporal variability and by an annual cycle of sea ice retreat, water column stratification, large phytoplankton blooms, and months of complete darkness. This region is also highly susceptible to increasingly changing climatic conditions that will significantly affect the hydrography, iron supply, primary production patterns and carbon cycling. This project focused on analyzing how differences in photosynthetic traits between the two major bloom-forming functional groups in the polynya, diatoms and the prymnesiophyte *Phaeocystis antarctica*, and investigate if these differences can explain their dominance and succession. The study was conducted as part of the Controls on Ross Sea Algal Community Structure (CORSAC) program during two cruises in December 2005-January, 2006, and November-December, 2006. A fast repetition rate fluorometer (FRRF) was used to assess photochemical efficiency on natural phytoplankton assemblages and on monoclonal cultures. Measurements were made on cultures to determinate differences in photorecovery kinetics, as well on a suite of experiments performed to test the effects of temperature, iron, CO₂ and micronutrients had on natural assemblages. In addition, FRRF measurements were made on 1,182 discrete samples representative of 98 profiles collected over the two cruises. *Phaeocystis antarctica* consistently photorecovered faster than the diatoms *Pseudo-nitzschia* sp., indicating different photosynthetic strategies and ecological niches; in addition, temperature and iron significantly promoted photosynthetic quantum yields, indicating a diffuse iron limitation of the natural assemblages used for the experiments and a high susceptibility to forecasted temperature increases in the region. Experiments also demonstrated that the Ross Sea phytoplankton is capable of maintaining high photosynthetic capacity after extensive periods in the dark. The dominance and successions in the blooms appears to be controlled by a combination of hydrography and in particular by the relative depths of the mixed layer and euphotic zone, as well by the water temperatures and possibly by iron concentrations. Diatom-dominated blooms were found in shallow mixed water layers characterized by higher temperature and fresher waters in the summer in the western part of the polynya, while *Phaeocystis antarctica* prevailed in colder regions with deeper mixed layer depths in the eastern part of the polynya. The dominance in the bloom significantly affected the relative macronutrient drawdown. Photosynthetic characteristic of natural assemblages were also modeled based on variable fluorescence rapid light curves (RLCs), and photophysiological differences were found between diatoms and *Phaeocystis antarctica*, with the latter having higher E_k and lower functional absorption cross sections (σ_{PSII}) and α values, but similar maximum electron transport rates (ETRs). Lastly, correlation between RLC- based modeled photosynthetic rates and ¹⁴C based primary production presented some discrepancies due to limitations and differences in methodologies.

Photobiological Studies of Ross Sea Phytoplankton

SECTION I. PROJECT INTRODUCTION

RESEARCH BACKGROUND AND MOTIVATION

Approximately 50% of planetary photosynthesis takes place in the marine environment (Falkowski 1994, Field *et al.* 1998). Photosynthetic conversion of solar energy into organic matter and the accompanying photoreduction of water into molecular oxygen is the single, most critical determinant of life on earth. Although marine photosynthetic biomass is approximately 1% of terrestrial biomass, it has a much faster carbon turnover, about one to three weeks, compared with the nine to twenty years on land (Field *et al.* 1998). Such rapid turnover rates suggest that the marine primary producers are sensitive to environmental factors, such as nutrient and trace metal supply, temperature, $p\text{CO}_2$, and changes in weather that may lead to changes water column structure. Over the last several decades, all these factors have shown accelerated rates of change, most likely driven by carbon loading in the atmosphere. These changes have recently caught the attention of the public, and are increasingly viewed as a serious threat to all ecosystems. One of the most critical questions is whether the photosynthetic performance of the world's ocean can be sustained under the increasing anthropogenic impact. Public awareness of global climate change and the improved understanding of environmental effects of rising concentration of carbon dioxide (CO_2) concentrations in the atmosphere stimulated a great interest in the understanding of oceanic primary production and the fate of the photosynthetically produced organic matter. This dissertation aims to contribute to this understanding by presenting results of phytoplankton photophysiological studies conducted in the Ross Sea, a highly productive region of the Southern Ocean (Smith and Nelson 1986, Smith and Comiso 2008). This region provides a proxy for studying processes occurring in the ice-covered Southern Ocean. Phytoplankton act as a major sink for atmospheric CO_2 in this region (Sweeney *et al.* 2000) by fixing and exporting carbon to depth by sinking and forming aggregates (Arrigo *et al.* 2008). However, the environmental conditions controlling the growth, taxonomic composition and primary productivity

rates of Ross Sea phytoplankton blooms are yet to be fully clarified. Despite the importance of Antarctic phytoplankton and productivity in determining the partitioning of biogeochemical pools of carbon, sulfur and silica, little is known about the patterns and mechanisms of these processes at high latitudes. The present work aims to elucidate factors controlling primary productivity in the Ross Sea by characterizing the photophysiological properties of dominant phytoplankton taxa in the Ross Sea; investigating the effects of varying patterns of temperature, integrated light availability and micronutrient concentrations on these characteristics; measuring the spatial distribution of photosynthetic quantum yield in the spring and summer by using an active fluorescence technique; and evaluating techniques and methodologies for assessing primary productivity rates based on chlorophyll fluorescence.

The Ross Sea, Antarctica

This study is based on data collected in the Ross Sea polynya. This polynya is an ice-free region surrounded by seasonally variable ice concentrations, and is roughly surrounded in late spring by Victoria Land in the west, Marie Byrd Land to the east, the Ross Sea Ice Shelf in the south, and seasonal sea ice in the north (Figure 1). The polynya's hydrography is controlled by the ice dynamics, combined with the local meteorological events, such as katabatic winds (Bromwich *et al.* 1993, Arrigo *et al.* 1998), deep water formation (Assmann and Timmermann 2005), as well as iceberg calving and movements (Dinniman *et al.* 2007).

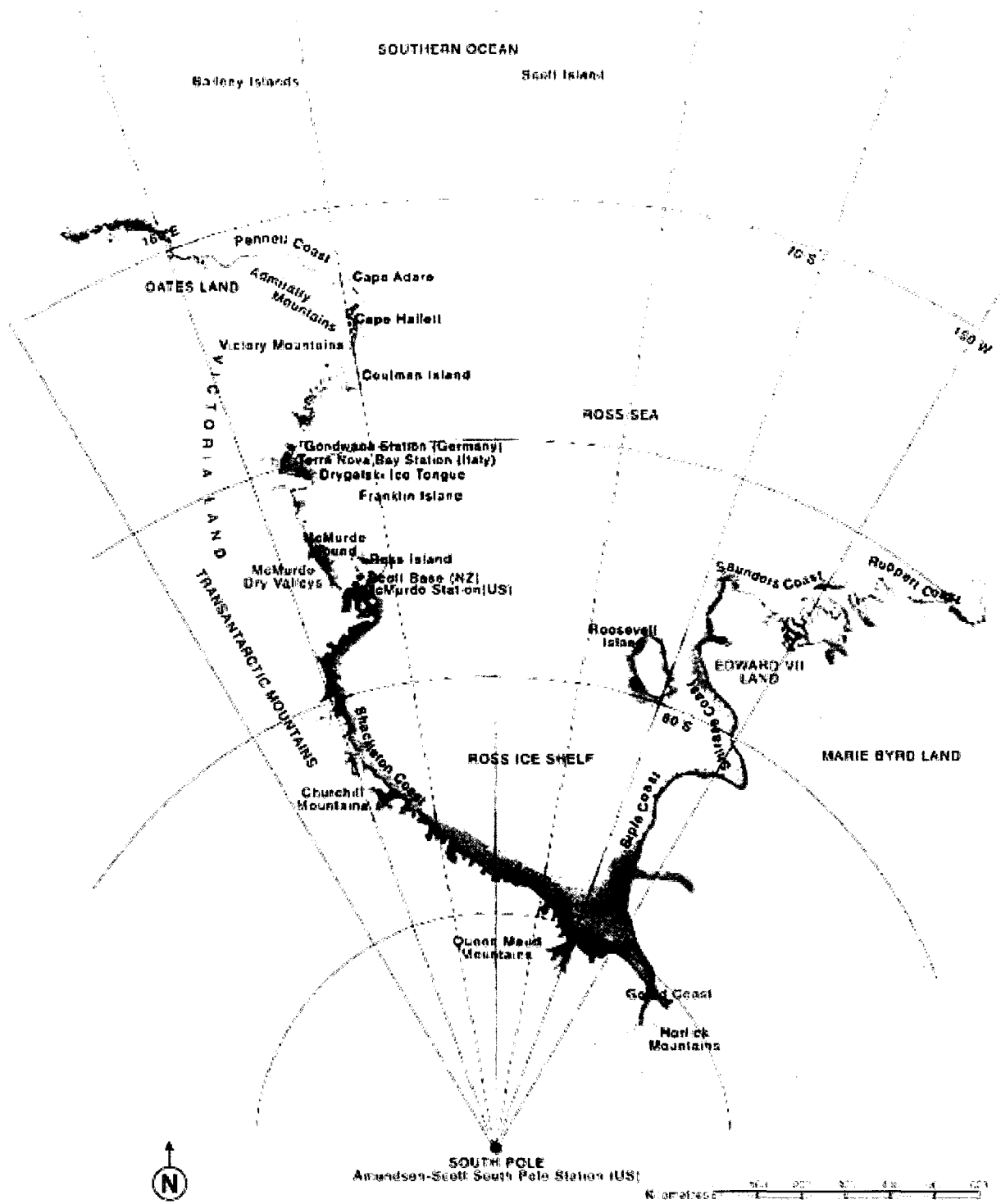


Figure 1 Map of the Ross Sea (Cape Adare, Antarctic Heritage Trust, New Zealand).

Usually the water column in the polynya is deeply mixed at the beginning of October (in some locations throughout the entire water column), becomes weakly stratified in early November, and more strongly stratified in December because of surface freshening due to ice melting and the seasonal increase in irradiance and sensible heat. Macronutrient concentrations in the polynya are always elevated (Smith *et al.* 2003b) and never limit phytoplankton productivity in the polynya; instead, productivity appears to be light-limited in the spring (Smith *et al.* 2000) and iron-limited in the summer (Fitzwater *et al.* 2000, Olson *et al.* 2000, Sedwick *et al.* 2000, Cochlan *et al.* 2002, Coale *et al.* 2003, Coale *et al.* 2005, Sedwick *et al.* 2007) due to the limited Aeolian and oceanographic micronutrient inputs (Fung *et al.* 2000, Peloquin and Smith 2007). Transiently higher concentrations of iron in the euphotic zone are usually correlated with glacial ice/iceberg melting (de Baar and De Jong 2001, Raiswell *et al.* 2008) and occasionally with deep water intrusions of modified circumpolar deep water (MCDW) (Peloquin and Smith 2007, Orsi and Wiederwohl 2009). Inter- and intra-annual sea ice concentrations, as well polynya size and duration, are extremely variable (Arrigo and van Dijken 2004, Cavalieri and Parkinson 2008, Smith and Comiso 2008). Such variability exerts a strong control on the extension and magnitude of the recurrent Ross Sea spring blooms (Smith and Nelson 1985, Comiso *et al.* 1993, Peloquin and Smith 2007). Usually a progression in the spring biomass and productivity occurs from late October (Smith and Gordon 1997, Arrigo *et al.* 1998, Smith *et al.* 2006) to December, when higher biomass and carbon fixation rates are observed in the polynya (Smith *et al.* 2000). Occasionally a secondary bloom occurs in February (austral summer) both in the Ross Sea polynya and in Terra Nova Bay (Innamorati *et al.* 1999, Peloquin and Smith 2007). Occasionally, small (spatially and temporally) blooms of cryptophytes are observed in limited coastal areas impacted by glacial runoff (Arrigo *et al.* 1999). Other taxa (dinoflagellates, silicoflagellates) are generally much less abundant, while some other groups (Cyanobacteria, prochlorophytes) are absent.

The Ross Sea polynya provides an ideal location for studies on climate change and carbon cycling because of its high latitude, high productivity, and well-defined boundaries. This study has been conducted using techniques and methods based on Fast Repetition Rate Fluorescence (FRRF) (Kolber *et al.* 1998) that allowed a new level of assessment and understanding of factors controlling primary production and floristic composition of the polynya's blooms. The objective of this study was to improve the understanding and forecast the effects of global climate change on biogeochemical cycling of key elements such as carbon, silica and sulfur in the region and throughout the Antarctic.

Ross Sea phytoplankton

The current paradigm for the phytoplankton succession in the Ross Sea polynya is that the spring bloom is dominated by the prymnesiophyte *Phaeocystis antarctica* (DeMaster *et al.* 1992, Arrigo *et al.* 1994, Arrigo *et al.* 1999, Smith and Asper 2001) when mixed layer depths are greater, and shifts to an assemblages dominated by diatoms when waters become more strongly stratified (Smith and Nelson 1985, Arrigo *et al.* 2000). Diatoms appear to persist in coastal areas along Victoria Land and receding ice edges (DiTullio and Smith 1996, Leventer and Dunbar 1996, Arrigo *et al.* 1999, Goffart *et al.* 2000).

Diatoms are thought to be efficiently grazed in the marginal ice zone (MIZ) by mesozooplankton (Carrada *et al.* 2000, Tagliabue and Arrigo 2003), whereas grazing on *Phaeocystis* (Huntley *et al.* 1987) is less clear. Grazing may be restricted to solitary forms (Smith *et al.* 2003a), although microzooplankton are occasionally found associated with colonies (Shields *et al.*, 2007), they do not appear to efficiently graze (Caron *et al.* 2000). Blooms of colonial *Phaeocystis* also do not have characteristic degradation pigments associated with ingestion by micro- or mesozooplankton (DiTullio and Smith 1996). However, some mucus-net grazers, such as pteropods, are present and may ingest *P. antarctica*, although grazing studies using these forms have not yet been conducted. Grazing

significantly impacts the carbon flux in December and January (Gowing *et al.* 2001), but grazing in the Ross Sea appears to be anomalously low when compared to other regions of the Southern Ocean with similar level of biomass and productivity (Tagliabue and Arrigo 2003 and references therein).

Several traits distinguish diatoms from *Phaeocystis*, with important implications relative to their dominance and their effect on biogeochemical cycles. Arrigo *et al.* (1999) found differences in the uptake stoichiometry between these two taxa, with *Phaeocystis* displaying a higher nitrogen requirement relative to phosphorus; furthermore, *Phaeocystis* has also higher iron requirements (DiTullio *et al.* 2007, Sedwick *et al.* 2007). *Phaeocystis antarctica* has been the subject of numerous studies that have demonstrated an extensive array of unusual characteristics that makes this taxon's eco- and photophysiology unique. For example, the high production of dimethylsulphoniopropionate (DMSP), the precursor of dimethylsulfide (DMS) (Matrai *et al.* 1993, DiTullio and Smith 1995), makes this taxon a central influence in the sulfur cycle. As a result, *Phaeocystis* may play an important role in the global radiation balance due to the formation of sulfate aerosols with high reflectance and the ability to provide cloud condensation nuclei (CCN) (Liss *et al.* 2005). *Phaeocystis* can fix greater quantities of carbon than diatoms - up to 60 % of the annual production in the Ross Sea (Smith *et al.* 2006) - due to the large standing stocks attained and the high amounts of carbon in its mucopolysaccharide colonial matrix (Mathot *et al.* 2000). It is also responsible for enhanced high concentrations of dissolved organic material (DOM) in the water that can promote elevated bacterial production (Carlson *et al.* 2000, Misic *et al.* 2006). *Phaeocystis* has several photophysiological acclimation strategies; for example, it can modify its thylakoid ultrastructure and pigment packaging capabilities (Moisan and Mitchell 1999, Moisan *et al.* 2006) to adapt to the highly variable light conditions of polar regions. It also can adapt to the varying light and iron conditions via high xanthophyll cycling rates in the presence of high iron concentrations, while a constant state of high energy quenching and increased absorption cross sections are maintained by an elevated xanthophylls

pool under low iron concentrations to avoid photoinhibition (van Leeuwe and Stefels 2007).

Phaeocystis produces UVR absorbing compounds such as mycosporine-like amino acids (MAAs) to avoid UVR photo-damage (Moisan and Mitchell 2001). Although this property is not exclusive to *Phaeocystis* in Antarctica, MAA production is triggered at higher concentrations by both UVA and UVB in *Phaeocystis*, while in diatoms MAA production is mostly triggered by UVA radiation (320-400 nm) (Lieselotte and Dale 1997). *Phaeocystis* has also been shown to be capable of resuming photosynthesis after long periods of darkness and entrapment in frozen ice (Tang *et al.* 2008). Colonial growth rates also have been shown to be greater than those of solitary cells under nutrient-replete conditions (Shields and Smith 2009). These traits may explain high survival rates of *Phaeocystis* through polar winters and its rapid biomass accumulation during the austral spring and summer in the polynya.

Chlorophyll fluorescence and photosynthetic characteristics

Chlorophyll fluorescence analysis is one of the most convenient and powerful tools to study the photophysiology of plants. Fluorescence measurements can be made rapidly and in a non-invasive and non-destructive manner. A variety of approaches and techniques have been developed to characterize a range of photosynthetic characteristics, such as efficiency of light utilization, yield of photosynthetic conversion, and the rate of photosynthetic electron transport. In addition, the fluorescence signal can serve as a proxy for chlorophyll biomass when measured under conditions of well-defined light history, and where the extent of fluorescence quenching can be quantified (Kiefer and Reynolds 1992). The depth of information present in the fluorescence signal, however, also contributes to the technique's weakness, as the extremely complicated patterns of fluorescence responses to physiological and environmental conditions make interpreting the signal difficult. Most of the fluorescence observed at ambient temperature is emitted by photosystem (PS) II and is modulated

by the level of photosynthetic activity within PSII reaction centers (RCII). In the simplest interpretation, fluorescence represents a radiative emission of the excess of absorbed light energy. Two other pathways, the photosynthetic energy utilization and heat dissipation, compete with fluorescence for the absorbed light, with both modulating fluorescence yield, Φ_F ,

$$\Phi_F = \frac{k_F}{k_F + k_D + k_T + k_P} \quad (\text{Eq. 1})$$

and the intensity of the fluorescence signal, F ,

$$F = E_A \Phi_F = E_a \frac{k_F}{k_F + k_D + k_T + k_P} \quad (\text{Eq. 2})$$

where E_A is the absorbed excitation energy, k_D is the rate constant for heat de-excitation, k_T is the rate constant for energy transfer to non-fluorescent pigments, and k_P is rate constant for photochemical reaction (Krause and Weis 1991).

Fluorescence yield is minimal (F_o) when all primary PSII acceptors, Q_A , are oxidized (RCII are in the "open" state), and $k_P = k_{Pmax} \gg k_F + k_D + k_T$:

$$F_o = E_A \Phi_{F_o} = E_A \frac{k_F}{k_F + k_D + k_T + k_{Pmax}} \quad (\text{Eq. 3})$$

As irradiance levels increase, the reduction level of Q_A increases in proportion to the level of photosynthetic activity, and k_P decreases as the fraction of RCII in "open state" is reduced.

Fluorescence yield reaches a maximum when all reaction centers become closed, with k_P approaching zero. These conditions are met at high light level, when the rate of excitation delivery to RCII far exceeds the capacity of the photosynthetic electron transport.

$$F_m = E_A \Phi_{Fm} \frac{k_F}{k_F + k_D + k_T} \quad (\text{Eq. 4})$$

Expressing the maximum yield of photochemistry, Φ_{PSII}^{\max} as

$$\Phi_{PSII}^{\max} = \frac{k_{P\max}}{k_F + k_D + k_T + k_{P\max}} \quad (\text{Eq. 5})$$

substituting Eq. 3 and 4 into Eq. 5 allows derivation of the photosynthetic yield to be expressed as a function of the F_o and F_m fluorescence signals:

$$\Phi_{PSII}^{\max} = \frac{F_m - F_o}{F_m} = \frac{F_v}{F_m} \quad (\text{Eq. 6})$$

where F_o and F_m are the fluorescence signals measured under darkness and under conditions of full saturation of PSII activity, respectively. Under intermediate irradiance, the photosynthetic yield changes from Φ_{PSII}^{\max} in the darkness to values close to zero under supersaturating light conditions.

Photosynthetic yield under ambient irradiance, Φ_{PSII}^S , can also be calculated from the fluorescence as

$$\Phi_{PSII}^S = \Phi_{PSII}^{\max} \frac{F_m - F_s}{F_m - F_o} = \Phi_{PSII}^{\max} PQ = \frac{F_m - F_s}{F_m} \quad (\text{Eq. 7})$$

where F_s is the fluorescence signal measured under ambient light (frequently referred to as steady-state fluorescence), and PQ is the photochemical quenching. In the absence of energy transfer PQ represents the fraction of open reaction centers.

In a fluorescence induction curve, the rate at which RC "close" and fluorescence rises from F_o to F_m reflects the reduction rate of Q_A and is controlled by the irradiance, the functional absorption cross-section of PSII (σ_{PSII} , $\text{m}^2 \text{ quanta}^{-1}$ or $\text{\AA}^{-2} \text{ quanta}^{-1}$), and the rate constant of the photosynthetic electron transport:

$$F_s = F_o + F_v(1 - PQ) = F_o + F_v \frac{E\sigma_{PSII}}{E\sigma_{PSII} + \frac{1}{\tau_{PSII}}} \quad (\text{Eq. 8})$$

where E is the ambient irradiance and τ_{PSII} is the turnover time of photosynthesis. Similarly, the photosynthetic yield under ambient irradiance can be expressed as

$$\Phi_{PSII}^S = \Phi_{PSII}^{\max} (1 - PQ) = \Phi_{PSII}^{\max} \frac{E\sigma_{PSII}}{E\sigma_{PSII} + \frac{1}{\tau_{PSII}}} \quad (\text{Eq. 9})$$

Technically, the photosynthetic responses under ambient light can be characterized by recording changes in the fluorescence signal over the range of the light regime (Eq. 7), or by characterizing the three photosynthetic characteristics: the maximum yield of photosynthesis, the functional absorption cross section, and the turnover time of photosynthesis (Eq. 9).

One of the biggest obstacles in applying the formalism described in Eq. 1-9 is the fact that under exposure to light, the rate constant of heat de-excitation also changes (see Eq. 2), affecting the fluorescence yield in a way that is independent of the primary photochemistry. This phenomenon, referred to as nonphotochemical quenching, or NPQ, competes with both the fluorescence and photosynthesis for the absorbed excitation energy. By doing so, it provides a photo-protective mechanism for dissipating the excess of excitation energy. When such mechanisms do not work effectively or heat is not released efficiently, the organisms become photo-inhibited or photo-damaged at high irradiance levels, when the rate of excitation delivery to PSII reaction centers exceeds that of the photosynthetic electron transport, leading to degradation of key photosynthetic proteins, such as D1. This will reduce or stop the electron flow in the chloroplast if not repaired or replaced quickly (Long *et al.* 1994).

The mechanisms of non-photochemical quenching operate over time scales ranging from tens of milliseconds to hours. At the short-time scales NPQ-related changes in the fluorescence signal become indistinguishable from the effects of photochemical quenching, complicating interpretation of the fluorescence signals.

Duysens and Sweers (1963) applied the concept of variable fluorescence to study photosynthetic characteristics of microalgae by using the fluorescence induction theory described by Kautsky and Hirsch (1931). Applications of modulated or active fluorescence for assessment of physiological state of phytoplankton in the marine environment in relation to resources and stress factors such as nutrients and light have increased significantly over the last twenty years. Early instruments utilized pump-and-probe fluorometry (PPF) to determine photosynthetic quantum yield (Mauzerall 1972, Falkowski *et al.* 1986, Kolber *et al.* 1990). The same approach was used in the Ross Sea in conjunction with flow cytometry to assess the photophysiology of individual genera (Olson *et al.* 2000). Subsequently, pulse amplitude fluorometry (PAM), which measures the photochemical efficiency of PS II utilizing multiple turnover (MT) flashlets (Schreiber *et al.* 1986, Genty *et al.* 1989), was introduced. Yet the most flexible approach toward rapid characterization of photosynthetic parameters based on fluorescence induction curves has been implemented in the form of fast repetition rate fluorometry (FRRF). This technique measures phytoplankton quantum yield using single turnover (ST) flash (Kolber and Falkowski 1992), and was very effective in assessing photosynthetic efficiencies and the availability of iron over large areas of the ocean (Kolber *et al.* 1994, Behrenfeld *et al.* 1996). Quantum yields measured by variable fluorescence are well correlated with nutrient availability and stress (Kolber *et al.* 1988, Greene *et al.* 1991, Kolber and Falkowski 1992, Behrenfeld *et al.* 1996, Parkhill *et al.* 2001, Sylvan *et al.* 2007, Schallenberg *et al.* 2008).

Differences between FRR and PAM fluorometry

The main differences between FRR and PAM fluorometry lies in the means by which excitation light is applied to saturate PSII, in the way the fluorescence signal is measured, and in the number of photosynthetic parameters that can be measured by these two techniques. FRRF is based on a sequence of high intensity, submicrosecond flashlets with adjustable time interval to produce a single

turnover (ST), multiple turnovers (MT), or relaxation flashes, allowing selective reduction and reoxidation of Q_A , Q_B , and PQ pool electron acceptors within PSII. In contrast, PAM fluorometry uses multiple turnover (MT) flashes to collectively reduce all these acceptors, without discriminating between intermediate reactions. In FRRF, the excitation flashlets are used to both stimulate the photosynthetic activity, and to measure the corresponding changes in the fluorescence yield. In PAM fluorometry, a separate low power excitation source is used to measure the change in the fluorescence yield. Finally, FRRF allows resolving the saturation characteristics of the fluorescence signal, allowing assessment of the functional absorption cross section, the yield of charge separation, and the kinetics of the photosynthetic electron transport between Q_A - Q_B , Q_B -PQ-pool, and PQ-pool-PSI pairs of electron donors/acceptors. PAM fluorometry, on the other hand, is limited to measurements of the yield of charge separation (the variable fluorescence). The MT flash in FRRF fluorometry is produced as a sequence of up to 5000 flashlets at 20 μ s interval (100 ms total length), while in PAM fluorometry the MT flash is produced as a continuous, 500 ms – 1000 ms flash.

When measured under low-to-intermediate light, the maximum F_v/F_m signals attained with FRRF-ST flash are generally 20-30% lower than that measured with PAM fluorometry, while the responses to FRRF-MT and PAM excitation are similar. Following exposure to high irradiances, however, the differences between the maximum F_v/F_m measured by ST and MT flashes disappear. This effect is most likely due to much faster photosynthetic turnover time under high irradiance conditions, which prevents the evolution of the high fluorescence state characteristic to MT flash.

Fluorescence in the Ross Sea

There are very few studies on Ross Sea phytoplankton ecophysiology using variable fluorescence. DiTullio *et al.* (2000) used the PAM technique to measure the vertical distribution of photochemical quantum efficiency, and interpreted the presence of high photosynthetic quantum

yields at depth to be the result of a rapid export of *P. antarctica* to depth in austral spring. They observed that photochemical quantum yield at depths of 450-500 m was similar to that measured at the surface, and argued that the assemblages at depth must have been close to the surface recently, and that rapid flux to depth must have occurred. This interpretation depends on the fact that polar phytoplankton photophysiological capacity degrades in darkness at rates similar to those found in temperate waters, but contrasts with results in the following chapters in which assemblages and cultures placed in darkness for a few weeks consistently increased their quantum yields. Olson *et al.* (2000) used a PPF combined with a flow cytometer to monitor phytoplankton photophysiology and the assemblage response to iron additions within short incubations at two stations in the Ross Sea. At both stations, the samples appeared to be iron limited and gradually increased their quantum yields over six days following iron addition. Smith *et al.* (submitted) describe the first variable fluorescence data from a month-long mooring deployment in the Ross Sea polynya. Such a long deployment of a bio-optical instrument was possible due to the absence of biofouling in the extremely cold waters of the polynya. These observations were complemented by regular fluorometric measurements at three depths on two separate moorings deployed for a month during the growing season of three consecutive years. They indicate exceptionally large seasonal- and inter- annual variations of biomass, while the FRRF results suggested a relaxation from spring iron limitation, most likely due to mixing events and, coincident reduction in irradiance limitation concurrent with dilution of the phytoplankton assemblage via mixing.

Iron and light variability in the Ross Sea

Phytoplankton dynamics in the Ross Sea polynya are largely controlled by the combination of iron availability, light, ice coverage and wind. Macronutrients are rarely limiting and don't appear to exert much forcing on bloom's dynamics and phytoplankton community composition (Smith *et al.*

2003a). In contrast, iron limitation and natural iron enrichment events, such as upwelling of circumpolar deep water along frontal zones (Measures and Vink 2001), intrusions of circumpolar deep water (Peloquin and Smith 2007), glacial ice melting (Leventer and Dunbar 1996, Sedwick and DiTullio 1997, Grotti *et al.* 2001), or iron remineralization of organic material in subsurface waters (Johnson *et al.* 1997) appear to be pivotal in such processes, especially in combination with light gradients. Low iron concentrations are considered the dominant factor limiting primary productivity in the Ross Sea (Martin *et al.* 1991, Olson *et al.* 2000, Sedwick *et al.* 2000, Sosik and Olson 2002, Peloquin and Smith 2007). This element is a critical part of the phytoplankton photosynthetic machinery, and is a component of a variety of other enzymes, such as nitrate and nitrite reductase. It therefore contributes to many fundamental physiological processes, such as photosynthesis, respiration, carbon fixation, and nutrient uptake. Differences in iron requirements between diatoms and *P. antarctica* have been documented (Coale *et al.* 2003, Sedwick *et al.* 2007), potentially explaining distinctive photophysiological patterns between haptophytes and diatoms in experiments presented in the following chapters, and the reported phytoplankton assemblage dynamics in the polynya. For example, differences in iron requirements confer to *P. antarctica* and diatoms different photorecovery and photo-resilience capabilities. These traits become critical in a highly variable irradiance field within the polynya, where optimization of quantum efficiency may be vital for the success of one group relative to the other. Experimental results to test these hypotheses are presented in the following chapters.

Aims and motivation of this research

There are several scientific questions that motivated the studies presented in this dissertation. The studies encompassed a wide range of spatial and temporal scales -from variable fluorescence measurements based on biophysical responses on the order of microseconds (describing cellular

processes and electron transport within the organism's photosynthetic apparatus and plastid membrane), to biomass distribution over the entire Ross Sea polynya, and spatial and temporal variations over several years. This study specifically investigated the photophysiological differences between diatoms and *P. antarctica*, and I postulate that *P. antarctica* has lower light and higher iron requirements than polar diatoms. My hypothesis is based on the observed dominance of *P. antarctica* in deeper mixed waters of the Ross Sea polynya (Arrigo *et al.* 1999, Smith and Asper 2001, Arrigo *et al.* 2003), with lower integrated light and higher iron concentrations than observed during the summer stratified conditions, where diatoms tend to dominate (Sedwick and DiTullio 1997, Smith and Asper 2001). This work also provides a valuable method to derive primary productivity based on variable fluorescence measurements. Such methods have been developed for other oceanic regions (Kromkamp and Peene 1999, Raateoja 2004), but until now it has not been applied or verified in the Southern Ocean.

Scientific relevance

The work performed within this dissertation produced significant results that improve our knowledge of polar phytoplankton photophysiology and ecology. The results also enable the interpretation of extensive bio-optical surveys conducted during several cruises in the Ross Sea polynya. This region is the most productive area in the entire Southern Ocean, and is presently undergoing significant changes in physical forcing. For example, the entire Ross Sea sector has exhibited a significant *increase* in ice concentrations in the past four decades (Kwok and Comiso 2002, Comiso and Nishio 2008, Smith and Comiso 2008)), although this trend is highly variable in space within the sector, with some regions (e.g., the eastern Ross Sea) decreasing significantly, and others (e.g., north of Cape Adare) greatly increasing through time. Regardless of the existing trends, the region almost undoubtedly will be affected in numerous ways by global climate change and human

activities (via physical forcing, as well as harvesting of selected species within the food web), and hence the regional and global biogeochemical cycles driven by its phytoplankton dynamics will be altered in ways that are impossible to predict at present (Arrigo *et al.* 1999). Furthermore, given that carbon flux between the atmosphere and ocean is mostly determined by photosynthetic carbon uptake, I attempt in this study to elucidate the mechanisms regulating photosynthesis in the Ross Sea and to develop, apply, and test new methodologies and instrumentation for the region.

Studies presented in the following chapters represent a rich baseline for future photophysiological studies on Ross Sea phytoplankton. The set of measurements and experiments reported here will allow better identification of future changes in the polynya phytoplankton photosynthetic rates and primary production, and therefore, if consistently monitored, will allow quantification of ecosystem shifts due to global climate change or localized impacts.

LITERATURE CITED

- Arrigo K. R., McLain C. R., Firestone K. J., Sullivan C. W., Comiso J. C. 1994. A comparison of CZCS and *in situ* pigment concentrations in the Southern Ocean. Report No. 13 in TM 104566, NASA
- Arrigo K. R., Weiss A. M., Smith W. O., Jr. 1998. Physical forcing of phytoplankton dynamics in the southwestern Ross Sea. *Journal of Geophysical Research* 103:1007-1021
- Arrigo K. R., Robinson D. H., Worthen D. L., Dunbar R. B., DiTullio G. R., VanWoert M., Lizotte M. P. 1999. Phytoplankton community structure and the drawdown of nutrients and CO₂ in the Southern Ocean. *Science* 283:365-367
- Arrigo K. R., DiTullio G. R., Dunbar R. B., Robinson D. H., VanWoert M. L., Worthen D. L., Lizotte M. P. 2000. Phytoplankton taxonomic variability in nutrient utilization and primary production in the Ross Sea. *Journal of Geophysical Research* 105:8827-8846
- Arrigo K. R., Worthen D. L., Robinson A. R. 2003. A coupled ocean-ecosystem model of the Ross Sea: 2. Iron regulation of phytoplankton taxonomic variability and primary production. *Journal of Geophysical Research* 108:3231
- Arrigo K. R., van Dijken G. L. 2004. Annual changes in sea-ice, chlorophyll *a*, and primary production in the Ross Sea, Antarctica. *Deep Sea Research I* 51:117-138
- Arrigo K. R., van Dijken G., Long M. 2008. Coastal Southern Ocean: A strong anthropogenic CO₂ sink. *Geophysical Research Letters* 35 doi: 10.1029/2008gl035624
- Assmann K., Timmermann R. 2005. Variability of dense water formation in the Ross Sea. *Ocean Dynamics* 55:68-87
- Behrenfeld M. J., Bale A. J., Kolber Z. S., Aiken J., Falkowski P. G. 1996. Confirmation of iron limitation of phytoplankton photosynthesis in the equatorial Pacific Ocean. *Nature* 383:508-511
- Bromwich D. H., Carrasco J. F., Liu Z., Tzeng R.-Y. 1993. Hemispheric atmospheric variations and oceanographic impacts associated with Katabatic surges across the Ross Ice Shelf, Antarctica. *Journal of Geophysical Research* 98:13045-13062
- Carlson C. A., Hansell D. A., Peltzer E. T., Smith W. O., Jr. 2000. Stocks and dynamics of dissolved and particulate organic matter in the southern Ross Sea, Antarctica. *Deep Sea Research II* 47:3201-3225
- Caron D. A., Dennett M. R., Lonsdale D. J., Moran D. M., Shalapyonok L. 2000. Microzooplankton herbivory in the Ross Sea, Antarctica. *Deep Sea Research II* 47:3249-3272
- Carrada G. C., Mangoni O., Russo G. F., Saggiomo V. 2000. Phytoplankton size-fractionated biomasses in the Ross Sea. Spatial and temporal evolution during the austral spring. In: Faranda F. M.,

- Guglielmo, L., Ianora, A. (ed) Ross Sea Ecology Italian Antarctic expeditions (1987–1995). Springer, Berlin, 205–216
- Cavaliere D. J., Parkinson C. L. 2008. Antarctic sea ice variability and trends, 1979–2006. *Journal of Geophysical Research* 113:doi:10.1029/2007JC004564
- Coale K. H., Wang X., Tanner S. J., Johnson K. S. 2003. Phytoplankton growth and biological response to iron and zinc addition in the Ross Sea and Antarctic Circumpolar Current along 170°W. *Deep Sea Research II* 50:635-653
- Coale K. H., Gordon M. R., Wang X. 2005. The distribution and behavior of dissolved and particulate iron and zinc in the Ross Sea and Antarctic circumpolar current along 170°W. *Deep Sea Research I* 52:295-318
- Cochlan W. P., Bronk D. A., Coale K. H. 2002. Trace metals and nitrogenous nutrition of Antarctic phytoplankton: experimental observations in the Ross Sea. *Deep Sea Research II* 49:3365-3390
- Comiso J. C., McLain C. R., Sullivan C. W., Ryan J. P., Leonard C. L. 1993. Coastal Zone Color Scanner pigment concentrations in the Southern-Ocean and relationship to geophysical surface-features. *Journal of Geophysical Research* 98:2419-2451
- Comiso J. C., Nishio F. 2008. Trends in the sea ice cover using enhanced and compatible AMSR-E, SSM/I, and SMMR data. *Journal of Geophysical Research* 113:doi:10.1029/2007JC004257
- de Baar H. J. W., De Jong J. T. M. 2001. Observations of iron distributions in seawater. In: Buffle J., van Leeuwen H. P. (eds) *The biogeochemistry of iron in seawater*, Vol 7. John Wiley and Sons, 396
- DeMaster D. J., Dunbar R. B., Gordon L. I., Leventer A. R., Morrison J. M., Nelson D. M., Nittrouer C. A., Smith W. O., Jr. 1992. Cycling and accumulation of biogenic silica and organic matter in high-latitude environments: the Ross Sea. *Oceanography* 5:146-153
- Dinniman M. S., Klinck J. M., Smith W. O., Jr. 2007. Influence of sea ice cover and icebergs on circulation and water mass formation in a numerical circulation model of the Ross Sea, Antarctica. *Journal of Geophysical Research* 112:doi:10.1029/2006JC004036
- DiTullio G. R., Smith W. O., Jr. 1995. Relationship between dimethylsulfide and phytoplankton pigment concentrations in the Ross Sea, Antarctica. *Deep Sea Research I* 42:873-892
- DiTullio G. R., Smith W. O., Jr. 1996. Spatial patterns in phytoplankton biomass pigment distributions in the Ross Sea. *Journal of Geophysical Research* 101:18467-18477
- DiTullio G. R., Grebmeier J. M., Arrigo K. R., Lizotte M. P., Robinson A. R., Leventer A., Barry J. P., VanWoert M. L., Dunbar R. B. 2000. Rapid and early export of *Phaeocystis antarctica* blooms in the Ross Sea, Antarctica. *Nature* 404:595-598
- DiTullio G. R., Garcia N., Riseman S., Sedwick P. N. 2007. Effects of iron concentration on pigment composition in *Phaeocystis antarctica* grown at low irradiance. *Biogeochemistry* 83:71-81

- Duysens L. N. M., Sweers H. E. 1963. Mechanisms of two photochemical reactions in algae as studied by means of fluorescence. In: Miyachi S. (ed) Studies on microalgae and photosynthetic bacteria. University Tokyo Press, Tokyo, Japan, 353-372
- Falkowski P. G., Wyman K., Ley A. C., Mauzerall D. 1986. Relationship of steady-state photosynthesis to fluorescence in eucaryotic algae. *Biochimica et Biophysica Acta* 849:183-192
- Falkowski P. G. 1994. The role of phytoplankton photosynthesis in global biogeochemical cycles. *Photosynthesis Research* 39:235-258
- Field C. B., Behrenfeld M. J., Randerson J. T., Falkowski P. G. 1998. Primary production of the biosphere: integrating terrestrial and oceanic components. *Science* 281:237-240
- Fitzwater S. E., Johnson K. S., Gordon R. M., Coale K. H., Smith W. O., Jr. 2000. Trace metal concentrations in the Ross Sea and their relationship with nutrients and phytoplankton growth. *Deep Sea Research II* 47:3159-3179
- Fung I. Y., Meyn S. K., Tegen I., Doney S. C., John J., Bishop J. 2000. Iron supply and demand in the upper ocean. *Global Biogeochemical Cycles* 14:281-295
- Genty B., Briantais J. M., Baker N. R. 1989. The relationship between the quantum yield of photosynthetic electron transport and quenching of chlorophyll fluorescence. *Biochimica et Biophysica Acta* 990:87-92
- Goffart A., Catalano G., Hecq J. H. 2000. Factors controlling the distribution of diatoms and *Phaeocystis* in the Ross Sea. *Journal of Marine Systems* 27:161-175
- Gowing M. M., Garrison D. L., Kunze H. B., Winchell C. J. 2001. Biological components of Ross Sea short-term particle fluxes in the austral summer of 1995-1996. *Deep Sea Research I* 48:2645-2671
- Greene R. M., Geider R. J., Falkowski G. P. 1991. Effect of iron limitation on photosynthesis in a marine diatom. *Limnology and Oceanography* 36:1772-1782
- Grotti M., Soggia F., Abemoschi M. L., Rivoar P., Magi E., Frache R. 2001. Temporal distribution of trace metals in Antarctic coastal waters. *Marine Chemistry* 76:189-209
- Huntley M. E., Marin V., Escritor F. 1987. Zooplankton grazers as transformers of ocean optics: A dynamic model. *Journal of Marine Research* 45:911-945
- Innamorati M., Mori C., Massi L., Lazzara L., Nuccio C. 1999. Phytoplankton biomass related to environmental factors in the Ross Sea. In: Faranda F. M., Guglielmo, L., Ianora, A. (ed) *Ross Sea Ecology*. Springer-Verlag, Berlin, 217– 230
- Johnson K. S., Gordon R. M., Coale K. H. 1997. What controls dissolved iron concentrations in the world ocean? *Marine Chemistry* 57:137-161

- Kautsky H., Hirsch A. 1931. Neue Versuche zur Kohlensäureassimilation. *Naturwissenschaften* 19:964-964
- Kiefer D. A., Reynolds R. A. 1992. Advances in understanding phytoplankton fluorescence and photosynthesis. In: Falkowski P. G., Woodhead A. D. (eds) *Primary Productivity and Biogeochemical Cycles in the Sea*. Plenum Press, New York, 155-174
- Kolber Z. S., Zehr J., Falkowski P. G. 1988. Effects of Growth Irradiance and Nitrogen Limitation on Photosynthetic Energy Conversion in Photosystem II. *Plant Physiology* 88:923-929
- Kolber Z. S., Wyman K. D., Falkowski P. G. 1990. Natural variability in photosynthetic energy conversion efficiency: A field study in the Gulf of Maine. *Limnology and Oceanography* 35:72-79
- Kolber Z. S., Falkowski P. G. 1992. Fast Repetition Rate (FRR) fluorometer for making in situ measurements of primary productivity. *Ocean 92 Conference*, Newport, Rhode Island, 637-641
- Kolber Z. S., Barber R. T., Coale K. H., Fitzwater S. E., Greene R. M., Johnson K. S., Lindley S., Falkowski G. P. 1994. Iron limitation of the phytoplankton photosynthesis in the equatorial Pacific Ocean. *Nature* 371:145-149
- Kolber Z. S., Prasil O., Falkowski P. G. 1998. Measurements of variable chlorophyll fluorescence using fast repetition rate techniques: defining methodology and experimental protocols. *Biochimica et Biophysica Acta* 1367:88-106
- Krause G. H., Weis E. 1991. Chlorophyll Fluorescence and Photosynthesis: The Basics. *Annual Review of Plant Physiology and Plant Molecular Biology* 42:313-349
- Kromkamp J., Peene J. 1999. Estimation of phytoplankton photosynthesis and nutrient limitation in the Eastern Scheldt estuary using variable fluorescence. *Aquatic Ecology* 33:101-104
- Kwok R., Comiso J. C. 2002. Southern Ocean Climate and Sea Ice Anomalies Associated with the Southern Oscillation. *Journal of Climate* 15:487-501
- Leventer A., Dunbar R. B. 1996. Factors influencing the distribution of diatoms and other algae in the Ross Sea. *Journal of Geophysical Research* 101:18489-18500
- Lieselotte R., Dale R. 1997. Photoinduction of UV-absorbing compounds in Antarctic diatoms and *Phaeocystis antarctica*. *Marine Ecology Progress Series* 160:13-25
- Liss P. S., Chuck A., Bakker D., Turner S. 2005. Ocean fertilization with iron: effects on climate and air quality. *Tellus B* 57:269-271
- Long S. P., Humphries S., Falkowski P. G. 1994. Photoinhibition of Photosynthesis in Nature. *Annual Review of Plant Physiology and Plant Molecular Biology* 45:633-662

- Martin J. H., Gordon R. M., Fitzwater S. E. 1991. The case for iron. *Limnology and Oceanography* 36:1793-1802
- Mathot S., Smith W. O., Jr., Carlson C. A., Garrison D. L., Gowing M. M., Vickers C. L. 2000. Carbon partitioning within *Phaeocystis antarctica* (Prymnesiophyceae) colonies in the Ross Sea, Antarctica. *Journal of Phycology* 36:1049-1056
- Matrai P. A., Vernet M., Hood R., Jennings A., Brody E., Saemundsdottir S. 1993. Light-dependence of carbon and sulfur production by polar clones of the genus *Phaeocystis*. *Marine Biology* 124:157-167
- Mauzerall D. 1972. Light-induced fluorescence changes in *Chlorella*, and the primary photoreactions for the production of oxygen. *Proceedings National Academy of Science* 69:1358-1362
- Measures C. I., Vink S. 2001. Dissolved Fe in the upper waters of the Pacific sector of the Southern Ocean. *Deep Sea Research II* 48:3913-3941
- Misic C., Castellano M., Ruggiero N., Povero P. 2006. Dissolved organic matter characterisation and temporal trends in Terra Nova Bay (Ross Sea, Antarctica). *Estuarine, Coastal and Shelf Science* 70:405-414
- Moisan T. A., Mitchell B. G. 1999. Photophysiological acclimation of *Phaeocystis antarctica* Karsten under light limitation. *Limnology and Oceanography* 44:247-258
- Moisan T. A., Mitchell B. G. 2001. UV absorption by mycosporine-like amino acids in *Phaeocystis antarctica* Karsten induced by photosynthetically available radiation. *Marine Biology* 138:217-227
- Moisan T. A., Ellisman M., Buitenhuis C., Sosinsky G. 2006. Differences in chloroplast ultrastructure of *Phaeocystis antarctica* in low and high light. *Marine Biology* 149:1281-1290
- Olson R. J., Sosik H. M., Chekalyuk A. M., Shalapyonok A. 2000. Effects of iron enrichment on phytoplankton in the Southern Ocean during late summer: active fluorescence and flow cytometric analyses. *Deep Sea Research II* 47:3181-3200
- Orsi A. H., Wiederwohl C. L. 2009. A recount of Ross Sea waters. *Deep Sea Research II* 56:778-795
- Parkhill J. P., Maillet G., Cullen J. J. 2001. Fluorescence-based maximal quantum yield for PSII as a diagnostic of nutrient stress. *Journal of Phycology* 37:517-529
- Peloquin J. A., Smith W. O., Jr. 2007. Phytoplankton blooms in the Ross Sea, Antarctica: Interannual variability in magnitude, temporal patterns, and composition. *Journal of Geophysical Research* 112 doi: 10.1029/2006JC003816
- Raateoja M. 2004. Fast repetition rate fluorometry (FRRF) measuring phytoplankton productivity: A case at the entrance to the Gulf of Finland, Baltic Sea. *Boreal Environmental Research* 9:236-276

- Raiswell R., Benning L. G., Tranter M., Tulaczyk S. 2008. Bioavailable iron in the Southern Ocean: the significance of the iceberg conveyor belt. *Geochemical Transactions* 9 doi: 10.1186/1467-4866
- Schallenberg C., Lewis M. R., Kelley D. E., Cullen J. J. 2008. Inferred influence of nutrient availability on the relationship between Sun-induced chlorophyll fluorescence and incident irradiance in the Bering Sea. *Journal of Geophysical Research* 113 doi: 10.1029/2007JC004355
- Schreiber U., Schliwa U., Bilger W. 1986. Continuous recording of photochemical and non-photochemical chlorophyll fluorescence quenching with a new type of modulation fluorometer. *Photosynthesis Research* 10:51-62
- Sedwick P. N., DiTullio G. R. 1997. Regulation of algal blooms in antarctic shelf waters by the release of iron from melting sea ice. *Geophysical Research Letters* 24:2515–2518
- Sedwick P. N., DiTullio G. R., Mackey D. J. 2000. Iron and manganese in the Ross Sea, Antarctica: Seasonal iron limitation in Antarctic shelf waters. *Journal of Geophysical Research* 105:11321-11336
- Sedwick P. N., Garcia N., Riseman S., Marsay C., DiTullio G. 2007. Evidence for high iron requirements of colonial *Phaeocystis antarctica* at low irradiance. *Biogeochemistry* 83:83-97
- Smith W. O., Jr, Nelson D. M. 1985. Phytoplankton bloom produced by a receding ice edge in the Ross Sea: spatial coherence with the density field. *Science* 227:163-166
- Smith W. O., Jr, Asper V. L. 2001. The influence of phytoplankton assemblage composition on biogeochemical characteristics and cycles in the southern Ross Sea, Antarctica. *Deep Sea Research I* 48:137-161
- Smith W. O., Jr, Asper V. A., Tozzi S., Lui X. submitted. Surface layer variability in the Ross Sea, Antarctica as assessed by continuous fluorescence measurements. *Progress In Oceanography*
- Smith W. O., Jr., Nelson D. M. 1986. The importance of ice-edge blooms in the Southern Ocean. *BioScience* 36:251-257
- Smith W. O., Jr., Gordon L. I. 1997. Hyperproductivity of the Ross Sea (Antarctica) polynya during austral spring. *Geophysical Research Letters* 24:233-236
- Smith W. O., Jr., Marra J., Hiscock M. R., Barber R. T. 2000. The seasonal cycle of phytoplankton biomass and primary productivity in the Ross Sea, Antarctica. *Deep Sea Research II* 47:3119-3140
- Smith W. O., Jr., Dennett M. R., Mathot S., Caron D. A. 2003a. The temporal dynamics of the flagellated and colonial stages of *Phaeocystis antarctica* in the Ross Sea. *Deep Sea Research II* 50:605-617
- Smith W. O., Jr., Dinniman M. S., Klinck J. M., Hofmann E. 2003b. Biogeochemical climatologies in the Ross Sea, Antarctica: seasonal patterns of nutrients and biomass. *Deep Sea Research II* 50:3083-3101

- Smith W. O., Jr., Shields A. R., Peloquin J. A., Catalano G., Tozzi S., Dinniman M. S., Asper V. A. 2006. Interannual variations in nutrients, net community production, and biogeochemical cycles in the Ross Sea. *Deep Sea Research II* 53:815-833
- Smith W. O., Jr., Comiso J. C. 2008. Influence of sea ice on primary production in the Southern Ocean: A satellite perspective. *Journal of Geophysical Research* 113 doi: 10.1029/2007JC004251
- Sosik H. M., Olson R. J. 2002. Phytoplankton and iron limitation of photosynthetic efficiency in the Southern Ocean during late summer. *Deep Sea Research I* 49:1195-1216
- Sweeney C., Smith W. O., Jr, Hales B., Bidigare R. R., Carlson C. A., Codispoti L. A., Gordon L. I., Hansell D. A., Millero F. J., Park M.-O., Takahashi T. 2000. Nutrient and carbon removal ratios and fluxes in the Ross Sea, Antarctica. *Deep Sea Research II* 47:3395-3421
- Sylvan J. B., Quigg A., Tozzi S., Ammerman J. W. 2007. Eutrophication-induced phosphorus limitation in the Mississippi River plume: Evidence from fast repetition rate fluorometry. *Limnology and Oceanography* 52:2679-2685
- Tagliabue A., Arrigo K. R. 2003. Anomalously low zooplankton abundance in the Ross Sea: An alternative explanation. *Limnology and Oceanography* 48:686-699
- Tang K., Smith W. O., Jr, Shields A. R., Elliott D. T. 2008. Survival and recovery of *Phaeocystis antarctica* (Primnesiophyceae) from prolonged darkness and freezing. *Proceedings of the Royal Society of London. Series B* 276:81-90
- van Leeuwe M. A., Stefels J. 2007. Photosynthetic responses in *Phaeocystis antarctica* towards varying light and iron conditions. *Biogeochemistry* 83:61-70

**SECTION II. THE PHOTO-PHYSIOLOGICAL DIFFERENCES AMONG CULTURED ROSS SEA DIATOMS,
PHAEOCYSTIS ANTARCTICA, AND NATURAL ASSEMBLAGES AND THEIR PHOTOSYNTHETIC
RESPONSES TO LIGHT, TEMPERATURE, MICRONUTRIENTS, AND pCO₂ VARIATIONS**

Parts of this section are included in collaborative manuscripts currently published:

Feng, Y., Hare, C.E., Rose, J.M., Handy, S.M., DiTullio, G.R., Lee, P.A., Smith, W.O. Jr., Peloquin, J., Tozzi, S., Sun, J., Zhang, Y., Dunbar, R.B., Long, M.C., Sohst, B., Hutchins, D.A. (2010) Interactive Effects of CO₂, Irradiance and Iron on Ross Sea Phytoplankton. *Deep Sea Research I* 57(3), 368-383

Rose J.M., Feng Y., DiTullio G., Dunbar R., Hare C. E., Lee P., Lohan M., Long M., Smith W.O., Jr., Sohst B., Tozzi S., Zhang Y. and Hutchins D. A. (2009) Synergistic effects of iron and temperature on Antarctic plankton assemblages. *Biogeosciences* 6, 3131–3147

ABSTRACT

I conducted field and laboratory manipulations to examine photophysiological differences between *Phaeocystis antarctica* and diatoms. *P. antarctica*, a prymnesiophyte that can dominate the phytoplankton in the Southern Ocean, displays a distinct photophysiological response to water column structure, irradiance, and micronutrient availability when compared to diatoms. Specifically, *P. antarctica* showed a rapid recovery from high light exposure, as indicated by the rapid return to initial, high quantum yields, in contrast to diatoms, which responded more slowly. Both organisms eventually recovered to initial quantum yields values, suggesting that high light exposure does not have a permanent effect on these organisms. Experiments with variable irradiance, micronutrients, temperature and pCO₂ suggest that iron has the greatest and most rapid impact on quantum yields, while the increased temperatures accelerated the rates of change of photophysiological processes, but does not modify the relative responses between functional groups.

INTRODUCTION

The Ross Sea polynya is characterized by regular occurrences of phytoplankton blooms during the austral spring and summer (El-Sayed *et al.* 1983, Smith and Nelson 1985, Arrigo and McClain 1994, Arrigo *et al.* 1998, Smith *et al.* 2000), with peaks of standing biomass and productivity usually observed in December (Smith *et al.* 2000, Smith *et al.* 2006), and sometimes followed by a secondary bloom in February (Innamorati *et al.* 1999, Peloquin and Smith 2007). Blooms in the Ross Sea are dominated by two phytoplankton functional groups, diatoms and the polymorphic prymnesiophyte *Phaeocystis antarctica* (Smith and Gordon 1997, Arrigo *et al.* 1999, Dennett *et al.* 2001). *P. antarctica* has a complex life cycle (Rousseau *et al.* 1994, Whipple *et al.* 2005, Rousseau *et al.* 2007, Verity *et al.* 2007) that includes solitary cells and a colonial stage, the latter which often dominates blooms. *P.*

antarctica colonies tend to bloom in early spring (Smith *et al.* 1998), predominantly in the south central Ross Sea (Arrigo *et al.* 1998, Hecq *et al.* 1999), in relatively weakly stratified waters (Arrigo *et al.* 1999, Smith and Asper 2001). Diatoms are frequently dominant in summer and in more strongly stratified water columns, including shallow mixed layers along the Victoria Land coast and near receding ice edges (Smith and Nelson 1986, DiTullio and Smith 1996, Goffart *et al.* 2000, Smith and Asper 2001). They appear to significantly contribute to carbon export (Fonda Umani *et al.* 2002), especially via the process of particle aggregation, despite the potentially high grazing rates in some coastal areas (Goffart *et al.* 2000). Diatom blooms are often dominated by *Fragilariopsis curta* (Smith and Nelson 1986, Dunbar *et al.* 1998, Goffart *et al.* 2000), with other *Fragilariopsis* species, such as *F. cylindrus*, found in lower densities. *Chaetoceros* spp. (Leventer and Dunbar 1996), *Nitzschia* and *Pseudo-nitzschia* spp. (Nuccio *et al.* 2000) and *Thalassiosira* spp. (Fonda Umani *et al.* 2002) are also commonly encountered. Phytoplankton distribution appears to be controlled by a variety of factors (Leventer and Dunbar 1996), including interactions of environmental forcing such as meteorological conditions (Arrigo *et al.* 1998), ice (Leventer and Dunbar 1996), irradiance (Lazzara *et al.* 1999), macronutrients, and micro-nutrients (Sedwick and DiTullio 1997, Coale *et al.* 2003), as well as grazing (Caron *et al.* 2000).

Some of the meteorological and physical forcing factors vary dramatically between years (Jacobs and Giulivi 1998). These variations affect the temporal and spatial distribution of diatoms and *P. antarctica*. Moreover, morphological, physiological and stoichiometric differences between diatoms and *P. antarctica* can affect the dynamics of carbon, silica and sulfur cycling. The productivity of the Ross Sea polynya is never limited by macronutrients; rather it is seasonally limited by light (Smith *et al.* 2000) in the early spring and by iron availability in the summer (Sedwick and DiTullio 1997, Fitzwater *et al.* 2000, Olson *et al.* 2000, Sedwick *et al.* 2000, Coale *et al.* 2005). On the other hand, photosynthetically active radiation (PAR, 400-700 nm) in the Ross Sea and its availability to

phytoplankton is controlled by seasonal variations in solar elevation and inclination, ice concentration, cloudiness, and the depth of the mixed layer. Changes in these forcing factors on several different spatial and temporal scale result in a variety of photophysiological responses such as: (a) *photoacclimation*, defined as a phenotypic response to a change in irradiance that often leads to rearrangements in the photosynthetic apparatus and changes in the photosynthetic kinetics, (b) *photoadaptation*, defined as population adjustments to changes in light regimes that occurs on a longer time scale and can involve several generations, and (c) *photoinhibition*, referred to as a combination of several different processes that result in the decline of PSII efficiency, usually as a result of high light exposure. *Photoinhibition* usually involves fast degradation of D1 protein following oxidative damage due to slow tyrosine electron donor activity. Alternatively, *photoinhibition* can be caused, or exacerbated by, reduced electron flow between quinones, resulting in a slower electron turnover and increased probability of charge recombination between the primary radical pair P680 and the primary acceptor pheophytin. This event produces triplet chlorophyll that reacts with O₂ to produce extremely reactive singlet oxygen (Vass *et al.* 1992). Either way, *photoinhibition* results in the degradation of D1 and inactivation of PSII and therefore, reduction in the pool of active PSII reaction centers. If this process becomes irreversible, or if the rates of repair lag the rates of photoinhibition, the organism is considered to be *photodamaged*. There are several mechanisms of *photoprotection* that organisms use. These aim to prevent photosynthetic apparatus damage by reducing the rates of excitation delivery to PSII reaction center, and/or dissipating the excess of excitation energy with alternative sink pathways (i.e., non-photochemical quenching). The *photoprotection* responses vary with the light intensity and exposure time. The majority of non-photochemical quenching are believed to occur through heat dissipation via the xanthophyll cycle (Demmig-Adams and Adams 1992). This study elucidates some of the biophysical responses of Ross Sea phytoplankton photosynthesis using

variable fluorescence techniques and is aimed at understanding how light, temperature, Fe, and CO₂ affect photosynthetic quantum yields.

MATERIAL AND METHODS

All experiments were conducted on board the *RVIB N.B. Palmer* as part of the “Controls on Ross Sea Algal Community Structure (CORSACS)” program during cruises NBPO6-01 (Dec. 2005 – Jan. 2006) and NBPO6-08 (Nov. – Dec. 2006).

Variable Chl *a* fluorescence measurements

Photosynthetic parameters based on chlorophyll *a* variable fluorescence were characterized using a Kolber bench-top fast repetition rate fluorometer (FRRF). This instrument is equipped with an array of blue LED lights (~470 nm) with a total power of about six watts cm⁻². In continuous wave (CW) mode the instrument can deliver up to 8000 μmol photons m⁻² s⁻¹ while performing FRR excitation. The FRR excitation flashlets are produced at pulse photon flux density (PPFD) of about 65,000 μmol photons m⁻² s⁻¹, with 150 ns rise time and 200 ns fall time. A thermo-electric cooled 10-mm avalanche photodiode (Advance Photonics, Inc) detector is connected to an elbow-shaped light pipe that collects the emission light from the bottom of the sample chamber. The instrument has a sensitivity of 0.01 μg L⁻¹ with 5-10% accuracy. The measurement protocol was optimized to obtain fluorescence saturation (F_m) by a rapid sequence of 80 flashlets, followed by 30 flashlets for the relaxation portion. Prior to measurements the instrument blanks were determined with distilled water to account for light scattering within the cuvette, and then with seawater that had been filtered through a Millex AA 0.8 μm Millipore Membrane to account for fluorescence of dissolved organic matter. The maximum

quantum yield efficiency for PSII (F_v/F_m) was calculated (Genty *et al.* 1989) by normalizing F_m by the difference between the fluorescence at saturation (F_m) and the minimum fluorescence (F_0):

$$\Phi_{PSII}^{\max} = \frac{F_m - F_0}{F_m} = \frac{F_v}{F_m} \quad (\text{Eq. 10})$$

Functional absorption cross section (σ_{PSII}) was calculated by fitting the fluorescence transient into a theoretical function describing the relationship between fluorescence and photosynthesis (Kolber *et al.* 1998).

Two different units of the instrument were used. They differed only in the LED array sizes and in the signal attenuation method, but provided similar performance. Samples were either placed into the cuvette via pipette or dispensed with a peristaltic pump. Maximum flow rate was 5 mL min^{-1} . To avoid condensation on the exterior of the cuvette due to the temperature difference between the seawater and the laboratory air, the light and cuvette chamber were constantly flushed with dry nitrogen gas.

Phytoplankton cultures and natural assemblages

Monoclonal, non-axenic cultures of *P. antarctica* (CCMP 1374) and *Pseudo-nitzschia sp.* (CCMP 1445) were obtained from the Pravasoli-Guillard National Center for Culture of Marine Phytoplankton. Stock cultures were kept in duplicate 15 mL Falcon Tubes in growth chambers at $-1^\circ\text{C} \pm 1$ in filter-sterilized f/2 media (Guillard 1975) under continuous irradiance (cold-white fluorescent lamps). Natural phytoplankton assemblages collected in the Ross Sea were used for experiments shortly after collection, following removal of macrozooplankton by prescreening with a $200 \mu\text{m}$ Nitex mesh. Prior to measurements, the natural samples were kept under the same conditions described above.

Photorecovery (PR) experiments

Due to the nature of the fluorescence measurements, true replications were impossible; instead, pseudo-replicates were measured whenever possible. A total of five experiments were performed during the summer cruise NBP06-01, and three more experiments were performed during the spring cruise (Table 1). For PR 1 incubation experiment *P. antarctica* (CCMP 1374) and *Pseudo-nitzschia* sp. (CCMP 1445) were kept in 1-L Qorpak bottles and acclimated at $150 \mu\text{mol photons m}^{-2} \text{s}^{-1}$ for 2 weeks. The F_v/F_m values of the cultures were measured at 0, 5, 10, 20 and 45 minutes after removal from the incubator while maintained at $<10 \mu\text{mol photons m}^{-2} \text{s}^{-1}$ on ice.

For PR 2 an unmodified, *P. antarctica*-dominated assemblage, and a culture of *Pseudo-nitzschia* sp. were used. They were acclimated to $300 \mu\text{mol photons m}^{-2} \text{s}^{-1}$ for several days, and their photosynthetic properties were monitored over 13 days. Following acclimation, the cultures were kept under low light ($<10 \mu\text{mol photons m}^{-2} \text{s}^{-1}$) for the first two hours, and then wrapped in aluminum foil to simulate complete darkness and returned to the incubator. The cultures were sampled six times during the first hour by removing of 10-15 mL subsamples to determinate the rapid photorecovery kinetics, six more times in the following 12 hours, and approximately once every 24 hours for the following 12 days to quantify the slow photorecovery kinetics.

The PR3 and PR4 experiments were performed over 32 and 24 hours, respectively. Prior to the experiments both cultures were acclimated in on-deck incubators at 50% E_0 for 48 hours under an average irradiance of $400 \mu\text{mol photons m}^{-2} \text{s}^{-1}$.

PR 5 lasted 24 hours and was designed to determine the effects of different exposures to inhibiting irradiance levels on photorecovery. Four 500 mL flasks with 250 mL of sterile Ross Sea water were inoculated with 50 mL of *P. antarctica*-dominated natural assemblage, and four flasks with *Pseudo-nitzschia* sp. These flasks were exposed to $850 \mu\text{mol photons m}^{-2} \text{s}^{-1}$ for a period of 2, 4, 6 and 8 hours. During the spring cruise all experiments were conducted in indoor incubators due to low air

temperatures using a surface water flow-through system. The stock cultures were maintained in a growth chamber at $150 \mu\text{mol photons m}^{-2} \text{s}^{-1}$ constant light.

The PR 6, 7, 8 experiments were performed with *P. antarctica* and *Pseudo-nitzschia* sp. cultures. In PR 6 very little photoinhibition was observed following three hours exposure to $300 \mu\text{mol photons m}^{-2} \text{s}^{-1}$; therefore, the experiment was repeated (PR 7 and 8) with $600 \mu\text{mol photons m}^{-2} \text{s}^{-1}$ over two and four hours, which resulted in more pronounced photoinhibition. Photorecovery was monitored for six hours after removal of the cultures from light.

A recovery index (REC_{ind}) was calculated as the difference in the photorecovery by comparing equal sections of the slopes of the fitted curve:

$$REC_{ind} = \left. \frac{F_v}{F_m} \right|_{t+1} - \left. \frac{F_v}{F_m} \right|_t \quad (\text{Eq. 11})$$

This approach differs from the recovery assessment calculated either as the relative recovery percentage (RR %) based on the maximum measured quantum yield,

$$RR(\%) = 100 \frac{\left. \frac{F_v}{F_m} \right|_i - \left. \frac{F_v}{F_m} \right|_{init}}{\left. \frac{F_v}{F_m} \right|_{max} - \left. \frac{F_v}{F_m} \right|_{init}} \quad (\text{Eq. 12})$$

or as the per cent recovery based on the maximum theoretical (F_v/F_m) of 0.65 (theoretical recovery, or TR %):

$$TR(\%) = 100 \frac{\left. \frac{F_v}{F_m} \right|_i - \left. \frac{F_v}{F_m} \right|_{init}}{0.65 - \left. \frac{F_v}{F_m} \right|_{init}} \quad (\text{Eq. 13})$$

In some of the experiments, the cultures achieved complete photorecovery and maximum photosynthetic quantum yields of 0.65, with RR approaching TR.

Ross Sea iron, light and CO₂ experiments 1 and 2 (RSC1 and RSC2)

FRRF measurements were used to investigate the combined effects of iron, light and CO₂ on photosynthetic parameters. Natural assemblages from near-surface water were collected in December 2005 and in November 2006 and were used to inoculate shipboard continuous cultures (Hutchins *et al.* 2003, Hare *et al.* 2005, Hare *et al.* 2007). Near-surface (10 to 15 m) water was collected using a trace-metal clean Teflon pump system (Bruland *et al.* 2005), and 50-L reservoirs were filled with 0.2 µm-filtered seawater to continuously provide fresh media to the 2.5-L incubation bottles. A factorial design was used, with three variables (irradiance, Fe and CO₂) at two levels each, for a total of eight treatments that were each replicated three times.

RSC1 experiment was performed under two irradiance levels: 10% of surface light (low irradiance), and 40% of surface light (high irradiance), whereas CO₂ concentrations of 360 and 750 ppm were used. Iron concentrations in the control were set by natural surface concentrations (ca. 0.2 nM), and the elevated iron treatment had concentrations in excess of 1 nM. The experiment was run for 19 days. In RSC2, the low and high irradiances were 77 and 365 mol photons m⁻² s⁻¹, respectively, with low and high CO₂ at 380 and 750 ppm. Iron concentrations were as in RSC1, and the experiment was run for 16 days.

Ross Sea temperature and iron experiment 1 (RST1)

This experiment involved batch cultures of natural assemblages collected during NBPO6-01, and included a factorial design with two variables: temperature and iron. Incubations were performed at 18% of surface irradiance. Two levels for each variable were used, and each treatment was run in triplicate. Incubation temperatures selected were at 0 and 4°C, with the latter adjusted gradually over a period of three hours. Iron concentrations were the same as in RSC1, and the experiment lasted seven days. Photophysiological responses were followed with variable fluorescence measurements.

Samples were dark-adapted in a cooler on ice for 30 to 40 minutes prior to fluorescence measurements to assess maximum potential photosynthetic quantum yields.

Ross Sea light and temperature experiment 2 (RST2)

During NBP06-08 FRRF measurements were used to investigate the combined effects of light and temperature on phytoplankton photophysiology in a manner similar to RST1. Incubations were run at irradiance levels of 77 and 365 mol photons $\text{m}^{-2} \text{s}^{-1}$ and 0 and 4°C using near-surface water collected using a trace-metal clean pump system (Bruland *et al.* 2005). Samples for FRRF measurement were dark-adapted in a cooler on ice for 30 to 40 minutes to assess maximum potential photosynthetic quantum yields.

Fe, Zn, Co, and Vitamin B₁₂ experiment (WHOI 1, 2 and 3)

Three experiments during NBP06-08 were performed to investigate the effects of trace metals and coenzyme B₁₂ limitation in natural phytoplankton assemblages (Bertrand *et al.* 2007). Water was collected from 5-8 m with the trace-metal clean pump system and placed into a 50-L carboy, and then transferred to 2- and 4.5-L polycarbonate bottles. All water transfers were done in a positive pressure, trace metal-clean space equipped with a laminar flow hood. Ambient temperature was maintained by a constant flow of surface seawater through the incubators. One nmol L^{-1} iron was added as FeCl_3 (Fluka) in pH 2 (SeaStar HCl) MilliQ water, and 1 nmol L^{-1} zinc, and 500 pmol L^{-1} cobalt was added as CoCl_2 (Fluka) in pH 2 (SeaStar HCl) MilliQ water. 100 pmol L^{-1} Vitamin B₁₂ (Sigma, cyanocobalamin, 99%) was added as a solution in Milli-Q water, cleaned for trace metals by running through a column with 2–3 mL of prepared Chelex-100 (BioRad) beads (Price *et al.* 1988/1989). All treatments were run in triplicate. The experiments had factorial design to test for single factor limitation and for possible iron co-limitation with coenzyme B₁₂, cobalt and zinc. The temperature was maintained at 0 ± 1 °C. The

first two experiments (WHOI 1 and 2) were performed in an environmental chamber with $150 \mu\text{mol photons m}^{-2} \text{s}^{-1}$ light, while the third experiment (WHOI 3) was performed in an on-deck incubator shielded with neutral density screen that transmitted 20% of ambient irradiance. A subset of treatment replicates were run in the environmental chamber as well. Samples for FRRF measurement were dark adapted in a cooler on ice for 30 to 40 minutes to measure maximum potential photosynthetic quantum yields.

Statistical analysis

Photorecovery kinetics of *Pseudo-nitzschia* and *P. antarctica* were analyzed by comparing slopes and intercepts of Ln:Ln regressions using general linear model (GLM) in SAS[®] (Bruin 2006) and by repeated measurements ANOVA also using SAS[®]. Comparisons between treatments in *RST1*, *RST2*, *RSC1*, *RSC2*, WHOI 1, 2 and 3 were analyzed by repeated measurements ANOVA and Least Squares Means analysis with Tukey-Kramer adjustment for multiple comparisons using SAS[®] 9.1.3 (SAS, 2003). For *RSC1* a cubic model was used to obtain a substantially better fit.

RESULTS

Photorecovery (PR) experiments

In PR1 the cultures, acclimated to $150 \mu\text{mol photons m}^{-2} \text{s}^{-1}$ light, did not show any sign of irradiance-induced stress or inhibition (Figure 2). The initial F_v/F_m value in the *P. antarctica* culture was $0.581 (\pm 0.001)$, and the average F_v/F_m over the first 45 minutes was $0.579 (\pm 0.017)$. *Pseudo-nitzschia* had a slightly lower initial F_v/F_m value (0.540 ± 0.002) which remained stable over the next hour. In PR 2, where cultures were acclimated to $300 \mu\text{mol photons m}^{-2} \text{s}^{-1}$, a mild photoinhibition in both the *P. antarctica*-dominated assemblage and the *Pseudo-nitzschia* culture was observed, with

initial F_v/F_m of 0.47 and 0.48, respectively. Their photorecovery kinetics, however, were quite different. *Pseudo-nitzschia* (Figure 3) recovered very slowly and showed only 30% photorecovery after 2 hours, whereas 30% recovery in *P. antarctica* took only 30 minutes. After 6 and 48 hours, *Pseudo-nitzschia* recovery was 50 and 99% respectively, whereas *P. antarctica* recovered 70 and 94% of the maximum quantum yield (0.65) by the 13th day. The absorption cross section (σ_{PSII}) in both cultures decreased during photorecovery, approaching about half of the initial value after two days. Photorecovery curves were significantly different ($T = -3.97$, $p = 0.0003$). PR 3 cultures were incubated in an on-deck incubator, and hence were exposed to natural light and greater irradiance than those in PR 2. The average irradiance exposure over 24 hours was $450 \mu\text{mol photons m}^{-2} \text{s}^{-1}$. The initial quantum yields for *P. antarctica* and *Pseudo-nitzschia* were 0.28 and 0.26, respectively (Figure 4). As in PR 2, *P. antarctica* recovered much faster, achieving about 48% recovery within the first hour, vs. only 10% recovery in *Pseudo-nitzschia*. Both cultures fully recovered after about 24 hours. In PR 4 the initial F_v/F_m for *P. antarctica* and *Pseudo-nitzschia* were 0.23 and 0.29, respectively. Again, *P. antarctica* recovered faster, achieving 55% recovery in the first hour vs. only 25% in *Pseudo-nitzschia* (Figure 5). Both species reached their relative maximum photosynthetic yields in ca. 8 hours, much faster than in the previous experiments. In PR 5 (Figure 6) the cultures underwent short exposures (2, 4, 6 and 8 hours) to $\sim 850 \mu\text{mol photons m}^{-2} \text{s}^{-1}$. Initial and final quantum yield in *P. antarctica* ranged from 0.37 following 2 hours exposure to 0.25 following 8 hours exposure, while those for *Pseudo-nitzschia* were 0.24 to 0.31. Photoinhibition was proportional to exposure time for *P. antarctica*, but not for *Pseudo-nitzschia*. There was a significant difference in the recovery time between species, with *P. antarctica* recovering faster than *Pseudo-nitzschia* (Figure 6). During the first photorecovery experiment of the spring cruise (PR 6), a 3-h exposure to $300 \mu\text{mol photons m}^{-2} \text{s}^{-1}$ induced limited photoinhibition in both cultures. Following the exposure *P. antarctica* displayed an F_v/F_m of 0.47, recovering to 0.52 after about five hours and to 0.55 after ca. 24 hours. *Pseudo-nitzschia* displayed

initial decrease in F_v/F_m to 0.45, increased to 0.47 after 24 h. In PR 7 and 8 (Figure 7 and 8) were the cultures were exposed for up to six hours, and once again *P. antarctica* showed faster recovery. In these experiments *P. antarctica* showed higher total theoretical recovery within one hour (30 and 11%), while in *Pseudo-nitzschia* the relative recovery was 21% following 2 hours high light exposure in PR 7 (Figure 7), and 15% following 4 hours high light exposure in PR 8 (Figure 8).

Iron and temperature (RST1)

Photosynthetic quantum yields in RST1 (Figures 9 and 10) steeply increased during the first three days following iron addition: by 34% in the low-temperature treatment and by 40% in the high-temperature treatment. The higher temperature appeared to provide an additional advantage to the iron-replete cultures, but the more rapid growth also depleted macronutrients faster, and the culture entered senescence by the fourth day. The iron-enriched, low-temperature culture maintained a relatively high photosynthetic quantum yield of ca. 0.55 for the entire experiment. Conversely, the quantum yields in the control treatment declined steadily from the experiment's onset. ANOVA analysis indicates that iron addition effects were significant, ($F=146.78$ $p<0.0001$), while temperature and the interaction between temperature and iron were not (Appendix 1; Tables 1 and 2). As expected, trends were observed in the absorption cross section values, where iron remains the first discriminatory variable, with temperature exerting a minor effect. In conjunction with RST1 (performed with a mid-summer *P. antarctica*-dominated assemblage under 20% of ambient light; $180 \mu\text{mol quanta m}^{-2}\text{s}^{-1}$), the marked iron limitation is evident.

Light and temperature (RST2)

In all the experiments, the cultures quickly depleted the available iron, as evidenced by the decrease in quantum yields. The fastest decline was observed in the high light/high temperature

treatment, followed by the low light/high temperature, high light/low temperature, and low light/high temperature, suggesting that temperature is a primary factor for the rate of iron utilization (Figure 11). The absorption cross section measurements do not display as clear of a trend between treatments (Figure 12). Both temperature ($F=29.37$ $p<0.0001$) and light ($F=16.15$ $p=0.0001$) had significant effects on the F_v/F_m and the σ_{PSII} (Appendix 1; Tables 3 and 4).

Iron, light and CO₂ (RSC1 & RSC2)

In both RSC1 (Figures 13 and 14) and RSC2 (Figures 15 and 16), quantum yields were initially low (0.3 in RSC1 and 0.4 in RSC2), recovering to ca. 0.6 within 6 days, and declining thereafter. High light exposure accelerated the decrease in quantum yields following the first week. Nevertheless, iron addition appeared to promote higher photosynthetic quantum yields relative to the controls. In RSC1 the light treatment had a significant effect on both F_v/F_m ($F=147.7$ $p<0.0001$) and σ_{PSII} ($F=15.73$ $p<0.0001$) (Appendix 1; Tables 5 and 6), while in RSC2 both iron and light treatments were significantly different from the controls (Appendix 1; Tables 7 and 8). CO₂ concentration did not affect the quantum yield or absorption cross section.

Fe, Zn, Co, and vitamin B₁₂ (WHOI 1, 2 and 3)

In all three experiments, *P. antarctica* dominated through the entire incubation. Iron limitation was clear, given the higher quantum yields measured in all iron-addition treatments. Utilization of nutrients in WHOI 1 and 2 did not affect Chl *a* in the iron treatments (M. Saito personal communication). In these experiments, F_v/F_m started at 0.44 and steadily declined in all treatments, with the exception of iron addition treatments (Figures 17 and 19). In WHOI 1 and 3 there was a higher Chl *a* accumulation relative to the nutrients removed. Similarly, in all three experiments the presence of iron induced responses that were consistently different from the controls and from the

treatments with Zn, Co, B₁₂ alone. A significant difference between iron treatments and the rest was systematically observed for F_v/F_m and σ_{PSII} (Appendix 1; Tables 9 – 14). The results were confirmed by LSM pair-wise comparison.

DISCUSSION

When organisms are acclimated to specific (and stable) conditions, they optimize their photophysiology so as to most efficiently utilize the limiting nutrient or in situ energy. Cells can adjust to high irradiances (e.g., PR 1); they can also maintain high photosynthetic capability over long periods of low light or darkness (PR 2). The remarkable ability of retaining photosynthetic competence during extended exposure to darkness as seen in (PR 2) has been reported for *P. antarctica* by Tang *et al.* (2008) who compared photosynthetic quantum yields of cultures kept in the dark and in the light over a two-month period in which they observed a steady exponential decline of F_v/F_m ; nonetheless, the cultures were still photosynthetically viable at the end of the experiment and systematically recovered when re-exposed to light. This capacity helps to shed some understanding on how Antarctic phytoplankton is capable of surviving the long austral winter with complete darkness and often being encased in ice (or freezing water) prior to being released in the spring.

A range of mechanisms of photoacclimation and photoadaptation operate in photosynthesis, each with different response times. For example, there are rapid (seconds to minutes) responses that do not require the synthesis of new biomolecules. These responses involve changes in the efficiency of light utilization through variations in functional absorption cross section and modulation of the electron transfer rate, as shown by the reciprocal trends of F_v/F_m and σ_{PSII} . When changes in the light regime persist, photoacclimation-type responses occur within ca. 60 minutes, and involve synthesis of proteins and pigments, and/or rearrangements of photosystem components. On longer time scales

(days to weeks), cells and populations adapt by changing their stoichiometric and pigment contents. All photorecovery experiments demonstrated the multi-kinetic photoacclimation; moreover, the consistently faster recovery in *P. antarctica* compared to *Pseudo-nitzschia* suggests much greater plasticity of photoadaptation mechanisms in this organism.

All experiments showed biphasic recovery kinetics that can be explained by cellular acclimation followed by population responses and adaptation. In PR 2, 3 and 4, diatoms achieved the theoretical maximum photosynthetic quantum yield of 0.65, while *Phaeocystis* barely matched this response in PR 2, while reaching a maximum of 0.61 in PR3 and 4. In either case, the cultures appeared to fully recover as demonstrated by extremely high photosynthetic quantum yields. PR 5 confirmed the faster photorecovery kinetics of *P. antarctica* when compared to *Pseudo-nitzschia*. No significant effect of the exposure time was observed within the same experiment, indicating that the photoacclimation responses are controlled mostly by the amplitude of the stimulus, and not by the dosage of light. The relatively short exposure to high irradiance did not significantly damage the cultures, as they rapidly regained most of their photosynthetic capability, demonstrating once again the high level of adaptation to extreme light fluctuations in the absence of iron and nutrient limitation and UV damaging radiation. The cells can adjust the absorption cross section of PSII by either undergoing state transitions, or undergoing non-photochemical quenching. On longer time scales cells tend to acclimate to a particular irradiance regime by changing their chlorophyll content (Richardson *et al.* 1983). Photoacclimation is also manifested by changes in pigment composition. For example, a significant shift at low irradiances from Chl *a*, 19-hexanoyloxyfucoxanthin and Chl *c_x* to diadinoxanthin, β -carotene, and diatoxanthin has been previously observed in *P. antarctica* (Moisan and Mitchell 1999). Extensive studies on Antarctic phytoplankton photobiology in the Ross Sea (SooHoo *et al.* 1987, Moisan and Mitchell 1999, van Hilst and Smith 2002, Moisan *et al.* 2006, van Leeuwe and Stefels 2007) indicate multiple responses by *P. antarctica* to light. For example, to maintain optimal

assimilation rates, *P. antarctica* increases its absorption cross section under low light conditions characteristic of the spring polynya. At the same time *P. antarctica* displays better tolerance than diatoms to high irradiance levels due to fast xanthophyll cycling, which may provide an advantage in fluctuating light environments (Moisan *et al.* 1998).

Another photoacclimation mechanism observed in *P. antarctica* involves increasing colonial size and changing cell concentration to compensate for the increased irradiance during the spring and summer, enhancing its “sun-screen factor” (Lieselotte and Dale 1997). Such self-shading and absorption cross section control may be less effective against rapid light changes, but may help to explain the frequent and persistent *P. antarctica* blooms in the Ross Sea polynya. *P. antarctica* also has a chlorophyll packaging ability (Moisan and Mitchell 1999), and it can modify its quantum yield efficiency over fast time scales to respond to shorter term light variability. *P. antarctica* has higher iron requirements when compared with diatoms (Coale *et al.* 2003), especially at low irradiance levels (Sedwick *et al.* 2007). Iron-limited *P. antarctica* cells remain in a permanent state of high energy quenching that prevents photoinhibition during exposure to high irradiance; it also maintains a high growth potential (van Leeuwe and Stefels 2007). *P. antarctica* can also significantly increase its diatoxanthin/diadinoxanthin ratio in response to high irradiance (van Leeuwe and Stefels 1998). It is therefore possible that the highly diverse and flexible photoacclimation mechanisms in *P. antarctica* are in large part responsible for its success in the Ross Sea polynya. In the spring it can efficiently utilize the available iron in the low-irradiance regime (Sedwick *et al.* 2000), yet can still photosynthesize at close to optimum rates in the summer, when iron becomes depleted, but the irradiance is high.

All of the WHOI experiments indicate the presence of iron limitation, but little or no evidence for other micronutrient or vitamin B₁₂ limitation, as previously suggested (Bertrand *et al.* 2007). All experiments were performed on acclimated natural assemblages that had already experienced

relatively low iron concentrations prior to collection. The significant and consistent reduction in σ_{PSII} in all iron treatments again demonstrates the plasticity and photoadaptability of *P. antarctica*. Such traits are critical in an environment where light fluctuations occur on different time scales and with different frequencies, including the regular 24 hours solar cycle, and stochastic light fluctuations due to cloudiness, surface wave action, ice, and continuous vertical mixing.

The Ross Sea is experiencing increases in sea ice coverage and lower air temperatures. These phenomena are mainly due to masking of the effects of greenhouse gas impacts by a stronger Southern Annular Mode (SAM) and the opposite impacts of stratospheric ozone depletion (Shindell and Schmidt 2004). The ozone layer is predicted to re-establish itself over Antarctica in the future, which will weaken and or reverse the SAM index, subjecting the Ross Sea to higher temperatures. Indeed, there can be little doubt that by the end of the 21st century the Ross Sea will be experiencing substantially warmer temperatures along with the rest of the Antarctic, and will have greatly reduced ice concentrations during summer. The investigations of the combined effects of temperature, iron concentrations, and irradiance should improve the predictions of Ross Sea responses to anthropogenic change. Temperature largely controls the enzymatic pathways of carbon assimilation in photosynthesis, but it also affects the electron transport system via the thermal effects on membrane fluidity. Such an effect was detectable in experiments at fixed light regimes and on quasi-acclimated cultures, allowing better discrimination of the effects of temperature.

Kinetic differences in photorecovery between *P. antarctica* and *Pseudo-nitzschia* suggest specific differences in their ecological strategies and niches. These traits most likely reflect evolutionary adaptation to the extreme environmental conditions of the polynya and polar environments. My results indicate how Ross Sea phytoplankton quantum yields and primary productivity are influenced by changes in environmental variables such as increased temperature and CO₂. On the other hand, increased temperature will also lead to increased stratification, due to both

increased meltwater inputs into the polynya and increased heat flux, further modifying the irradiance regime in the polynya. Alternatively it has been noted for the Western Antarctic Peninsula (WAP) that ice disappearance can lead to deeper mixing due to stronger winds and differently promote higher primary production (Montes-Hugo *et al.* 2009). All the phytoplankton benefited from added iron, indicating strong and widespread iron limitation within the polynya surface waters.

The enhanced photophysiological plasticity and better photoprotective capability in *P. antarctica* (especially from UVR), may be due to its capability to produce mycosporine-like-amino acids (MAAs) (Lieselotte and Dale 1997, Moisan and Mitchell 2001) at concentrations far exceeding those in diatoms. Also, MAA production in *P. antarctica* is triggered by both UVA and UVB, while diatoms respond mainly to UVA. In temperate regions, diatoms such as *Pseudo-nitzschia* are selectively photoinhibited by UVB, while harvesting UVA (Mengelt and Prezelin 2005), but similar responses have not been observed in high-latitude species. This difference in UVR-protection mechanisms and acclimation strategies is critical to better understanding the factors controlling blooms and production in the Ross Sea, given the potentially high levels of UVR in spring.

Diatoms and *P. antarctica* contribute differently to carbon cycling and export (Gowing *et al.* 2001). Given the magnitude of Ross Sea's primary productivity, it is pivotal to understand the differences in the photosynthetic mechanisms of the major taxa to better infer the fate of the organic matter and to improve representations in numerical models. It is forecasted that polar waters will become increasingly stratified (Sarmiento and Le Quéré 1996, Sarmiento *et al.* 2004) due to global climate change. Therefore, a shift from blooms dominated by *P. antarctica* in the Ross Sea to those dominated by diatoms has been hypothesized, with a consequent reduction in the carbon export (Arrigo *et al.* 1999). However, this prediction does not account for the potentially reduced in situ irradiance environment or altered iron fluxes. Results from the studies presented here suggest that photophysiological differences between diatoms and *P. antarctica* are strongly affected by light

conditions and iron concentrations, and these are much more important determinants of the relative abundances and species succession in the polynya. Numerical models of primary production in the Ross Sea should therefore be modified to account for the different photophysiological responses of these taxa and their respective controls by light and iron to generate more accurate predictions of future environments and ecosystems.

Table 1 Synthesis of photorecovery experiments results. Initial (start) and final (end) photosynthetic quantum yield for each experiment, In:ln fit correlation coefficients (r^2), intercept (a) and slope (b), T value (t) and p-value (p) from comparison of GLM slopes.

Experiment ID	Culture	F_v/F_m		Fit				
		Start	End	r^2	a	b	t	p
PR1	<i>P. antarctica</i> CCMP 1374	0.58	0.58	No significant photoinhibition				
	<i>Pseudo-nitzschia</i> sp. CCMP 1445	0.54	0.58					
PR2	<i>P. antarctica</i> -dominated natural assemblage	0.47	0.65	0.822	0.030	-0.587	-3.9700	0.0003
	<i>Pseudo-nitzschia</i> sp. CCMP 1445	0.48	0.65	0.909	0.049	-0.663		
PR3	<i>P. antarctica</i> -dominated natural assemblage	0.28	0.61	0.919	0.118	-0.911	-1.7000	0.0965
	<i>Pseudo-nitzschia</i> sp. CCMP 1445	0.26	0.65	0.929	0.213	-1.190		
PR4	<i>P. antarctica</i> -dominated natural assemblage	0.23	0.61	0.941	0.175	-0.819	-1.0400	0.3092
	<i>Pseudo-nitzschia</i> sp. CCMP 1445	0.29	0.65	0.971	0.199	-0.934		
PR5	<i>P. antarctica</i> -dominated natural assemblage	0.38	0.53	0.732	0.051	-0.813		
		0.35	0.54	0.778	0.067	-0.904		
		0.27	0.51	0.148	0.077	-1.014		
		0.25	0.47	0.818	0.202	-1.464		
	<i>Pseudo-nitzschia</i> sp. CCMP 1445	0.24	0.58	0.997	0.186	-1.646		
		0.23	0.54	0.886	0.205	-1.764		
		0.24	0.55	0.996	0.184	-1.610		
		0.31	0.50	0.931	0.141	-1.394		
PR6	<i>P. antarctica</i> CCMP 1374	0.47	0.55	No significant photoinhibition				
	<i>Pseudo-nitzschia</i> sp. CCMP 1445	0.45	0.48					
PR7	<i>P. antarctica</i> CCMP 1374	0.30	0.48	0.971	0.093	-1.258		
	<i>Pseudo-nitzschia</i> sp. CCMP 1445	0.30	0.38	0.902	0.047	-1.243		
PR8	<i>P. antarctica</i> CCMP 1374	0.29	0.46	0.862	0.111	-1.345		
	<i>Pseudo-nitzschia</i> sp. CCMP 1445	0.32	0.38	0.683	0.047	-1.200		

Table 2. Synthesis of other experimental conditions used during CORSACS I and II

Date		Length	Cruise	Experiment	Culture	Incubation	Irradiance		Temp.		CO2		Other variables
Start	End	Days	ID	ID		location	$\mu\text{mol photons m}^{-2} \text{s}^{-1}$		°C		ppm		
12/27/2005	1/14/2006	19	NBP0601	RSC1	P.a. Natural assemblage	On deck	10% E ₀	40% E ₀	surface w.		360	750	Fe ~0.2 / > 1nM
1/15/2006	1/21/2006	7		RST1	P.a. Natural assemblage	On deck	18% E ₀		0	4	Ambient		Fe ~0.15 / > 1nM
11/16/2006	11/23/2006	9		RST2	Natural assemblage	Van	50	320	0	4	Ambient		-
11/24/2006	12/2/2006	16	NBP0608	RSC2	Natural assemblage	Van	77	365	0		380	750	Fe ~0.2 / > 1nM
11/16/2006	11/24/2006	8		WHO11	P.a. Natural assemblage	Van	150		± 1		Ambient		Fe, Co, Zn, B12
11/22/2006	11/29/2006	7		WHO12	P.a. Natural assemblage	Van	150		± 1		Ambient		Fe, Co, Zn, B12
12/2/2006	12/9/2006	7		WHO13	P.a. Natural assemblage	On deck	20 % E ₀		surface w. (± 1)		Ambient		Fe, Co, Zn, B12

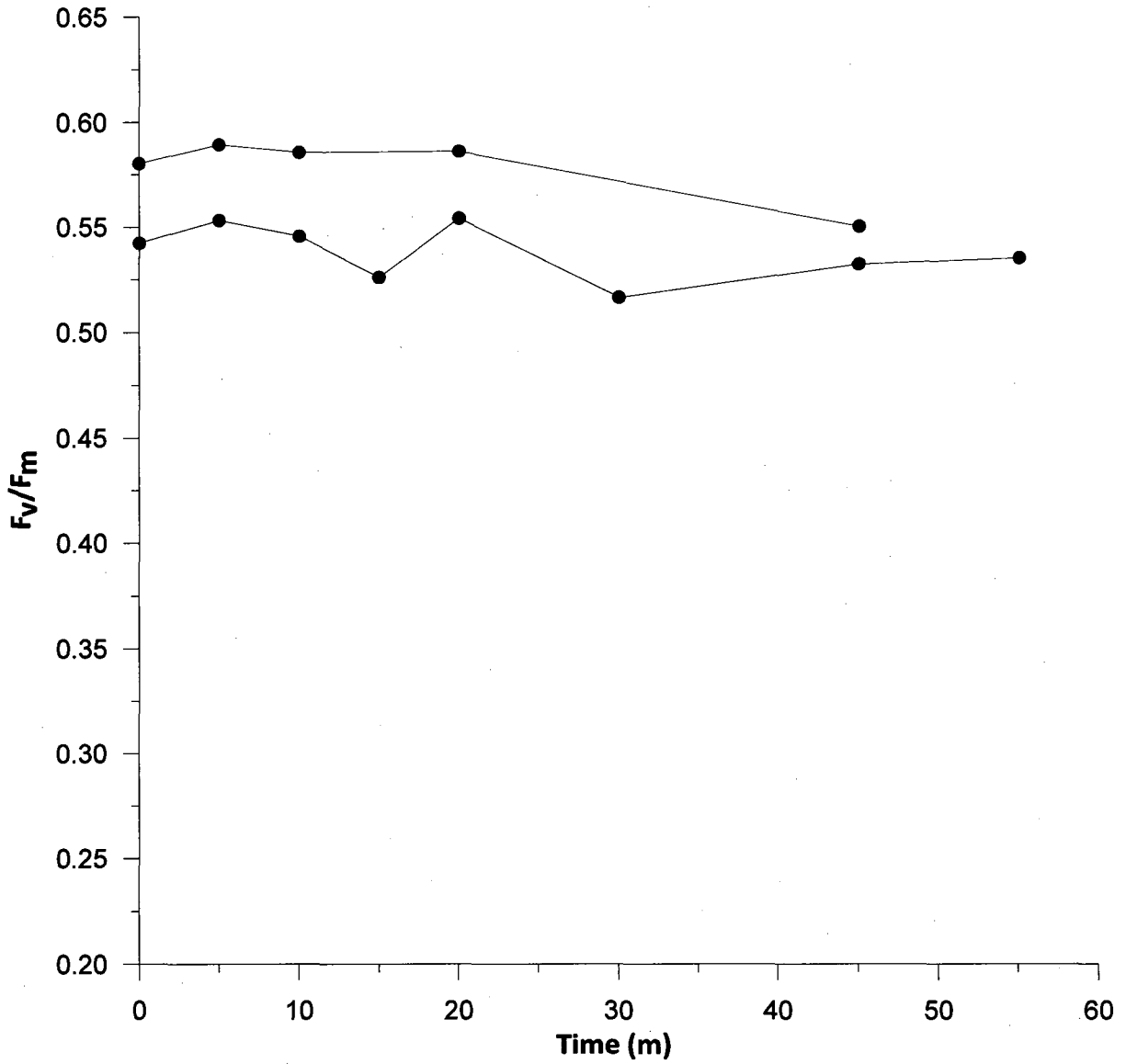


Figure 2. Potential photochemical efficiency of PSII vs. time for photorecovery experiment 1 with *P. antarctica* (●) and *Pseudo-nitzschia* (●) preconditioned at $150 \mu\text{mol photons m}^{-2} \text{s}^{-1}$. No significant photoinhibition was detected.

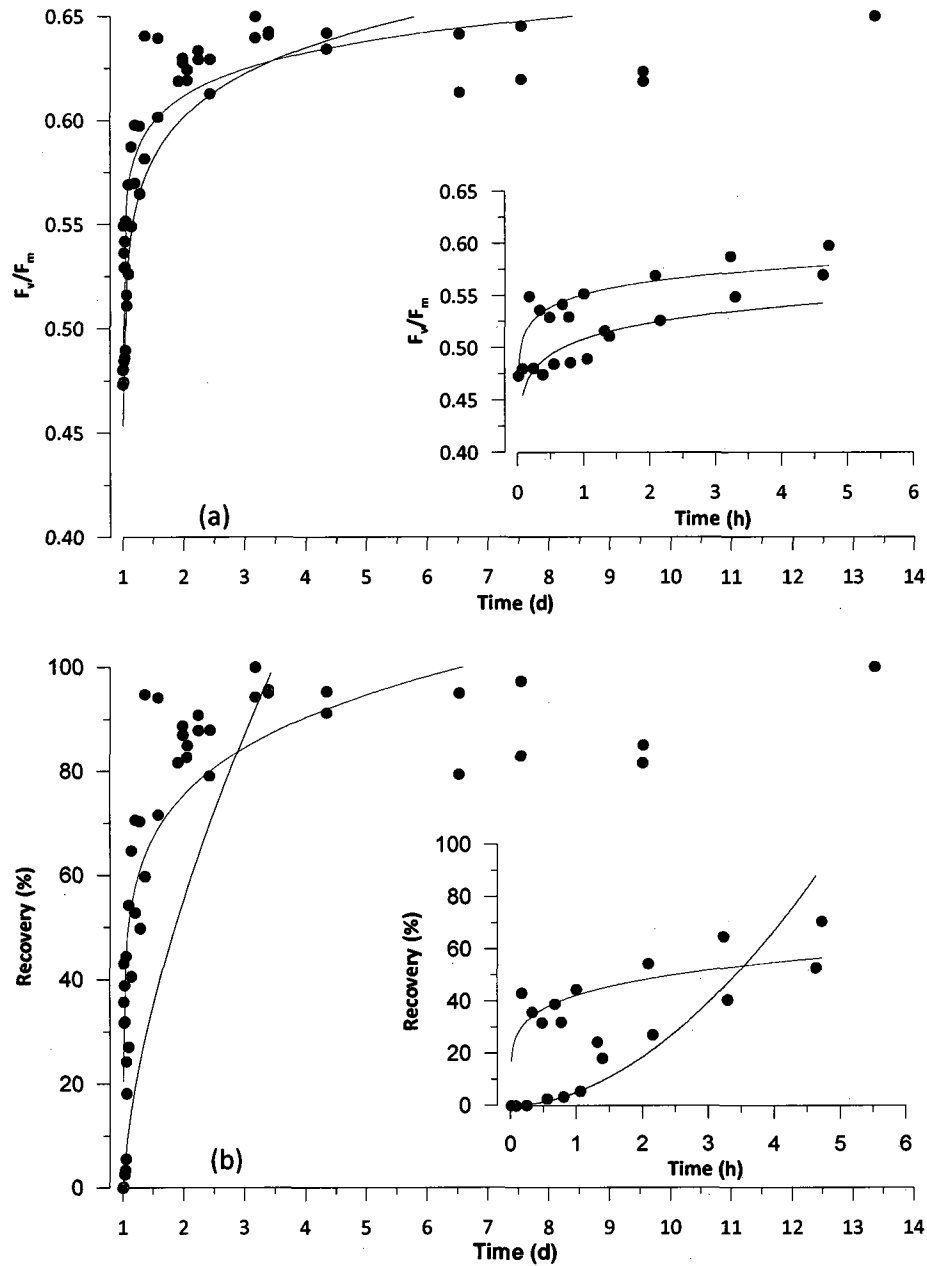


Figure 3. Potential photochemical efficiency of PSII vs. time (a) and percentage recovery of F_v/F_m over time (b) for 13-h photorecovery experiment 2; *P. antarctica* dominated natural assemblage (●) and *Pseudo-nitzschia* (○) preconditioned at $300 \mu\text{mol photons m}^{-2} \text{s}^{-1}$ for 48 h. Solid lines are Ln:Ln fit regression. *P. antarctica* reached 70% of total recovery in the first 5 h and showed faster photorecovery than *Pseudo-nitzschia*. Nearly to full recovery was achieved after 3 d and maintained for the 13 d of the experiment.

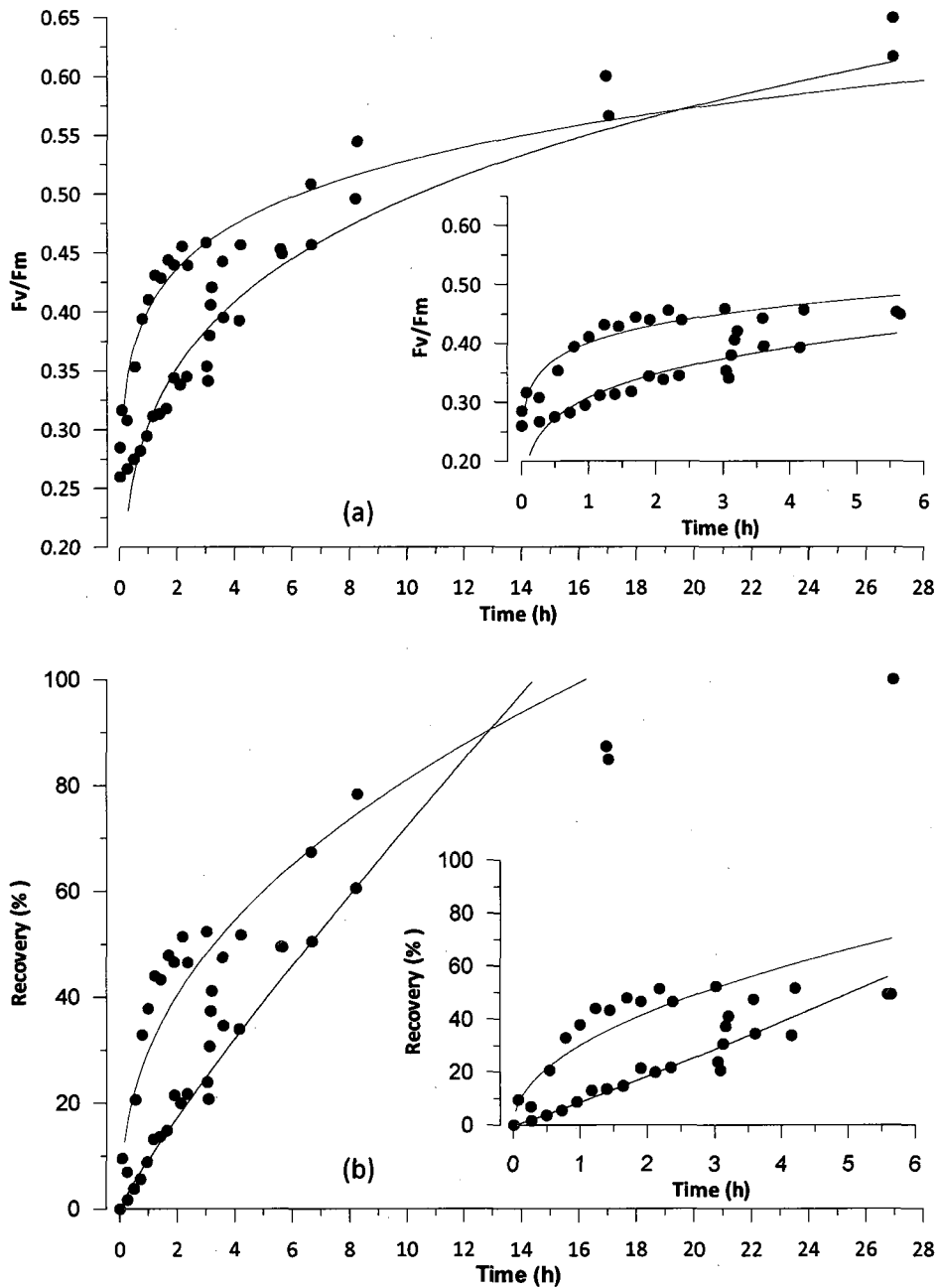


Figure 4. Potential photochemical efficiency of PSII vs. time (a) and percent recovery of F_v/F_m over time (b) for 28-h photorecovery experiment #3; *P. antarctica* dominated natural assemblage (●) and *Pseudo-nitzschia* (●) preconditioned at 50% E_0 (ca. 400 $\mu\text{mol photons m}^{-2} \text{s}^{-1}$) for 48 h. Solid lines are Ln:Ln fit regression. *P. antarctica* consistently recovered faster than *Pseudo-nitzschia* over the first 6 hours and reached full recovery by the 28th hour.

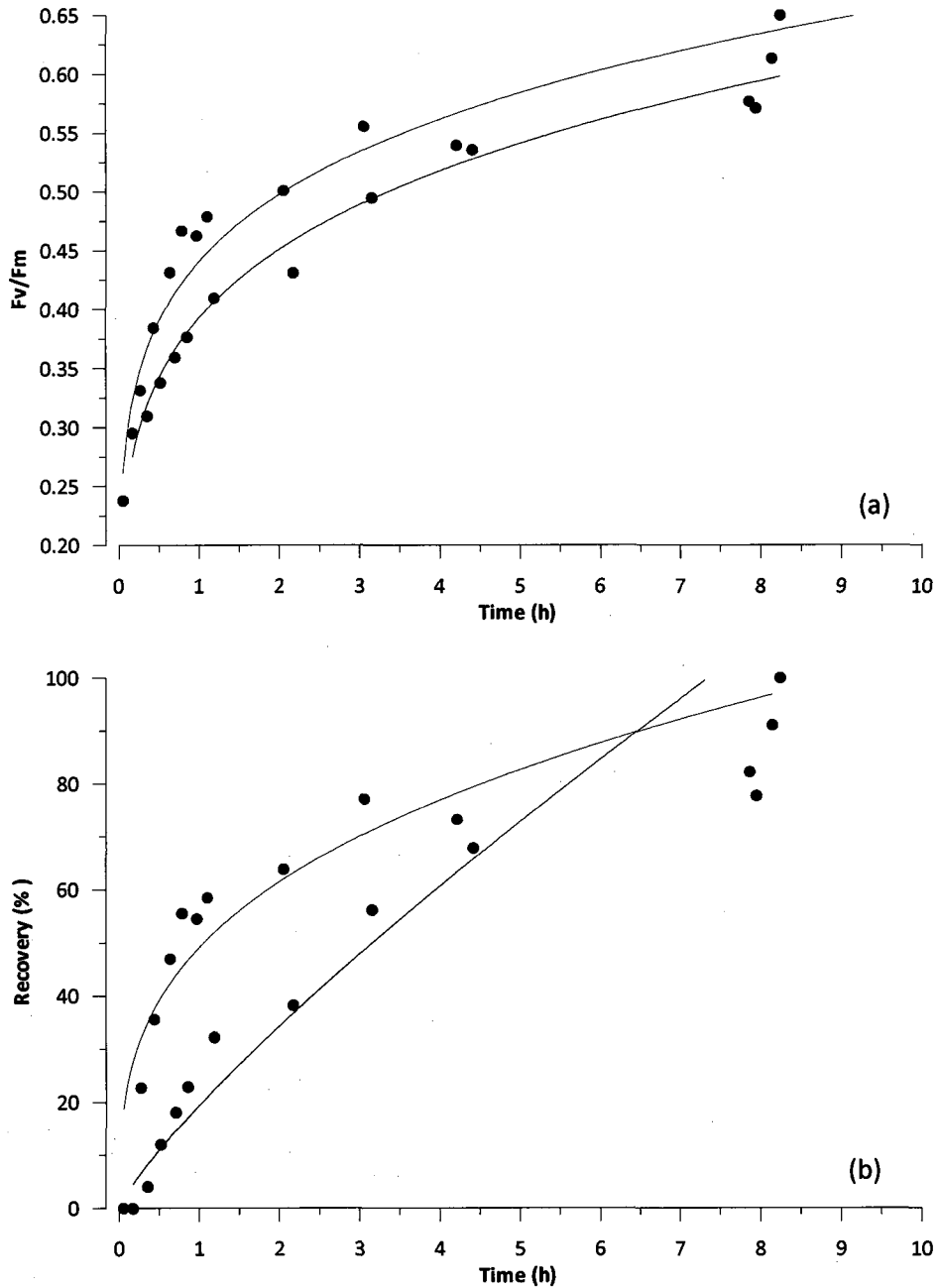


Figure 5. Potential photochemical efficiency of PSII vs. time (a) and percentage recovery of F_v/F_m over time (b) for 10-h photorecovery experiment 4; *P. antarctica* dominated natural assemblage (●) and *Pseudo-nitzschia* (●) preconditioned at 50% E_0 (ca. $400 \mu\text{mol photons m}^{-2} \text{s}^{-1}$) for 48 h. Solid lines are Ln:Ln fit regression. *P. antarctica* consistently recovered faster than *Pseudo-nitzschia* over the first 5 h, reaching ca. 80% of the initial value.

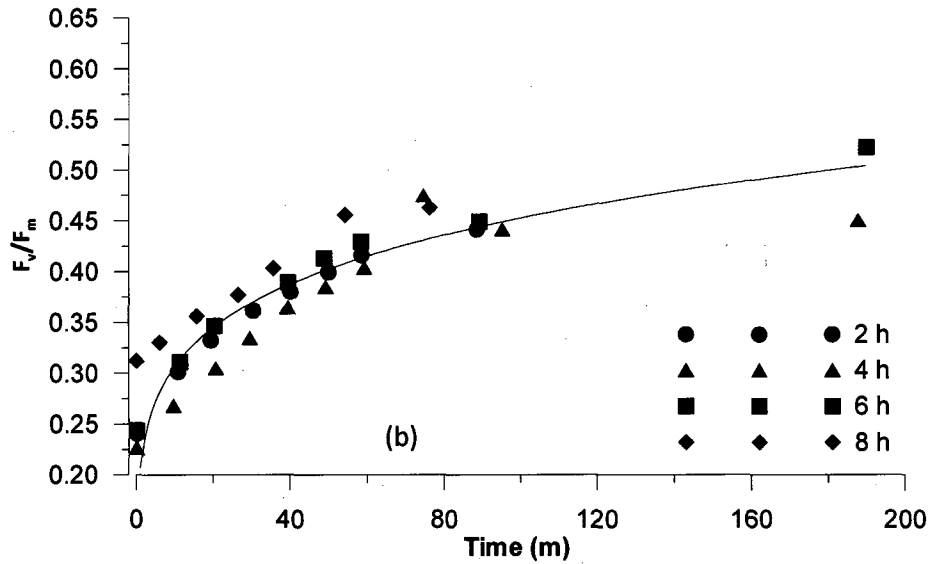
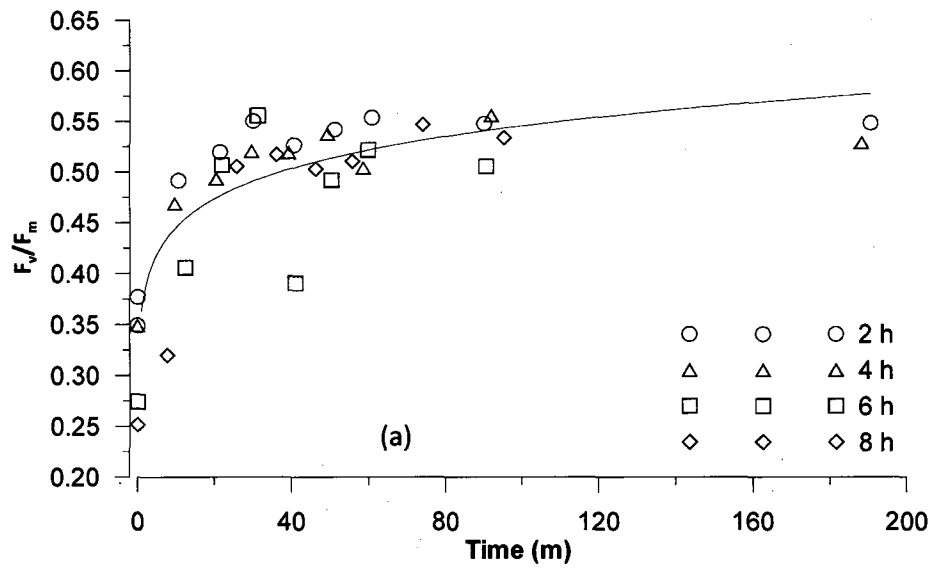


Figure 6. Potential photochemical efficiency of PSII vs. time for *P. antarctica* dominated natural assemblage (a) and *Pseudo-nitzschia* (b) for photorecovery experiment # 5, preconditioned at 850 $\mu\text{mol photons m}^{-2} \text{s}^{-1}$ for 2 (circles), 4 (triangles), 6 (squares), and 8 h (diamonds). Solid lines are Ln:Ln fit regression for pooled data. *P. antarctica* recovered faster than *Pseudo-nitzschia*, and there was no significant difference between exposure times.

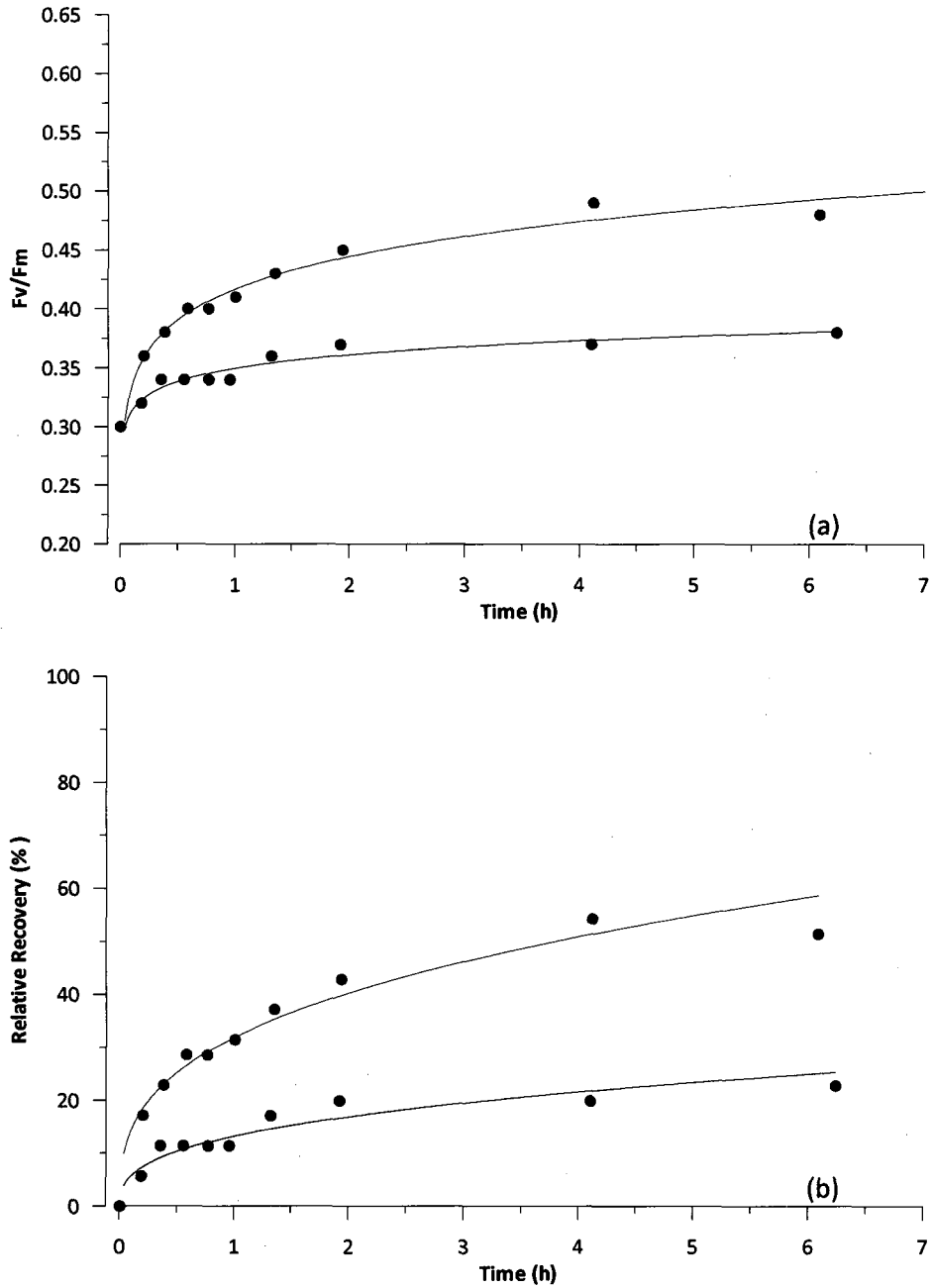


Figure 7. Potential photochemical efficiency of PSII vs. time (a) and percentage recovery of F_v/F_m over time (b) for 6-h photorecovery experiment 7; *P. antarctica* (●) and *Pseudo-nitzschia* (●) preconditioned 2 h at $600 \mu\text{mol photons m}^{-2} \text{s}^{-1}$. Solid lines are Ln:Ln fit regression. *P. antarctica* exhibited slower overall recovery compared to previous experiments, but recovered ca. 40% in the first 6 h vs. only 20% in the diatom culture.

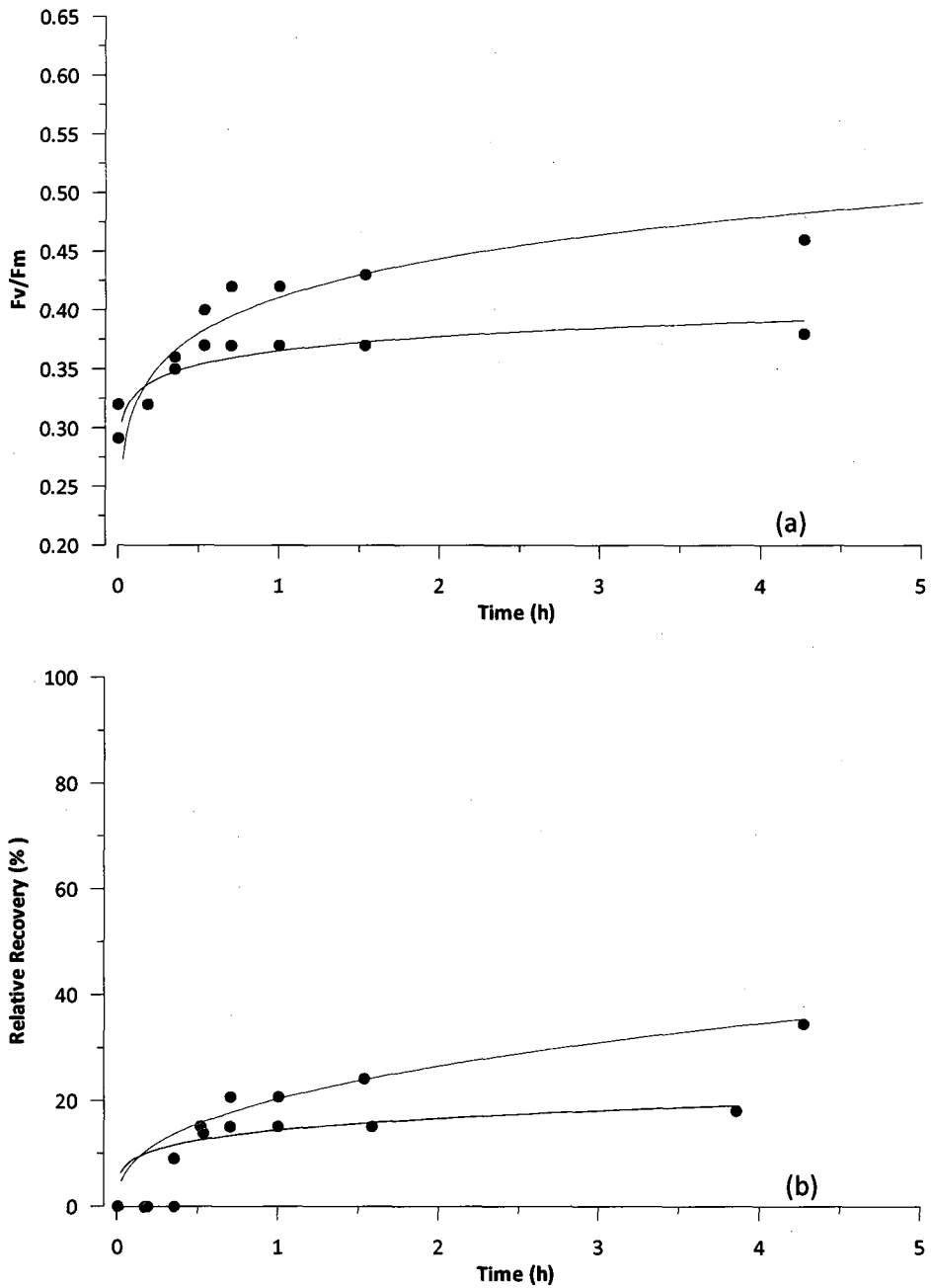


Figure 8. Potential photochemical efficiency of PSII vs. time (a) and percent recovery of F_v/F_m over time (b) for 4-h photorecovery experiment #8; *P. antarctica* (●) and *Pseudo-nitzschia* (○) preconditioned 4 h at $600 \mu\text{mol photons m}^{-2} \text{s}^{-1}$. Solid lines are Ln:Ln fit regression. The 2-h difference compared to PR #7 resulted in minimal reduction in initial and final fluorescence quantum yields, with *P. antarctica* always recovering faster than *Pseudo-nitzschia*.

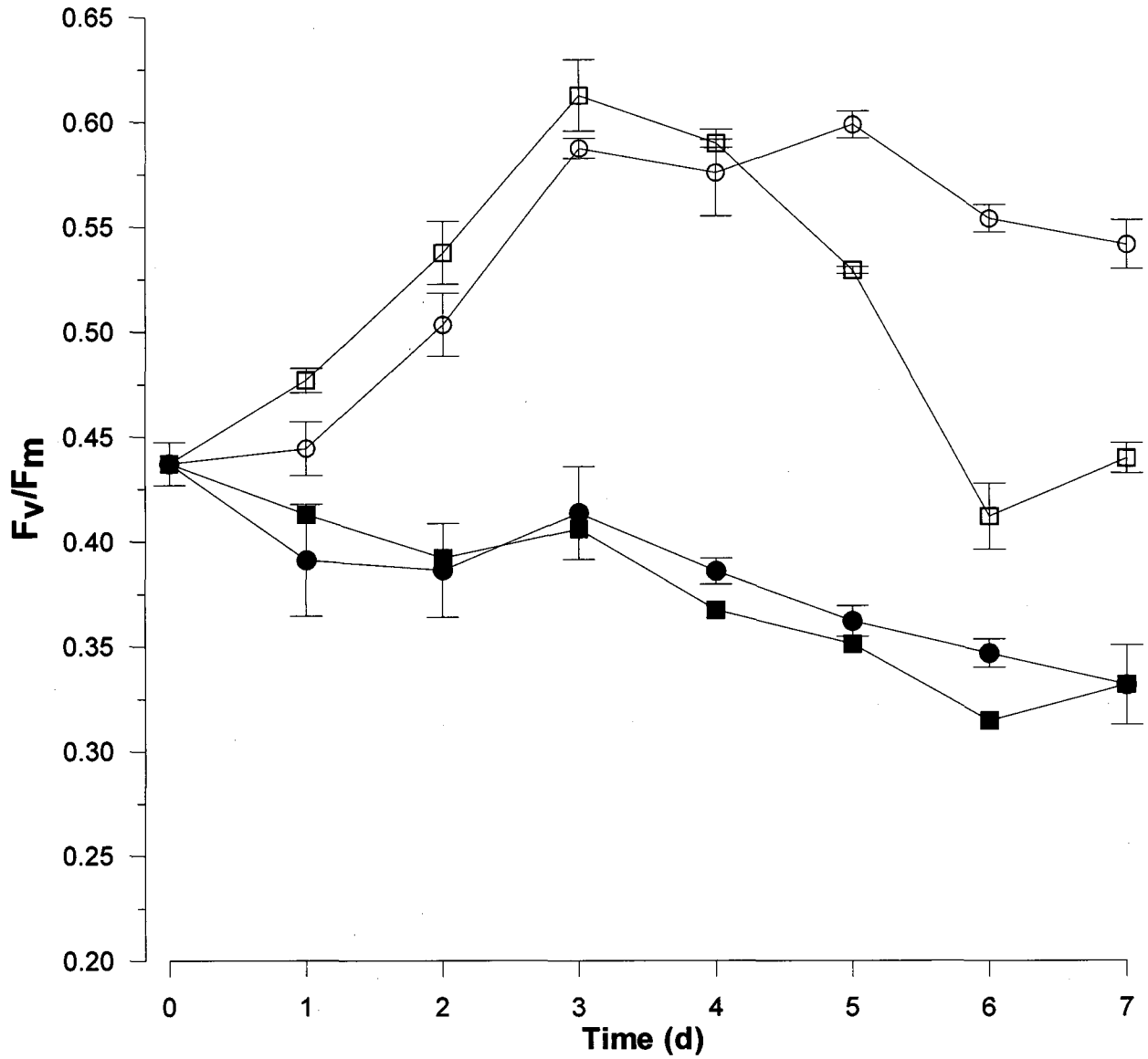


Figure 9. RST1 experiment potential photochemical efficiency of PSII vs. time. High temperature + iron (□); Low temperature + iron (○); High temperature (■); Low temperature (●). Iron significantly increased the photochemical quantum yield relative to the control treatments, while temperature had a positive effect only on the first 3-4 d.

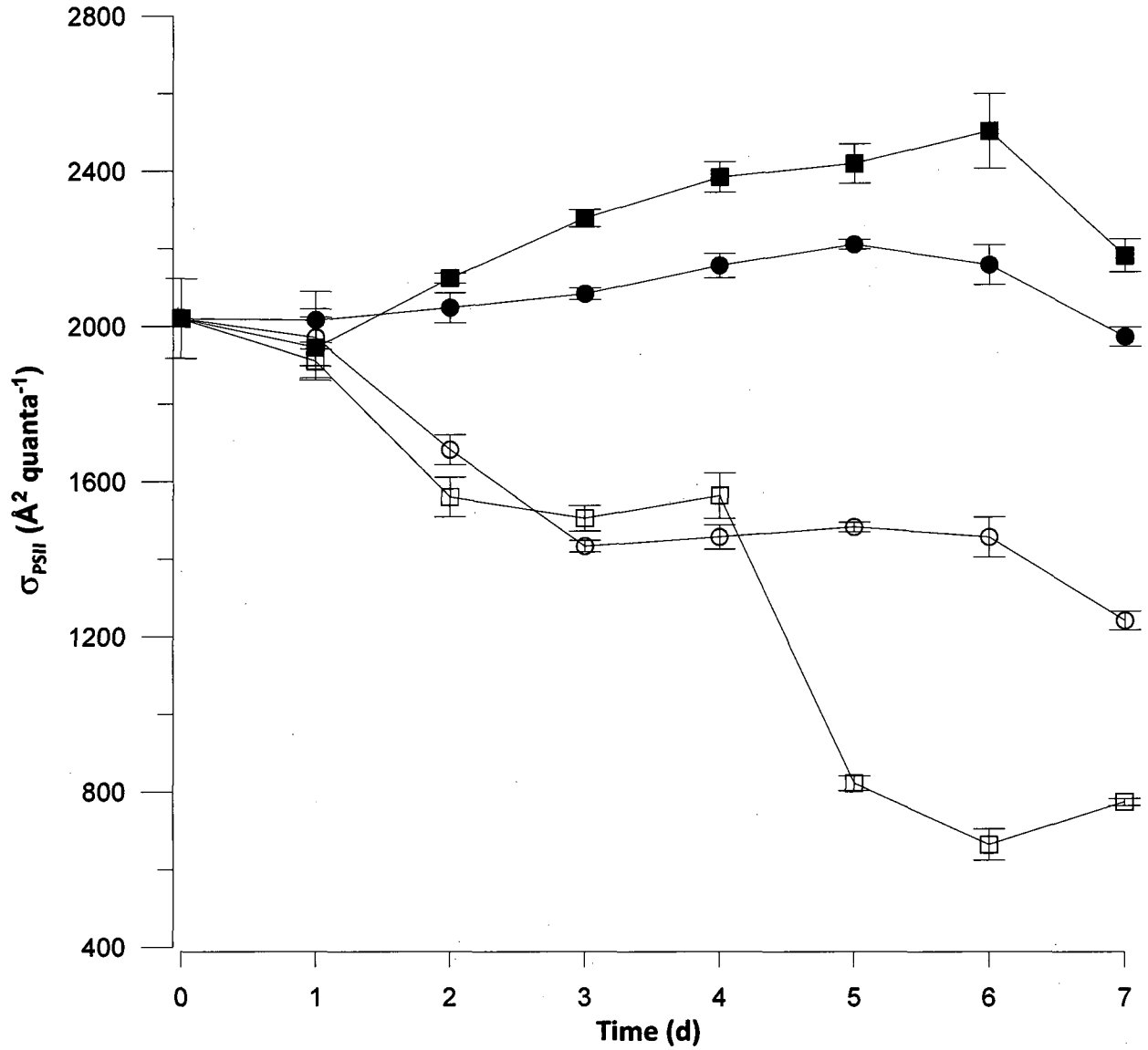


Figure 10. RST1 experiment absorption cross section (σ_{PSII}) vs. time. Low temperature + iron (\circ); High temperature + iron (\square); Low temperature (\bullet); High temperature (\blacksquare). In the iron control treatments σ_{PSII} stayed constant through the 7-d experiment, while in the iron treatment the higher efficiency was achieved with a smaller absorption cross section due to more efficient electron transport through PSII.

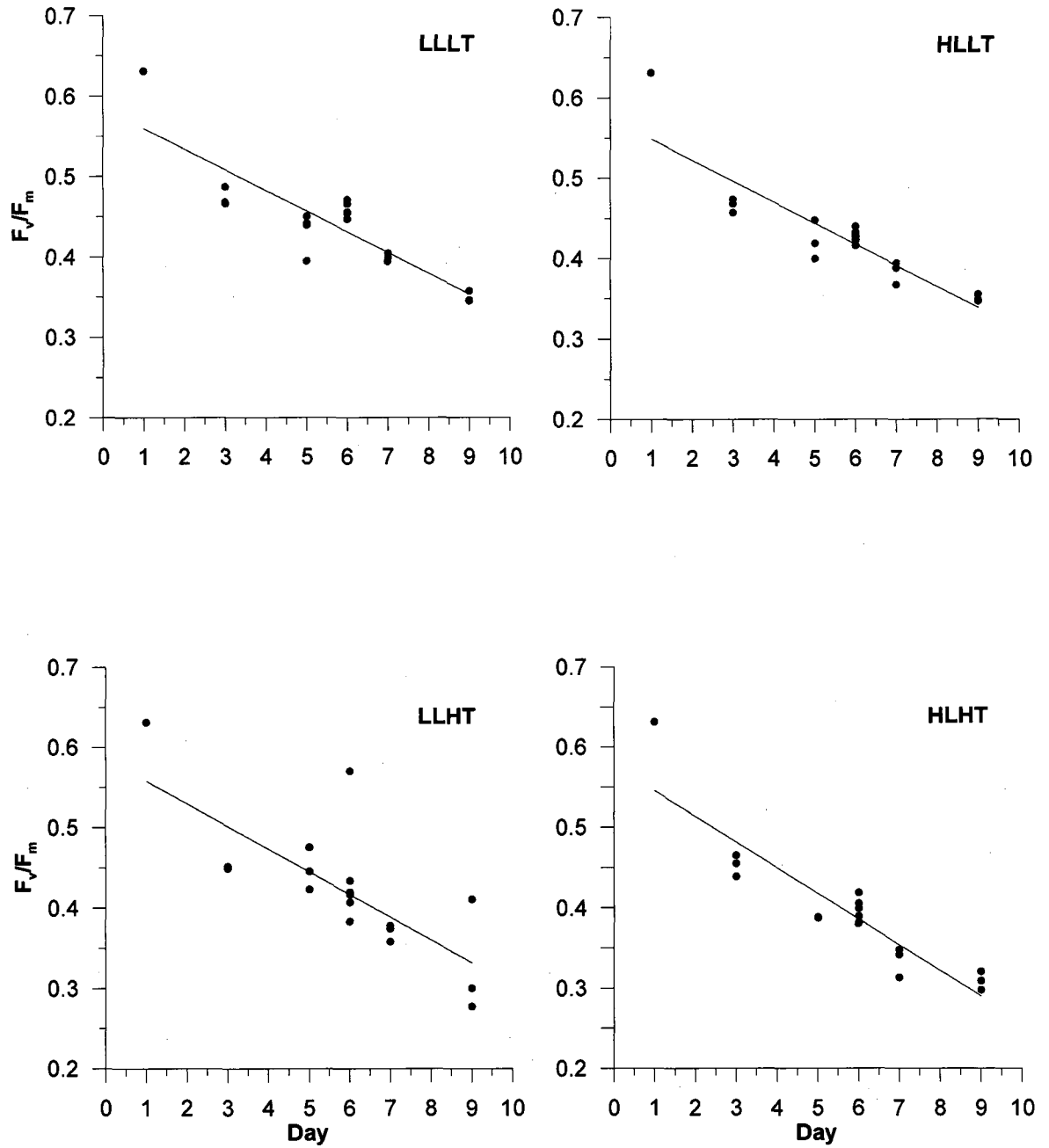


Figure 11. RST2 potential photochemical efficiency of PSII vs. time. Low light (LL, $77 \mu\text{mol photons m}^{-2} \text{s}^{-1}$); high light (HL, $365 \mu\text{mol photons m}^{-2} \text{s}^{-1}$); low temperature (LT, 0°C); high temperature (HT, 4°C). Due to iron limitation photochemical quantum yield steadily declined in all treatments. Rates of F_v/F_m decline were statistically significant for temperature and light, but with no significant interaction. Higher light and temperature resulted in a steeper decrease of potential photochemical efficiency of PSII.

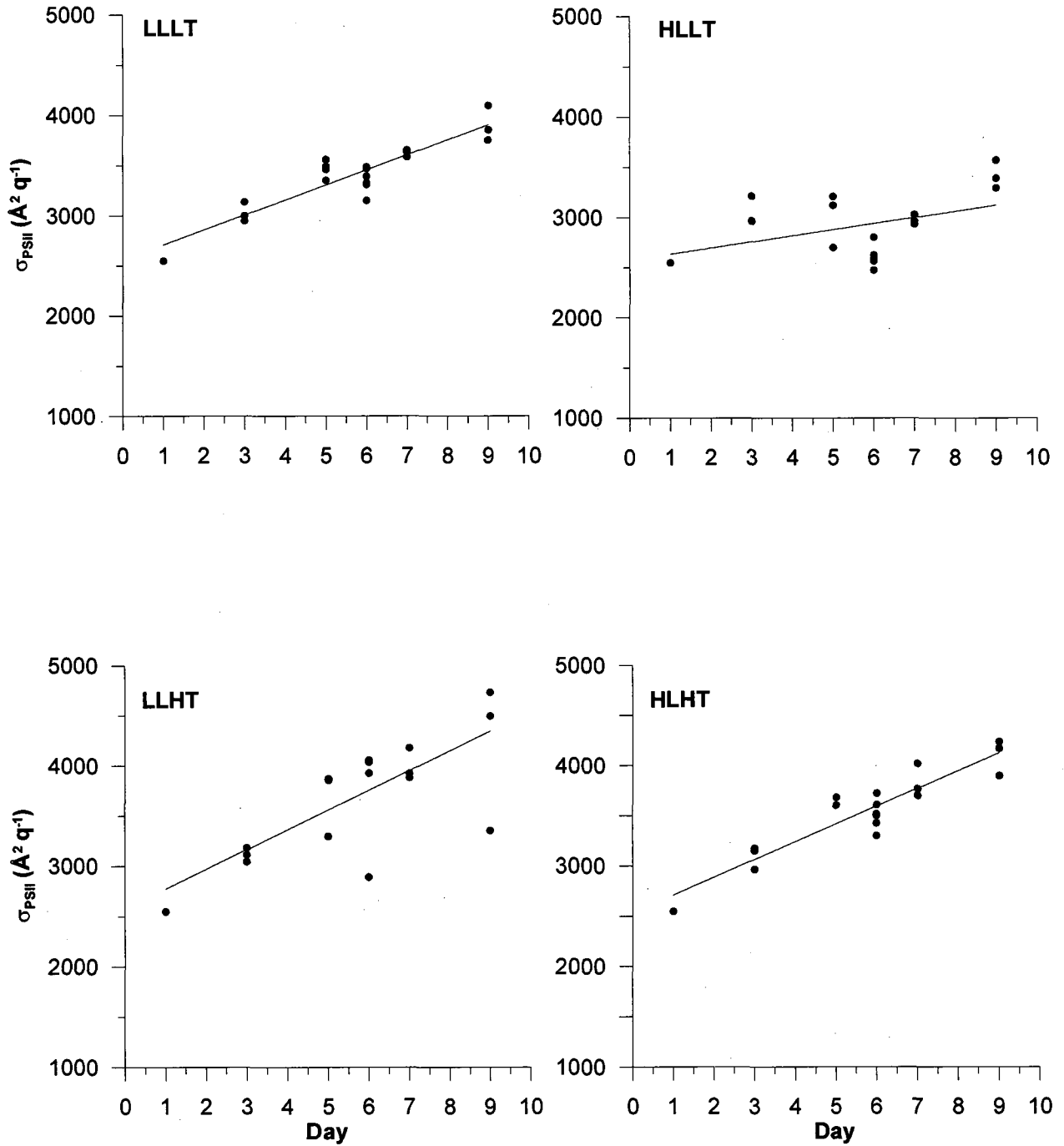


Figure 12. RST2 experiment absorption cross section (σ_{PSII}) vs. time. Low light (LL, $77 \mu\text{mol photons m}^{-2} \text{s}^{-1}$); high light (HL, $365 \mu\text{mol photons m}^{-2} \text{s}^{-1}$); low temperature (LT, 0°C); high temperature (HT, 4°C). σ_{PSII} was affected by both temperature and light but there was no detectable interaction effect. Absorption cross section correlated positively with both temperature and light.

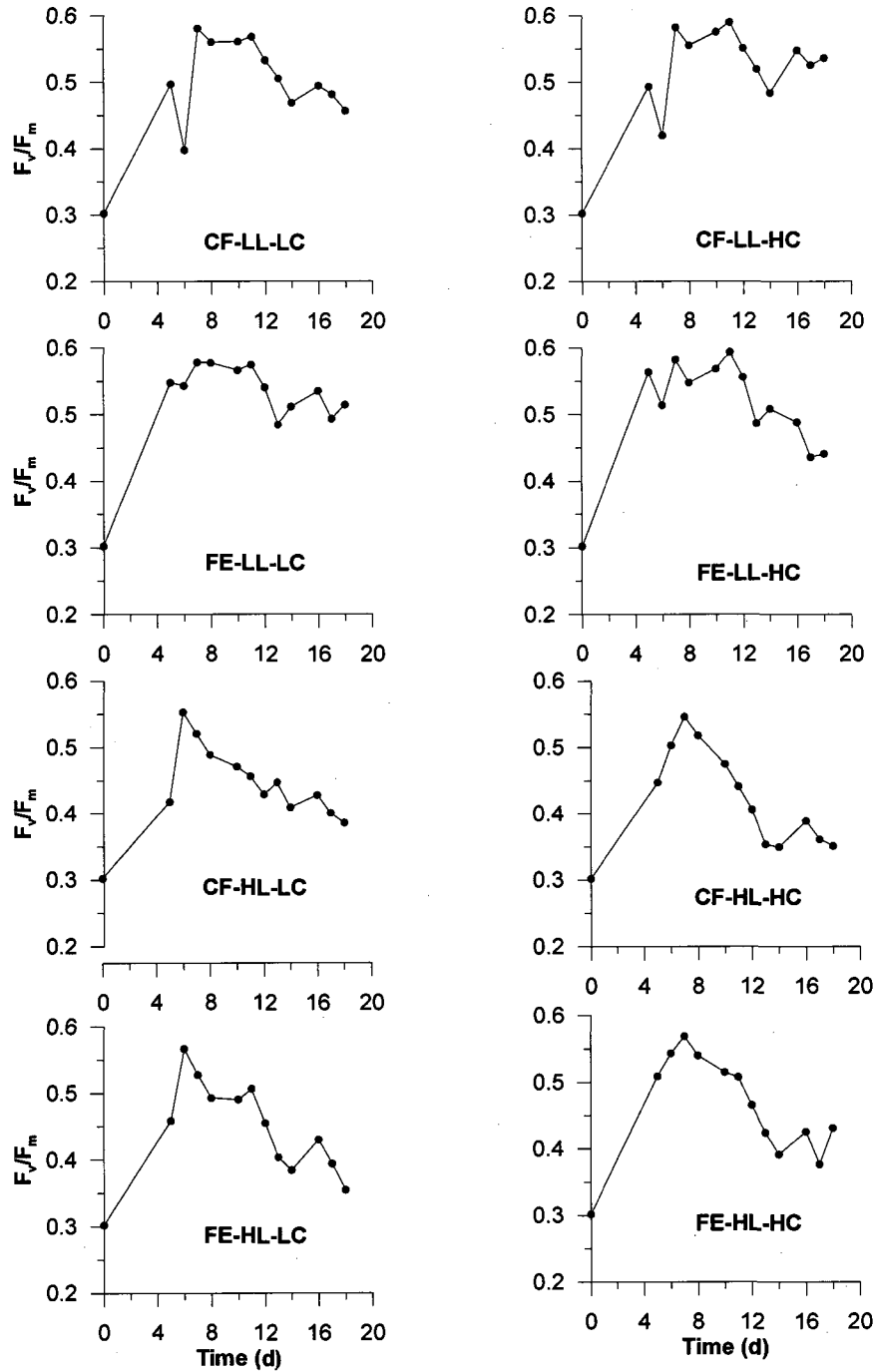


Figure 13. RSC1 potential photochemical efficiency of PSII vs. time. + iron (FE, > 1 nM Fe) iron control (CF, <0.2 nM Fe); high light (HL, 40% E₀); low light (LL, 10% E₀); low CO₂ (LC, 360 ppm); high CO₂ (HC, 750 ppm). Iron and light both had significant effects by increasing photochemical quantum yield and keeping it higher for most of 16 d under lower light.

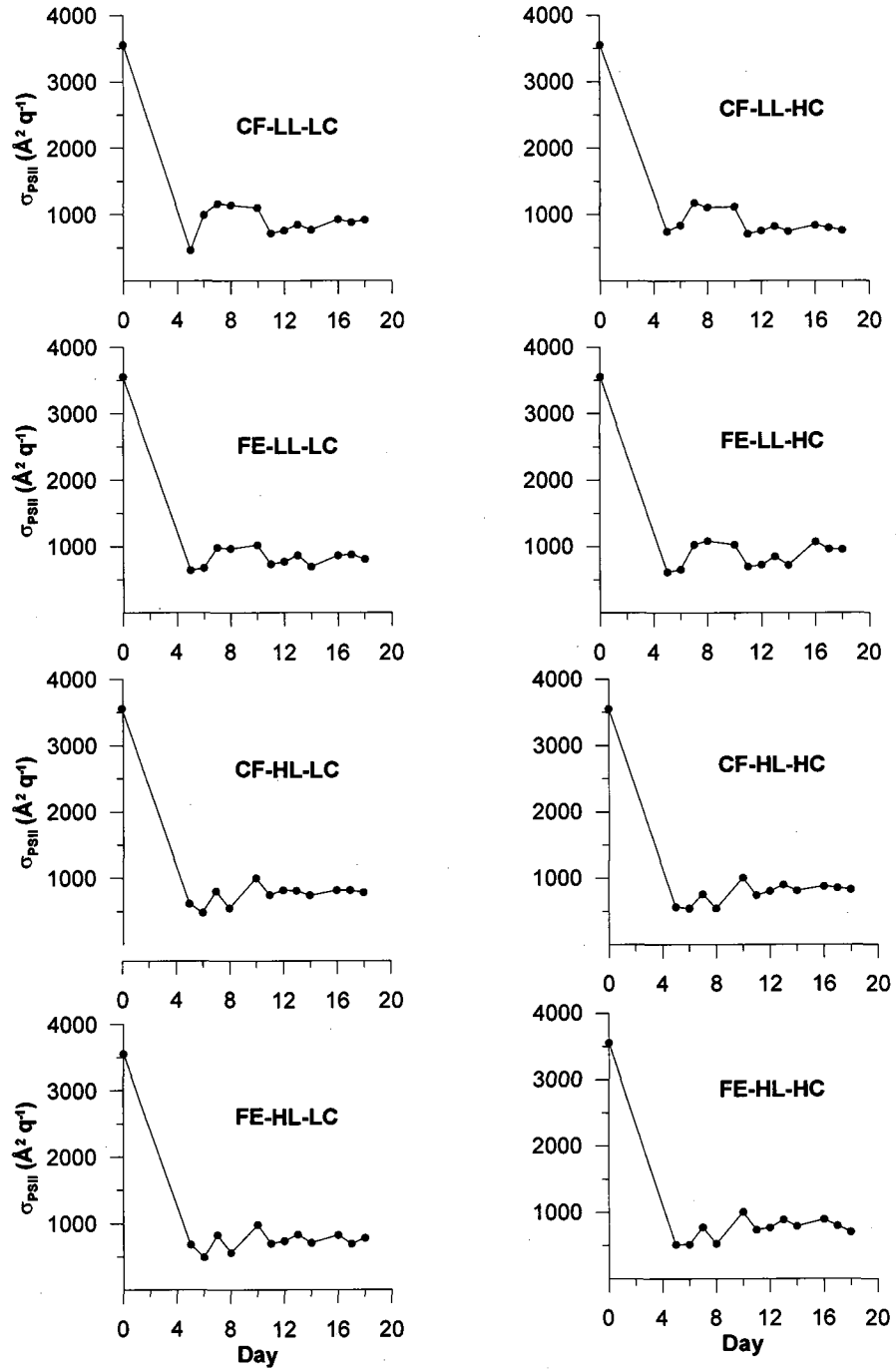


Figure 14. RSC1 absorption cross section (σ_{PSII}) vs. time. + iron (FE, > 1 nM Fe) iron control (CF, <0.2 nM Fe); high light (HL, 40% E_0); low light (LL, 10 % E_0); low CO_2 (LC, 360 ppm); high CO_2 (HC, 750 ppm). No significant difference was observed between treatments.

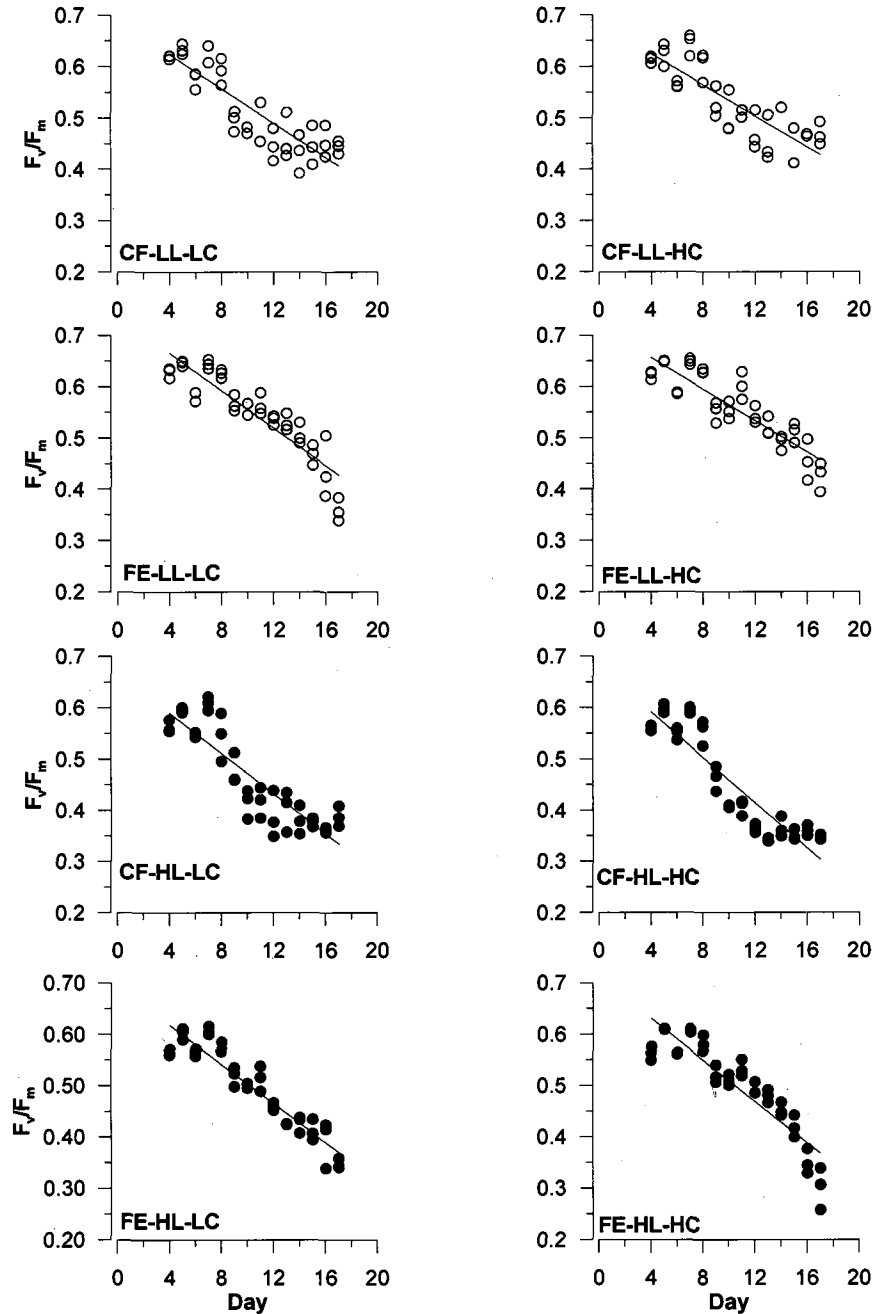


Figure 15. RSC2 potential photochemical efficiency of PSII vs. time. + iron (FE, > 1.0 nM Fe) iron control (CF, <math><0.2\text{ nM Fe}</math>); high light (HL, $365\ \mu\text{mol photons m}^{-2}\text{ s}^{-1}$); low light (LL, $77\ \mu\text{mol photons m}^{-2}\text{ s}^{-1}$); low CO_2 (LC, 380 ppm); high CO_2 (HC, 750 ppm). Iron and light both had significant effects on treatments by increasing photochemical quantum yield and keeping it higher for most of the experimental duration under lower light. Only iron and light had significant effect on F_v/F_m CO_2 had no significant effect. Iron treatment and lower light had higher average quantum yields.

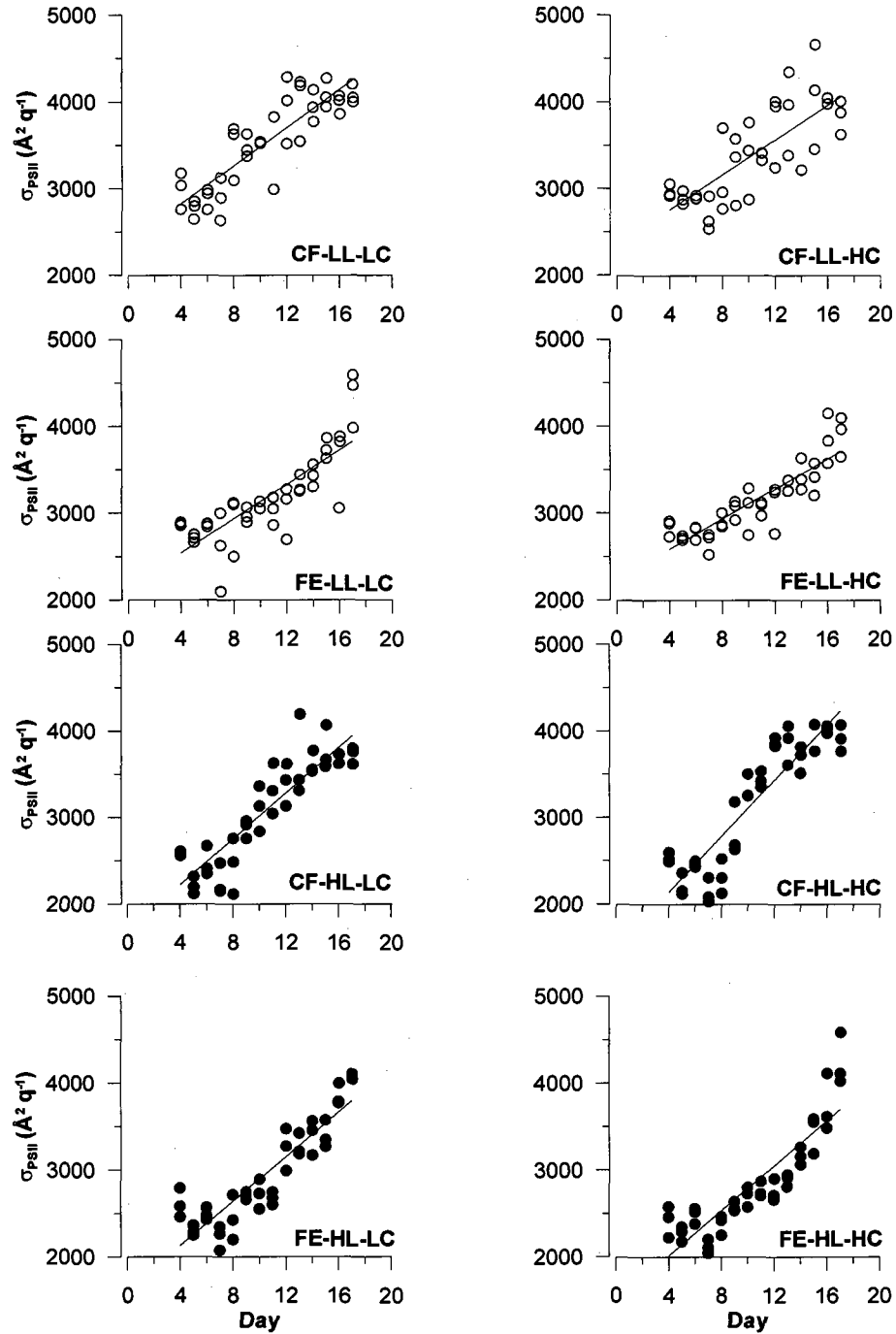


Figure 16. RSC2 absorption cross section (σ_{PSII}) vs. time. + iron (FE, > 1.0 nM Fe) iron control (CF, <0.2 nM Fe); high light (HL, 365 $\mu\text{mol photons m}^{-2} \text{s}^{-1}$); low light (LL, 77 $\mu\text{mol photons m}^{-2} \text{s}^{-1}$); low CO_2 (LC, 380 ppm); high CO_2 (HC, 750 ppm). Trends of the potential photochemical efficiency of PSII vs. time indicate that active compensation mechanisms to iron limitation and light inhibition were employed to maintain optimal electron transport in PSII.

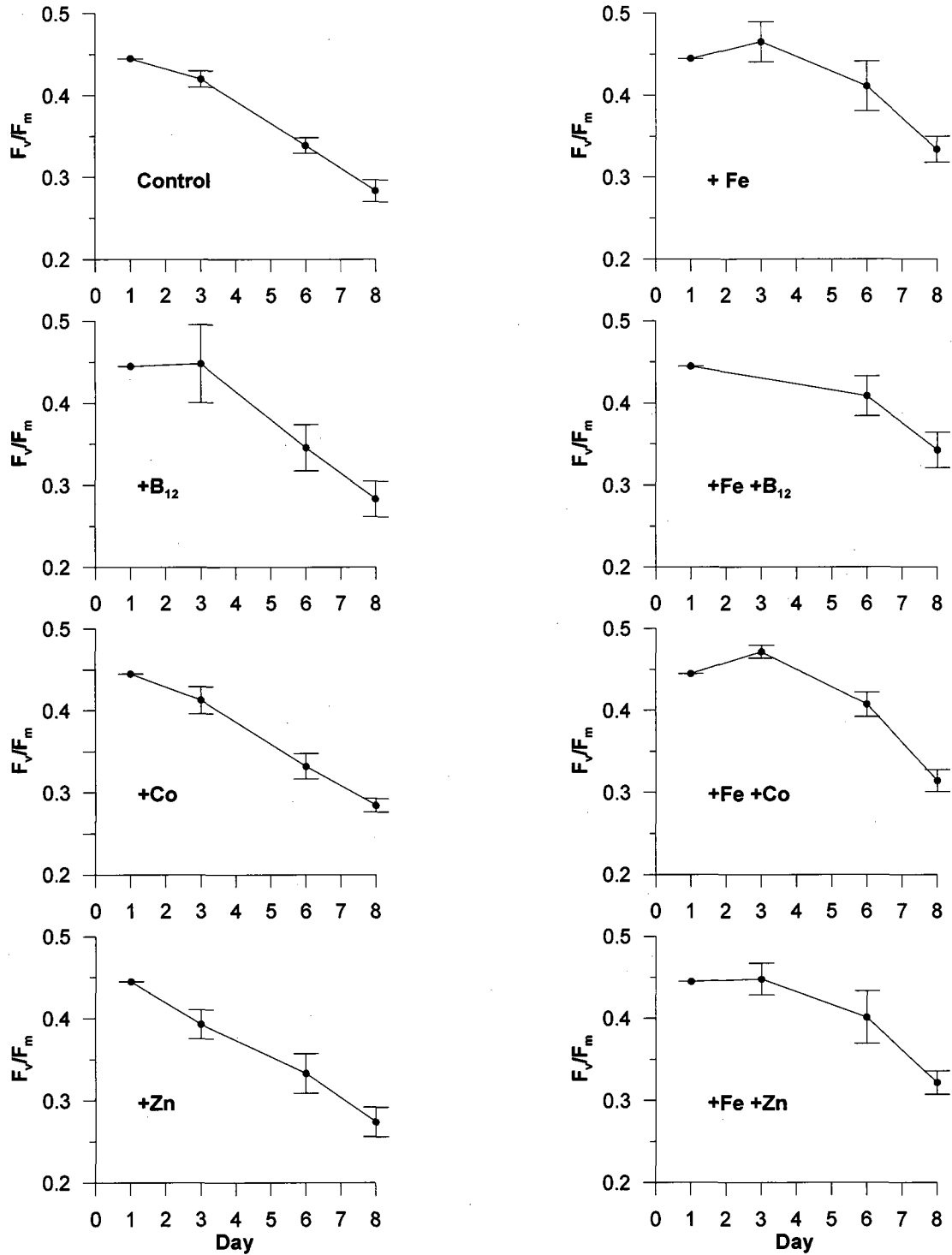


Figure 17. WHOI experiment 1, potential photochemical efficiency of PSII vs. time for micronutrient addition bioassays. Treatments containing iron were the only one significantly different from the control, indicating significant iron limitation in the incubated *P. antarctica*-dominated assemblage.

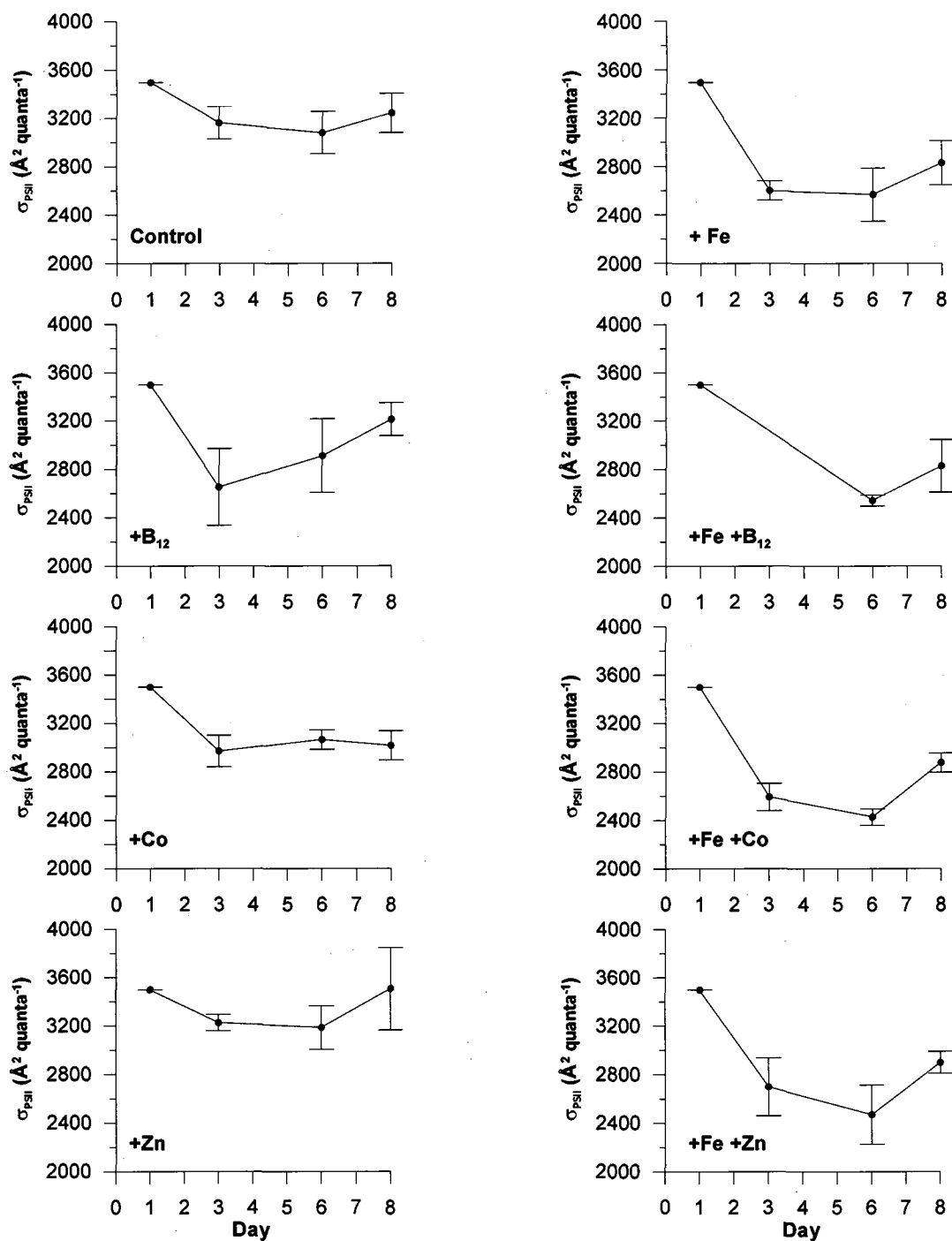


Figure 18. WHOI experiment 1 in growth chamber at $\pm 1^\circ\text{C}$ and $150 \mu\text{mol photons m}^{-2} \text{s}^{-1}$, absorption cross section (σ_{PSII}) vs. time. In all treatments with iron, σ_{PSII} was significantly reduced relative to the initial value and throughout the experiment, supporting the conclusion that a significant iron limitation was occurred in the natural assemblage.

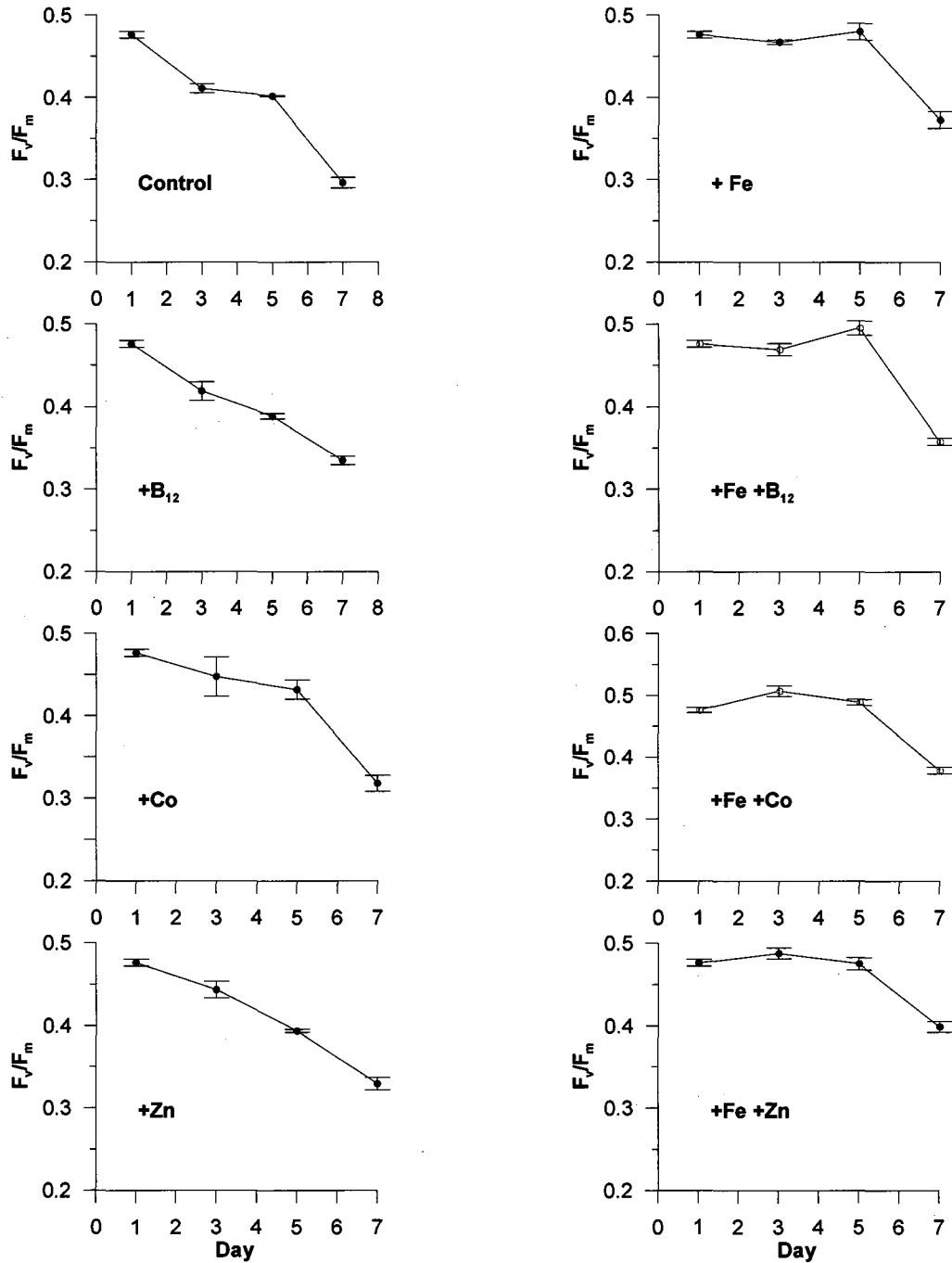


Figure 19. WHOI experiment 2 potential photochemical efficiency of PSII vs. time in micronutrient addition bioassays. Treatments containing iron were the only one significantly different from the control, and had higher quantum yields for the first 5 days of the incubation, indicating significant iron limitation.

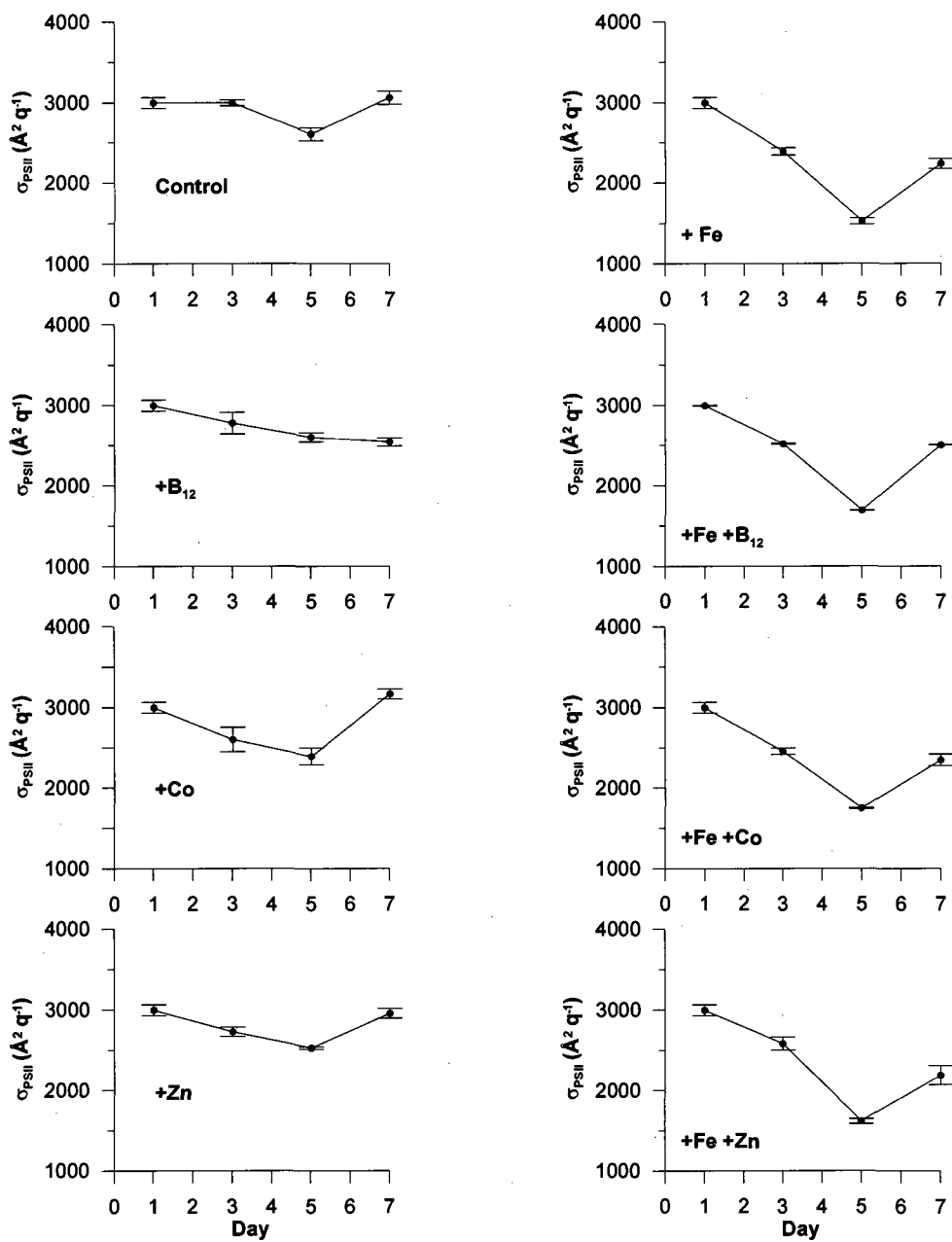


Figure 20. WHOI experiment 2, absorption cross section (σ_{PII}) vs. time. In all treatments with iron, σ_{PII} was significantly reduced relative to the initial value and throughout the duration of the experiment, suggesting significant iron limitation. In all iron treatments the quantum yields were high and stable for the first five days whereas σ_{PII} reached its minimum on the fifth day.

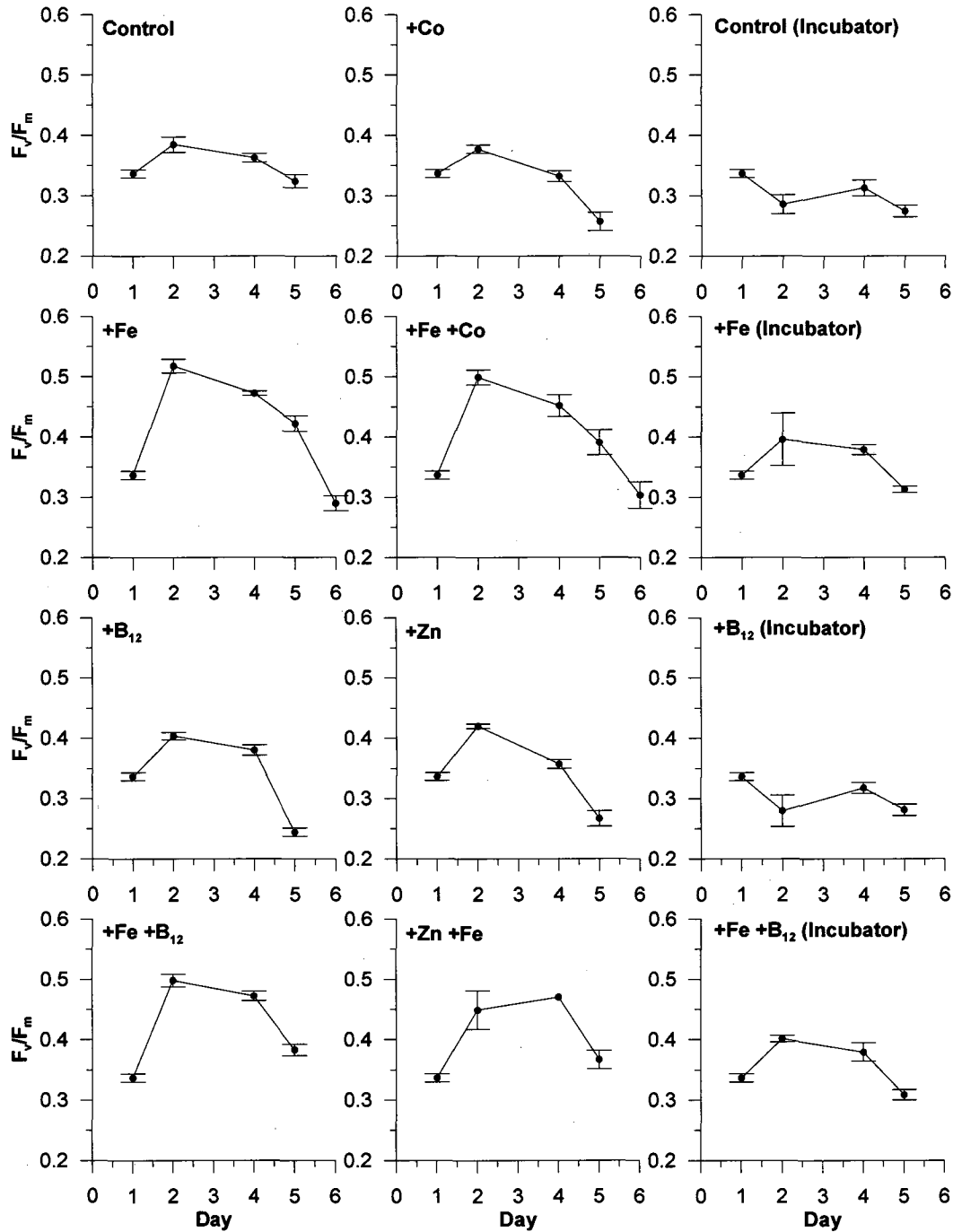


Figure 21. WHOI experiment 3 potential photochemical efficiency of PSII vs. time in micronutrient addition bioassays. Treatments containing iron were the only ones significantly different from the control, demonstrating higher quantum yields, thus confirming significant iron limitation.

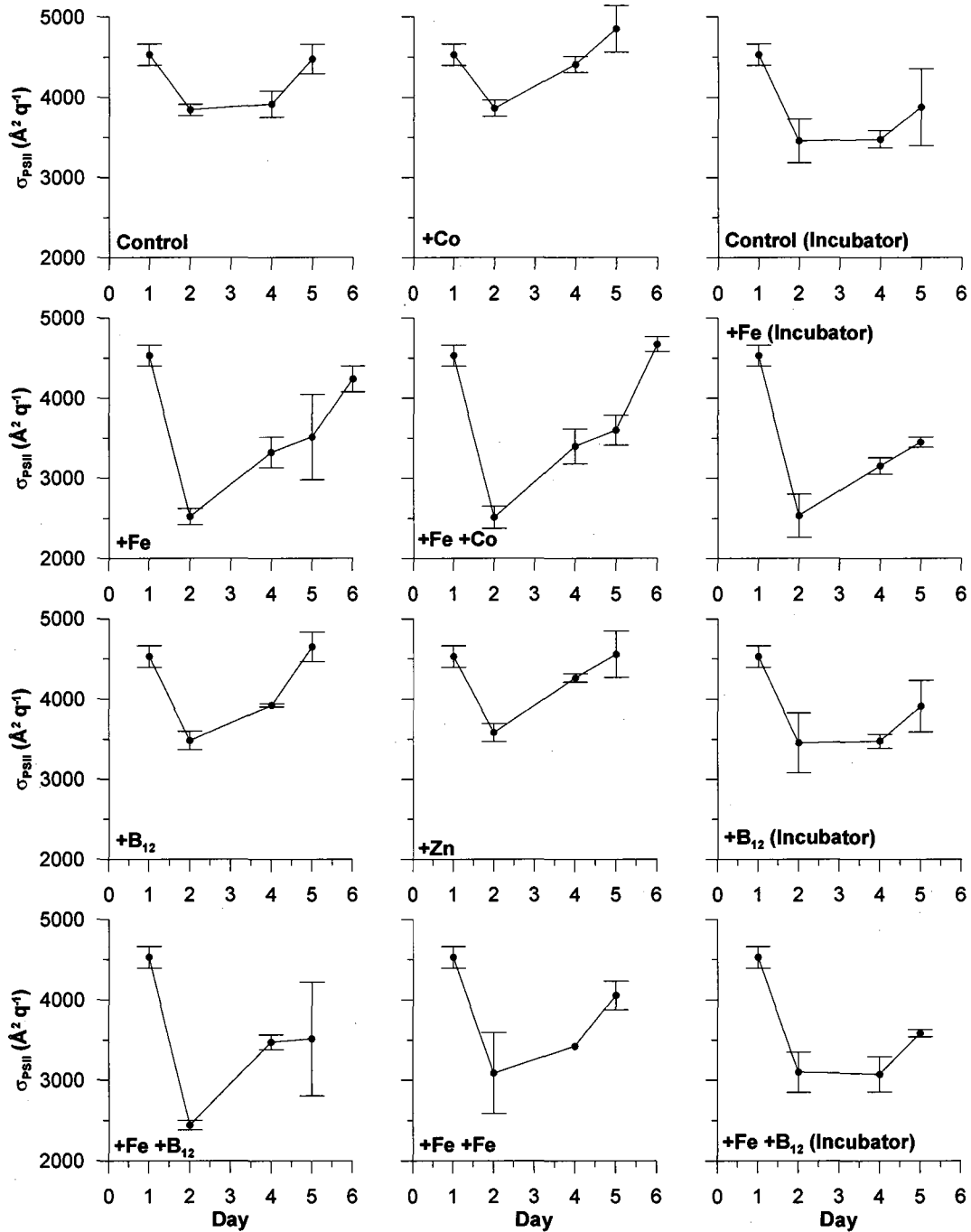


Figure 22. WHOI experiment 3 absorption cross section (σ_{PII}) vs. time. In all treatments with iron, σ_{PII} was rapidly reduced relative to initial values, suggesting significant iron limitation.

LITERATURE CITED

- Arrigo K. R., McClain C. R. 1994. Spring phytoplankton production in the western Ross Sea. *Science* 266:261-263
- Arrigo K. R., Weiss A. M., Smith W. O., Jr. 1998. Physical forcing of phytoplankton dynamics in the southwestern Ross Sea. *Journal of Geophysical Research* 103:1007-1021
- Arrigo K. R., Robinson D. H., Worthen D. L., Dunbar R. B., DiTullio G. R., VanWoert M., Lizotte M. P. 1999. Phytoplankton community structure and the drawdown of nutrients and CO₂ in the Southern Ocean. *Science* 283:365-367
- Bertrand E. M., Saito M. A., Rose J. M., Riesselman C. R., Lohan M. C., Noble A. E., Lee P. A., DiTullio G. R. 2007. Vitamin B12 and iron co-limitation of phytoplankton growth in the Ross Sea. *Limnology and Oceanography* 52:1079-1093
- Bruin J. 2006. Newtest: command to compute new test
<http://www.ats.ucla.edu/stat/stata/ado/analysis/>
- Bruland K. W., Rue E. L., Smith G. J., DiTullio G. R. 2005. Iron, macronutrients and diatom blooms in the Peru upwelling regime: brown and blue waters of Peru. *Marine Chemistry* 93:81-103
- Caron D. A., Dennett M. R., Lonsdale D. J., Moran D. M., Shalapyonok L. 2000. Microzooplankton herbivory in the Ross Sea, Antarctica. *Deep Sea Research II* 47:3249-3272
- Coale K. H., Wang X., Tanner S. J., Johnson K. S. 2003. Phytoplankton growth and biological response to iron and zinc addition in the Ross Sea and Antarctic Circumpolar Current along 170°W. *Deep Sea Research II* 50:635-653
- Coale K. H., Gordon M. R., Wang X. 2005. The distribution and behavior of dissolved and particulate iron and zinc in the Ross Sea and Antarctic circumpolar current along 170°W. *Deep Sea Research I* 52:295-318
- Demmig-Adams B., Adams W. W. 1992. Photoprotection and other responses of plants to high light stress. *Annual Review of Plant Physiology and Plant Molecular Biology* 43:599-626
- Dennett M. R., Mathot S., Caron D. A., Smith W. O., Jr., Lonsdale D. J. 2001. Abundance and distribution of phototrophic and heterotrophic nano- and microplankton in the southern Ross Sea. *Deep Sea Research II* 48:4019-4037
- DiTullio G. R., Smith W. O., Jr 1996. Spatial patterns in phytoplankton biomass pigment distributions in the Ross Sea. *Journal of Geophysical Research* 101:18467-18477
- Dunbar R. B., Leventer A. R., Mucciarone D. A. 1998. Water column sediment fluxes in the Ross Sea, Antarctica: Atmospheric and sea ice forcing. *Journal of Geophysical Research* 103:30,741-30,760

- El-Sayed S. Z., Biggs D. C., Holm-Hansen O. 1983. Phytoplankton standing crop, primary productivity, and near-surface nitrogenous nutrient fields in the Ross Sea, Antarctica. *Deep Sea Research* 30:871-886
- Fitzwater S. E., Johnson K. S., Gordon R. M., Coale K. H., Smith W. O., Jr. 2000. Trace metal concentrations in the Ross Sea and their relationship with nutrients and phytoplankton growth. *Deep Sea Research II* 47:3159-3179
- Fonda Umani S., Accornero A., Budillon G., Capello M., Tucci S., Cabrini M., Del Negro P., Monti M., De Vittor C. 2002. Particulate matter and plankton dynamics in the Ross Sea Polynya of Terra Nova Bay during the Austral Summer 1997/98. *Journal of Marine Systems* 36:29-49
- Genty B., Briantais J. M., Baker N. R. 1989. The relationship between the quantum yield of photosynthetic electron transport and quenching of chlorophyll fluorescence. *Biochimica et Biophysica Acta* 990:87-92
- Goffart A., Catalano G., Hecq J. H. 2000. Factors controlling the distribution of diatoms and *Phaeocystis* in the Ross Sea. *Journal of Marine Systems* 27:161-175
- Gowing M. M., Garrison D. L., Kunze H. B., Winchell C. J. 2001. Biological components of Ross Sea short-term particle fluxes in the austral summer of 1995-1996. *Deep Sea Research I* 48:2645-2671
- Guillard R. R. L. 1975. Culture of phytoplankton for feeding marine invertebrates. In: Chanley W. L. S. a. M. H. (ed) *Culture of Marine Invertebrate Animals*. Plenum Press, New York, 26-60
- Hare C. E., DiTullio G. R., Trick C. G., Wilhelm S. W., Bruland K. W., Rue E. L., Hutchins D. A. 2005. Phytoplankton community structure changes following simulated upwelled iron inputs in the Peru upwelling region. *Aquatic Microbial Ecology* 38:269-282
- Hare C. E., DiTullio G. R., Riseman S. F., Crossley A. C., Popels L. C., Sedwick P. N., Hutchins D. A. 2007. Effects of changing continuous iron input rates on a Southern Ocean algal assemblage. *Deep-Sea Research II* 54:732-746
- Hecq J. H., Guglielmo L., Goffart A., Catalano G., Goosse H. 1999. Modelling approach of the ross sea plankton ecosystem. In: Faranda F., Guglielmo, L., Ianora, A (ed) *Ross Sea Ecology. Italian Antarctic Expeditions 1986–1995*. Springer, Berlin, 395–412
- Hutchins D. A., Pustizzi F., Hare C. E., DiTullio G. R. 2003. A shipboard natural community continuous culture system for ecologically relevant low-level nutrient enrichment experiments. *Limnology and Oceanography-Methods* 1:82-91
- Innamorati M., Mori C., Massi L., Lazzara L., Nuccio C. 1999. Phytoplankton biomass related to environmental factors in the Ross Sea. In: Faranda F. M., Guglielmo, L., Ianora, A. (ed) *Ross Sea Ecology*. Springer-Verlag, Berlin, 217– 230
- Jacobs S. S., Giulivi C. F. 1998. Interannual ocean and sea ice variability in the Ross Sea, in *Ocean, Ice, and Atmosphere*. In: Jacobs S. S., Weiss R. F. (eds), Vol 75. AGU, Washington DC, 83-99

- Kolber Z. S., Prasil O., Falkowski P. G. 1998. Measurements of variable chlorophyll fluorescence using fast repetition rate techniques: defining methodology and experimental protocols. *Biochimica et Biophysica Acta* 1367:88-106
- Lazzara L., Saggiomo V., Innamorati M., Mangoni O., Massi L., Mori G., Nuccio C. 1999. Photosynthetic parameters, irradiance and production estimates in the Western Ross Sea. In: F.M.Faranda L. G., A. Ianora (ed) *Ross Sea Ecology. Italian Antarctic Expeditions (1987-1995)*. Springer Verlag, Berlin, 259-273
- Leventer A., Dunbar R. B. 1996. Factors influencing the distribution of diatoms and other algae in the Ross Sea. *Journal of Geophysical Research* 101:18489-18500
- Lieselotte R., Dale R. 1997. Photoinduction of UV-absorbing compounds in Antarctic diatoms and *Phaeocystis antarctica*. *Marine Ecology Progress Series* 160:13-25
- Mengelt C., Prezelin B. B. 2005. UVA enhancement of carbon fixation and resilience to UV inhibition in the genus *Pseudo-nitzschia* may provide a competitive advantage in high UV surface waters. *Marine Ecology Progress Series* 301:81-93
- Moisan T. A., Olaizola M., Mitchell B. G. 1998. Xanthophyll cycling in *Phaeocystis antarctica*: changes in cellular fluorescence. *Marine Ecology Progress Series* 169:113-121
- Moisan T. A., Mitchell B. G. 1999. Photophysiological acclimation of *Phaeocystis antarctica* Karsten under light limitation. *Limnology and Oceanography* 44:247-258
- Moisan T. A., Mitchell B. G. 2001. UV absorption by mycosporine-like amino acids in *Phaeocystis antarctica* Karsten induced by photosynthetically available radiation. *Marine Biology* 138:217-227
- Moisan T. A., Ellisman M., Buitenhuis C., Sosinsky G. 2006. Differences in chloroplast ultrastructure of *Phaeocystis antarctica* in low and high light. *Marine Biology* 149:1281-1290
- Montes-Hugo M., Doney S. C., Ducklow H. W., Fraser W., Martinson D., Stammerjohn S. E., Schofield O. 2009. Recent Changes in Phytoplankton Communities Associated with Rapid Regional Climate Change Along the Western Antarctic Peninsula. *Science* 323:1470-1473 doi: 10.1126/science.1164533
- Nuccio C., Innamorati M., Lazzara L., Mori G., Massi L. 2000. Spatial and temporal distribution of phytoplankton coenoses in the Ross Sea. In: F. Faranda L. G., A. Ianora (ed) *Ross Sea Ecology. Italian Antarctic Expeditions (1987-1995)*. Springer Verlag, Berlin, 231-245
- Olson R. J., Sosik H. M., Chekalyuk A. M., Shalapyonok A. 2000. Effects of iron enrichment on phytoplankton in the Southern Ocean during late summer: active fluorescence and flow cytometric analyses. *Deep Sea Research II* 47:3181-3200

- Peloquin J. A., Smith W. O., Jr. 2007. Phytoplankton blooms in the Ross Sea, Antarctica: Interannual variability in magnitude, temporal patterns, and composition. *Journal of Geophysical Research* 112 doi: 10.1029/2006JC003816
- Price N. M., Harrison G. I., Hering J. G., Hudson R. J., Nirel P. M. V., Palenik B., Morel F. M. M. 1988/1989. Preparation and chemistry of the artificial algal culture medium Aquil. *Biological Oceanography* 6:443-461
- Richardson K., Beardall J., Raven J. A. 1983. Adaptation of unicellular algae to irradiance: an analysis of strategies. *New Phytologist* 93:157-191
- Rousseau V., Vaultot D., Casotti R., Cariou V., Lenz J., Gunkel J., Baumann M. 1994. The life cycle of *Phaeocystis* (Prymnesiophyceae): evidence and hypotheses. *Journal of Marine Systems* 5:23-39
- Rousseau V., Chrétiennot-Dinet M.-J., Jacobsen A., Verity P., Whipple S. 2007. The life cycle of *Phaeocystis*: state of knowledge and presumptive role in ecology. *Biogeochemistry* 83:29-47
- Sarmiento J. L., Le Quéré C. 1996. Oceanic Carbon Dioxide Uptake in a Model of Century-Scale Global Warming. *Science* 274:1346-1350 doi: 10.1126/science.274.5291.1346
- Sarmiento J. L., Slater R., Barber R., Bopp L., Doney S. C., Hirst A. C., Kleypas J., Matear R., Mikolajewicz U., Monfray P., Soldatov V., Spall S. A., Stouffer R. 2004. Response of ocean ecosystems to climate warming. *Global Biogeochemical Cycles* 18:doi:1029/2003GB002134
- Sedwick P. N., DiTullio G. R. 1997. Regulation of algal blooms in antarctic shelf waters by the release of iron from melting sea ice. *Geophysical Research Letters* 24:2515–2518
- Sedwick P. N., DiTullio G. R., Mackey D. J. 2000. Iron and manganese in the Ross Sea, Antarctica: Seasonal iron limitation in Antarctic shelf waters. *Journal of Geophysical Research* 105:11321-11336
- Sedwick P. N., Garcia N., Riseman S., Marsay C., DiTullio G. 2007. Evidence for high iron requirements of colonial *Phaeocystis antarctica* at low irradiance. *Biogeochemistry* 83:83-97
- Shindell D. T., Schmidt G. A. 2004. Southern Hemisphere climate response to ozone changes and greenhouse gas increases. *Geophysical Research Letters* 31:doi:10.1029/2004GL020724
- Smith W. O., Jr, Nelson D. M. 1985. Phytoplankton bloom produced by a receding ice edge in the Ross Sea: spatial coherence with the density field. *Science* 227:163-166
- Smith W. O., Jr, Asper V. L. 2001. The influence of phytoplankton assemblage composition on biogeochemical characteristics and cycles in the southern Ross Sea, Antarctica. *Deep Sea Research I* 48:137-161
- Smith W. O., Jr, Shields A. R., Catalano G., Peloquin J. A., Tozzi S., Dinniman M. S., Asper A. A. 2006. Interannual variations in nutrients, net community production, and biogeochemical cycles in the Ross Sea. *Deep-Sea Research II* 53:815-833

- Smith W. O., Jr., Nelson D. M. 1986. The importance of ice-edge blooms in the Southern Ocean. *BioScience* 36:251-257
- Smith W. O., Jr., Gordon L. I. 1997. Hyperproductivity of the Ross Sea (Antarctica) polynya during austral spring. *Geophysical Research Letters* 24:233-236
- Smith W. O., Jr., Carlson C. A., Ducklow H. W., Hansell D. A. 1998. Growth dynamics of *Phaeocystis antarctica*-dominated plankton assemblages from the Ross Sea. *Marine Ecology Progress Series* 168:229-244
- Smith W. O., Jr., Marra J., Hiscock M. R., Barber R. T. 2000. The seasonal cycle of phytoplankton biomass and primary productivity in the Ross Sea, Antarctica. *Deep Sea Research II* 47:3119-3140
- SooHoo J. B., Palmisano A. C., Kottmeier S. T., Lizotte M. P., SooHoo S. L., Sullivan C. W. 1987. Spectral light absorption and quantum yield of photosynthesis in sea ice microalgae and a bloom of *Phaeocystis pouchetii* from McMurdo Sound, Antarctica. *Marine Ecology Progress Series* 39:175-189
- Tang K., Smith W. O., Jr, Shields A. R., Elliott D. T. 2008. Survival and recovery of *Phaeocystis antarctica* (Primnesiophyceae) from prolonged darkness and freezing. *Proceedings of the Royal Society of London. Series B* 276:81-90
- van Hilst C. M., Smith W. O., Jr 2002. Photosynthesis/irradiance relationships in the Ross Sea, Antarctica, and their control by phytoplankton assemblage composition and environmental factors. *Marine Ecology Progress Series* 226:1-12
- van Leeuwe M. A., Stefels J. 1998. Effects of iron and light stress on the biochemical composition of antarctic *Phaeocystis sp.* (Primnesiophyceae). II. Pigment composition. *Journal of Phycology* 34:496-503
- van Leeuwe M. A., Stefels J. 2007. Photosynthetic responses in *Phaeocystis antarctica* towards varying light and iron conditions. *Biogeochemistry* 83:61-70
- Vass I., Styring S., Hundal T., Koivuniemi A., Aro E., Andersson B. 1992. Reversible and irreversible intermediates during photoinhibition of photosystem II: stable reduced QA species promote chlorophyll triplet formation. *Proceedings of the National Academy of Sciences of the United States of America* 89:1408-1412
- Verity P., Brussaard C., Nejstgaard J., van Leeuwe M., Lancelot C., Medlin L. 2007. Current understanding of *Phaeocystis* ecology and biogeochemistry, and perspectives for future research. *Biogeochemistry* 83:311-330
- Whipple S. J., Patten B. C., Verity P. G. 2005. Life cycle of the marine alga *Phaeocystis*: A conceptual model to summarize literature and guide research. *Journal of Marine Systems* 57:83-110

**SECTION III. LARGE SCALE VARIATIONS IN PHYTOPLANKTON PHOTOSYNTHETIC ACTIVITY IN THE
ROSS SEA (ANTARCTICA) POLYNYAS RELATED TO ENVIRONMENTAL PARAMETERS AND BLOOM
DYNAMICS**

ABSTRACT

Bio-optical approaches, including active fluorescence techniques, are increasingly utilized to improve the understanding of phytoplankton ecology and dynamics. Here I present results from two cruises to the Ross Sea (Antarctica), where I used fast repetition rate fluorometry (FRRF) to relate phytoplankton photobiology to water mass characteristics and assemblage composition. Spatial and temporal distributions of photosynthetic activity is related to biogeochemical patterns and physical forcing that select for either the prymnesiophyte *Phaeocystis antarctica* or diatoms. *P. antarctica* often dominates spring assemblages and appears to have higher resilience to high light fluxes and fluctuations, while diatoms dominate the warmer, more stratified waters and tend to have reduced quantum yields during austral summer. Significant differences in nutrient uptake were observed, as dissolved N:P ratios were inversely proportional to the dissolved silicate pool, indicating higher nitrogen vs. phosphorus requirement in diatoms compared to *P. antarctica*. Fluorescence quantum yields were generally higher in early spring when the polynya was well homogenized, with few gradients of physico-chemical properties. In late spring and summer fluorescence quantum yields were lower and reflected the stronger water mass gradients. Absorption cross sections were high in early spring, reflecting adaptations to lower average light availability, and decreased significantly in the summer, especially in waters with shallow mixed layers. Dominance of *P. antarctica* in the spring and in some areas during summer appears to be related to its photophysiological resilience and faster photoadaptation, while diatoms bloomed in shallow mixed layers in the summer, likely due to their higher photosynthetic competency.

INTRODUCTION

The objective of this chapter is to examine the spatial and temporal distribution of phytoplankton photosynthetic quantum yields in the Ross Sea polynya as measured with FRR fluorometry during austral spring (November- December) and summer (January-February). These results are correlated with environmental variables, phytoplankton biomass and taxonomic composition as determined by pigment analysis. My goal is to better understand factors regulating polar phytoplankton growth and how blooms impact the region biogeochemistry.

The Ross Sea

The Ross Sea displays substantial spatial and temporal variability (Jacobs and Giulivi 1998, Smith *et al.* 2006). The region is surrounded by Victoria Land on the west and Marie Byrd Land in the southeast and is partially covered by the Ross Ice Shelf (RIS). The Ross Sea sector is also characterized by a cyclonic gyre, located between the Antarctic Circumpolar Current (ACC) and the Antarctic continental shelf. The ocean circulation on the Ross Sea's continental shelf is strongly linked to oceanic and atmospheric circulation, as well as ice extent. The shelf supports substantial primary and secondary production (Smith *et al.* 2007), and has two distinctively different (eastern and western) biogeochemical regions (Nelson *et al.* 1996, Smith *et al.* 1996, Goffart *et al.* 2000, Sweeney *et al.* 2000a) where environmental conditions follow changes in ice coverage, nutrient sources and sinks, and light availability.

Ecophysiology and photobiology of high-latitude phytoplankton functional groups.

The main phytoplankton functional groups in the Ross Sea are the haptophyte *Phaeocystis antarctica* (El-Sayed *et al.* 1983, Smith and Gordon 1997) and diatoms, such as *Pseudo-nitzschia sp.*, *Fragilariopsis cylindrus*, *Nitzschia sp.*, *Chaetoceros sp.*, *Thalassiosira sp.*, *Thalassiothrix sp.*,

Rhizosolenia sp. and *Corethron* sp. (Smith and Nelson 1985, DeMaster *et al.* 1992, Leventer and Dunbar 1996, Dennett *et al.* 2001, Garrison *et al.* 2003). The former usually predominates during early spring, while the latter are more common during austral summer (Arrigo *et al.* 1999), especially in the western Ross Sea and in regions of melting ice, which generally exhibit increased stratification. Diatom distribution appears to be strongly controlled by ice coverage and dynamics (Leventer and Dunbar 1988, 1996). Furthermore, diatoms appear to have slower growth rates compared to *P. antarctica* throughout most of the region, especially during early spring (Smith *et al.* 1996, Smith *et al.* 1999). As a result, *P. antarctica* dominates the spring phytoplankton and has the potential for early and rapid export of carbon to deep water and sediments (DiTullio *et al.* 2000). This finding is in contrast with sedimentation rates below the euphotic zone measured in the northern hemisphere (Wassmann 1994); additionally, such rapid export events have never been detected in any sediment traps deployed in the Ross Sea (Dunbar *et al.*, 1998).

P. antarctica has three different morphotypes: flagellated single cells, non-flagellated single cells, and colonies of non-flagellated single cells embedded in a mucous sheath (Rousseau *et al.* 1994, Rousseau *et al.* 2007). It is still unclear which factors promote the colony formation and regulate their size (e.g., Lancelot *et al.*, 1998; Jakobsen and Tang, 2002). Nutrient concentrations and ratios are believed to play a role (Rousseau *et al.* 1994, Lancelot *et al.* 1998), and enlargement of the colonies may in part represent a response to grazing (Tang 2003, Tang *et al.* 2008). Temperature and light likely affect the morphotypes, the photosynthetic and growth rates, and the exudation rates of dissolved organic carbon and nitrogen (DOC and DON) (Jahnke 1989, Verity *et al.* 1990, Hu and Smith 1998). The percentage of organic carbon in the mucus matrix of the colonies is highly variable (4 – 50%) (Matrai *et al.* 1993, Mathot *et al.* 2000). When *P. antarctica* dominates, higher rates of nitrate removal (relative to carbon) are observed compared to diatom-dominated waters (Arrigo *et al.* 1999). A deeper mixed layer has been suggested to provide an advantage due to better buoyancy control

offered by the mucilaginous matrix (Lancelot *et al.* 1998), photosynthetic plasticity, and higher growth rates at lower light levels (Arrigo *et al.* 1999). *P. antarctica* blooms often occur near receding ice edges and are sometimes followed by diatom blooms (Landry *et al.* 2002, Buesseler *et al.* 2003, Smith *et al.* 2003). It has been suggested that iron concentrations, which are relatively elevated in spring due to ice melt and winter mixing (Sedwick and DiTullio 1997) and reduced in summer due to biological uptake (Sedwick *et al.* 2000), significantly affect assemblage composition in the Ross Sea as well. On the other hand, iron stress has little control on pigment composition and therefore chromatic adaptation (van Leeuwe *et al.* 1998), but has a strong effect on the efficiency of the electron transfer rate (ETR). Despite all of these observations, there is little consensus on the main factors regulating the presence, competition, and succession between these two phytoplankton functional taxa in the Ross Sea polynya.

Role of iron

Low iron concentrations have been considered as a possible limiting factor of phytoplankton in the Southern Ocean (Martin 1990, Timmermans *et al.* 1998, de Baar *et al.* 1999, Boyd *et al.* 2000). Iron is an essential component of the photosynthetic machinery, but it is also involved in other enzymes, such as nitrate reductase. A major source of iron to the surface Ross Sea waters is the upwelling of circumpolar deep water along frontal zones (Measures and Vink 2001, Dinniman *et al.* 2003). Melting glacial and sea ice provides a second iron source, stimulating biomass increases late in the season along the marginal ice zone (MIZ) (Sedwick and DiTullio 1997). Remineralization of organic material in subsurface waters and sediment resuspension also contribute to the iron balance (Johnson *et al.* 1997). It has been observed that *P. antarctica* dominates in more deeply mixed waters, with presumably higher iron concentrations (Arrigo *et al.* 1999, Arrigo *et al.* 2003) and lower integrated irradiance. Conversely, waters with lower iron concentrations (highly stratified summer conditions)

appear to select for diatoms (Sedwick and DiTullio 1997, Smith and Asper 2001). However, as these two types of habitats overlap, there is no statistical difference between the environments dominated by different functional groups of phytoplankton with respect to either mixed layer depth or photosynthetic parameters (van Hilst and Smith 2002).

Fluorescence, fluorescence induction, and variable fluorescence

Fluorescence by photosynthetic pigments represents one of the dissipative pathways for absorbed excitation energy. As this signal is proportional to the pigment concentration, it has been long used to assess phytoplankton abundance (Lorenzen 1966). Fluorescence allows for the rapid and non-destructive measurement of chlorophyll *a*, making it extremely useful both in aquatic and terrestrial ecosystems due to its sensitivity and convenience (Krause and Weis 1991). Despite this, *in vivo* fluorescence is only a proxy, not an exact measure of chlorophyll *a* concentration and algal biomass. The fluorescence yield (the ratio of the emitted fluorescence to the absorbed excitation energy) of a photosynthetic organism is controlled by a variety of factors. It changes with species composition, the physiological state, and the light exposure and history of the photosynthetic assemblage. Blue (440 – 480 nm) or red (~665 nm) light, corresponding to the blue (or red) absorption bands of chlorophyll, is usually utilized as excitation energy. The fluorescence signal is generally detected at 680 – 690 nm, corresponding to the peak of chlorophyll *a* emission from photosystem II (PSII).

Fluorescence induction, also known as variable fluorescence, was first described by Kautsky and Hirsch (1931), and manifests itself as an increase in the fluorescence yield following brief (μ s to ms) exposure to light. In response, the photosynthetic electron transport progressively saturates, and the excess excitation energy is reemitted as fluorescence with gradually increasing quantum yields (or decreasing photochemical quenching). Under prolonged exposure to strong light (minutes to hours)

another mechanism, called non-photochemical quenching, is observed, in which the fluorescence intensity decreases due redistribution of the deactivation pathways between heat, fluorescence, and photosynthesis (Schreiber *et al.* 1986). Several models of these phenomena have been proposed (Trissl *et al.* 1993), generally converging to a relatively simple expression of the photosynthetic yields (Φ_{PSII}) as a function of the measured fluorescence signals:

$$\Phi_{PSII} = \frac{F_m - F'}{F_m} = \frac{F_v'}{F_m} \quad (\text{Eq. 14})$$

where Φ_{PSII} is the maximum quantum yield of PSII, F_m is the fluorescence at saturation, and F' is fluorescence measured under ambient light (Genty *et al.* 1989). The Φ_{PSII} approaches the maximum level when measured in the dark - that is, with all reaction centers open.

In the past twenty years the use of active fluorescence to measure and monitor phytoplankton photosynthetic activity by variable fluorescence has increased. Variable fluorescence has been measured with pump and probe fluorometry (PPF) (Mauzerall 1972, Falkowski *et al.* 1986, Kolber *et al.* 1990). This approach has been previously used in the Ross Sea in combination with flow cytometry to measure the photophysiology of different genera (Olson *et al.* 2000). The PPF fluorometry evolved into fast repetition fluorometry (FRRF) (Kolber *et al.* 1998). In the 1980's pulse amplitude fluorometry (PAM), which measures photochemical efficiency of PS II utilizing multiple turnover flashes (Schreiber and Bilger 1986), was developed. Variable fluorescence has been widely used as a method for assessing the photochemical status and response of phytoplankton to a variety of factors, including nutrient (Kromkamp and Peene 1999, Parkhill *et al.* 2001, Sylvan *et al.* 2007) and trace-metal limitation (Kolber *et al.* 1994, Behrenfeld and Kolber 1999, Boyd *et al.* 2000, Olson *et al.* 2000). FRRF and PAM methodologies have been compared in laboratory and field studies (Suggett *et al.* 2003) and in the field (Rottgers 2007). The main difference between the FRRF and the PAM methods is the way that PSII redox state is manipulated by light excitation (Kromkamp and Forster

2003). With the FRRF technique the primary electron acceptor, Q_A , is reduced with a short ($\sim 100 \mu\text{s}$) sequence of flashlets within a single turnover of PSII reaction center (ST excitation). Besides measuring the photosynthetic yields (Eq. 14), the fluorescence saturation profile measured by FRR technique allows assessment of the functional absorption cross section of PSII. The FRRF can also produce multiple turnover (up to 100 ms) excitation sequence to reduce both the (Q_A), and the secondary (QP pool) electron acceptors (MT excitation). Finally, by controlling the time interval between excitation flashlets, FRR technique allows to quantify the kinetics of the photosynthetic electron transport. In the PAM approach, a multiple-turnover flash is used to measure the photosynthetic yields. Comparison of the two in the North Sea and in the South Atlantic (Rottgers 2007) resulted in significant differences, but the photosynthetic yields measured by these two techniques generally scaled linearly. In laboratory tests the PAM technique generally measured photosynthetic quantum yields about 20% higher than the FRRF technique at low light intensity; these differences largely disappear at high irradiances (Suggett *et al.* 2003).

MATERIAL AND METHODS

Study Area

All sampling was conducted in the Ross Sea Polynya within the “Controls on Ross Sea Algal Community Structure (CORSACS)” project during two cruises on the *RVIB N. B. Palmer* (Cruises NBP06-01, December 2005-January 2006 and NBP06-08, November-December 2006) and a short cruise as part of the “Interannual Variability in the Ross Sea (IVARS)” project at the end of January 2006. Cruise details are provided in table 3. The ability to relate the taxonomic photophysiological responses to the measured photosynthetic activity in the context of the environmental conditions is a significant step towards a better understanding of the phytoplankton dynamics in the polynya. The CORSACS data presented here in provides a comprehensive overview of physical, chemical and biological conditions

and processes in the Ross Sea Polynya during the austral spring and summer. Further insight on the sources and mechanisms controlling the bioavailable iron in the polynya may be gained by experimentation and measurements of iron concentration in the Ross Sea with a goal of better interpretation of all photophysiological data.

Hydrography

Hydrographic properties of the Ross Sea continental shelf were assessed by 102 CTD casts at 74 stations during NBP06-01 (Appendix 2; Table 1) and 72 CTD casts at 43 stations on NBP06-08 (Appendix 2; Table 2). Station locations are shown in figures 23 and 24. A SeaBird Electronics Model SBE-911+ was used to measure conductivity, temperature, and depth. The instruments were mounted on a SeaBird, epoxy coated, 24-bottle rosette sampler with 10-L Bullister bottles controlled by a SeaBird pylon. Data from the sensors were transmitted in real time to SBE-11 deck unit via a conducting cable and were digitally recorded on a Windows computer with SBE Seasave software (Ver. 5.37d).

Irradiance

Surface irradiance was collected every second and recorded every minute with a Biospherical QSR-240 PAR sensor mounted on the mast above the ship bridge as part of the ship's underway data. Irradiance profiles were recorded at each CTD cast with a submersible Biospherical QSP 2300 PAR sensor and processed together with all other CTD sensors using SBE Seasave software.

Nutrient analysis

Inorganic dissolved nutrients (nitrate, nitrite, phosphate, ammonium and silicic acid) were measured on all samples. Samples for nutrient analyses (60 mL) were collected with an acid-washed

syringe and filtered through a 0.2 µm Gelman Acrodiscs into 125 mL polypropylene bottles. Analyses were performed on a Lachat QuickChem Autanalyzer using standard automated techniques. Samples were processed immediately after collection, and if necessary, stored at 4° C for no more than 12 hours.

Chlorophyll

Samples for total chlorophyll *a* (Chl *a*) were collected from the Niskin bottles into clean, dark polyethylene bottles and immediately filtered through 25 mm GF/F Whatman glass microfiber filters (nominal pore size 0.7 µm) using a vacuum of less than 5 psi. Filters were immediately placed in borosilicate tubes with 90% acetone, capped for 24 hours, and extracted at -20° C in the dark (JGOFS 1994). Following extraction the filters were removed and fluorometric determination of chlorophyll *a* by a non-acidification method (Welschmeyer 1994) was completed with a Turner Designs TD700 fluorometer. The fluorometer was calibrated at the beginning and at end of each cruise using commercially purified chlorophyll *a*. Prior to the measurements the fluorometer was zeroed with 90% acetone.

HPLC pigments

Pigments were quantified with HPLC techniques according to DiTullio and Geesey (2002). The measured pigments included chlorophyll *a* (Chl *a*), fucoxanthin (Fuco), 19'-hexanoyloxyfucoxanthin (19-Hex) and chlorophyll *c*₃ (Chl *c*₃). Fuco, Chl *c*₃ and 19-Hex were used as chemotaxonomic proxies for diatoms (Jeffrey 1980, Claustre *et al.* 1994) and prymnesiophytes (Gieskes and Kraay 1986, DiTullio and Smith 1995). 19-Hex is considered to be a robust indicator of *Phaeocystis* biomass in the Ross Sea, based on the reported predominance of *Phaeocystis* and minor contribution of other prymnesiophytes in the region (Palmisano *et al.* 1986, DiTullio *et al.* 2000, Goffart *et al.* 2000).

Variable Chl *a* fluorescence measurements

To measure fluorescence yields, I used an MBARI 4th generation bench-top FRR fluorometer. This instrument is equipped with an array of blue LED lights (~470 nm) with a total power of about 6 watts cm⁻². In continuous wave (CW) mode the instrument can deliver up to 8000 μmol photons m⁻² s⁻¹ while performing FRR excitation. The FRR excitation flashlets are produced at pulse photon flux density (PPFD) of about 65,000 μmol photons m⁻² s⁻¹, with 150 ns rise time and 200 ns fall time. A thermo-electric cooled 10-mm avalanche photodiode (Advance Photonics, Inc) detector is connected to an elbow-shaped light pipe that collects the emission light from the bottom of the sample chamber. The instrument has a sensitivity of 0.01 μg L⁻¹ with 5-10% accuracy. The measurement protocol was optimized to obtain fluorescence saturation (F_m) by a rapid sequence of 80 flashlets, followed by 30 flashlets at exponentially increasing intervals to characterize the relaxation kinetics of fluorescence transients. Instrument blanks were determined with distilled water to account for light scattering within the cuvette, and then with seawater that had been filtered through a Millex AA 0.8 μm Millipore Membrane to account for fluorescence of dissolved organic matter. Water samples for FRRF measurements were collected from Niskin bottles, and immediately placed on ice and kept under low light (5–10 μmol photons m⁻² s⁻¹) for low light adaptation for approximately 30-40 min. Minimal (F_0) and maximal (F_m) fluorescence and the effective absorption cross section (σ_{PSII}) were calculated from each ST saturation curve using LIFT.exe developed at MBARI. Reference and baseline corrections were used to estimate other photosynthetic parameters, including the effective absorption cross section (σ_{PSII}), and the minimum turnover time of PSII photochemistry (τ_{Qa}) (Kolber *et al.* (1998). Functional absorption cross section (σ_{PSII}) was calculated by fitting the fluorescence transient into a theoretical function describing the fluorescence-photosynthesis relationship (Kolber *et al.* 1998).

Two different instruments were used on the two cruises. They differed in the LED array sizes and in the signal attenuation method, but provided similar performance. Samples were either placed into the cuvette via pipettes or dispensed through the cuvette with a peristaltic pump with maximum flow rate of 5 mL min^{-1} . To avoid condensation on the cuvette due to the temperature difference between the cold seawater and the warm laboratory air, the light and cuvette chamber were constantly flushed with dry nitrogen gas.

A PAM submersible unit prototype (SubPAM; Gademann Instruments) was used in bench-top mode. This SubPAM unit differs from previous PAM instruments because it is equipped with a photomultiplier tube (PMT) that enhances the signal, allowing to make measurements in both low and high phytoplankton biomass regimes. Waters samples retrieved from Niskin bottles were placed on ice, and kept under low light ($5\text{--}10 \mu\text{mol photons m}^{-2} \text{ s}^{-1}$) for approximately 30-40 minutes and subsequently measured. The PAM sampling chamber was kept on ice to minimize sample temperature stress. Samples (60 mL) were loaded into the chamber by gravity or by weak pressure from a syringe and measured three times. To obtain F_v/F_m values, the saturation pulse ranged from 0.8 to 1.0 s, and care was taken to insure that the saturation pulse fully achieved the maximum fluorescence.

Seawater blanks

Over 100 filtered seawater blanks (FSW) were measured during the two cruises (Figure 27). Seawater blanks were obtained by filtering samples by applying gentle and constant pressure with a 60 mL syringe through MF-Millipore MCE Membrane Millex AA 0.8 mm filters. The observed FSW blanks ranged from 0.07 – 4.38% of the corresponding F_m signal, with the average of $0.87 \pm 1.38\%$. Blanks were measured on samples with chlorophyll concentrations ranging between 0.28 and $6.16 \mu\text{g}$

L^{-1} and on full profiles. The FRRF was periodically blanked with a DI water sample to account for the cuvette light scattering to monitor for bio-fouling through time, and to determinate whether cuvette cleaning was necessary. The cleaning procedure involved multiple rinses with DI water and scraping with cotton or foam Q-tips.

Light calculations

Light attenuation coefficients (k_d) were calculated according to the following equations:

$$E_z = E_{0^-} \times e^{k_d \times z} \quad (\text{Eq. 15})$$

$$k_d = \frac{\ln E_{0^-}}{\ln E_z} \quad (\text{Eq. 16})$$

where E is the irradiance at depth z , and E_{0^-} is the irradiance below the sea surface. The euphotic zone depth (Z_{eu}) (Eq. 17-19) is defined as the depth at which the irradiance equals 1% of the surface value (E_{0^-}):

$$\frac{E_z}{E_{0^-}} = \frac{1}{100} \quad (\text{Eq.17})$$

$$\frac{\ln 100}{k_d} = Z_{eu} \quad (\text{Eq. 18})$$

$$\frac{4.6}{k_d} = Z_{eu} \quad (\text{Eq. 19})$$

Maps and contour plots of latitudinal sections have been generated with Ocean Data View (Schlitzer 2008). As the sampling along transects did not follow the chronological or geographical order, the data cannot produce a truly synoptic image of the sampled properties, potentially causing smearing of features' signals and trends during the interpolation process. 2 and 3D scatter plots were generated with Grapher 7.4 (Golden Softer Inc.®).

RESULTS

Physical features of surface waters (0-200 m)

During NBP0601 stations were occupied between 74.5 °S, 165.25 °E and 78.65 °S 164.75°W in the Bay of Whales, encompassing most of the polynya over the Ross Sea shelf (Figure 23). Five transects (at 74.5°S, 75.0°S, 76.0°S, 76.5°S, and 77.5°S; Appendix 3; Figures 1-5) and a sixth transect that I will refer to as the IVARS transect (parallel the Ross ice shelf between 168.5°E and 177.8°W) were completed (Appendix 3; Figure 6). Meltwater from sea ice and glacial ice on the west side of the polynya created two shallow water lenses with warmer and fresher characteristics. Mixed layer depths (MLD), defined as the depth in the water column where the density changes from the surface density by an arbitrary incremental difference $\Delta\sigma_t$ ($\Delta\sigma_t = (\rho - 1) 1000 \text{ kg m}^{-3}$). For this region the range of values that have been used in previous studies is from $\Delta\sigma_t = 0.02$ to 0.125. Using a $\Delta\sigma_t$ of 0.05 (kg m^{-3}), MLD varied from extremely shallow (10 m) to very deep (> 175 m) and averaged 36 m. The deepest MLD were found at 74.5° S and along the 77.5 °S transect, while the shallow MLDs were mostly found on the west side of the polynya (Appendix 2; Table 1).

During NBP0608 the surveyed area was smaller, principally due to the higher ice coverage and reduced polynya size. All stations were within 76°S, 170°E and 78°S, 180°. Three full transects were performed at 76.0°S, 76.5°S and 77.5°S (Appendix 3; Figures 7-9), plus the IVARS transect (Appendix 3; Figure 10). Mixed layer depths were calculated based on a $\Delta\sigma_t$ of 0.02 (kg m^{-3}) because the polynya had reduced density variability, and nutriclines appeared to coincide with this $\Delta\sigma_t$. Despite the presence of a few stations with shallow MLD (<10 m) on the western side of the polynya, the average MLD in the polynya during the spring was about 52 m, approximately 25 m deeper than in the summer. Long *et al.* (submitted) calculated mixed layer depth for the same data set applying as an additional criteria the Brunt-Väisälä or buoyancy frequency ($N^2 = -(g/\rho)d\rho/dz$), which provides a

measure of the strength of stratification and helped them identify the most appropriate $\Delta\sigma_t$ value to corroborate the calculation of MLD depths; result in Long *et al.* (submitted) are comparable to the one calculated here. Moreover surface salinity data during NBP0608 do not show sufficiently big variability or temporal trends that would indicate significant freshwater contributions to the surface waters. Mean sea surface temperatures ($-1.7\pm 0.2^\circ\text{C}$) during the cruise were too cold to allow melting of significant quantities of ice; and temperature-induced buoyancy effects were minimal. Similarly, the euphotic zone (depth of 1% surface irradiance) was deeper during the spring than in the summer and averaged 34 m, with a maximum of 82 m, while in the summer the deepest Z_{eu} was at 58 m (Appendix 2; Table 1 and 2).

Chlorophyll *a* standing stocks, pigment and nutrient concentrations

During NBP0601 high chlorophyll *a* standing stocks observed, ranging from 0.034 to 7.47 $\mu\text{g L}^{-1}$ (average $2.13 \pm 0.86 \mu\text{g L}^{-1}$), and were confined to low density waters in close proximity to receding ice edges. Along the 75°S transect silicate concentrations were consistently depleted in the upper 25-30 m, corresponding to the presence of warmer waters (0 and +2°C) (Appendix 3; Figure 2). Along the 76.0°S and 76.5°S transects, the chlorophyll maximum deepened and two distinct assemblages were identified, with the western side dominated by diatoms and the eastern side by *P. antarctica* (Appendix 3; Figures 3 and 4). Higher biomass, up to 6 $\mu\text{g L}^{-1}$ chl *a*, was found along the 77.5°S transect at the end of December (Dec. 29), with the assemblage dominated by *P. antarctica*. The biomass decreased to about to 2 $\mu\text{g L}^{-1}$ chl *a* two weeks later in the same location (Appendix 3; Figure 5). Ratios of Fuco:19-Hex > 1 indicated the presence of diatoms, which also was accompanied by significant silicate reduction in the euphotic zone. The highest silicate removal occurred at the most western stations (88, 98, 93 and 94) in the polynya, where the water temperatures were the highest (between 1 and 2.5°C) and which had intermediate chlorophyll concentrations of 1.5 to 2.4 $\mu\text{g L}^{-1}$.

Diatom presence in this region was indicated by high ratio of Fuco:Chl *a* and high silicate removal, while *P. antarctica* presence was indicated by high 19-Hex:chlorophyll *a* ratios (DiTullio and Smith 1995).

During NBP0608 we found relatively high biomass along the IVARS transect in proximity of the Ross Ice Shelf. This bloom was dominated by *P. antarctica* colonies, with chlorophyll concentrations reaching $7 \mu\text{g L}^{-1}$ and with up to $2 \mu\text{g L}^{-1}$ of chl *a* in the greater than $20 \mu\text{m}$ size fraction. The 77°S transect was characterized by relatively low biomass, with slight accumulation in the low density surface waters ($\sigma\text{-t} < 27.78 \text{ kg m}^{-3}$) at 174°E ($\sim 2.5 \mu\text{g L}^{-1}$ chl *a*) and 177°E ($\sim 3 \mu\text{g L}^{-1}$ chl *a*) (in Appendix 3; Figure 9). The northern transect at 76.5°S , close to the receding ice pack, displayed higher biomass in the top 50 m of the water column along the entire transect relative to the adjacent lines. Significant accumulation of biomass was observed at most eastern part of the transect at 178°W . Much lower chl *a* concentrations were observed along the 77.0°S transect, while the highest phytoplankton abundances were found between 175°E and 179°E and west of 172°E in proximity of the Ross Sea ice shelf, with concentrations up to $6 \mu\text{g L}^{-1}$ chl *a* and negligible dissolved silicate uptake (Appendix 3; Figure 10).

FRRF and PAM

Extensive testing over a full range of depths and chlorophyll concentrations demonstrated that dissolved fluorescence material contributed less than 1% to the total fluorescence signal. Contrary to Cullen's and Davis (2003) findings, the FSW had no significant effect on the F_v/F_m value. Similar results regarding the effect of FSW blanks were also shown for a larger dataset covering tropical Pacific Ocean by Behrenfeld *et al.* (2006b), in which FSW fluorescence values were negligible relative to total sample fluorescence, even in highly oligotrophic waters.

On NBP0601 the upper 50 m populations exhibited reduced photosynthetic efficiencies, with $F_v/F_m < 0.50$, possibly due to photoinhibition. The depth of the photoinhibition increased with latitude and MLD (Appendix 3; Figures 1-5). Quantum yields in the top 10 m averaged 0.35 (S.D. ± 0.054 ; $n=106$), and in the upper one m F_v/F_m ranged between 0.23 and 0.49. Fluorescence quantum yields displayed nutrient-like profiles during NBP0608, and only mild photoinhibition at the surface was observed, with an average F_v/F_m of 0.48 (S.D. ± 0.048 $N=66$) in the top 10 m. On both cruises, lower quantum yields ($F_v/F_m \sim 0.30$) were measured in the upper water column at locations dominated by diatoms (as suggested by lower dissolved silicate and or pigment ratios). Higher quantum yields ($F_v/F_m > 0.55$) were usually found below the mixed layer. On NBP0601 the F_v/F_m was highly correlated with dissolved macronutrients (Figure 29 c, d) and temperature (Figure 28 f). No clear relationship was found between fluorescence quantum yields and other parameters on the spring cruise (Figure 29). Absorption cross sections were significantly greater on NBP0601 (average $\sigma_{PSII} = 969 \text{ \AA}^2 \text{ quanta}^{-1}$) than on NBP0608 (average $\sigma_{PSII} = 809 \text{ \AA}^2 \text{ quanta}^{-1}$), and the difference increased when only the surface values are compared ($1003 \text{ \AA}^2 \text{ quanta}^{-1}$ for NBP0601 vs. $826 \text{ \AA}^2 \text{ quanta}^{-1}$ for NBP0608) (Figure 30).

Discrete chlorophyll a concentrations were regressed against CTD fluorometric values and discrete FRRF F_m measurements during NBP0601 (Figure 25), and with PAM F_m for NBP0608 (Figure 26). The correlation of chl a and CTD fluorescence and with the MBARI FRRF were similar ($r^2=0.770$; $n=580$, and $r^2=0.774$; $n=546$), while in the spring the MBARI FRRF data correlated against discrete chl a with a correlation coefficient ($r^2=0.877$; $n=359$), higher than the CTD fluorometer ($r^2=0.760$; $n=463$) and the PAM ($r^2=0.009$; $n=379$). Correlation between PAM and MBARI FRRF F_m was extremely weak and insignificant ($r^2=0.09$; $n=379$). Such weak correlation is surprising and unexpected, and at this time without a satisfactory explanation.

DISCUSSION

Deep-water formation in the Ross Sea (Jacobs *et al.* 1970) and the sensitivity of the region to climate change and fluctuations (Sarmiento and Orr 1991, Sarmiento *et al.* 1998) extends the potential significance of the polynya's biogeochemical processes. The Ross Sea biogeochemistry is strongly controlled by the algal assemblages' temporal evolution and abundance. Polynya blooms are at times dominated by *P. antarctica* and other times by diatoms, but in general these two assemblages are present together at a variable relative abundance. This is evident from the disappearance ratios of nitrogen to silica that reflects the lack of complete dominance of diatoms or *P. antarctica*. Given the distinctive differences these two taxa have on biogeochemical cycles of nitrogen, phosphorus, silica, sulfur (Nelson and Smith 1986, DeMaster *et al.* 1992, Arrigo *et al.* 1999, Smith *et al.* 2006), and most importantly, carbon (Smith and Asper 2001, Smith *et al.* 2006), it is important to understand the factors that control their presence, abundance, growth rates, and photosynthetic characteristics. Diatoms and *P. antarctica* differ in their impacts on the biological pump in the Ross Sea polynya due different export rates and modes (Sweeney *et al.* 2000b, Gowing *et al.* 2001). They are selectively grazed by different organisms, and hence play different roles in supporting local ecosystems (Ducklow 2008). Despite the well recognized role of *Phaeocystis* as a critical genus for its influences on biogeochemical cycles food webs and climate (Wassmann 1994, Verity and Smetacek 1996), the true nature and contribution amount of carbon export from the euphotic zone and benthic input by *P. antarctica* in the Ross Sea remains controversial (Gowing *et al.* 2001, Accornero *et al.* 2003, Reigstad and Wassmann 2007), as blooms mostly occur in deeply mixed water column and sedimentation rates appear to be much higher than in other oceanic regions (Wassmann 1994). High sedimentation and export rates from the euphotic zone of *P. antarctica* in the Ross Sea have been suggested (DiTullio *et al.* 2000, Asper and Smith 2003), although has been also reported that these cells are less inclined to form aggregates than diatoms and therefore do not contribute significantly in direct carbon export as

a result of direct sedimentation or aggregate formation, but possibly instead by mucus flocs (Passow and Wassmann 1994) and by repackaging by grazers (Gowing *et al.* 2001, Shields and Smith 2008). Diatoms are thought to have a high potential for carbon export by direct sinking due to their lack of motile flagella and their dense silica frustules, but in the polynya grazing and repackaging is still considered the main carbon export pathway for this genus in the polynya (Hopkins 1987, DeMaster *et al.* 1992, Dunbar *et al.* 1998).

In this study, we did not identify a single, dominant factor responsible for selecting diatoms or *P. antarctica* in the Ross Sea polynya. Macronutrients never limit production (Smith and Harrison 1991); instead, a hypothesis that phytoplankton spatial and temporal distribution is driven by iron and light availability and by differences in photophysiology and resource utilization (Olson *et al.* 2000, van Hilst and Smith 2002) appears to be strongly supported. Extensive probing of photophysiological responses of phytoplankton assemblages during the surveys combined with the broad suite of core measurements and ancillary data shows the diatom-dominated blooms are mostly confined to shallow mixed layer depths and warmer waters during summer. Vertical structure of variable fluorescence derived parameters, highlighted the persistent photoinhibition of subsurface phytoplankton population, which implicates suboptimal photosynthetic and primary production rates during the summer (Smith *et al.* 2000), while in the spring the only instances of such photoinhibition were found along the continental ice shelf in correspondence of warmer waters and higher biomass possibly indicating a combined irradiance and micronutrient co-limitation (Sunda and Huntsman 1997, Boyd *et al.* 1999, Maldonado *et al.* 1999) or stronger UV irradiation effect (Neale *et al.* 1998, Jeffrey *et al.* 2006). The latter being the probable cause of the extensive summer subsurface photoinhibition (Jeffrey *et al.* 2006). The consistent high photosynthetic quantum yield below the MLD both in the spring and summer suggests full recovery from the subsurface photoinhibition for the organisms sunken or mixed below the MLD as well. The fluorescence quantum yield during the summer, when

macronutrients can be significantly depleted in the upper water column, correlated with lower values where nutrients were most depleted. Due to the never limiting macronutrient concentrations (Smith and Harrison 1991), this result corroborates the idea of a likely irradiance and iron co-limitation (Moore *et al.* 2007). Correlation of vertical distribution of F_v/F_m during the spring cruise with temperature distribution, with lower values in warmer waters also is most likely due to the same type of co-limitation given that warmer waters were confined to surface layers in which nutrients were more depleted and irradiance was higher. The nutrients and temperature range during the spring cruise were very narrow, while the photosynthetic quantum yields vertical structure was homogenous with consistently high values reflecting the mostly deeply mixed polynya waters and indicating no major stressor or limiting photosynthetic factor.

There is no clear relationship between iron concentrations and phytoplankton blooms and/or photophysiology in our data despite a well established functional relationship between iron abundance and photosynthetic quantum yields and productivity (Olson *et al.* 2000, Timmermans *et al.* 2001, Behrenfeld *et al.* 2006a, Moore *et al.* 2007). Nonetheless, the lack of correlation between iron concentrations and phytoplankton photophysiology in our study can be explained in several ways. First, the relative scarcity of iron measurements relative to other variables makes this data set only partially representative of very heterogeneous distribution of iron concentrations in the polynya. Furthermore, iron sources and iron recycling processes in the polynya are not well understood, making the assessment of the spatial and temporal distribution of bioavailable iron difficult, especially given the potential sources such as melting icebergs, subsurface hydrothermal vents, local upwelling, and intrusions of modified circumpolar deep water. As a result, iron concentrations in the polynya are driven by sources which vary in time and space, as well as by net uptake and regeneration. The related processes are regulated over time scales much longer than those controlling F_v/F_m and phytoplankton growth, particularly at low temperatures. Therefore, the lack of correlation between

iron concentration and fluorescence quantum yields is not surprising considering also that part of the fluorescence response is due to many other processes related to the hydrographic regime such as vertical density structure and mixing as well the light history.

Nonetheless, the high quantum yields and high biomass accumulation observed in November during NBP0608 cruise suggests relatively high growth rates and primary productivity combined with low grazing and loss rates, as demonstrated previously (Caron *et al.* 2000). Diatom dominance in summer in shallow mixed layers with increased stratification and higher temperatures is consistent with their ability to adapt to higher irradiance levels, whereas *P. antarctica* dominated in deeper mixed layers in spring when iron availability is sufficient to satisfy the substantial prymnesiophyte iron requirement (Coale *et al.* 2004, Sedwick *et al.* 2007). Higher functional absorption cross section found in correspondence of diatom dominated surface waters during the summer is an indicator of possible nutrient stress (Berges *et al.* 1996, Holeyton *et al.* 2005). As shown in the previous chapter, *P. antarctica* had faster rates of photorecovery, potentially conferring an advantage in the deeply mixed waters. In summer, especially in shallow mixed layers with fewer light fluctuations, diatoms have a distinct advantage and are selected by their higher photosynthetic capacity and their higher iron affinity (and lower absolute demand). These characteristics allow diatoms to efficiently utilize the micronutrients at lower concentrations, while potentially displaying faster growth rates (Smith *et al.* 1999) with less photoadaptation stress. Being able to link the taxonomic photophysiological responses to the measured photosynthetic activity in the context of the environmental conditions is a significant step towards a better understanding of the phytoplankton dynamics in the polynya. The CORSACS data presented here provides a comprehensive overview of physical, chemical and biological conditions and processes in the Ross Sea Polynya during the austral spring and summer, a theoretical basis of the dynamics of the Ross Sea Shelf waters, and insights into the factors driving the phytoplankton blooms' temporal evolution. Further measurements of iron concentrations in the Ross

Sea will give insight on the sources and mechanisms controlling the bioavailable iron and facilitate the interpretation of photophysiological data.

The study and dataset here presented are invaluable when considering the many difficulties of remote sensing techniques for this area. For example, nutrient fields for the polynya and for any other oceanic regions are impossible to retrieve remotely, hydrography can only be estimated from remotely sensed ice and wind data and with the support of numerical circulation models, and chlorophyll concentrations and fluorescence measurements from satellite can be limited for this region by extensive cloud and ice coverage. Despite these limitations, the Ross Sea has been the object of research and expeditions since the mid-1800s, yet there are still many unanswered questions, especially those involving the characterization of the physical and biological interactions in the polynya, their effects on the biogeochemistry of the region, and the areas influence and connection to other oceanic regions. These unanswered questions are even more compelling when considering the climate changes that the Southern Ocean and in particular the Ross Sea is undergoing. Understanding phytoplankton communities' evolution and distributions in the Ross Sea is still unclear and such understanding is important to better estimate the region's productivity, food web and carbon fluxes.

Table 3. Cruises number of stations and available variable fluorescence measurements synthesis.

	Start sampling	End sampling	# CTD casts	# CTD Stations	# FRR Samples	# FRR Stations	#PAM Samples	# PAM Stations
NBP0601	12/27/05	1/23/06	102	74	668	56	-	-
IVARS	1/31/05	2/1/06	12	12	132	11	-	-
NBP0608	11/06/06	12/06/06	72	43	382	31	408	35
Total			188		1182	98	408	35

Table 4. Minimum, maximum, mean and standard deviation for main physical, chemical and biological water properties for cruises NBP0601 and NBP0608.

Variable	Cruise				Cruise			
	NBP0601				NBP0608			
	Min	Max	Mean	SD	Min	Max	Mean	SD
Temperature (°C)	-1.95	2.75	-0.73	0.86	-2.08	-0.97	-1.78	0.13
Salinity (psu)	33.893	34.805	34.376	0.161	33.676	34.794	34.488	0.10
Sigma (kg m^{-3})	27.069	27.981	27.633	0.151	27.544	28.016	27.766	0.80
PAR ($\mu\text{E m}^{-2} \text{s}^{-1}$)	0	1600	58	165	0	1347	52	139
Mixed layer depth (m)	10	179	36	26	7	317	65	52
Euphotic depth (m)	9	58	26	9	17	82	34	13
GFF Chl a ($\mu\text{g L}^{-1}$)	0.034	7.47	2.13	0.86	0.00	7.29	2.11	1.61
>20 mm Chl a ($\mu\text{g L}^{-1}$)	0.013	4.67	0.96	0.82	0.00	2.17	0.46	0.42
Nitrate (μM)	2.5	32.7	23.4	5.8	23.0	33.6	28.7	1.8
Phosphate (μM)	0.11	2.79	1.72	0.43	1.64	2.55	2.08	0.15
Silicate (μM)	30	106	75	9.5	75	93	82	2.8

Table 5. Correlations between fluorescence quantum yields (F_V/F_M), dissolved macronutrients and temperature for NBP0601. (a=intercept, m=slope).

	Units	mean	S.D.	min	max	a	m	r^2
F_V/F_M vs.	-	0.451	0.093	0.207	0.631			
Chl α	$\mu\text{g L}^{-1}$	1.695	1.464	0.01	7.380	0.497	-0.026	0.400
N	μM	24.027	5.473	11.924	32.774	0.181	0.013	0.737
Si	μM	75.667	9.688	43.97	94.115	0.036	0.006	0.668
P	μM	1.774	0.428	0.469	2.790	0.179	0.164	0.752
T	$^{\circ}\text{C}$	-0.792	0.818	-1.924	1.991	0.555	-0.086	0.752

Table 6. Correlation between fluorescence quantum yields (F_V/F_M), dissolved macronutrients and temperature for NBPO608. (a=intercept, m=slope).

	Units	mean	S.D.	min	max	a	m	r^2
F_V/F_M vs.		0.533	0.05	0.355	0.646			
Chl <i>a</i>	$\mu\text{g L}^{-1}$	2.528	1.741	0.01	7.296	0.574	-0.016	
N	μM	28.238	1.875	23.0	32.8	0.073	0.0162	0.038
Si	μM	81.769	2.83	75.86	93.56	0.442	0.001	0.06
P	μM	2.039	0.152	1.641	2.365	0.203	0.160	0.24
T	$^{\circ}\text{C}$							

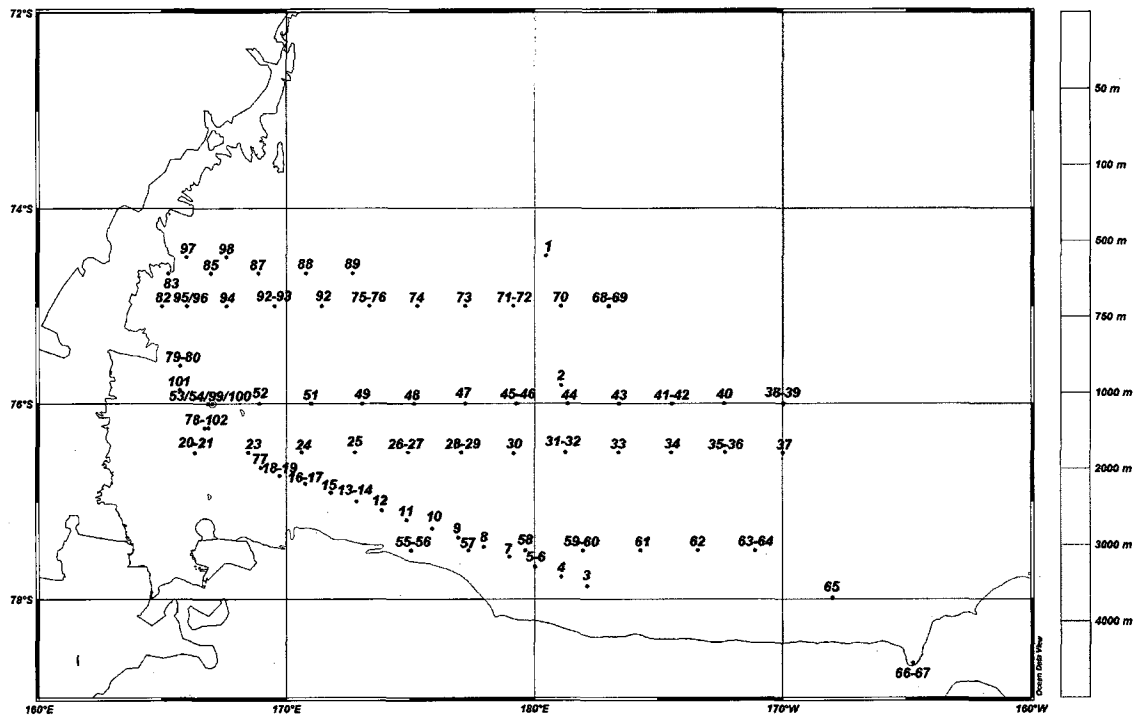


Figure 23. Map showing bathymetry of the study area and station locations of R/V N.B. Palmer cruise NBP0601 sampled between December 27, 2005 and January 23, 2006.

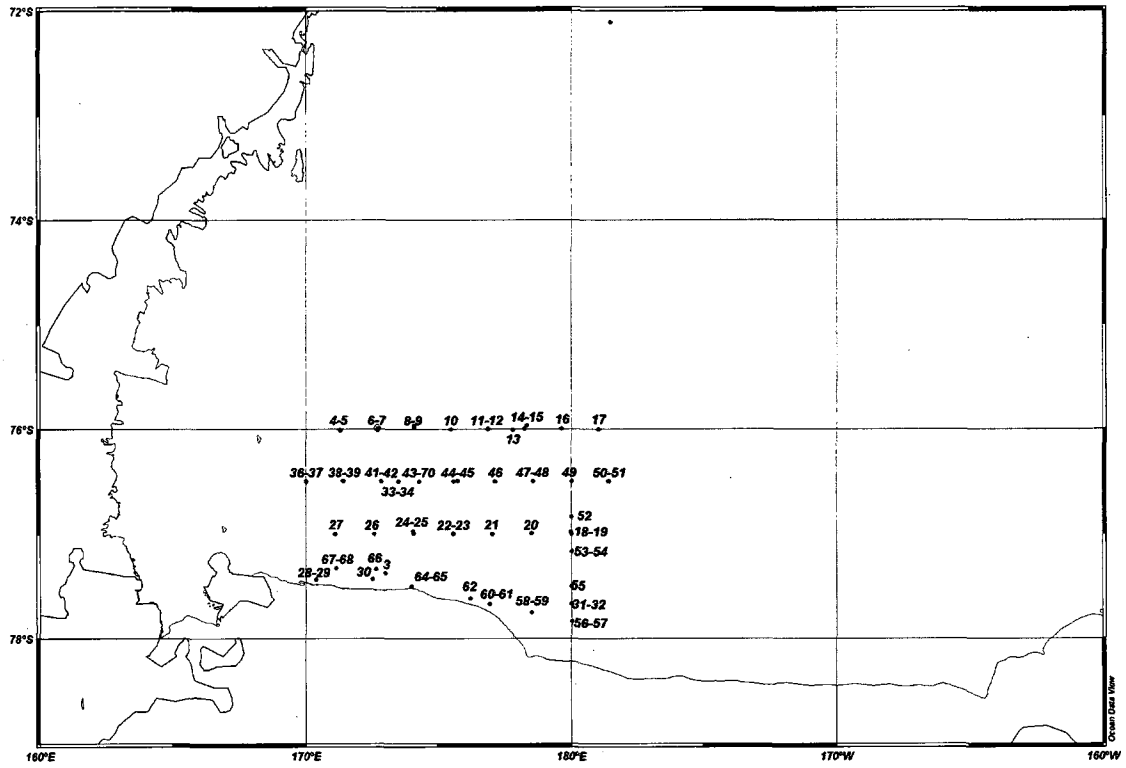


Figure 24. Map showing bathymetry of the study area and station locations of R/V N.B. Palmer cruise NBP0601 sampled between November 6 and December 6, 2006.

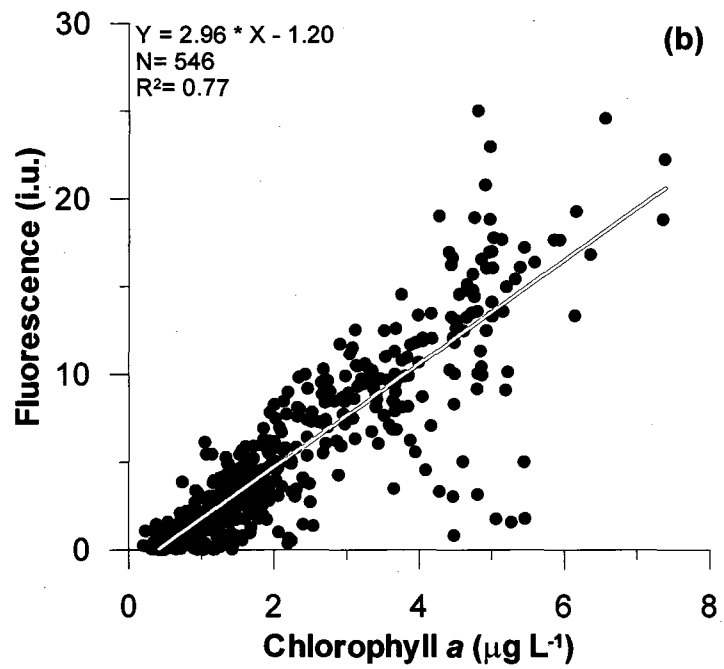
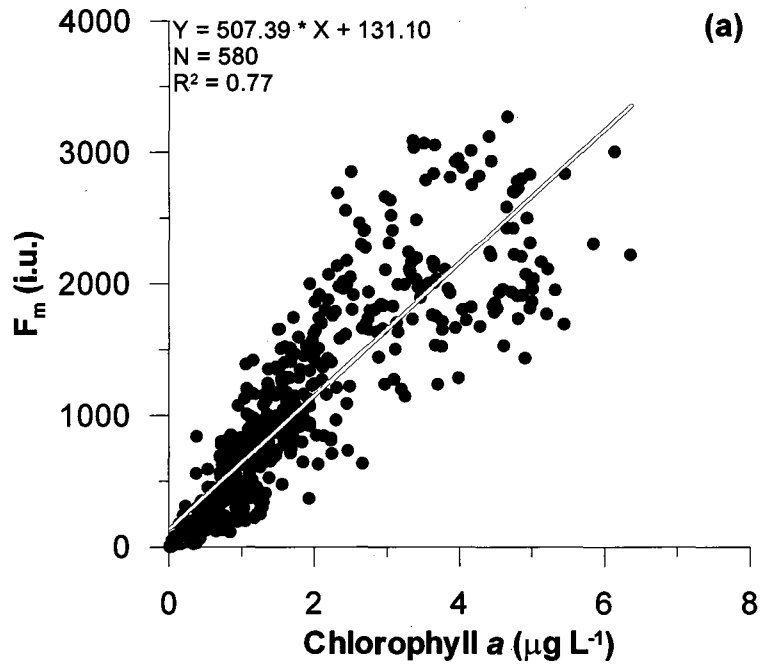


Figure 25. Scatter plot showing relationship between chlorophyll a concentration and MBARI F_m (a) and ship underway Turner AU 10 Fluorometer fluorescence (b) for cruise NBP0601.

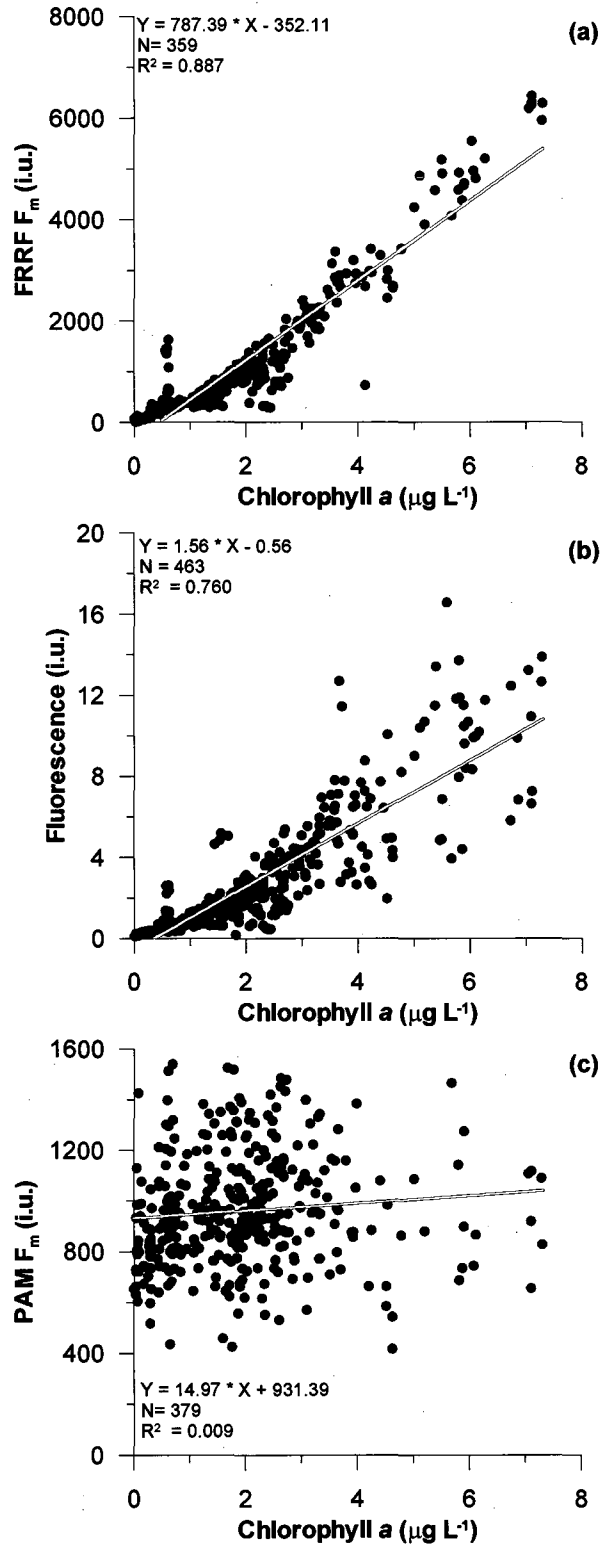


Figure 26. Scatter plot of chlorophyll *a* concentration versus MBARI F_m (a), versus ship underway Turner AU 10 Fluorometer fluorescence (b) and PAM F_m (c) for cruise NBP0608.

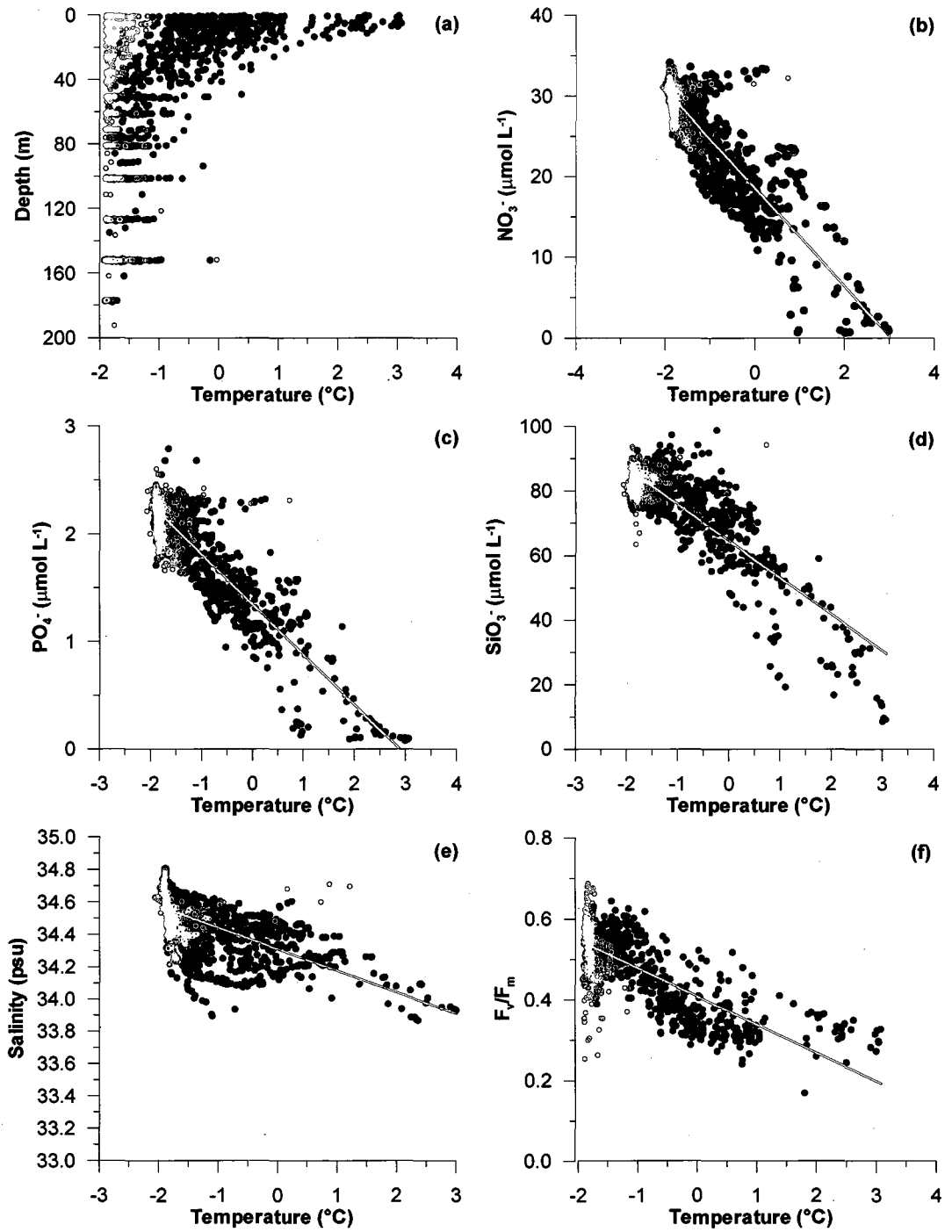


Figure 28. Scatter plots of water column temperature versus depth (a), nitrate (b), phosphate (c), silicate (d), salinity (e), and fluorescence quantum yields (f) for NBP0601(•) and NBP0608 (○).

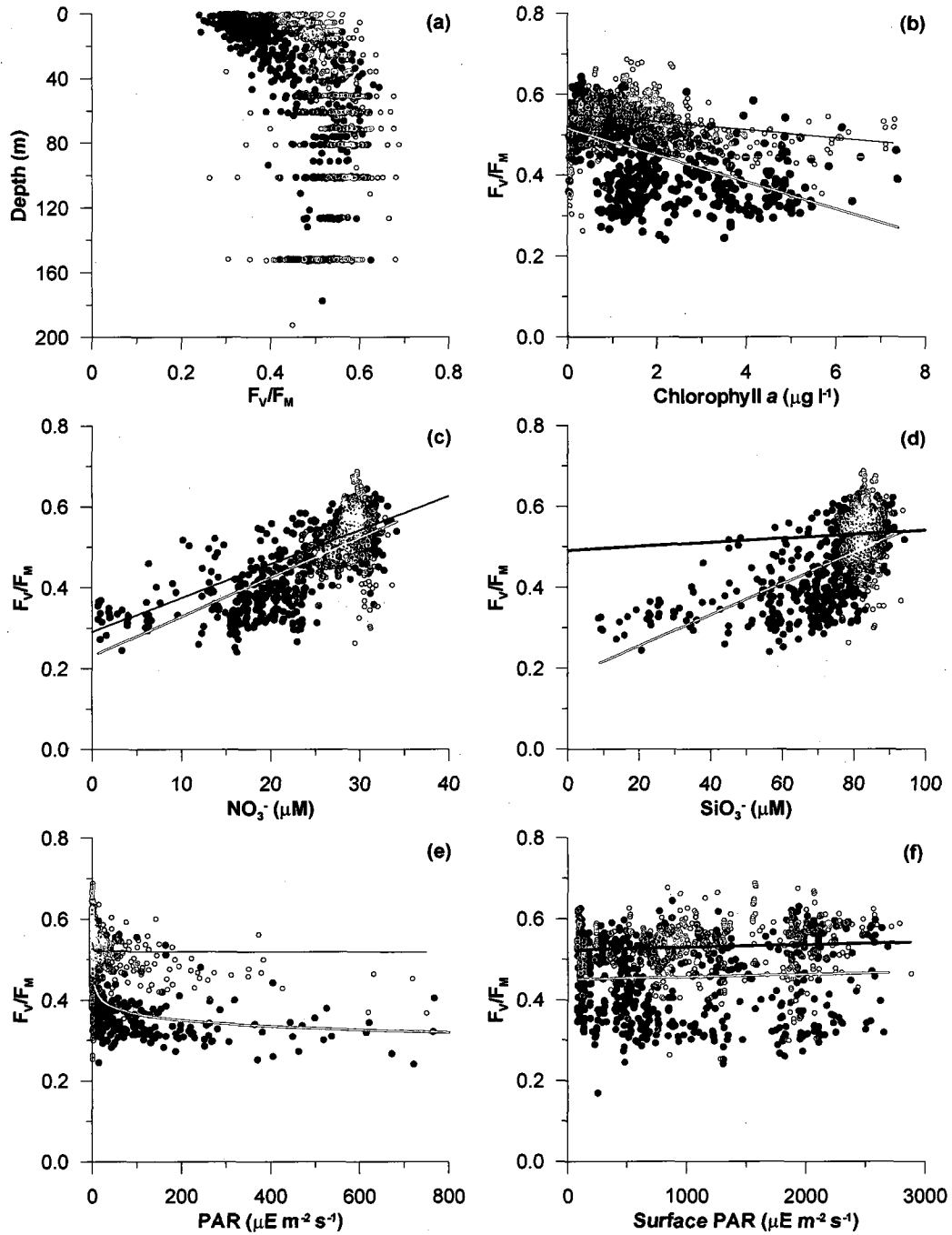


Figure 29. Scatter plots of water column fluorescence quantum yields versus depth (a), nitrate (b), phosphate (c), silicate (d), salinity (e), and fluorescence quantum yields (f) for NBP0601 (•) and NBP0608 (◦). Regression fit for NBP0601 (red line) and NBP0608 (black line).

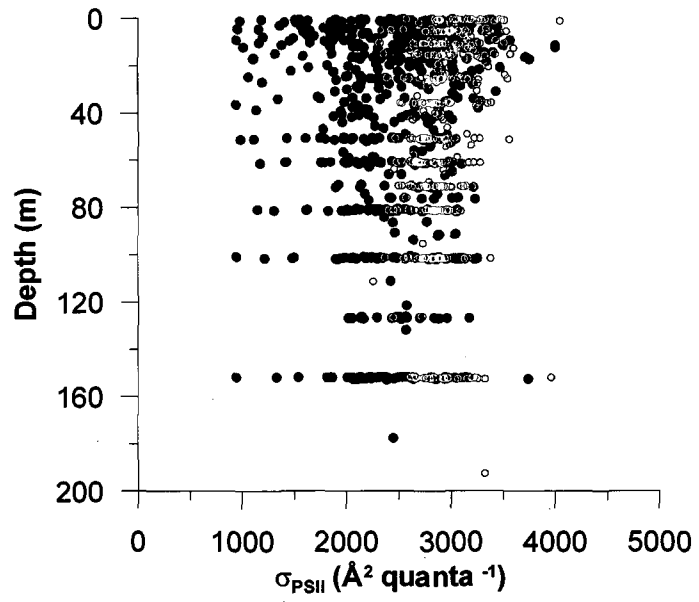


Figure 30. Distribution in water column of absorption cross section for NBP0601 (•), and for NBP0608 (○).

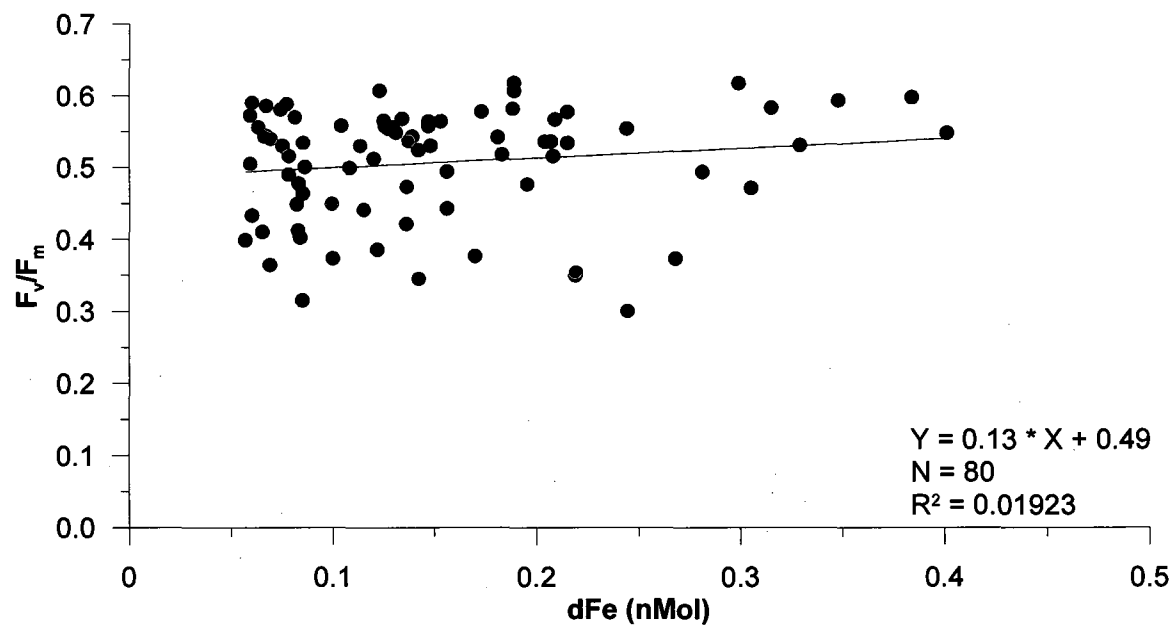


Figure 31. Scatter plots of dissolved iron vs. fluorescence quantum yields for NBP0601 (•) and NBP0608 (•).

LITERATURE CITED

- Accornero A., Manno C., Arrigo K. R., Martini A., Tucci S. 2003. The vertical flux of particulate matter in the polynya of Terra Nova Bay. Part I. Chemical constituents. *Antarctic Science* 15:119-132 doi:10.1017/S0954102003001111
- Arrigo K. R., Robinson D. H., Worthen D. L., Dunbar R. B., DiTullio G. R., VanWoert M., Lizotte M. P. 1999. Phytoplankton community structure and the drawdown of nutrients and CO₂ in the Southern Ocean. *Science* 283:365-367
- Arrigo K. R., Worthen D. L., Robinson A. R. 2003. A coupled ocean-ecosystem model of the Ross Sea: 2. Iron regulation of phytoplankton taxonomic variability and primary production. *Journal of Geophysical Research* 108:3231
- Asper V. L., Smith W. O., Jr. 2003. Abundance, distribution and sinking rates of aggregates in the Ross Sea, Antarctica. *Deep Sea Research I* 50:131-150
- Behrenfeld M. J., Kolber Z. S. 1999. Widespread Iron Limitation of Phytoplankton in the South Pacific Ocean. *Science* 283:840-843
- Behrenfeld M. J., Worthington K., Sherrell R. M., Chavez F. P., Strutton P., McPhaden M., Shea D. M. 2006a. Controls on tropical Pacific Ocean productivity revealed through nutrient stress diagnostics. *Nature* 442:1025-1028
- Behrenfeld M. J., Worthington K., Sherrell R. M., Chavez F. P., Strutton P., McPhaden M., Shea D. M. 2006b. Controls on tropical Pacific Ocean productivity revealed through nutrient stress diagnostics. *Nature* 442:1025
- Berges J. A., Charlebois D. O., Mauzerall D. C., Falkowski P. G. 1996. Differential Effects of Nitrogen Limitation on Photosynthetic Efficiency of Photosystems I and II in Microalgae. *Plant Physiol.* 110:689-696 doi: 10.1104/pp.110.2.689
- Boyd P., LaRoche J., Gall M., Frew R., McKay R. M. L. 1999. Role of iron, light, and silicate in controlling algal biomass in subantarctic waters SE of New Zealand. *Journal of Geophysical Research* 104:13395-13408 doi: 10.1029/1999jc900009
- Boyd P. W., Watson A. J., Law C. S., Abraham E. R., Trull T., Murdoch R., Bakker D. C. E., Bowie A. R., Buesseler K. O., Chang H., Charette M., Croot P., Downing K., Frew R., Gall M., Hadfield M., Hall J., Harvey M., Jameson G., LaRoche J., Liddicoat M., Ling R., Maldonado M. T., McKay R. M., Nodder S., Pickmere S., Pridmore R., Rintoul S., Safi K., Sutton P., Strzepek R., Tanneberger K., Turner S., Waite A., Zeldis J. 2000. A mesoscale phytoplankton bloom in the polar Southern Ocean stimulated by iron fertilization. *Nature* 407:695-702
- Buesseler K. O., Barber R. T., Dickson M.-L., Hiscock M. R., Moore J. K., Sambrotto R. 2003. The effect of marginal ice-edge dynamics on production and export in the Southern Ocean along 170°W. *Deep Sea Research II* 50:579-603

- Caron D. A., Dennett M. R., Lonsdale D. J., Moran D. M., Shalapyonok L. 2000. Microzooplankton herbivory in the Ross Sea, Antarctica. *Deep Sea Research II* 47:3249-3272
- Claustre H., Kerhervé P., Marty J. C., Prieur L., Videau C., Hecq J. H. 1994. Phytoplankton dynamics associated with a geostrophic front: ecological and biogeochemical implications. *Journal of Marine Systems* 52:711–742
- Coale K. H., Johnson K. S., Chavez F. P., Buesseler K. O., Barber R. T., Brzezinski M. A., Cochlan W. P., Millero F. J., Falkowski P. G., Bauer J. E., Wanninkhof R. H., Kudela R. M., Altabet M. A., Hales B. E., Takahashi T., Landry M. R., Bidigare R. R., Wang X., Chase Z., Strutton P. G., Friederich G. E., Gorbunov M. Y., Lance V. P., Hilting A. K., Hiscock M. R., Demarest M., Hiscock W. T., Sullivan K. F., Tanner S. J., Gordon R. M., Hunter C. N., Elrod V. A., Fitzwater S. E., Jones J. L., Tozzi S., Koblizek M., Roberts A. E., Herndon J., Brewster J., Ladizinsky N., Smith G., Cooper D., Timothy D., Brown S. L., Selph K. E., Sheridan C. C., Twining B. S., Johnson Z. I. 2004. Southern Ocean Iron Enrichment Experiment: Carbon Cycling in High- and Low-Si Waters. *Science* 304:408-414
- Cullen J. J., Davis R. F. 2003. The blank can make a big difference in oceanographic measurements. *Limnology and Oceanography Bulletin* 12:29-35
- de Baar H. J. W., de Jong J. T. M., Nolting R. F., Timmermans K. R., van Leeuwe M. A., Bathmann U., Rutgers van der Loeff M., Sildam J. 1999. Low dissolved Fe and the absence of diatom blooms in remote Pacific waters of the Southern Ocean. *Marine Chemistry* 66:1-34
- DeMaster D. J., Dunbar R. B., Gordon L. I., Leventer A. R., Morrison J. M., Nelson D. M., Nittrouer C. A., Smith W. O., Jr. 1992. Cycling and accumulation of biogenic silica and organic matter in high-latitude environments: the Ross Sea. *Oceanography* 5:146-153
- Dennett M. R., Mathot S., Caron D. A., Smith W. O., Jr., Lonsdale D. J. 2001. Abundance and distribution of phototrophic and heterotrophic nano- and microplankton in the southern Ross Sea. *Deep Sea Research II* 48:4019-4037
- Dinniman M. S., Klinck J. M., Smith W. O., Jr. 2003. Cross-shelf exchange in a model of the Ross Sea circulation and biogeochemistry. *Deep Sea Research II* 50:3103-3120
- DiTullio G. R., Smith W. O., Jr. 1995. Relationship between dimethylsulfide and phytoplankton pigment concentrations in the Ross Sea, Antarctica. *Deep Sea Research I* 42:873-892
- DiTullio G. R., Grebmeier J. M., Arrigo K. R., Lizotte M. P., Robinson A. R., Leventer A., Barry J. P., VanWoert M. L., Dunbar R. B. 2000. Rapid and early export of *Phaeocystis antarctica* blooms in the Ross Sea, Antarctica. *Nature* 404:595-598
- DiTullio G. R., Geesey M. E. 2002. Photosynthetic pigments in marine algae and bacteria In: Bitton G. (ed) *The encyclopedia of environmental microbiology*. John Wiley & Sons, New York, 2453–2470

- Ducklow H. 2008. Microbial services: challenges for microbial ecologists in a changing world. *Aquatic Microbial Ecology* 53:13-19
- Dunbar R. B., Leventer A. R., Mucciarone D. A. 1998. Water column sediment fluxes in the Ross Sea, Antarctica: Atmospheric and sea ice forcing. *Journal of Geophysical Research-Oceans* 103:30741-30759
- El-Sayed S. Z., Biggs D. C., Holm-Hansen O. 1983. Phytoplankton standing crop, primary productivity, and near-surface nitrogenous nutrient fields in the Ross Sea, Antarctica. *Deep Sea Research* 30:871-886
- Falkowski P. G., Wyman K., Ley A. C., Mauzerall D. 1986. Relationship of steady-state photosynthesis to fluorescence in eucaryotic algae. *Biochimica et Biophysica Acta* 849:183-192
- Garrison D. L., Jeffries M. O., Gibson A., Coale S. L., Neenan D., Fritsen C., Okolodkov Y. B., Gowing M. M. 2003. Development of sea ice microbial communities during autumn ice formation in the Ross Sea. *Marine Ecology-Progress Series* 259:1-15
- Genty B., Briantais J. M., Baker N. R. 1989. The relationship between the quantum yield of photosynthetic electron transport and quenching of chlorophyll fluorescence. *Biochimica et Biophysica Acta* 990:87-92
- Gieskes W. W. C., Kraay G. W. 1986. Analysis of phytoplankton by HPLC before, during and after mass occurrence of the microflagellate *Corymbellus aureus* during the spring bloom in the open northern North Sea in 1983. *Marine Biology* 92:45-52
- Goffart A., Catalano G., Hecq J. H. 2000. Factors controlling the distribution of diatoms and *Phaeocystis* in the Ross Sea. *Journal of Marine Systems* 27:161-175
- Gowing M. M., Garrison D. L., Kunze H. B., Winchell C. J. 2001. Biological components of Ross Sea short-term particle fluxes in the austral summer of 1995-1996. *Deep Sea Research I* 48:2645-2671
- Holeton C. L., Nedelec F., Sanders R., Brown L., Moore C. M., Stevens D. P., Heywood K. J., Statham P. J., Lucas C. H. 2005. Physiological state of phytoplankton communities in the Southwest Atlantic sector of the Southern Ocean, as measured by fast repetition rate fluorometry. *Polar Biology* 29:44-52
- Hopkins T. L. 1987. Midwater food web in McMurdo Sound, Ross Sea, Antarctica. *Marine Biology* 96:93-106
- Hu S., Smith W. O., Jr. 1998. The effects of irradiance on nitrate uptake and dissolved organic nitrogen release by phytoplankton in the Ross Sea. *Continental Shelf Research* 18:971-990
- Jacobs S. S., Amos A. F., Bruchhausen P. 1970. Ross-Sea Oceanography and Antarctic Bottom Water Formation. *Deep Sea Research* 17:935-962

- Jacobs S. S., Giulivi C. F. 1998. Interannual ocean and sea ice variability in the Ross Sea, in Ocean, Ice, and Atmosphere. In: Jacobs S. S., Weiss R. F. (eds), Vol 75. AGU, Washington DC, 83-99
- Jahnke J. 1989. The light and temperature dependence of growth rate and elemental composition of *Phaeocystis globosa scherfell* and *P. poucheti* (Har.) Lagerh. in batch cultures. Netherlands Journal of Sea Research 23:15-21
- Jeffrey S. W. 1980. Algal pigment systems. In: Falkowski P. (ed) Primary Productivity in the Sea. Plenum, New York, 35-58
- Jeffrey W. H., Pakulski J. D., Connelly S., Baldwin A. J., Karentz D., Phillips-Kress J., Sobrino C., Franklin L., Neale P. J. 2006. Effects of Ultraviolet Radiation on Bacterioplankton Production in the Ross Sea, Antarctica. EOS, transactions, American Geophysical Union 87
- JGOFS 1994. Protocols for the Joint Global Ocean Flux Study (JGOFS) core measurements, Vol 24. UNESCO, Paris
- Johnson K. S., Gordon R. M., Coale K. H. 1997. What controls dissolved iron concentrations in the world ocean? Marine Chemistry 57:137-161
- Kautsky H., Hirsch A. 1931. Neue Versuche zur Kohlensäureassimilation. Naturwissenschaften 19:964-964
- Kolber Z. S., Wyman K. D., Falkowski P. G. 1990. Natural variability in photosynthetic energy conversion efficiency: A field study in the Gulf of Maine. Limnology and Oceanography 35:72-79
- Kolber Z. S., Barber R. T., Coale K. H., Fitzwater S. E., Greene R. M., Johnson K. S., Lindley S., Falkowski G. P. 1994. Iron limitation of the phytoplankton photosynthesis in the equatorial Pacific Ocean. Nature 371:145-149
- Kolber Z. S., Prasil O., Falkowski P. G. 1998. Measurements of variable chlorophyll fluorescence using fast repetition rate techniques: defining methodology and experimental protocols. Biochimica et Biophysica Acta 1367:88-106
- Krause G. H., Weis E. 1991. Chlorophyll Fluorescence and Photosynthesis: The Basics. Annual Review of Plant Physiology and Plant Molecular Biology 42:313-349
- Kromkamp J., Peene J. 1999. Estimation of phytoplankton photosynthesis and nutrient limitation in the Eastern Scheldt estuary using variable fluorescence. Aquatic Ecology 33:101-104
- Kromkamp J. C., Forster R. M. 2003. The use of variable fluorescence measurements in aquatic ecosystems: differences between multiple and single turnover measuring protocols and suggested terminology. European Journal of Phycology 38:103-112
- Lancelot C., Keller M. D., Rousseau V., Smith W. O., Jr. 1998. Phaeocystis physiological ecology. In: Anderson D. M., Cembella, A.D., Hallegraeff, G.M. (ed) Physiological Ecology of Harmful Algal Blooms, Vol 41. Springer-Verlag, Berlin

- Landry M. R., Selph K. E., Brown S. L., Abbott M. R., Measures C. I., Vink S., Allen C. B., Calbet A., Christensen S., Nolla H. 2002. Seasonal dynamics of phytoplankton in the Antarctic Polar Front region at 170°W. *Deep Sea Research II* 49:1843-1865
- Leventer A., Dunbar R. B. 1988. Recent diatom record of McMurdo Sound, Antarctica: Implications for history of sea ice extent. *Paleoceanography* 3:259-274
- Leventer A., Dunbar R. B. 1996. Factors influencing the distribution of diatoms and other algae in the Ross Sea. *Journal of Geophysical Research* 101:18489-18500
- Long M. C., Dunbar R. B., Tortell P. D., Smith W. O., Jr., Mucciarone D. A., DiTullio G. R. *submitted*. Vertical structure, seasonal drawdown, and net community production in the Ross Sea, Antarctica. *Journal of Geophysical Research*
- Lorenzen C. J. 1966. A method for the continuous measurement of in vivo chlorophyll concentration. *Deep Sea Research* 13:223-227
- Maldonado M. T., Boyd P. W., Harrison P. J., Price N. M. 1999. Co-limitation of phytoplankton growth by light and Fe during winter in the NE subarctic Pacific Ocean. *Deep Sea Research Part II: Topical Studies in Oceanography* 46:2475-2485
- Martin J. H. 1990. Glacial-interglacial CO₂ change: The iron hypothesis. *Paleoceanography*. 5:1-13
- Mathot S., Smith W. O., Jr., Carlson C. A., Garrison D. L., Gowing M. M., Vickers C. L. 2000. Carbon partitioning within *Phaeocystis antarctica* (Prymnesiophyceae) colonies in the Ross Sea, Antarctica. *Journal of Phycology* 36:1049-1056
- Matrai P. A., Vernet M., Hood R., Jennings A., Brody E., Saemundsdottir S. 1993. Light-dependence of carbon and sulfur production by polar clones of the genus *Phaeocystis*. *Marine Biology* 124:157-167
- Mauzerall D. 1972. Light-induced fluorescence changes in *Chlorella*, and the primary photoreactions for the production of oxygen. *Proceedings National Academy of Science* 69:1358-1362
- Measures C. I., Vink S. 2001. Dissolved Fe in the upper waters of the Pacific sector of the Southern Ocean. 48:3913
- Moore C. M., Seeyave S., Hickman A. E., Allen J. T., Lucas M. I., Planquette H., Pollard R. T., Poulton A. J. 2007. Iron-light interactions during the CROZet natural iron bloom and EXPORT experiment (CROZEX) I: Phytoplankton growth and photophysiology. *Deep Sea Research Part II: Topical Studies in Oceanography* 54:2045-2065
- Neale P. J., Cullen J. J., Davis R. F. 1998. Inhibition of marine photosynthesis by ultraviolet radiation: Variable sensitivity of phytoplankton in the Weddell-Scotia Sea during the austral spring. *Limnology and Oceanography* 43:433-448

- Nelson D. M., Smith W. O., Jr. 1986. Phytoplankton bloom dynamics of the western Ross Sea ice edge-- II. Mesoscale cycling of nitrogen and silicon. *Deep Sea Research I* 33:1389-1412
- Nelson D. M., DeMaster D. J., Dunbar R. B., Smith W. O., Jr 1996. Cycling of organic carbon and biogenic silica in the Southern Ocean: Estimates of water-column and sedimentary fluxes on the Ross Sea. *Journal of Geophysical Research* 101:18,519-518,532
- Olson R. J., Sosik H. M., Chekalyuk A. M., Shalapyonok A. 2000. Effects of iron enrichment on phytoplankton in the Southern Ocean during late summer: active fluorescence and flow cytometric analyses. *Deep Sea Research II* 47:3181-3200
- Palmisano A. C., SooHoo J. B., SooHoo S. L., Kottmeier S. T., Craft L. L., Sullivan C. W. 1986. Photoadaptation in *Phaeocystis pouchetii* advected beneath annual sea ice in McMurdo Sound, Antarctica. *Journal of Plankton Research* 8:891-906
- Parkhill J. P., Maillet G., Cullen J. J. 2001. Fluorescence-based maximal quantum yield for PSII as a diagnostic of nutrient stress. *Journal of Phycology* 37:517-529
- Passow U., Wassmann P. 1994. On the trophic fate of *Phaeocystis pouchetii* (Hariot): IV. The formation of marine snow by *P. pouchetii*. *Marine Ecology Progress Series* 104:153-116
- Reigstad M., Wassmann P. 2007. Does *Phaeocystis spp.* contribute significantly to vertical export of organic carbon? *Biogeochemistry* 83:217-234
- Rottgers R. 2007. Comparison of different variable chlorophyll *a* fluorescence techniques to determine photosynthetic parameters of natural phytoplankton. *Deep Sea Research I* 54:437-451
- Rousseau V., Vaulot D., Casotti R., Cariou V., Lenz J., Gunkel J., Baumann M. 1994. The life cycle of *Phaeocystis* (Prymnesiophyceae): evidence and hypotheses. *Journal of Marine Systems* 5:23-39
- Rousseau V., Chrétiennot-Dinet M.-J., Jacobsen A., Verity P., Whipple S. 2007. The life cycle of *Phaeocystis*: state of knowledge and presumptive role in ecology. *Biogeochemistry* 83:29-47
- Sarmiento J. L., Orr J. C. 1991. Three-dimensional simulations of the impact of Southern Ocean nutrient depletion on atmospheric CO₂ and ocean chemistry. *Limnology and Oceanography* 36:1928-1950
- Sarmiento J. L., Hughes T. M. C., Stouffer R. J., Manabe S. 1998. Simulated response of the ocean carbon cycle to anthropogenic climate warming. *Nature* 393:245-249
- Schlitzer R. 2008. Ocean Data View. <http://odv.awi.de>
- Schreiber U., Bilger W. 1986. Continuous recording of photochemical and non-photochemical chlorophyll fluorescence quenching with a new type of modulation fluorometer. *Photosynthesis Research* 10:51-62

- Schreiber U., Schliwa U., Bilger W. 1986. Continuous recording of photochemical and non-photochemical chlorophyll fluorescence quenching with a new type of modulation fluorometer. *Photosynthesis Research* 10:51-62
- Sedwick P. N., DiTullio G. R. 1997. Regulation of algal blooms in Antarctica shelf waters by release of iron from melting sea ice. *Geophysical Research Letters* 24:2515-2518
- Sedwick P. N., DiTullio G. R., Mackey D. J. 2000. Iron and manganese in the Ross Sea, Antarctica: Seasonal iron limitation in Antarctic shelf waters. *Journal of Geophysical Research* 105:11321-11336
- Sedwick P. N., Garcia N., Riseman S., Marsay C., DiTullio G. 2007. Evidence for high iron requirements of colonial *Phaeocystis antarctica* at low irradiance. *Biogeochemistry* 83:83-97
- Shields A. R., Smith W. O., Jr. 2008. An examination of the role of colonial *Phaeocystis antarctica* in the microbial food web of the Ross Sea. *Polar Biology* 31:1091-1099
- Smith W., Nelson D., Mathot S. 1999. Phytoplankton growth rates in the Ross Sea, Antarctica, determined by independent methods: temporal variations. *Journal of Plankton Research* 21:1519-1536
- Smith W. O., Jr, Nelson D. M. 1985. Phytoplankton bloom produced by a receding ice edge in the Ross Sea: spatial coherence with the density field. *Science* 227:163-166
- Smith W. O., Jr, Asper V. L. 2001. The influence of phytoplankton assemblage composition on biogeochemical characteristics and cycles in the southern Ross Sea, Antarctica. *Deep Sea Research I* 48:137-161
- Smith W. O., Jr, Ainley D. G., Cattaneo-Vietti R. 2007. Trophic interactions within the Ross Sea continental shelf ecosystem. *Philosophical Transactions of the Royal Society B: Biological Sciences* 362:95-111
- Smith W. O., Jr., Harrison W. G. 1991. New production in polar regions: the role of environmental controls. *Deep Sea Research I* 38:1463-1479
- Smith W. O., Jr., Nelson D. M., DiTullio G. R., Leventer A. R. 1996. Temporal and spatial patterns in the Ross Sea: Phytoplankton biomass, elemental composition, productivity and growth rates. *Journal of Geophysical Research* 101:18455-18465
- Smith W. O., Jr., Gordon L. I. 1997. Hyperproductivity of the Ross Sea (Antarctica) polynya during austral spring. *Geophysical Research Letters* 24:233-236
- Smith W. O., Jr., Marra J., Hiscock M. R., Barber R. T. 2000. The seasonal cycle of phytoplankton biomass and primary productivity in the Ross Sea, Antarctica. *Deep Sea Research II* 47:3119-3140

- Smith W. O., Jr., Dinniman M. S., Klinck J. M., Hofmann E. 2003. Biogeochemical climatologies in the Ross Sea, Antarctica: seasonal patterns of nutrients and biomass. *Deep Sea Research II* 50:3083-3101
- Smith W. O., Jr., Shields A. R., Peloquin J. A., Catalano G., Tozzi S., Dinniman M. S., Asper V. A. 2006. Interannual variations in nutrients, net community production, and biogeochemical cycles in the Ross Sea. *Deep Sea Research II* 53:815-833
- Suggett D. J., Oxborough K., Baker N. R., MacIntyre H. L., Kana T. M., Geider R. J. 2003. Fast repetition rate and pulse amplitude modulation chlorophyll *a* fluorescence measurements for assessment of photosynthetic electron transport in marine phytoplankton. *European Journal of Phycology* 38:371-384
- Sunda W. G., Huntsman S. A. 1997. Interrelated influence of iron, light and cell size on marine phytoplankton growth. *Nature* 390:389
- Sweeney C., Hansell D. A., Carlson C. A., Codispoti L. A., Gordon L. I., Marra J., Millero F. J., Smith W. O., Jr., Takahashi T. 2000a. Biogeochemical regimes, net community production and carbon export in the Ross Sea, Antarctica. *Deep Sea Research II* 47:3369-3394
- Sweeney C., Smith W. O., Jr, Hales B., Bidigare R. R., Carlson C. A., Codispoti L. A., Gordon L. I., Hansell D. A., Millero F. J., Park M.-O., Takahashi T. 2000b. Nutrient and carbon removal ratios and fluxes in the Ross Sea, Antarctica. *Deep Sea Research II* 47:3395-3421
- Sylvan J. B., Quigg A., Tozzi S., Ammerman J. W. 2007. Eutrophication-induced phosphorus limitation in the Mississippi River plume: Evidence from fast repetition rate fluorometry. *Limnology and Oceanography* 52:2679-2685
- Tang K., Smith W. O., Jr, Shields A. R., Elliott D. T. 2008. Survival and recovery of *Phaeocystis antarctica* (Primnesiophyceae) from prolonged darkness and freezing. *Proceedings of the Royal Society of London. Series B* 276:81-90
- Tang K. W. 2003. Grazing and colony size development in *Phaeocystis globosa* (Prymnesiophyceae): the role of a chemical signal. *Journal of Plankton Research* 25:831-842
- Timmermans K. R., van Leeuwe M. A., de Jong J. T. M., McKay R. M. L., Nolting R. F., Witte H. J., van Ooyen J., Swagerman M. J. W., Kloosterhuis H., de Baar H. J. W. 1998. Iron stress in the Pacific region of the Southern Ocean: evidence from enrichment bioassays. *Marine Ecology Progress Series* 166:27-41
- Timmermans K. R., Davey M. S., van der Wagt B., Snoek J., Geider R. J., Veldhuis M. J. W., Gerringa L. J. A., De Baar H. J. W. 2001. Co-limitation by iron and light of *Chaetoceros brevis*, *C. dictyota* and *C. calcitrans* (Bacillariophyceae). *Marine Ecology Progress Series* 217:287-297
- Trissl H. W., Gao Y., Wulf K. 1993. Theoretical fluorescence induction curves derived from coupled differential equations describing the primary photochemistry of photosystem II by an exciton-radical pair equilibrium. *Biophysical Journal* 64:974-988

- van Hilst C. M., Smith W. O., Jr 2002. Photosynthesis/irradiance relationships in the Ross Sea, Antarctica, and their control by phytoplankton assemblage composition and environmental factors. *Marine Ecology Progress Series* 226:1-12
- van Leeuwe M. A., Timmermans K. R., Witte H. J., Kraay G. W., Veldhuis M. J. W., de Baar H. J. W. 1998. Effects of iron stress on chromatic adaptation by natural phytoplankton communities in the Southern Ocean. *Marine Ecology Progress Series* 166:43-52
- Verity P. G., Smayda T. J., Sakshaug E. 1990. Photosynthesis excretion and growth rate of *Phaeocystis* colonies and solitary cells. *Polar Research* 10:117-128
- Verity P. G., Smetacek V. 1996. Organism life cycles, predation, and the structure of marine pelagic ecosystems. *Marine Ecology Progress Series* 130:277-293
- Wassmann P. 1994. Significance of sedimentation for the termination of *Phaeocystis* blooms. *Journal of Marine Systems* 5:81-100
- Welschmeyer N. A. 1994. Fluorometric analysis of chlorophyll *a* in the presence of chlorophyll *b* and phaeopigments. *Limnology and Oceanography* 39:1985-1992

**SECTION IV. PHYTOPLANKTON PHOTOPHYSIOLOGY AND PRIMARY PRODUCTIVITY DERIVED FROM
VARIABLE FLUORESCENCE MEASUREMENTS IN THE ROSS SEA, ANTARCTICA**

ABSTRACT

The Ross Sea polynya is a highly productive region of the Southern Ocean with strong seasonal and spatial variability in phytoplankton biomass and productivity. This variability is mostly related to ice dynamics and polynya evolution during the austral spring and summer. During the late spring and austral summer of 2005/2006 we combined the use of ^{14}C -productivity measurements with bio-optical methods to derive phytoplankton primary productivity with much higher spatial and temporal resolution than possible with radiolabeling of discrete samples. Our objective was to explore and compare advantages and deficiencies using fast repetition rate fluorometry (FRRF) and rapid light curves (RLCs) in assessing phytoplankton photosynthetic performance and estimating productivity in the Ross Sea. Our observations indicate a poor correlation between ^{14}C - and FRRF-derived productivity, possibly because of the differential limitations of each by micronutrients, as well as by the fundamental differences in both methodologies. Regions dominated by diatoms and *Phaeocystis antarctica* were characterized by significantly different fluorescence signatures, as indicated by FRRF and RLCs measurements. Diatoms, dominant in the eastern coastal polynya (in warmer, fresher surface waters) displayed ~50% larger absorption cross section (σ_{psII}) than *P. antarctica*, despite being acclimated and exposed to higher irradiance levels. *P. antarctica*-dominated blooms in the western portion of the polynya displayed higher photoadaptation index (E_k) and ~50% lower slope of light-limited photosynthetic rates (α). Thus, the photochemical characteristics may provide the two functional groups with a means to flourish in the variable environments that develop in the Ross Sea.

INTRODUCTION

The objective of this chapter is to explore the feasibility of deriving primary production rates from variable fluorescence measurements in the Ross Sea by comparing oxygenic photosynthetic rates with ^{14}C -based photosynthetic measurements. In addition, I wished to determine if photosynthetic parameters derived from rapid light curves (RLC) can be used to discriminate assemblages dominated by diatoms and *Phaeocystis antarctica*.

The Ross Sea, Antarctica

The Ross Sea is an extremely productive region of the Southern Ocean (Smith and Nelson 1985, Arrigo and McClain 1994). The abundance of marine mammals, fish and birds suggests that intense primary productivity occurs and sustains a rich ecosystem (Smith *et al.* 2007). Primary productivity in the polynya (an area of open water surrounded by ice) is usually dominated by diatoms and *Phaeocystis antarctica* (Smith and Gordon 1997). No single factor appears to control the dominance of the blooms (Arrigo *et al.* 1999, van Hilst and Smith 2002). Diatoms often dominate near the ice edge, while *P. antarctica*, a colonial prymnesiophyte, often dominates in the south central portion of the polynya (Arrigo *et al.* 1999). The assemblage composition and primary productivity rates influence the polynya biogeochemistry by selectively partitioning the fixed carbon and by altering the sulfur cycling via the production of DMSP/DMS by *P. antarctica* (DiTullio and Smith 1995, Arrigo *et al.* 1999, del Valle *et al.* 2007). Annual blooms coincide with sea ice retreat and the seasonal increases in solar radiation. Production at the ice edge can be extremely high, averaging $1 \text{ g C m}^{-2} \text{ d}^{-1}$ (Wilson *et al.* 1986). The distribution of biomass in the polynya is at times dominated by single taxa in local blooms, but more often, even at high biomass concentration, assemblages are a mixture of the two main phytoplankton groups (Smith and Asper 2001).

Despite the fact that phytoplankton biomass is extremely variable on small (less than 10 km), meso- (from 10 to 100 km) and large (> 100 km) scales (Arrigo and McLain, 1994; Peloquin and Smith, 2007), it is impossible to assess rate processes on the same scales, as methodology is unavailable to routinely quantify productivity over all spatial scales. Recently ^{14}C -primary productivity and variable fluorescence have been correlated for several different regions (Table 7), but never for the Southern Ocean and the Ross Sea. Despite the high correlation between the primary productivity rates measured with ^{14}C -uptake and those derived from FRRF measurements at station ALOHA by Corno *et al.* (2006), significant spatial and temporal variability occurred. Similarly, Moore *et al.* (2003) obtained high correlations between ^{14}C -productivity and estimates made with a FRRF-based model for a sector of the English Channel, producing high temporal and spatial resolution data that enable them to assess uncoupled patterns and processes in highly dynamic frontal systems. However, the Ross Sea environment is much different than those other regions. For example, during the growing season the Ross Sea experiences 24-h photoperiods, as well as rapidly (on the order of days to weeks) changing mixed layer depths (Smith *et al.*, submitted). Given the extreme spatial complexity of the region, it is important to assess the rates of productivity on similar spatial scales.

Fast repetition rate fluorometry

Bio-optics has allowed significant advances in the study of phytoplankton. There are many ways in which optical measurements have been applied to oceanic investigations, and range from the use of the Secchi disk in the late 1800's to determine the light penetration in the water and therefore of the suspended matter in the water column (Weinberg 1976), to application of *in vivo* fluorescence to measure and map chlorophyll and phytoplankton biomass over large regions (Lorenzen 1966), to the use of satellite data for delineating the global distribution and patterns of these primary producers (Yoder *et al.* 1993). Bio-optical remote sensing also allows estimating the amount of carbon

sequestered by oceanic primary production on a global scale (Behrenfeld and Falkowski 1997). In 1963 Duysens and Sweers were first to apply the concept of variable fluorescence to the study of photosynthetic microalgae using the fluorescence induction theory described by Kautsky and Hirsch (1931). Thereafter, pump and probe fluorometry (PPF) (Falkowski *et al.* 1986), pulse amplitude fluorometry (PAM), which measures photochemical efficiency of PS II utilizing multiple turnover flashlets (Schreiber and Bilger 1986), and fast repetition rate fluorometry (FRRF) (Kolber and Falkowski 1992), a technique that uses single turnover (ST) flashes to determine photosynthetic parameters such as the absorption cross section (σ_{PSII}) and the rate of oxidation of the primary electron acceptor in PSII, the plastoquinone Q_A in addition to the photochemical efficiency of photosystem two (PSII). Variable fluorescence-based estimates of primary productivity have the potential to assess phytoplankton production at a much greater space and time resolution, and with significant lower cost than the ^{14}C - and O_2 -methods allow. The fluorescence measurements take seconds to minutes to complete RLC curves, depending on the number of light levels, and the exposure time at each level before the measurement. Primary productivity is calculated based on the estimation of electron transport rate (ETR) and derivation of the oxygen production (P_{O_2}) (Kolber and Falkowski 1993, Boyd *et al.* 1997, Kromkamp and Peene 1999, Suggett *et al.* 2001, Raateoja *et al.* 2004, Smyth *et al.* 2004). The measurement of ETR provides the rate at which light dependent reactions proceed within the thylakoid membrane, allowing estimates of oxygen production. The main limitation in assessing primary productivity from fluorescence-based ETR measurements is the lack of adequate models linking fluorescence and photosynthesis. Common to the existing models is the assumption that some parameters remain constant, (i.e., the photosynthetic quotient (PQ) and the number of reaction centers (RC) per mole of chlorophyll), when in fact these parameters are likely to change with taxa and physiological state of the cells. These assumptions skew the relationship between the primary production measured with ^{14}C -uptake and those calculated from variable fluorescence, with the latter

usually reaching P_{\max}^B at higher irradiance levels. Only a small fraction of the photosynthetically-produced electrons are used for carbon fixation, while the highly-variable remainder is dissipated through alternative electron sinks such as photorespiration and reduction of molecular oxygen as part of Mehler reaction (reduction of O_2 by PSI). Dissimilarities between these two techniques are also generated by the different time-scales of the respective measurements: almost instantaneous for fluorescence and up to 24 h for ^{14}C -measurements, although repeating multiple bio-optical casts over 24 h at the same location to integrate the physiological states that the assemblages experience may alleviate that specific problem. In addition, the absorption cross section in phytoplankton chloroplasts is a function of an actual distribution of spectral irradiance that generally cannot be matched by the FRRF excitation light source, potentially resulting in overestimation of the FRRF-based absorption cross section. Spectral scaling of FRRF-based σ_{PSII}' may address this mismatch (Suggett *et al.* 2001). This scaling takes into account the differences in pigment absorption efficiency between natural and FRRF light.

In summary, it would be inappropriate to directly compare gross photosynthesis measured with the variable fluorescence techniques to the net carbon fixation measured with the radiolabeling method without a site-specific intercalibration between these two methods. On the other hand, active fluorescence methods and protocols (such as RLCs), in addition to allowing the calculation of the gross photosynthesis, permit a better characterization of the details of photosynthetic capacity and potential photosynthetic activity over a wide range of ambient irradiance levels (Ralph and Gademann 2005). RLCs measurements utilize a series of fluorescence transients performed under gradually increasing background irradiance levels. Such measurements allow the almost instantaneous determination of ETR at the predetermined irradiance range, providing estimates of α , E_k and ETR_{\max} of electron transport, in a manner similar to P-E curves. The measured characteristics generally depend on the state of light adaptation, which changes over the course of the day and by

season. Whether this represents an advantage or limitation depends on the objective of the study. In some cases, the ability to characterize the plasticity of photosynthetic apparatus in response to light exposure offers an opportunity to understand the mechanisms and photosynthetic consequences of light adaptations. Our finding in terms of the temporal and spatial distribution of the two taxa within the polynya is consistent with previous studies (DiTullio and Smith 1996, Arrigo *et al.* 1999, Smith and Asper 2001) with dominance in the spring of *P. antarctica* in the southeastern polynya and diatom-dominated assemblages in the summer on the western side of the polynya.

MATERIAL AND METHODS

Study site

Data for this study were collected during the first cruise of the Controls on Ross Sea Algal Community Structure (CORSACS) project on the *RVIB N. B. Palmer* (Cruise NBP06-01) in December, 2005 and January, 2006. The polynya was sampled between 74.5° and 77.5° S and 165° E and 170°W (Figure 32).

A SeaBird Electronics Model SBE-911+ was used to measure conductivity, temperature, and depth. The sensors were mounted on a SeaBird, epoxy-coated 24-bottle rosette sampler with 10-L Bullister bottles. Data from sensors were transmitted in real time to a deck unit via a conducting cable and were digitally recorded with SBE SeaSave software (Ver. 5.37d). Mixed-layer depths were defined as the depths from which there was a $\Delta\sigma_t$ of 0.02 from a stable surface value, and were calculated with a MatLab© program that recalled a routine from the SEAWATER Library (Morgan 1993) to calculate σ_t using the UNESCO 1983 (EOS 80) polynomial (Fofonoff and Millard 1983).

Radiometry and optical environment

Surface irradiance was recorded with a Biospherical cosine PAR sensor (QSR-2200) mounted above the ship's bridge. The *in situ* downward irradiance (E_d) was determined with a Biospherical PAR spherical scalar collector (QSP2300) mounted on the rosette and processed with all other CTD sensors. The average diffuse attenuation coefficient of E_d over the mixed layer depth K_d (m^{-1}) and the euphotic zone depth (z_{eu} , m) were calculated for all stations using

$$E_z = E_0 \times e^{-k_d \times z} \quad (\text{Eq.20})$$

$$k_d = \frac{\ln E_{0^-}}{\ln E_z} \quad (\text{Eq. 21})$$

where E is the irradiance at depth z, and E_{0^-} is the irradiance below the sea surface (Kirk 1983). The euphotic zone depth (Z_{eu}) (Eq. 22-23) is defined as the depth at which the irradiance equals 1% of the surface value (E_{0^-}):

$$\frac{E_z}{E_{0^-}} = \frac{1}{100} \quad (\text{Eq. 22})$$

$$\frac{\ln 100}{k_d} = Z_{eu} \quad (\text{Eq. 22})$$

$$\frac{4.6}{k_d} = Z_{eu} \quad (\text{Eq. 23})$$

Chlorophyll

Samples for total chlorophyll *a* (Chl *a*) were collected into clean, dark polyethylene bottles and immediately filtered through 25 mm GF/F Whatman glass microfiber filters (nominal pore size 0.7 μm) using a vacuum of less than 5 psi. Filters were immediately placed in borosilicate tubes with 90% acetone, capped, and extracted for 24 hours at -20°C in the dark (JGOFS, 1994). Following extraction the filters were removed and fluorometric determination of chlorophyll *a* by a non-acidification technique was made with a Turner Designs TD700 fluorometer. The fluorometer was calibrated at the beginning and at end of each cruise with a pure chlorophyll *a* solution (Sigma). Prior to the measurements the fluorometer was zeroed with 90% acetone.

Primary productivity and P vs. E determinations

Daily primary production was measured by 24-h on-deck simulated-*in situ* incubations with $^{14}\text{C-NaHCO}_3$. 265 mL of water were collected from seven depths corresponding to the 100, 50, 25, 15,

5, 1, 0.1% irradiance below the sea surface (E_0). Each bottle was inoculated with 10 μCi of $\text{NaH}^{14}\text{CO}_3$ and placed in an on-deck incubator in UV-transparent tubes wrapped in neutral density filters to attenuate the light and reproduce the irradiance from which the sample was collected, and cooled with flowing surface seawater. After 24 h samples were filtered through 25 mm GF/F Whatman glass microfiber filters (nominal pore size 0.7 μm) and Poretics membranes with nominal pore size of 20 μm under a vacuum of less than 5 psi. 100 μL 0.1N HCl was added to all filters to remove inorganic ^{14}C adsorbed to the filters, and aerated for 24 h before the addition of scintillation fluor (5 mL Ecolume®). Total added $\text{NaH}^{14}\text{CO}_3$ was measured by collecting 0.1 mL unfiltered, unacidified sample and adding 100 μL β -phenylethylamine and scintillation cocktail. Radioactivity was measured with a Packard liquid scintillation counter.

Photosynthetic parameters were measured using 2-mL samples collected from the 50% isolume at selected stations (Table 2). A sample (65 mL) was inoculated with 150 μCi of $\text{NaH}^{14}\text{CO}_3$, and 2 mL subsamples placed in a glass LSC vials that were placed in a 32-sample photosynthesetron that had a light gradient from near zero to ca. 500 $\mu\text{mol quanta m}^{-2} \text{s}^{-1}$. The samples were cooled by coolant from a water bath set at -1°C which flowed through an aluminum block that held the samples, and was illuminated from below by a halogen projector diode-emitting lamp.

PAR was measured periodically for each sample bottle position in the photosynthesetron using a 4π Biosperical QSL 2100 scalar sensor fitted with a micro-sensor. Carbon fixation rates normalized to Chl *a* concentrations, and P vs. E curves were fit to the empirical model (Webb *et al.* 1974, Platt *et al.* 1980):

$$P^B = P_{\max}^B \left[1 - e^{\frac{-\alpha E}{P_{\max}^B}} \right] \quad (\text{Eq. 25})$$

For terms and definitions refer to Table 9. Photoinhibition was rarely observed at the maximum irradiance levels used (Shields and Smith 2009), and hence was ignored in all analyses. Data

were fit to equation 25 with SigmaPlot® (version 9) to derive the initial slope (α) of the curve ($\text{mg C (mg Chl } a)^{-1} \text{ m}^{-3} \text{ h}^{-1} (\mu\text{E m}^{-2} \text{ s}^{-1})^{-1}$), the maximum photosynthetic rate (P_{max}^B ($\text{mg C (mg Chl } a)^{-1} \text{ h}^{-1}$) and the light saturation index E_k ($\mu\text{E m}^{-2} \text{ s}^{-1}$). The latter was derived by:

$$E_k = \frac{P_{\text{max}}^B}{\alpha} \quad (\text{Eq. 26})$$

Variable fluorescence

Measurements of photochemical efficiency of PSII were made with a MBARI 4th generation bench-top fast repetition rate fluorometer (FRRF) (Kolber *et al.* 1994). This fluorometer is equipped with an array of blue LED lights (~470 nm) with a total power of about 6 watts cm^{-2} . In continuous wave mode the instrument can deliver up to 8000 $\mu\text{mol photons m}^{-2} \text{ s}^{-1}$ of background light while performing FRR excitation. The FRR excitation flashlets are produced at pulse photon flux density (PPFD) of about 65,000 $\mu\text{mol photons m}^{-2} \text{ s}^{-1}$, with 150 ns rise time and 200 ns fall time. A thermo-electric cooled 10-mm avalanche photodiode (Advance Photonics, Inc) detector is connected to an elbow-shaped light pipe that collects the emission light from the bottom of the sample chamber. The instrument has a sensitivity of 0.01 $\mu\text{g L}^{-1}$ with 5-10% accuracy. The measurement protocol was optimized to obtain fluorescence saturation (F_m) by a rapid sequence of 80 flashlets, followed by 30 flashlets at exponentially increasing intervals to characterize the relaxation kinetics of fluorescence transients. Prior to measurements the instrument blanks were determined with distilled water to account for light scattering within the cuvette, and then with seawater filtered through a Millex AA 0.8 μm Millipore membrane to account for fluorescence of dissolved organic matter. Water samples for FRRF measurements were collected from the sampling bottles, and immediately placed on ice and kept under low light ($5\text{--}10 \mu\text{mol photons m}^{-2} \text{ s}^{-1}$) for low-light adaptation (approximately 30-40 min). Minimal (F_0) and maximal (F_m) fluorescence and the effective absorption cross section (σ_{psii}) where

calculated from each single turnover (ST) saturation curve using the proprietary software LIFT.exe developed by Dr. Z. Kolber at MBARI. Reference and baseline corrections were applied to retrieve other photosynthetic parameters including the effective absorption cross section (σ_{PSII}), and the minimum turnover time of PSII photochemistry (τ_{QA}) according to Kolber *et al.* (1998). Functional absorption cross section (σ_{PSII}) was calculated by fitting the fluorescence transient into a theoretical function describing the relationship between fluorescence and photosynthesis (Kolber *et al.* 1998).

Maximum photochemical efficiency of PSII is calculated as:

$$\frac{F_v}{F_m} = \frac{F_m - F_0}{F_m} \quad (\text{Eq.27})$$

This is measured on dark-adapted samples while the effective photochemical efficiency of PSII (Φ_{PSII}) (Genty *et al.* 1989) is measured on light adapted samples and it is given by:

$$\Phi_{PSII} = \frac{F'_m - F'}{F'_m} = \frac{\Delta F'}{F'_m} = \frac{F_v'}{F'_m} \quad (\text{Eq. 28})$$

When both dark- and light-adapted measurements were available, as in the case of the RLCs, the photochemical quenching (qP) was calculated as follows:

$$qP = \frac{\Phi_{PSII}}{F_v/F_m} = \frac{F'_m - F'/F'_m}{F_m - F_0/F_m} = \frac{F'_m - F'}{F_m - F_0} \quad (\text{Eq. 29})$$

Φ_{PSII} was used to estimate the relative electron transport rate ($rETR$) through the photosynthetic chain:

$$rETR = \Phi_{PSII} \times E \times \sigma_{PSII} \quad (\text{Eq. 30})$$

Variable fluorescence based primary productivity models

The FRRF based primary productivity (P_{FRRF}) is based on the electron transport rate (ETR) through PSII, and is a function of the following factors:

- The amount of light energy (E_z) available at depth.

- The absorption cross section of PSII for the sample cells (σ_{PSII})
- The photochemical quenching coefficient (qP)
- The photosynthetic efficiency of PSII (ϕ_e)
- The number of PSII reaction centers per unit of chlorophyll (n_{PSII})
- The proportion of PSII reaction centers that are functional (f)

Fluorescence-based estimates of photosynthetic rates (P_f^B , (mol e⁻ [Chl]⁻¹ a s⁻¹)) are based on the formula of Kolber and Falkowski (1993):

$$P_f^B = E \cdot \sigma_{PSII} \cdot qP \cdot \phi_e \cdot n_{PSII} \cdot (\Delta\phi_m / 0.65) \quad (\text{Eq. 31})$$

Similarly the gross photosynthetic oxygen evolution rates are calculated with the following equation:

$$P_{O_2}^B = E \cdot \sigma_{PSII} \cdot qP \cdot \phi_e \cdot f \cdot n_{PSII} \quad (\text{Eq. 32})$$

where P_{O_2} is the oxygen evolution rate (mol O₂ photon⁻¹ s⁻¹) and can be formulated as function of irradiance or depth; E is the irradiance ($\mu\text{mol photons m}^{-2} \text{s}^{-1}$); σ_{PSII} is the absorption cross section for PSII (m² photon⁻¹); qP is the photochemical quenching coefficient equivalent to $(F_m - F)/F_v$; ϕ_e is the photon yield of electron transfer by PSII with a theoretical maximum value of 0.25 (mol O₂ mol photon⁻¹), although higher values have been measured (Kromkamp *et al.* 2001). Photon yields are often referred to as $(1/k)$; f is the fraction of functional PSII reaction centers; and n_{PSII} is the number of reaction centers of PSII per chlorophyll a (mol photon [mol Chl a]⁻¹), and usually ranges between 200 and 800. Several formulations and derivations of Eq. 32 have been published (Babin *et al.* 1996, Boyd *et al.* 1997, Flameling and Kromkamp 1998, Hartig *et al.* 1998, Suggett *et al.* 2001, Moore *et al.* 2003, Raateoja 2004, Smyth *et al.* 2004, Estevez-Blanco *et al.* 2006, Cosgrove 2007, Prieto *et al.* 2008), and can be summarized by:

$$P_{O_2}^B(z) = A \cdot E(z) \cdot \sigma_{PSII}(z) \cdot qP(z) \cdot \phi_e(z) \cdot f(z) \cdot n_{PSII}(z) \cdot \text{Chl } a(z) \quad (\text{Eq. 33})$$

In this equation Chl *a* is the chlorophyll *a* concentration in mg m⁻³, *A* is a constant that can change based on the input variable units, and represents the product of the conversion of *E* from μE m⁻²s⁻¹ to mol quanta m⁻² s⁻¹ (6.022 x 10²³), seconds to hours (3600), and σ_{PSII} from Å² quanta⁻¹ to m² quanta⁻¹ (10²⁰). φ_e is defined by the requirement of four photons per O₂ evolved (0.25), and *f* is expressed as Δφ_m/0.65 to calculate *f*. Generally chlorophyll concentration is expressed in units of moles (892 g per mole of Chl *a*), and *n*_{PSII} as 1/500 (Chl *a* RCII⁻¹).

By correlating either fluorescence-based gross oxygen evolution rates (P^B_{O₂}) to photosynthetic rates based on carbon fixation, or by assuming a predetermined photosynthetic quotient (PQ) (mol O₂ evolved [mol CO₂]⁻¹), it is possible to estimate primary production (in units of mg C m⁻³ h⁻¹) from variable fluorescence measurements by modifying equation 14 to convert the oxygen evolution rate to the photosynthetic carbon fixation rate per unit volume of seawater *P_z* (mol⁻¹CO₂ m⁻³ h⁻¹).

Normalizing this by the chlorophyll concentration at depth *z* to P^B_{FRRF} (mol⁻¹C [μg Chl *a* L⁻¹] m⁻³ h⁻¹) yields the following :

$$P_{FRRF}^B(z) = (A \cdot E(z) \cdot \sigma_{PSII}(z) \cdot qP(z) \cdot \phi_e(z) \cdot f(z) \cdot n_{PSII}(z) \cdot Chl\ a(z)) \cdot PQ^{-1} \quad (\text{Eq. 34})$$

where *A* also includes the conversion of moles of carbon to grams (12 g C mol⁻¹ C).

Rapid light curves

Rapid light curves were performed with the MBARI FRRF by recording fluorescence transients following short exposure at 0, 10, 20, 30, 40, 45, 50, 55, 60, 65, 70, 80, 90, 100, 150, 200, 300, 400, 500, and 600 μE m⁻² s⁻¹. ETR was calculated for each measurement and subsequently fitted with an exponential

$$ETR_e = ETR_{max} \left[1 - e^{-\frac{-aE}{ETR_{max}}} \right] \quad (\text{Eq. 35})$$

or hyperbolic function

$$ETR_r = \frac{\alpha \cdot E_k \cdot E}{E_k + E} \quad (\text{Eq. 36})$$

within the FRRF data processing software to calculate the initial slope (α), the minimum saturating irradiance (E_k), and the maximum ETR (ETR_{max}) under light-saturating conditions. When using Eq. 36, E_k can be calculated as

$$E_k = \frac{ETR_{max}}{\alpha} \quad (\text{Eq. 37})$$

When using Eq. 37, ETR_{max} can be calculated as

$$ETR_{max} = E_k \cdot \alpha \quad (\text{Eq. 38})$$

Maps and contour plots were generated with Ocean Data View (Schlitzer 2008), and 2D scatter plots were generated with ODV and Grapher 7.4 (Golden Soften Inc.®).

RESULTS

The distribution of physical and optical properties within the Ross Sea polynya during CORSACS I was extremely heterogeneous. Mixed layer depths west of 170°E and north of 77°S were generally shallower than the average Z_{mix} , and regions of more deeply mixed waters were found north and east of the polynya (Figure 33c). Attenuation coefficients and euphotic zone depths reflect the same patterns (Figure 33a,b). The observed patchiness could be due to the sampling pattern within the polynya, given that the cruise took place during a time of rapid change and expansion of the polynya; moreover, short-term mixing events driven by storms occurred within the one-month sampling as well; therefore, over the duration of the cruise these events undoubtedly affected the reconstructed spatial fields, producing a picture that is far from synoptic. Nonetheless, a remarkable correspondence is found between deep mixed layer (Figure 33c) (that is, regions where the mixed layer depth was greater than the euphotic zone depth) and reduced Fuco:Hex ratios (Figure 33d).

These regions on the east boundary of the polynya were generally characterized by elevated silicic acid concentrations ($>78 \mu\text{mol L}^{-1}$), indicating a dominance of *P. antarctica*. Conversely, extremely high Fuco:Hex ratios and reduced silicic acid concentrations were found in the shallower mixed layers along the coast of Victoria Land, where waters were also on average warmer and with lower salinity.

Comparison of $\text{ETR}_e \cdot F_m$, $\text{ETR}_r \cdot F_m$ and $\text{rETR} \cdot F_m$ with ^{14}C -productivity rates, and ETR_e , ETR_r and rETR with ^{14}C - productivity rates normalized to biomass for the NBP0601 cruise (Figure 34) showed surprisingly weak correlations, with r^2 between 0.48 and 0.53 using a power function for fitting. Due to the lack of RLC measurements on NBP0608, only rETR were calculated and compared to ^{14}C -productivity rates, and correlation coefficients of 0.55 and 0.42 were found (Figure 35).

P. antarctica blooms were found in the northeastern part of the polynya in early January, while a diatom bloom occurred in the northwest part of the region at the end of January. Stations with phytoplankton assemblage dominated by *P. antarctica* (CTD cast 36, 37, 39, 40), and by diatoms (CTD casts 88, 89, 91, 97) were analyzed in detail (Figure 36). This comparison showed a marked difference in photosynthetic performance measured with RLCs and ^{14}C -uptake between assemblages dominated by the two taxa. Specifically, RLC-derived α and E_k are significantly higher ($p=3.72 \cdot 10^{-18}$) than those found in *P. antarctica*, (Figure 36j, l), E_k values are significantly lower ($p=3.64 \cdot 10^{-5}$) (Figure 36l), while there was no significant difference between RLC derived P_{max} ($p=0.13$) (Figure 36k). There were also statistical differences between average temperatures at stations dominated by diatoms (averaging $0.62 \text{ }^\circ\text{C}$ in the top 60 m) and *P. antarctica* ($-0.64 \text{ }^\circ\text{C}$). Nitrogen concentrations not surprisingly were similar ($p=0.059$), while silicic acid concentrations were expectedly significantly lower at the diatom-dominated sites, averaging $56.7 \mu\text{mol L}^{-1}$ vs. $79.2 \mu\text{mol L}^{-1}$ at the *P. antarctica*-dominated locations. Phosphate concentrations were significantly ($p=0.003$) higher at *P. antarctica*-dominated locations, averaging $1.60 \mu\text{mol L}^{-1}$ vs. $1.26 \mu\text{mol L}^{-1}$ at diatom stations. Chlorophyll *a* concentrations were significantly higher ($p=2.7 \cdot 10^{-12}$) at the *P. antarctica* sites as well, as was the

fraction of the pigment in the size class bigger than 20 μm ($p < 0.001$) (Figures 36e, f). No significant differences in photosynthetic quantum yields measured by FRRF were observed ($p=0.15$) (Figure 36h), while absorption cross sections were significantly higher at the diatom dominated sites ($p < 0.001$) (Figure 36i). Primary production rates as measured by ^{14}C -uptake were significantly higher ($p < 0.001$) at the *P. antarctica* sites, but when normalized to chlorophyll the difference disappeared ($p=0.45$), with average P_b of 0.54 and 0.52 $\text{mg C m}^{-3} \text{ h}^{-1} (\mu\text{g chl L}^{-1})^{-1}$ for diatoms and *P. antarctica*. All results for diatoms and *P. antarctica* are summarized in Table 8.

DISCUSSION

High spatial and temporal resolution of *in situ* measurements of biological activity in polar environments are extremely difficult and rare. Polar regions in general and the Ross Sea specifically have a high spatial and temporal variability (Smith *et al.* 2010), and active fluorescence can help providing insight into the forcing factors controlling phytoplankton photosynthetic rates. Variable fluorescence has become accepted as a technique for rapid and nondestructive assessment of photosynthetic biomass and rates (Falkowski and Kiefer 1985, Falkowski *et al.* 1986). RLC-derived photosynthetic parameters may help explain the physiological characteristics responsible for the ability of phytoplankton to bloom under specific environmental conditions. However, the method is far from simple, and many assumptions are inherent in the conversion of fluorescent measurements to *in situ* rates. These results of trying to correlate FRRF-based photosynthetic rates (ETRs) to ^{14}C -based phytoplankton productivity estimates for the Ross Sea highlighted both the difficulties and the potential benefits of using the two techniques. The FRRF ETRs are based on instantaneous measurements mostly representative of physiological conditions immediately preceding sampling. Conversely, ^{14}C -uptake measurements integrate and represent assemblage physiological conditions over the 24-h incubation period and of on deck conditions not always sufficiently well reflecting the *in*

situ conditions (Smith *et al.* 2000). More importantly, FRRF-based photosynthetic rates are representative of gross production rates, where ^{14}C -measurements are of estimates that more closely approach net production rates (Marra and Barber 2004). Such differences may explain weak correlation between ETR and ^{14}C -based production rates (Figure 34). The FRRF measurements performed during NBP0601 and NBP0608 were made on discrete samples collected at discrete depths, and were low-light adapted prior to measurements. Dark adaptation was initiated during the CTD up-cast (when the sampling bottles were closed) and continued in the lab, as low-light adaptation was necessary to perform measurements under consistent conditions and minimize variations due to recent light exposure. The low light adaptation also was utilized to prevent Calvin-Benson enzyme inactivation and dark-induced NPQ. Nonetheless, ETR profiles exhibit all the features seen in the ^{14}C -based profiles, with reduced rates at the surface due to photoinhibition, maximum subsurface values, and exponential declines correlated to light attenuation within the water column. ETR measurement appears to better represent photosynthetic rates in the lower portion of the euphotic zone than ^{14}C -measurements, especially where absolute irradiance levels were below $10 \mu\text{E m}^{-2} \text{s}^{-1}$ and photosynthesis was strongly light-limited. Under this light regime ^{14}C -assimilation rates were in most cases almost independent of the light levels at which samples were incubated. With the FRRF instrument and protocols used, it is difficult to predict oxygen evolution and carbon fixation in the Ross Sea polynya from photobiological measurements alone.

Nonetheless, FRRF and RLC measurements allowed the determination of photophysiological differences between diatoms and *P. antarctica* relevant to their respective strategies of light utilization. Despite similar photosynthetic yields, the rates of photosynthetic electron transport appear to be much higher in diatoms than in *P. antarctica*, while irradiance saturation levels were higher and absorption cross sections lower in the latter. These results are counterintuitive, given the higher irradiance levels (shallow mixed layers) at which the diatoms normally occur and previous

results from field and laboratory studies of *P. antarctica*. The lower functional absorption cross section in *P. antarctica* can be interpreted as a selected trait to achieve higher photoresilience when blooming in a relatively highly mixed water column, while the larger functional absorption cross section of diatoms, together with high electron transport capacity, can result from the adaptation to a stable shallow mixed layer with high average irradiance levels or can also be due to stressors as iron and light co-limitation (Moore *et al.* 2007). Fast electron transport rates might be explained by enhanced performance of Photosystem I due to higher iron concentrations in the warm, fresh water lenses resulted from ice melting, but no Fe concentrations were measured to test this hypothesis.

From the comparison of the average parameters values for the station dominated by diatoms and *P. antarctica* in Table 8, temperature and salinity appear to be strong indicators and predictors for the dominance of the two phytoplankton groups in the Ross Sea polynya. Also evident from the same table is the fact that diatom blooms have lower biomass, based on chlorophyll concentrations, but approximately equal primary production rates when normalized to chlorophyll. Such comparisons might not be appropriate if the amount of chlorophyll per cell can significantly change, but since it is likely that diatoms are exposed to higher irradiance fluxes in the shallow mixed layers that might lead to less chlorophyll per cell, the comparisons become problematic. High production rates are associated with deeper mixed layer depths in the profiles dominated by *P. antarctica*, which may imply the potential importance of alternating exposure during a 24-h period to darker and brighter periods which can ultimately influence the assemblage composition (Mortain-Bertrand 1989, Litchman and Klausmeier 2001). The dominance of *P. antarctica* in deeper mixed layers with their higher frequencies of fluctuating light relative to the environmental conditions at stations dominated by diatoms is supported by results of photorecovery experiments (Section II) and to lower rates of xanthophyll cycling found in laboratory experiments (Kropuenske *et al.* 2009, Mills *et al.* 2010). That is, the higher xanthophyll cycling rates found in diatoms can contribute to their dominance in the

shallow mixed layers via their capability to dissipate higher radiant energy experienced and their higher P_{\max} values attained.

The association of diatoms with warmer waters currently mainly in the west part of the polynya (Jacobs *et al.* 2002) has been used to suggest that an increase of diatom- dominated blooms in the future will occur in polar regions and in the Ross Sea (Arrigo *et al.* 1999). Such an argument is valid only when the increase temperature leads to increased ice melting and stratification, but is not sustainable when considering the photophysiological differences between *P. antarctica* and diatoms, because temperature alone might not be differentially affecting the physiology of the two phytoplankton groups. Furthermore, accelerated glacial ice melting due to the predicted atmospheric temperature increases may increase the iron supply to the polynya and possibly allowing the spring *P. antarctica* blooms to persist throughout the summer and significantly reduce the dominance of diatoms in blooms. The photophysiological differences (the different photoresilience and photosynthetic capacity elucidated in this section) provide an additional constraint on the growth, composition and spatial and temporal distribution of phytoplankton observed in the southern Ross Sea.

The difference in the N:P ratio uptake for the profiles dominated by the two phytoplankton groups also indicates the significantly different biogeochemical impacts that these have in the southern Ross Sea. Such impacts have been discussed previously (Arrigo *et al.* 2000, Dunbar *et al.* 2003), but could result in long-term alterations of nutrient distributions that result from remineralization of organic matter at depth. Specifically, the elevated N:P ratios in *P. antarctica* blooms over long time periods may result in altered N:P ratios in the deeper waters of the Ross Sea, which in turn are components of Mode Water and Deep Water that influence other regions of the ocean. Clearly, the altered ratios also influence the exported biogenic matter composition, which in turn may have an impact of sediment composition and food web stoichiometry. There is no data

suggesting that either diatoms or *P. antarctica* drawdown ratios are ever close to Redfield ratios (Dunbar *et al.* 2003) instead the evidence of higher N:P drawdown in *P. antarctica* blooms and lower in diatoms is persistent during the seasons. Divergence from the canonical Redfield ration during *P. antarctica* and diatoms blooms has implication on CO₂ drawdown as well and they are likely to impact carbon cycling should stratification increase in the Ross Sea as predicted (Arrigo *et al.* 1999, Arrigo *et al.* 2000).

Our FRRF RLCs results for photosynthetic performance are consistent with the ¹⁴C-derived P vs. E results of van Hilst and Smith (2002), as α increased with time (that is, as the bloom progressed through the growing season). P vs. E coefficient at are usually mainly controlled by irradiance and temperature at high latitudes (Harrison and Platt 1986), but the temperature range in the polynya upper water column is not sufficient to justify a considerable role affecting P vs. E coefficients (Sakshaug 1989) while there are significant changes in irradiance on diel and seasonal timescales. The higher RLC based α found in diatoms at higher irradiance level are clear indicators of the adaptation by this genus in the polynya to thrive at the higher irradiance level found in the shallow MLD. RLC based E_k (an estimate of the optima irradiance for maximal photosynthesis) higher in *P. antarctica* than in profiles dominated by diatoms can be interpreted as a trait to faster adaptation to higher irradiance level exposure by the former. This result is consistent with the faster photorecovery found in *P. antarctica* (Section II). RLC based P_{max} are only slightly higher later in the season and in profiles diatom dominated suggesting an acclimation to higher irradiance.

Despite some limitations, the estimates of primary production and photosynthetic performance by active fluorescence techniques present advantages over the radiocarbon and oxygen techniques. First of all the measurements are relatively easy to perform and can be made in real-time using a wide variety of instruments, allowing high spatial and temporal coverage at relatively low cost. Moreover, active fluorescence-based measurements are chlorophyll-specific, representing truly

phototrophic production, while radiocarbon and oxygen-based measurements represent community metabolism, and include the impacts of heterotrophic processes (Marra and Barber 2004). The contribution of heterotrophic production to the total production can be significant when measured over 24-h intervals; furthermore, the contribution varies seasonally in the Ross Sea and appears to be a function of both heterotrophic biomass and its coupling to food web processes (Nelson, unpublished). Applying variable fluorescence techniques to assess photosynthetic performance, and to characterize the specific photosynthetic characteristics (efficiency of light utilization, photosynthetic yields, and electron transport rates) can provide information about energy utilization, as well as about the linkages between the physics, chemistry and biology in the ocean. That should allow to better understand the variability of oceans' productivity, its responses and feedbacks to climate change, and possibly to predict future patterns in the oceanic carbon cycle. The next generation of instruments and protocols will offer improved capabilities for the measurement of an increasing suite of photophysiological parameters, while the knowledge of the inherently high spatial and temporal scales of these variables should enhance the accuracy and prediction over wider range of environmental conditions and ecosystems. Better understanding of the nutrient and energy cycles in the Ross Sea will allow better models of the carbon cycle in the region and enhance the estimates of the areas importance to the Southern Ocean as a whole (Arrigo et al. 2008).

Table 7. Summary of studies comparing active fluorescence techniques and carbon and oxygen based estimates of photosynthetic production. PPF = pump and probe fluorescence; PAM = pulse-amplitude-modulated; FRRF = fast repetition rate fluorescence. n_{PSII} indicates the number of PSII reaction centers (PSII RC); ϕ_c quantum yield of electron transport (mg C e^{-1}); PQ is equal to the photosynthetic quotient ($\text{mol O}_2 \text{ mol C}^{-1}$), $P_f(\text{C})$ is electron transport rate based primary production express in C units ($\text{mol C mol Chl a}^{-1} \text{ s}^{-1}$)

Reference	Assumption				Technique	Location
	n_{PSII}	ϕ_c	PQ	$P_f(\text{C})$		
Kolber and Falkowski(1993)	0.0018	0.25	1.1	$0.5-2.4 \cdot^{14}\text{C}$	PPF	NW Atlantic Ocean
Boyd <i>et al.</i> (1997)	0.00125	0.25	1.2	$0.3-13 \cdot^{14}\text{C}$	PPF	NE Atlantic Ocean
Flameling and Kromkamp (1988)	-			$\cdot\text{O}_2$	PAM	Laboratory/cultures
Hartig <i>et al.</i> (1998)					PAM	German Wadden Sea*
Suggett <i>et al.</i> (2001)	0.0033	0.25	*	$0.6-2.4 \cdot^{14}\text{C}$	FRRF	North Atlantic Ocean
Moore <i>et al.</i> (2003)	0.002	0.25	1.4	$1.0-5.0 \cdot^{14}\text{C}$	FRRF	English Channel
Smyth <i>et al.</i> (2004)	0.002	0.25	1.2	$0.4-1.2 \cdot^{14}\text{C}$	FRRF	Celtic Sea
Corno <i>et al.</i> (2006)	0.0033	0.25	1.1	$1.1-1.6 \cdot^{14}\text{C}$	FRRF	North Pacific Ocean
Raateoja (2006)	0.002	0.25	*	$0.6-1.6 \cdot^{14}\text{C}$	FRRF	Baltic Sea
Raateoja (2006)	0.002	0.18	1.5	$0.4-0.7 \cdot^{14}\text{C}$	FRRF	Baltic Sea
Raateoja (2006)	0.002	0.18	1.5	$0.2-2.4 \cdot^{14}\text{C}$	FRRF	Baltic Sea
Estevez-Blanco <i>et al.</i> (2006)			1.4		FRRF	Atlantic Ocean (N Spain)
Cosgrove (2007)					PAM	Laboratory/cultures
Current Study	0.002	0.25			FRRF	Ross Sea, Antarctica

*Benthic microphytobenthos

Table 8. T-test comparison of diatom and *P. antarctica* dominated stations (*= p < 0.05; **=p < 0.01;

***= p< 0.001).

	Diatom Average (S.D.)	<i>P. antarctica</i> Average (S.D.)	p
T(°C)	0.62 (1.15)	-0.65 (0.41)	***
Salinity (PSU)	34.27 (0.25)	34.11 (0.02)	***
Nitrate ($\mu\text{mol L}^{-1}$)	19.88 (8.85)	22.65 (2.73)	*
Phosphate ($\mu\text{mol L}^{-1}$)	1.26 (0.61)	1.60 (0.16)	**
Silicate ($\mu\text{mol L}^{-1}$)	56.71 (14.67)	79.17 (2.85)	***
Chl α GFF ($\mu\text{g L}^{-1}$)	1.38 (0.49)	3.48 (1.06)	***
Chl α 20 μm ($\mu\text{l L}^{-1}$)	0.77 (0.31)	1.63 (0.39)	***
K_d (m^{-1})	0.23 (0.14)	0.20 (0.02)	-
Z_{eu} (m)	26.27 (11.81)	22.50 (2.61)	**
Z_{mix} (m)	34.32 (7.56)	50.46 (13.68)	**
F_v/F_m	0.40 (0.09)	0.43 (0.06)	-
σ ($\text{\AA}^2 \text{ quanta}^{-1}$)	1586 (207)	1077 (217)	**
α ($\text{e}^- \text{RC}^{-1}/\mu\text{E m}^{-2}$)	9.71 (1.26)	5.9 (1.08)	**
E_k ($\mu\text{E m}^{-2} \text{s}^{-1}$)	20.20 (5.84)	30.00 (10.97)	**
P_{max} ($\text{e}^- \text{RC}^{-1} \text{s}^{-1}$)	197.03 (62.35)	176.95 (71.87)	-
rETR	$6.6 \cdot 10^{+4}$ ($1.1 \cdot 10^{+5}$)	$1.4 \cdot 10^{+4}$ ($2.2 \cdot 10^{+4}$)	**
rETR F_m	$6.2 \cdot 10^{+7}$ ($1.0 \cdot 10^{+8}$)	$2.9 \cdot 10^{+7}$ ($4.7 \cdot 10^{+7}$)	*
PP ($\text{mg C}^{-1} \text{h}^{-1}$)	0.80 (0.55)	1.96 (1.69)	**
P^B ($\text{mg C (mg chl } a)^{-1} \text{h}^{-1}$)	0.54 (0.32)	0.52 (0.42)	-

Table 9. List of parameters used, their definitions and units. a.u. = arbitrary units.

Parameter	Definition	Units
^{14}C	Isotope used to trace the incorporation of inorganic HCO_3 into organic matter during photosynthesis	---
α^{B}	Initial slope of the PI curve (Maximum light – utilization coefficient)	$\text{mg C (mg chl } a)^{-1} \text{ h}^{-1} (\mu\text{E m}^{-2} \text{ s}^{-1})^{-1}$
P^{B}	Photosynthetic rate normalized to chlorophyll a	$\text{mg C (mg chl } a)^{-1} \text{ h}^{-1}$
$P^{\text{B}}_{\text{max}}$	Maximum (light-saturated) photosynthetic rate normalized to chlorophyll a	$\text{mg C (mg chl } a)^{-1} \text{ h}^{-1}$
P_{ETR}	Fluorescence based photosynthetic rate	$\text{e}^- \text{ chl } a \text{ s}^{-1}$
E or PAR	Irradiance or Photosynthetically Active Radiation	$\mu\text{E m}^{-2} \text{ s}^{-1}$
E_k	Light saturation parameter ($=P_{\text{max}} / \alpha^*$)	$\mu\text{E m}^{-2} \text{ s}^{-1}$
ETR	Electron Transport Rate	$\mu\text{e}^- (\text{mg chl-} a)^{-1} \text{ s}^{-1}$
rETR	Relative Electron Transport Rate	relative units
a^*	Chl a specific absorption coefficient	$\text{m}^{-2} (\text{mg chl } a)^{-1}$
$\phi_{\text{c, max}}$	Maximum quantum yield for carbon fixation	mg C E^{-1}
ϕ_e	Photoinhibition parameter	
FRRF	Fast Repetition Rate Fluorometer	---
F_o	Minimum fluorescence measured in the dark	a.u.
F_m	Maximum fluorescence measured in the dark	a.u.
F_v	Variable fluorescence ($F_m - F_o$)	a.u.
F_v/F_m	Photochemical efficiency measured in the dark	Dimensionless
F'	Steady-state fluorescence at any point	a.u.
F_o'	Minimum fluorescence measured under actinic light	a.u.
F_m'	Maximum fluorescence measured under actinic light	a.u.
F_v'	Variable fluorescence ($F_m' - F_o'$) under actinic light	a.u.
F_q'	Difference of F_m' and F' ($F_m' - F'$)	a.u.
F_q'/F_m'	Photochemical efficiency	Dimensionless
$\Delta F'/F_m'$ or Φ_{PSII}	Photochemical efficiency measured under actinic light	Dimensionless
qP	Photochemical quenching coefficient	Dimensionless (always ≤ 1)
σ_{PSII}	Absorption cross section of PSII measured in the dark	$\text{\AA}^2 \text{ quanta}^{-1}$ or $10^{-20} \text{m}^2 \text{ quanta}^{-1}$
σ_{PSII}'	Absorption cross section of PSII under actinic light	$\text{\AA}^2 \text{ quanta}^{-1}$ or $10^{-20} \text{m}^2 \text{ quanta}^{-1}$
n_{PSII}	Number of PSII reaction centers	$\text{mol chl } a (\text{mol RCII})^{-1}$

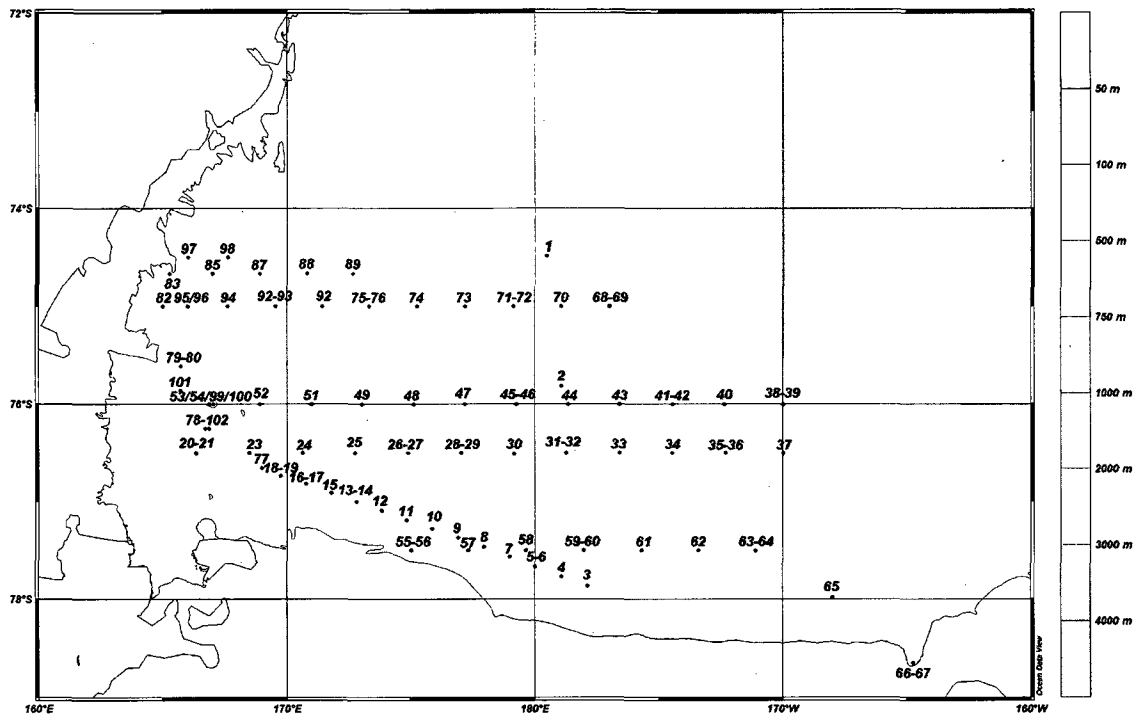


Figure 32. Map showing bathymetry of the study area and station locations of R/V N.B. Palmer cruise NBP0601 sampled between December 27, 2005 and January 23, 2006.

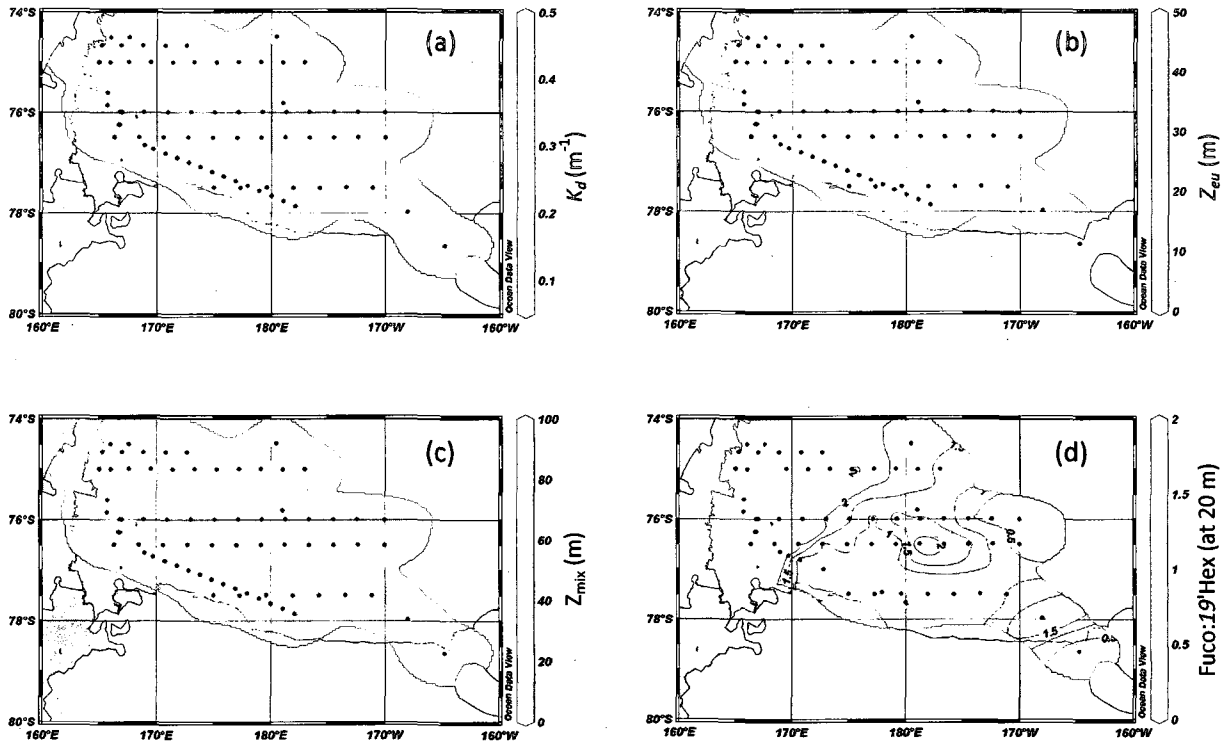


Figure 33. Distributions of (a) attenuation coefficients (K_d , m^{-1}); (b) euphotic zone depths (Z_{eu} , m); (c) mixed layer depths (Z_{mix} , m); (d) Fuco: 19'hexanoyloxyfucoxanthin ratio at 20 m (<0.2 were considered to be dominated by *Phaeocystis antarctica*).

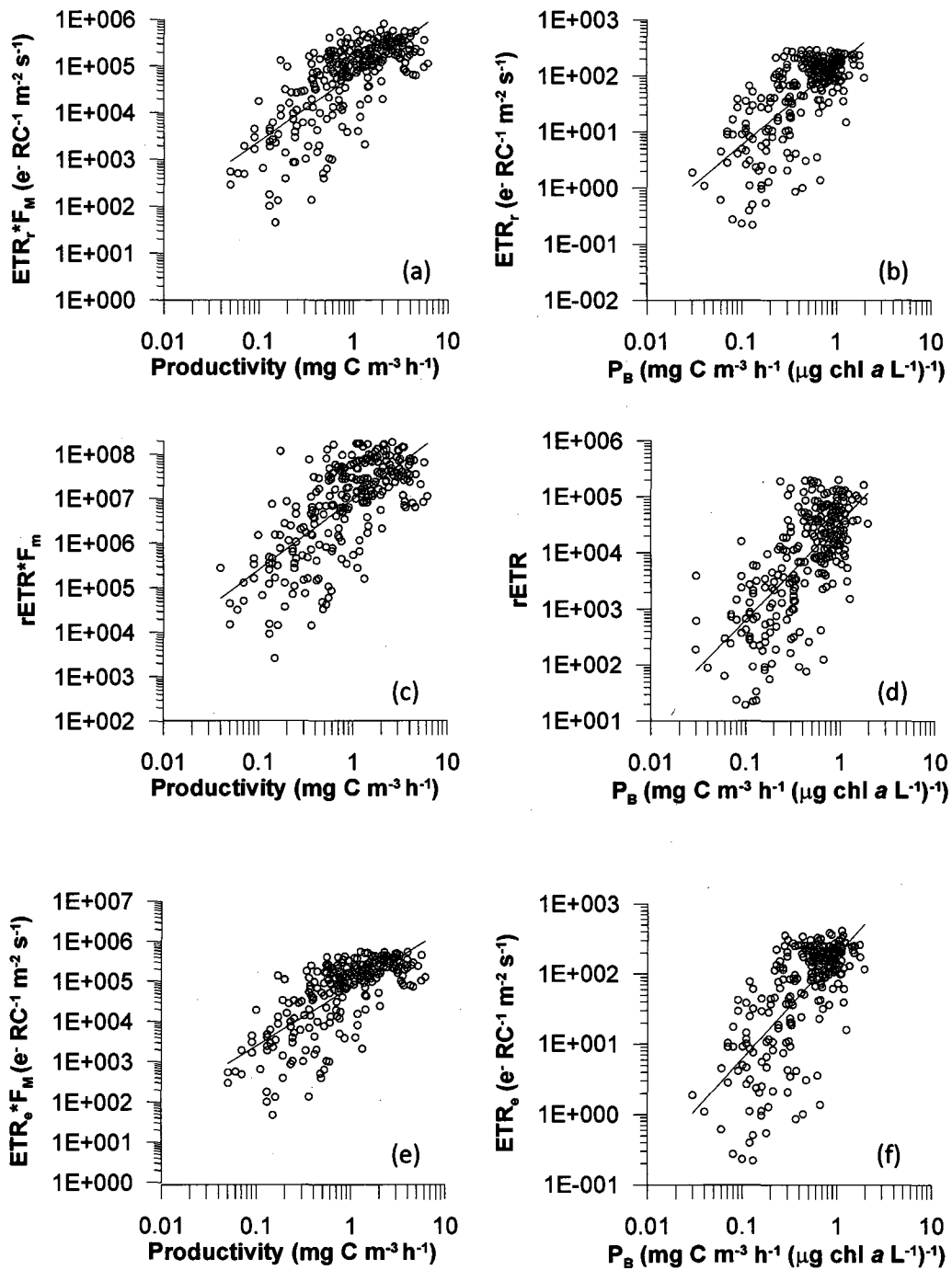


Figure 34. Correlations between electron transport rates calculated (a) from fitting rapid light curves (RLC) with rectangular hyperbolic function (ETR_r) and multiplied by the maximum fluorescence (F_m) and ^{14}C -primary productivity (PP); (b) ETR_r and productivity normalized to chlorophyll a (P_B); (c) relative electron transport ($rETR$) multiplied by F_m and PP; (d) $rETR$ and P_B ; (e) ETR calculated from exponential fitting (ETR_e) multiplied by F_m and PP; (f) ETR_e and P_B .

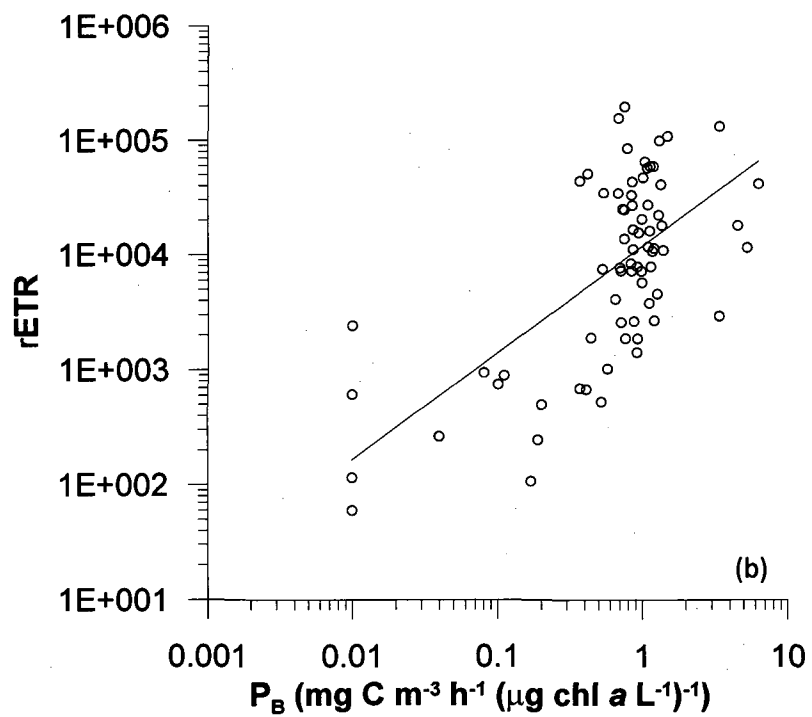
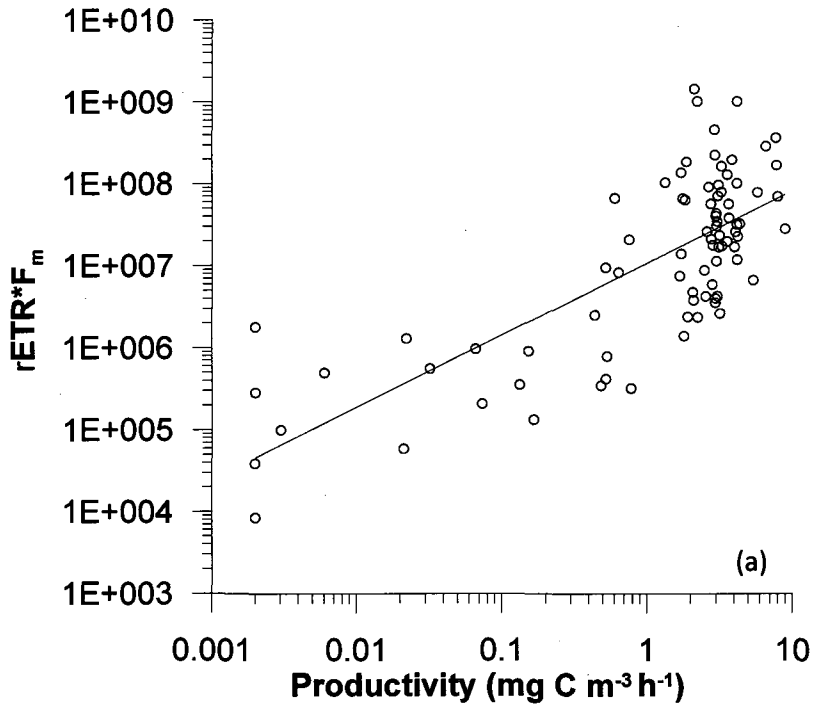


Figure 35. Correlation between relative electron transport rates (rETR) multiplied by the maximum fluorescence (F_m) and ^{14}C -primary productivity (PP) displayed on a \log_{10} scale and fitted with power function); (b) rETR and productivity normalized to chlorophyll a (P_B).

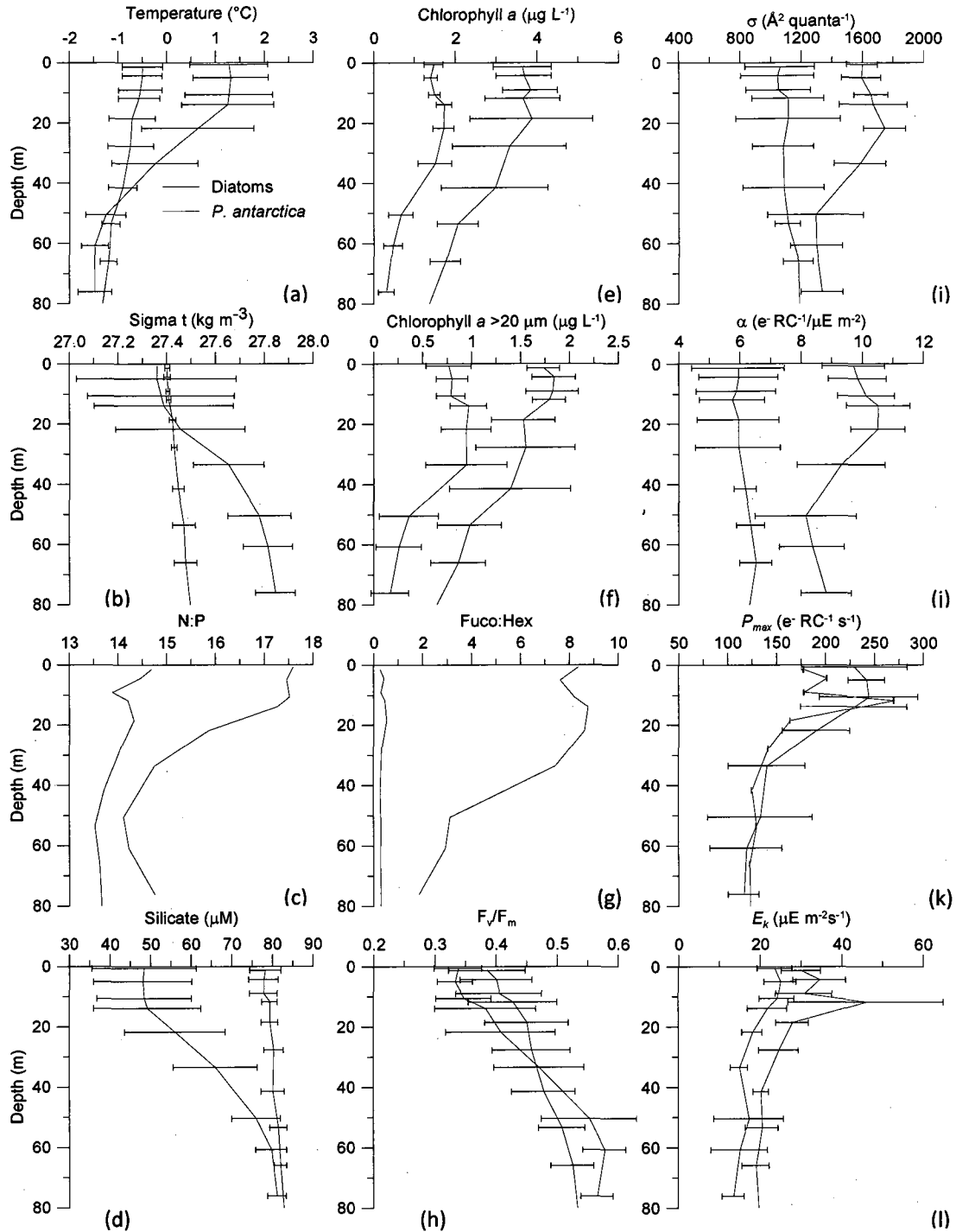


Figure 36. Averaged profiles of stations dominated by *P. antarctica* (red line, averaged CTD casts 36, 37, 39, 40) and by diatoms (green line, averaged CTD cast 88, 89, 91, 97). (a) Temperature; (b) water density; (c) N:P ratio; (d) Silicate concentration; (e) total chlorophyll *a* concentration; (f) greater than 20 μm chlorophyll *a* concentration; (g) Fuco:Hex ratio; (h) F_v/F_m ; (i) absorption cross section; (j) RLC derived α ; (k) RLC derived P_{max} ; (l) RLC derived E_k .

LITERATURE CITED

- Arrigo K. R., McClain C. R. 1994. Spring phytoplankton production in the western Ross Sea. *Science* 266:261-263
- Arrigo K. R., Robinson D. H., Worthen D. L., Dunbar R. B., DiTullio G. R., VanWoert M., Lizotte M. P. 1999. Phytoplankton community structure and the drawdown of nutrients and CO₂ in the Southern Ocean. *Science* 283:365-367
- Arrigo K. R., DiTullio G. R., Dunbar R. B., Robinson D. H., VanWoert M. L., Worthen D. L., Lizotte M. P. 2000. Phytoplankton taxonomic variability in nutrient utilization and primary production in the Ross Sea. *Journal of Geophysical Research* 105:8827-8846
- Babin M., Morel A., Claustre H., Bricaud A., Kolber Z. S., Falkowski P. G. 1996. Nitrogen- and irradiance-dependent variations of the maximum quantum yield of carbon fixation in eutrophic, mesotrophic and oligotrophic marine systems. *Deep-Sea Research* 43:1241-1272
- Behrenfeld M. J., Falkowski P. G. 1997. A consumers guide to phytoplankton primary productivity models. *Limnology and Oceanography* 42:1479-1491
- Boyd P. W., Aiken J., Kolber Z. S. 1997. Comparison of radiocarbon and fluorescence based (pump and probe) measurements of phytoplankton photosynthetic characteristics in the Northeast Atlantic Ocean. *Marine Ecology Progress Series* 149:215-226
- Corno G., Letelier R. M., Abbott M. R., Karl D. M. 2006. Assessing primary production variability in the North Pacific subtropical gyre: a comparison of fast repetition rate fluorometry and ¹⁴C measurements. *Journal of Phycology* 42:51-60
- Cosgrove J. 2007. *Marine phytoplankton primary production and ecophysiology using chlorophyll *a* fluorescence*. Dissertation, Murdoch University, Perth, WA Australia pp. 247
- del Valle D. A., Kieber D. J., Bisgrove J., Kiene R. P. 2007. Light-stimulated production of dissolved DMSO by a particle-associated process in the Ross Sea, Antarctica. *Limnology and Oceanography* 52:2456-2466
- DiTullio G. R., Smith W. O., Jr. 1995. Relationship between dimethylsulfide and phytoplankton pigment concentrations in the Ross Sea, Antarctica. *Deep Sea Research* 42:873-892
- DiTullio G. R., Smith W. O., Jr 1996. Spatial patterns in phytoplankton biomass pigment distributions in the Ross Sea. *Journal of Geophysical Research* 101:18467-18477
- Dunbar R. B., Arrigo K. R., DiTullio G. D., Leventer A., Lizotte M. P., Van Woert M. L., Robinson D. H. 2003. Non-Redfield production and export of marine organic matter: a recurrent part of the annual cycle in the Ross Sea, Antarctica. In: *Biogeochemistry of the Ross Sea, Vol 78*. American Geophysical Union, 179-196

- Duysens L. N. M., Sweers H. E. 1963. Mechanisms of two photochemical reactions in algae as studied by means of fluorescence. In: Miyachi S. (ed) *Studies on microalgae and photosynthetic bacteria*. University Tokyo Press, Tokyo, Japan, 353-372
- Estevez-Blanco P., Cermeno P., Espineira M., Fernandez E. 2006. Phytoplankton photosynthetic efficiency and primary production rates estimated from fast repetition rate fluorometry at coastal embayments affected by upwelling (Rias Baixas, NW of Spain), 1153-1165
- Falkowski P. G., Kiefer D. A. 1985. Chlorophyll *a* fluorescence in phytoplankton: relationship to photosynthesis and biomass. *Journal of Plankton Research* 7:715-731
- Falkowski P. G., Wyman K., Ley A. C., Mauzerall D. 1986. Relationship of steady-state photosynthesis to fluorescence in eucaryotic algae. *Biochimica et Biophysica Acta* 849:183-192
- Flameling I. A., Kromkamp J. 1988. Light dependence of quantum yields for PSII charge separation and oxygen evolution in eucaryotic algae. *Limnology and Oceanography* 43:284-297
- Flameling I. A., Kromkamp J. 1998. Light dependence of quantum yields for PSII charge separation and oxygen evolution in eucaryotic algae. *Limnology and Oceanography* 43:284-297
- Fofonoff P., Millard R. C. J. 1983. Algorithms for computation of fundamental properties of seawater, in UNESCO technical papers in marine science Series, 44, Unesco (ed), pp. 53
- Genty B., Briantais J. M., Baker N. R. 1989. The relationship between the quantum yield of photosynthetic electron transport and quenching of chlorophyll fluorescence. *Biochimica et Biophysica Acta* 990:87-92
- Harrison W. G., Platt T. 1986. Photosynthesis-irradiance relationships in polar and temperate phytoplankton populations. *Polar Biology* 5
- Hartig P., Wolfstein K., Lippemeier S., Colijn F. 1998. Photosynthetic activity of natural microphytobenthos populations measured by fluorescence (PAM) and ¹⁴C-tracer methods: a comparison. *Marine Ecology Progress Series* 166:53-62
- Jacobs S. S., Giulivi C. F., Mele P. A. 2002. Freshening of the Ross Sea During the Late 20th Century. *Science* 297:386-389
- Kautsky H., Hirsch A. 1931. Neue Versuche zur Kohlensäureassimilation. *Naturwissenschaften* 19:964-964
- Kirk J. T. O. 1983. *Light and Photosynthesis in Aquatic Ecosystem*, Vol. Cambridge Univ. Press, Cambridge pp. 401
- Kolber Z. S., Falkowski P. G. 1992. Fast Repetition Rate (FRR) fluorometer for making in situ measurements of primary productivity. *Ocean 92 Conference*, Newport, Rhode Island, 637-641

- Kolber Z. S., Falkowski G. P. 1993. Use of active fluorescence to estimate phytoplankton photosynthesis in situ. *Limnology and Oceanography* 38:1646-4665
- Kolber Z. S., Barber R. T., Coale K. H., Fitzwater S. E., Greene R. M., Johnson K. S., Lindley S., Falkowski G. P. 1994. Iron limitation of the phytoplankton photosynthesis in the equatorial Pacific Ocean. *Nature* 371:145-149
- Kolber Z. S., Prasil O., Falkowski P. G. 1998. Measurements of variable chlorophyll fluorescence using fast repetition rate techniques: defining methodology and experimental protocols. *Biochimica et Biophysica Acta* 1367:88-106
- Kromkamp J., Peene J. 1999. Estimation of phytoplankton photosynthesis and nutrient limitation in the Eastern Scheldt estuary using variable fluorescence. *Aquatic Ecology* 33:101-104
- Kromkamp J. C., Domin A., Dubinsky Z., Lehmann C., Schanz F. 2001. Changes in photosynthetic properties measured by oxygen evolution and variable chlorophyll fluorescence in a simulated entrainment experiment with the cyanobacterium *Planktothrix rubescens*. *Aquatic Sciences* 63:363-382
- Kropuenske L. R., Mills M. M., Dijken G. L. v., Bailey S., Robinson D. H., Welschmeyer N. A., Arrigo K. R. 2009. Photophysiology in two major Southern Ocean phytoplankton taxa: Photoprotection in *Phaeocystis antarctica* and *Fragilariopsis cylindrus*. *Limnology and Oceanography* 54:1176-1196
- Litchman E., Klausmeier C. A. 2001. Competition of phytoplankton under fluctuating light. *American Naturalist* 157:170-187
- Lorenzen C. J. 1966. A method for the continuous measurement of in vivo chlorophyll concentration. *Deep Sea Research* 13:223-227
- Marra J., Barber R. T. 2004. Phytoplankton and heterotrophic respiration in the surface layer of the ocean. *Geophysical Research Letters* 31 doi: 10.1029/2004gl019664
- Mills M. M., Kropuenske L. R., Van Dijken G. L., Alderkamp A. C., Mine Berg G., Robinson H. D., Welschmeyer N. A., Arrigo K. R. 2010. Photophysiology in two Southern Ocean taxa: Photosynthesis of *Phaeocystis antarctica* (Prymnesiophyceae) and *Fragilariopsis cylindrus* (Bacillariophyceae) under simulated mixed layer irradiance. *Journal of Phycology*:submitted
- Moore C. M., Suggett D., Holligan P. M., Sharples J., Abraham E. R., Lucas M. I., Rippert T. P., Fisher N. R., Simpson J. H., Hydes D. J. 2003. Physical controls on phytoplankton physiology and production at a shelf sea front: a fast repetition rate fluorometer based study. *Marine Ecology Progress Series* 259:29-45
- Moore C. M., Seeyave S., Hickman A. E., Allen J. T., Lucas M. I., Planquette H., Pollard R. T., Poulton A. J. 2007. Iron-light interactions during the CROZet natural iron bloom and EXport experiment (CROZEX) I: Phytoplankton growth and photophysiology. *Deep Sea Research Part II: Topical Studies in Oceanography* 54:2045-2065

- Morgan P. 1993. SEAWATER library. In: CSIRO D. o., Oceanography (ed)
- Mortain-Bertrand A. 1989. Effects of light fluctuations on the growth and productivity of Antarctic diatoms in culture. *Polar Biology* 9:245-252
- Platt T., Gallegos L., Harrison W. G. 1980. Photoinhibition of photosynthesis in natural assemblages of marine phytoplankton. *Journal of Marine Research* 38:687-701
- Prieto L., Vaillancourt R. D., Hales B., Marra J. 2008. On the relationship between carbon fixation efficiency and bio-optical characteristics of phytoplankton. *Journal of Plankton Research* 30:43-56
- Raateoja M. 2004. Fast repetition rate fluorometry (FRRF) measuring phytoplankton productivity: A case at the entrance to the Gulf of Finland, Baltic Sea. *Boreal Environmental Research* 9:236-276
- Raateoja M., Seppala J., Kuosa H. 2004. Bio-optical modelling of primary production in the SW Finnish coastal zone, Baltic Sea: fast repetition rate fluorometry in Case 2 waters. *Marine Ecology-Progress Series* 267:9-26
- Raateoja M. 2006. Photobiological studies of Baltic Sea phytoplankton. Dissertation, Finnish Institute of Marine Research, Finland, Helsinki pp. 44
- Ralph P. J., Gademann R. 2005. Rapid light curves: A powerful tool to assess photosynthetic activity. *Aquatic Botany* 82:222-237
- Sakshaug E. 1989. The physiological ecology of polar phytoplankton. In: Rey L., Alexander V. (eds) Sixth Conference of the Comité Arctique International. EJ Brill, Leiden, 61-89
- Schlitzer R. 2008. Ocean Data View. <http://odv.awi.de>
- Schreiber U., Bilger W. 1986. Continuous recording of photochemical and non-photochemical chlorophyll fluorescence quenching with a new type of modulation fluorometer. *Photosynthesis Research* 10:51-62
- Shields A. R., Smith W. O., Jr. 2009. Size-fractionated photosynthesis/irradiance relationships during *Phaeocystis antarctica*-dominated blooms in the Ross Sea, Antarctica *Journal of Plankton Research* 31:701-712
- Smith W. O., Jr, Nelson D. M. 1985. Phytoplankton bloom produced by a receding ice edge in the Ross Sea: spatial coherence with the density field. *Science* 227:163-166
- Smith W. O., Jr, Asper V. L. 2001. The influence of phytoplankton assemblage composition on biogeochemical characteristics and cycles in the southern Ross Sea, Antarctica. *Deep Sea Research I* 48:137-161

- Smith W. O., Jr, Ainley D. G., Cattaneo-Vietti R. 2007. Trophic interactions within the Ross Sea continental shelf ecosystem. *Philosophical Transactions of the Royal Society B: Biological Sciences* 362:95-111
- Smith W. O., Jr, Asper V. A., Tozzi S., Luiu X. 2010. Surface layer variability in the Ross Sea, Antarctica as assessed by continuous fluorescence measurements. *Progress In Oceanography*:submitted
- Smith W. O., Jr., Gordon L. I. 1997. Hyperproductivity of the Ross Sea (Antarctica) polynya during austral spring. *Geophysical Research Letters* 24:233-236
- Smith W. O., Jr., Marra J., Hiscock M. R., Barber R. T. 2000. The seasonal cycle of phytoplankton biomass and primary productivity in the Ross Sea, Antarctica. *Deep Sea Research II* 47:3119-3140
- Smyth T. J., Pemberton K. L., Aiken J., Geider R. J. 2004. A methodology to determine primary production and phytoplankton photosynthetic parameters from Fast Repetition Rate Fluorometry. *Journal of Plankton Research* 26:1337-1350
- Suggett D., Kraay G. W., Holligan P., Davey M. S., Aiken J., Geider R. J. 2001. Assessment of photosynthesis in a spring cyanobacterial bloom by use of a fast repetition rate fluorometer. *Limnology and Oceanography* 46:802-810
- van Hilst C. M., Smith W. O., Jr 2002. Photosynthesis/irradiance relationships in the Ross Sea, Antarctica, and their control by phytoplankton assemblage composition and environmental factors. *Marine Ecology Progress Series* 226:1-12
- Webb W. L., Newron M., Starr D. 1974. Carbon dioxide exchange of *Alnus rubra*: a mathematical model. *Oecologia* 17:281-291
- Weinberg S. 1976. Submarine daylight and ecology. *Marine Biology* 37:291-304
- Wilson D. L., Smith W. O., Jr., Nelson D. M. 1986. Phytoplankton bloom dynamics of the western Ross Sea ice edge--I. Primary productivity and species-specific production. *Deep Sea Research I* 33:1375-1387
- Yoder J. A., McClain C. R., Feldman G. C., Esaias W. 1993. Annual cycles of phytoplankton chlorophyll concentrations in the global ocean: A satellite view. *Global Biogeochem. Cycles* 7:181-194

SECTION V. SUMMARY

1. A significant difference in the photosynthetic recovery rates was found between diatoms and *Phaeocystis antarctica*, with the latter always being faster.
2. Faster photorecovery in *Phaeocystis antarctica* indicates a better adaptation to fluctuating light regimes commonly found in regions where the mixed layer depths are deeper than the euphotic zone.
3. *Pseudonitzschia sp.* and *Phaeocystis antarctica*, despite being kept in the dark for 14 days, maintain full photosynthetic capability during that time, proving a high photoadaptation and photoresilience to extended periods of darkness that can be experienced at higher latitudes.
4. *Pseudonitzschia sp.* and *Phaeocystis antarctica*, when exposed to high irradiance levels, photorecovered independently of the exposure time, with *Phaeocystis antarctica* always recovering faster.
5. All experiments involving iron additions resulted in increased photosynthetic quantum yields, indicating iron limitation of Ross Sea polynya natural assemblages collected during the austral spring and summer.
6. Increased temperature had an additive effect in conjunction with iron in enhancing photosynthetic quantum yield, implying higher productivity in a projected warmer polynya.
7. Increased CO₂ did not affect photosynthetic rates measured by variable fluorescence either in austral spring or summer.
8. Only iron influenced photosynthetic quantum yields; no evidence was found for co-limitation with vitamin B₁₂.

9. Extensive testing over a full range of depths and chlorophyll concentrations demonstrated that dissolved fluorescence material contributed less than 1% to the total fluorescence signal.
10. Hydrography and photosynthetic quantum yields in the Ross Sea polynya are much more homogenous in the spring than in the summer. Water temperatures in November and December 2006 were significantly colder, averaging -1.78°C , and within variations of about 1°C , while in December 2005, January 2006 water was warmer, averaging -0.73°C , and with a range of over 4°C .
11. Photosynthetic quantum yields were significantly higher in the spring; in the summer photoinhibition in the upper 50 m was commonly observed, with higher photosynthetic quantum yields only below the mixed layer depth.
12. Poor correlation between iron concentrations and photosynthetic quantum yields was potentially explained due to an offset in spatial and temporal collection of the samples.
13. Rapid light curves and the determination of photosynthetic parameters allow characterization of assemblages dominated by diatoms or *P. antarctica*; despite having similar photosynthetic quantum yields and ETR_{max} , diatoms are characterized by higher α and σ_{PSII} while *P. antarctica* by higher E_k .
14. Elucidating the effects of environmental factors on structuring the phytoplankton dynamics in the Ross Sea significantly contributes to a better understanding Ross Sea ecosystem.

15. Understanding forcing factors that control phytoplankton blooms and succession in the Ross Sea can improve our understanding of carbon and other element cycles at the regional scale; furthermore, the cascading impacts on these biogeochemical cycles on much broader scales, especially in light of likely extreme changes in the area due to planetary climate trends, is also improved.
16. Submersible FRRF profiler will allow better determination of *in situ* ETR and modeled production.

APPENDIX 1

Table 1. RST1 repeated measure GLM results for F_v/F_m .

Source	DF	Sum of Squares	Mean Square	F Value	Pr > F
Model	4	0.44970427	0.11242607	38.96	<.0001
Error	91	0.26260952	0.00288582		
Corrected Total	95	0.71231379			

R-Square	Coeff Var	Root MSE	F_v/F_m Mean
0.631329	12.02176	0.05372	0.446855

Source	DF	Type III SS	Mean Square	F Value	Pr > F
Temperature	1	0.01147016	0.01147016	3.97	0.0492
Fe	1	0.4235723	0.4235723	146.78	<.0001
Temperature*Fe	1	0.00384877	0.00384877	1.33	0.2512
Day	1	0.01081304	0.01081304	3.75	0.056

Table 2. RST1 repeated measure GLM results for σ_{PSII} .

Source	DF	Sum of Squares	Mean Square	F Value	Pr > F
Model	4	11533589.61	2883397.4	28.34	<.0001
Error	91	9260088.89	101759.22		
Corrected Total	95	20793678.5			

R-Square	Coeff Var	Root MSE	σ_{PSII} Mean
0.554668	17.45723	318.9972	1827.307

Source	DF	Type III SS	Mean Square	F Value	Pr > F
Temperature	1	192.879	192.879	0	0.9654
Fe	1	9792519.762	9792519.762	96.23	<.0001
Temperature*Fe	1	603611.778	603611.778	5.93	0.0168
Day	1	1137265.19	1137265.19	11.18	0.0012

Table 3. RST2 repeated measure GLM results for F_v/F_m .

Source	DF	Sum of Squares	Mean Square	F Value	Pr > F
Model	4	0.54329017	0.13582254	160.03	<.0001
Error	78	0.06620113	0.00084873		
Corrected Total	82	0.6094913			

R-Square	Coeff Var	Root MSE	F_v/F_m Mean
0.891383	6.676798	0.029133	0.436332

Source	DF	Type III SS	Mean Square	F Value	Pr > F
Temperature	1	0.02492888	0.02492888	29.37	<.0001
Light	1	0.0137108	0.0137108	16.15	0.0001
Temperature*Light	1	0.00032808	0.00032808	0.39	0.5359
day	1	0.33406084	0.33406084	393.6	<.0001

Table 4. RST2 repeated measure GLM for σ_{PSII} .

Source	DF	Sum of Squares	Mean Square	F Value	Pr > F
Model	4	17218756.07	4304689.02	65.29	<.0001
Error	78	5143025.72	65936.23		
Corrected Total	82	22361781.79			

R-Square	Coeff Var	Root MSE	σ_{PSII} Mean
0.770008	7.678473	256.7805	3344.161

Source	DF	Type III SS	Mean Square	F Value	Pr > F
Temperature	1	5017630.859	5017630.859	76.1	<.0001
Light	1	2382997.235	2382997.235	36.14	<.0001
Temperature*Light	1	384588.457	384588.457	5.83	0.0181
day	1	8264061.445	8264061.445	125.33	<.0001

Table 5. RSC1 repeated measure GLM for F_v/F_m .

Source	DF	Sum of Squares	Mean Square	F Value	Pr > F
Model	10	1.61659531	0.16165953	70.92	<.0001
Error	298	0.67927664	0.00227945		
Corrected Total	308	2.29587195			

R-Square	Coeff Var	Root MSE	F_v/F_m Mean
0.704131	10.03956	0.047744	0.475555

Source	DF	Type III SS	Mean Square	F Value	Pr > F
Light	1	0.33671585	0.33671585	147.72	<.0001
Iron	1	0.01395351	0.01395351	6.12	0.0139
Iron*Light	1	0.00096032	0.00096032	0.42	0.5168
CO ₂	1	0.05744392	0.05744392	25.2	<.0001
Light*CO ₂	1	0.00899101	0.00899101	3.94	0.0479
Iron*CO ₂	1	0.0026575	0.0026575	1.17	0.2811
Iron*Light*CO ₂	1	0.01372209	0.01372209	6.02	0.0147
Day	1	0.61854888	0.61854888	271.36	<.0001
Day2	1	0.33115708	0.33115708	145.28	<.0001
Day3	1	0.17819243	0.17819243	78.17	<.0001

Table 6. RSC1 repeated measure GLM for σ_{PSII} .

Source	DF	Sum of Squares	Mean Square	F Value	Pr > F
Model	10	161523224.9	16152322.5	303.39	<.0001
Error	298	15865587.1	53240.2		
Corrected Total	308	177388812			

R-Square	Coeff Var	Root MSE	σ_{PSII} Mean
0.91056	22.57291	230.7384	1022.192

Source	DF	Type III SS	Mean Square	F Value	Pr > F
Light	1	837291.43	837291.43	15.73	<.0001
Iron	1	51438.98	51438.98	0.97	0.3264
Iron*Light	1	12432.81	12432.81	0.23	0.6293
CO ₂	1	298624.48	298624.48	5.61	0.0185
Light*CO ₂	1	72330.01	72330.01	1.36	0.2447
Iron*CO ₂	1	45500.52	45500.52	0.85	0.356
Iron*Light*CO ₂	1	20440.94	20440.94	0.38	0.536
Day	1	81538459.55	81538459.55	1531.52	<.0001
Day2	1	43648155.24	43648155.24	819.83	<.0001
Day3	1	27784098.96	27784098.96	521.86	<.0001

Table 7. RSC2 repeated measure GLM for F_v/F_m .

	DF	Sum of Squares	Mean Square	F Value	Pr > F
Model	8	6.74112238	0.8426403	501.35	<.0001
Error	976	1.64040066	0.00168074		
Corrected Total	984	8.38152304			

R-Square	Coeff Var	Root MSE	F_v/F_m Mean
0.804284	8.10481	0.040997	0.505833

Source	DF	Type III SS	Mean Square	F Value	Pr > F
Light	1	0.89340766	0.89340766	531.56	<.0001
Iron	1	0.32392026	0.32392026	192.72	<.0001
Iron*Light	1	0.00748585	0.00748585	4.45	0.0351
CO ₂	1	0.00205982	0.00205982	1.23	0.2685
Light*CO ₂	1	0.01253689	0.01253689	7.46	0.0064
Iron*CO ₂	1	0.0062821	0.0062821	3.74	0.0535
Iron*Light*CO ₂	1	0.0070184	0.0070184	4.18	0.0413
Day	1	5.43554784	5.43554784	3234.02	<.0001

Table 8. RSC2 repeated measure GLM for σ_{PSII} .

Source	DF	Sum of Squares	Mean Square	F Value	Pr > F
Model	8	264902317.9	33112789.7	334.65	<.0001
Error	976	96573547.7	98948.3		
Corrected Total	984	361475865.6			

R-Square	Coeff Var	Root MSE	σ_{PSII} Mean
0.732835	9.955296	314.5605	3159.73

Source	DF	Type III SS	Mean Square	F Value	Pr > F
Light	1	22332993.1	22332993.1	225.7	<.0001
Iron	1	18075730	18075730	182.68	<.0001
Iron*Light	1	382903.4	382903.4	3.87	0.0494
CO ₂	1	399343.3	399343.3	4.04	0.0448
Light*CO ₂	1	330897.6	330897.6	3.34	0.0677
Iron*CO ₂	1	239338	239338	2.42	0.1202
Iron*Light*CO ₂	1	1475062.2	1475062.2	14.91	0.0001
Day	1	224370801.7	224370801.7	2267.56	<.0001

Table 9. WHOI 1 repeated measure GLM for F_v/F_m .

Treatment	Estimate	SE	t value	Pr > t
B12	0.009208	0.015041	0.61	0.5426
Co	0.010642	0.015041	0.71	0.4819
Control	0.009308	0.015041	0.62	0.5383
Fe	0.059736	0.015041	3.97	0.0002
FeB12	0.068367	0.015041	4.55	<0.0001
FeCo	0.040242	0.015041	2.68	0.0095
FeZn	0.047625	0.015041	3.17	0.0024
Zn	0	.	.	.

Table 10. WHOI 1 repeated measure GLM for σ_{PSII} .

Treatment	Estimate	SE	t value	Pr > t
B12	-294.294	128.2685	-2.29	0.0252
Co	-490.962	128.2685	-3.83	0.0003
Control	-262.158	128.2685	-2.04	0.0452
Fe	-672.447	128.2685	-5.24	<.0001
FeB12	-677.576	128.2685	-5.28	<.0001
FeCo	-630.233	128.2685	-4.91	<.0001
FeZn	-606.56	128.2685	-4.73	<.0001
Zn	0	.	.	.

Table 11. WHOI 2 repeated measure GLM for F_v/F_m .

Treatment	Estimate	SE	t value	Pr > t
B12	0.007833	0.005198	1.51	0.1367
Co	-0.01497	0.005198	-2.88	0.0054
Control	-0.0338	0.005198	-6.5	<.0001
Fe	0.041533	0.005198	7.99	<.0001
FeB12	0.028867	0.005198	5.55	<.0001
FeCo	0.0476	0.005198	9.16	<.0001
FeZn	0.0693	0.005198	13.33	<.0001
Zn	0	.	.	.

Table 12. WHOI 2 repeated measure GLM for σ_{PSII} .

Treatment	Estimate	SE	t value	Pr > t
B12	-399.973	52.29929	-7.65	<.0001
Co	251.7733	52.29929	4.81	<.0001
Control	148.4133	52.29929	2.84	0.0061
Fe	-692.06	52.29929	-13.23	<.0001
FeB12	-458.227	52.29929	-8.76	<.0001
FeCo	-570.287	52.29929	-10.9	<.0001
FeZn	-706.02	52.29929	-13.5	<.0001
Zn	0	.	.	.

Table 13. WHOI 3 repeated measure GLM for F_v/F_m .

Treatment	Estimate	SE	t value	Pr > t
B12	-0.0226	0.00923	-2.45	0.0171
Co	-0.0099	0.00923	-1.07	0.2875
Control	0.057033	0.00923	6.18	<.0001
Fe	0.155267	0.00923	16.82	<.0001
FeB12	0.116	0.00923	12.57	<.0001
FeCo	0.123933	0.00923	13.43	<.0001
FeZn	0.099767	0.00923	10.81	<.0001
Zn	0	.	.	.

Table 14. WHOI 3 repeated measure GLM for σ_{PSII} .

Treatment	Estimate	SE	t value	Pr > t
B12	92.95667	187.3002	0.5	0.6214
Co	291.77	187.3002	1.56	0.1242
Control	-80.5567	187.3002	-0.43	0.6686
Fe	-1044.9	187.3002	-5.58	<.0001
FeB12	-1043.55	187.3002	-5.57	<.0001
FeCo	-957.303	187.3002	-5.11	<.0001
FeZn	-500.277	187.3002	-2.67	0.0096
Zn	0	.	.	.

APPENDIX 2

Table 1. NBPO601 CTD cast, station, date, locations, mix layer depths (z_{mix} , m), light extinction coefficient (K_d m^{-1}); euphotic zone depth (z_{eu} , m) defined as 1% of E_0 and MBARI FRRF measurements.

CTD	Station	Date	Latitude	Longitude	K_d	$Z_{mix(0.05)}$	Z_{eu}	FRRF
1	1	12/27/2005	-74° 29.16'	-179° -31.22'	0.26	18	18	x
2	2	12/28/2005	-75° 48.91'	-178° -56.75'	0.20	29	23	x
3	3	12/28/2005	-77° 51.94'	-177° -52.69'	0.19	84	25	
4	4	12/28/2005	-77° 45.94'	-178° -56.18'	0.21	84	21	
5	5	12/28/2005	-77° 39.99'	-179° -59.98'	0.22	50	21	
6	5	12/28/2005	-77° 39.99'	-179° -59.98'	0.20	11	23	
7	6	12/29/2005	-77° 33.79'	178° 58.21'	0.32	22	14	x
8	7	12/29/2005	-77° 27.8'	177° 55.99'	0.20	18	23	
9	8	12/29/2005	-77° 22.12'	176° 54.01'	0.20	17	23	x
10	9	12/29/2005	-77° 16.55'	175° 51.73'	0.38	50	12	
11	10	12/29/2005	-77° 11.26'	174° 49.45'	0.35	22	13	
12	11	12/29/2005	-77° 5.47'	173° 48.89'	0.21	26	22	
13	12	12/29/2005	-77° 0.00'	172° 48.00'	0.24	25	19	
14	12	12/29/2005	-77° 0.00'	172° 47.98'	0.20	21	23	
15	13	12/30/2005	-76° 54.54'	171° 46.81'	0.21	30	22	
16	14	12/30/2005	-76° 49.15'	170° 45.72'	0.23	65	20	
17	14	12/30/2005	-76° 49.11'	170° 45.67'	0.22	56	21	
18	15	12/30/2005	-76° 43.99'	169° 43.00'	0.18	29	25	
19	15	12/30/2005	-76° 43.99'	169° 42.98'	0.24	44	19	
20	16	12/31/2005	-76° 30.1'	166° 19.23'	0.10	12	46	
21	16	1/1/2006	-76° 29.98'	166° 19.63'	0.09	11	49	x
22	17	1/1/2006	-76° 29.98'	168° 28.18'	0.20	49	23	x
23	18	1/1/2006	-76° 29.98'	170° 36.49'	0.15	32	30	
24	18	1/1/2006	-76° 29.98'	170° 36.49'	0.16	26	29	x
25	19	1/2/2006	-76° 29.98'	172° 45.00'	0.19	20	25	x
26	20	1/2/2006	-76° 30.00'	174° 53.68'	0.30	26	15	x
27	20	1/2/2006	-76° 30.00'	174° 53.68'	0.39	20	12	
28	21	1/2/2006	-76° 30.00'	177° 1.99'	0.16	32	29	
29	21	1/2/2006	-76° 30.00'	177° 1.99'	0.17	33	27	x
30	22	1/3/2006	-76° 30.44'	179° 9.43'	0.20	60	23	x
31	23	1/3/2006	-76° 29.96'	-178° -44.89'	0.20	29	23	
32	23	1/3/2006	-76° 29.96'	-178° -44.89'	0.19	27	24	x
33	24	1/4/2006	-76° 30.01'	-176° -36.97'	0.27	37	17	x
34	25	1/4/2006	-76° 30.00'	-174° -28.69'	0.19	48	25	x
35	26	1/4/2006	-76° 29.95'	-172° -20.08'	0.21	32	22	

CTD	Station	Date	Latitude	Longitude	K_d	$Z_{mix(0.05)}$	Z_{eu}	FRRF
36	26	1/4/2006	-76° 29.95'	-172° -20.08'	0.22	27	21	x
37	27	1/5/2006	-76° 30.1'	-169° -59.97'	0.24	55	19	x
38	28	1/5/2006	-76° 0.01'	-170° -0.06'	0.17	43	27	
39	28	1/5/2006	-76° 0.01'	-170° -0.06'	0.18	63	25	x
40	29	1/6/2006	-75° 59.98'	-172° -23.13'	0.19	56	25	x
41	30	1/6/2006	-75° 59.98'	-174° -28.05'	0.20	35	23	
42	30	1/6/2006	-75° 59.98'	-174° -28.05'	0.23	42	20	x
43	31	1/7/2006	-75° 59.98'	-176° -37.01'	0.22	31	21	x
44	32	1/7/2006	-75° 59.98'	-178° -40.8'	0.15	31	30	x
45	33	1/7/2006	-75° 59.98'	179° 14.93'	0.15	44	32	
46	33	1/7/2006	-75° 59.98'	179° 14.93'	0.14	46	33	x
47	34	1/8/2006	-75° 59.95'	177° 10.66'	0.14	76	32	x
48	35	1/8/2006	-75° 59.98'	175° 6.7'	0.14	44	34	x
49	36	1/8/2006	-75° 59.96'	173° 2.24'	0.13	41	34	
50	36	1/8/2006	-75° 59.96'	173° 2.24'	0.12	49	39	x
51	37	1/9/2006	-75° 59.95'	170° 58.68'	0.15	46	30	x
52	38	1/9/2006	-75° 59.98'	168° 53.98'	0.15	39	31	
53	39	1/9/2006	-75° 59.98'	166° 50.31'	0.36	10	13	
54	39	1/9/2006	-75° 59.98'	166° 50.32'	0.32	10	15	x
55	40	1/10/2006	-77° 29.98'	174° 59.98'	0.11	70	43	x
56	40	1/10/2006	-77° 29.98'	174° 59.98'	0.11	57	42	
57	41	1/11/2006	-77° 30.01'	177° 18.4'	0.16	54	28	x
58	42	1/11/2006	-77° 29.98'	179° 37.09'	0.16	34	29	x
59	43	1/11/2006	-77° 30.00'	-178° -3.52'	0.12	53	38	
60	43	1/11/2006	-77° 30.00'	-178° -3.52'	0.12	44	40	x
61	44	1/12/2006	-77° 30.04'	-175° -44.71'	0.13	31	37	x
62	45	1/12/2006	-77° 29.98'	-173° -26.29'	0.14	25	32	
63	46	1/12/2006	-77° 30.07'	-171° -7.63'	0.19	22	24	
64	46	1/12/2006	-77° 30.07'	-171° -7.63'	0.17	29	28	x
65	47	1/13/2006	-77° 58.92'	-168° -0.85'	0.12	27	39	x
66	48	1/13/2006	-78° 38.95'	-164° -45'	0.16	20	28	
67	48	1/13/2006	-78° 39.13'	-164° -45.01'	0.14	27	33	x
68	49	1/15/2006	-74° 59.95'	-177° -0.64'	0.10	179	48	
69	49	1/15/2006	-75° 0.03'	-176° -59.56'	0.12	24	39	x
70	50	1/15/2006	-75° 0.00'	-178° -56.18'	0.13	59	35	x
71	51	1/15/2006	-74° 59.95'	179° 8.2'	0.18	31	26	
72	51	1/15/2006	-74° 59.95'	179° 8.2'	0.18	31	26	x
73	52	1/15/2006	-74° 59.98'	177° 12.04'	0.18	37	25	x
74	53	1/16/2006	-75° 0.04'	175° 16.21'	0.13	26	36	x
75	54	1/16/2006	-74° 59.95'	173° 19.9'	0.12	24	40	

CTD	Station	Date	Latitude	Longitude	K_d	$Z_{mix(0.05)}$	Z_{eu}	FRRF
76	54	1/16/2006	-74° 59.95'	173° 19.91'	0.13	22	36	x
77	55	1/18/2006	-76° 39.43'	168° 58.41'	0.15	27	31	x
78	56	1/18/2006	-76° 15.00'	166° 49.99'	0.32	16	15	x
79	57	1/18/2006	-75° 36.64'	165° 43.45'	0.08	178	58	
80	57	1/18/2006	-75° 36.64'	165° 43.45'	0.18	28	25	x
81	58	1/19/2006	-74° 59.96'	165° 0.00'	0.23	44	20	
82	58	1/19/2006	-75° 0.00'	164° 59.44'	0.22	29	21	x
83	59	1/19/2006	-74° 39.97'	165° 15.00'	0.31	10	15	x
84	60	1/19/2006	-74° 40.00'	166° 58.02'	0.22	11	21	
85	60	1/19/2006	-74° 40.00'	166° 58.02'	0.21	11	22	x
86	61	1/20/2006	-74° 39.95'	168° 52.00'	0.19	34	25	
87	61	1/20/2006	-74° 39.95'	168° 52.00'	0.24	33	19	x
88	62	1/20/2006	-74° 40.00'	170° 48.07'	0.17	26	27	x
89	63	1/20/2006	-74° 39.99'	172° 39.99'	0.18	40	26	x
90	64	1/20/2006	-75° 0.10'	171° 25.74'	0.13	41	35	
91	64	1/20/2006	-75° 0.25'	171° 25.84'	0.11	43	43	x
92	65	1/21/2006	-74° 59.95'	169° 30.82'	0.19	13	24	
93	65	1/21/2006	-74° 59.95'	169° 30.82'	0.20	13	23	x
94	66	1/21/2006	-74° 59.98'	167° 35.98'	0.23	15	20	
95	67	1/21/2006	-75° 0.00'	166° 0.00'	0.31	11	15	
96	67	1/22/2006	-75° 0.00'	166° 0.00'	0.29	20	16	x
97	68	1/22/2006	-74° 30.00'	166° 0.04'	0.49	27	9	x
98	69	1/22/2006	-74° 30.00'	167° 35.98'	0.21	11	22	
99	70	1/22/2006	-76° 0.00'	166° 59.98'	0.25	12	18	
100	70	1/22/2006	-75° 59.98'	166° 59.98'	0.26	13	18	x
101	71	1/23/2006	-75° 51.58'	165° 42.03'	0.26	45	18	x
102	72	1/23/2006	-76° 15.07'	166° 41.97'	0.29	23	16	x

Table 2. NBPO608 CTD cast, station, date, locations, mix layer depths (z_{mix} , m), light extinction coefficient (K_d m^{-1}) and euphotic zone depth (z_{eu} , m) defined as 1% of E_0 and available variable fluorescence measurements.

CTD	Station	Date	Latitude	Longitude	$Z_{mix(0.02)}$	Z_{eu}	K_d	FRRF	FRRF	PAM
3	1	11/15/2006	-77° 22.48'	172° 59.98'	317	74	0.06			
4	2	11/15/2006	-76° 0.28'	171° 15.25'	28	23	0.20			
5	2	11/15/2006	-76° 0.64'	171° 17.92'	22	26	0.18	x		x
6	3	11/16/2006	-75° 59.86'	172° 41.44'	74	43	0.11			
7	3	11/16/2006	-75° 59.41'	172° 42.58'	77	43	0.11	x	x	x
8	4	11/16/2006	-75° 59.17'	174° 4.39'	78	47	0.10			
9	4	11/16/2006	-75° 57.85'	174° 4.70'	99	50	0.09	x	x	x
10	5	11/17/2006	-75° 59.98'	175° 26.98'	88	40	0.12	x	x	x
11	6	11/17/2006	-76° 0.10'	176° 50.04'	90	61	0.08		x	
12	6	11/17/2006	-75° 59.53'	176° 51.31'	85	67	0.07	x	x	x
13	7	11/17/2006	-76° 0.40'	177° 46.81'	65	32	0.15		x	
14	8	11/17/2006	-75° 59.71'	178° 13.06'	88	39	0.12			
15	8	11/17/2006	-75° 57.76'	178° 18.01'	93	42	0.11	x	x	x
16	9	11/18/2006	-75° 59.75'	179° 36.28'	60	46	0.10	x	x	x
17	10	11/18/2006	-76° 0.04'	-179° 0.25'	114	82	0.06	x	x	x
18	11	11/18/2006	-76° 59.95'	179° 59.97'	89	39	0.12			
19	11	11/18/2006	-76° 59.05'	179° 57.86'	80	39	0.12	x	x	x
20	12	11/18/2006	-76° 59.65'	178° 29.77'	86	41	0.11	x	x	x
21	13	11/19/2006	-76° 59.91'	177° 1.86'	31	30	0.15	x	x	x
22	14	11/19/2006	-76° 59.89'	175° 33.45'	173	47	0.10		x	
23	14	11/19/2006	-76° 59.62'	175° 34.09'	150	48	0.10	x	x	x
24	15	11/19/2006	-76° 59.64'	174° 4.08'	73	30	0.15			
25	15	11/19/2006	-76° 58.27'	174° 2.65'	110	33	0.14	x	x	x
26	16	11/20/2006	-76° 59.98'	172° 34.36'	48	36	0.13	x	x	x
27	17	11/20/2006	-76° 59.91'	171° 5.84'	140	52	0.09	x	x	x
28	18	11/20/2006	-77° 25.99'	170° 21.73'	172	49	0.09			
29	18	11/20/2006	-77° 25.99'	170° 21.73'	47	57	0.08	x	x	x
30	19	11/21/2006	-77° 25.75'	172° 31.39'	40	60	0.08	x	x	x
31	20	11/22/2006	-77° 40.03'	179° 59.80'	69	36	0.13			
32	21	11/22/2006	-77° 40.18'	-179° 59.65'	79	35	0.13	x	x	x
33	22	11/22/2006	-76° 30.10'	173° 29.95'	94	29	0.16			
34	22	11/22/2006	-76° 30.10'	173° 29.95'	82	29	0.16	x	x	x
36	22	11/22/2006	-76° 30.10'	173° 29.95'	78	22	0.21			
37	23	11/23/2006	-76° 29.95'	170° 0.08'	82	21	0.22	x	x	x

CTD	Station	Date	Latitude	Longitude	Z _{mix(0.02)}	Z _{eu}	K _d	FRRF	FRRF	PAM
38	23	11/23/2006	-76° 29.59'	169° 59.5'	137	26	0.18			
39	24	11/24/2006	-76° 29.77'	171° 25.27'	108	32	0.15	x	x	x
40	24	11/24/2006	-76° 29.53'	171° 24.61'	35	24	0.19	x		
41	25	11/24/2006	-76° 30.01'	172° 51.4'	12	29	0.16		x	
42	25	11/24/2006	-76° 29.95'	172° 51.44'	38	29	0.16	x	x	x
43	25	11/24/2006	-76° 30.10'	172° 51.28'	14	35	0.13	x	x	x
44	26	11/25/2006	-76° 29.96'	174° 16.93'	71	32	0.14	x	x	x
45	27	11/25/2006	-76° 29.71'	175° 43.41'	32	22	0.21	x	x	x
46	27	11/25/2006	-76° 30.10'	175° 35.23'	30	26	0.18	x	x	x
47	28	11/25/2006	-76° 29.98'	177° 8.68'	18	28	0.17			
48	29	11/25/2006	-76° 29.98'	178° 34.17'	27	27	0.17	x	x	x
49	29	11/25/2006	-76° 30.01'	178° 34.36'	12	29	0.16	x	x	x
50	30	11/26/2006	-76° 29.92'	-179° 59.92'	36	45	0.10			
51	31	11/26/2006	-76° 29.53'	-178° 35.67'	18	26	0.17	x	x	x
52	31	11/26/2006	-76° 29.98'	-178° 36.85'	25	47	0.10		x	x
53	32	11/26/2006	-76° 50.15'	179° 59.89'	44	27	0.17	x		
54	33	11/26/2006	-77° 10.03'	-179° 59.5'	21	39	0.12			x
55	33	11/26/2006	-77° 10.03'	-179° 59.51'	22	29	0.16		x	x
56	34	11/27/2006	-77° 29.92'	179° 59.80'	152	40	0.12	x		x
57	35	11/27/2006	-77° 49.97'	-179° 59.59'	162	45	0.10			
58	35	11/27/2006	-77° 49.97'	-179° 59.59'	41	23	0.20			
59	36	11/27/2006	-77° 44.98'	178° 29.93'	65	23	0.20	x	x	x
60	36	11/27/2006	-77° 44.98'	178° 29.93'	36	17	0.27			
61	37	11/28/2006	-77° 39.95'	176° 54.97'	39	17	0.26	x	x	x
62	37	11/28/2006	-77° 39.95'	176° 54.97'	35	17	0.27	x	x	
63	38	11/28/2006	-77° 36.91'	176° 11.94'	28	24	0.19	x	x	
64	38	11/28/2006	-77° 36.91'	176° 12.05'	28	21	0.22			
65	39	11/28/2006	-77° 29.96'	173° 59.82'	32	22	0.21		x	
66	39	11/28/2006	-77° 29.96'	173° 59.83'	25	19	0.24			
67	40	11/29/2006	-77° 20.15'	172° 39.00'	42	21	0.22			
68	41	11/29/2006	-77° 19.54'	171° 7.86'	13	18	0.26	x	x	
69	41	11/29/2006	-77° 19.54'	171° 7.86'	19	26	0.18	x	x	
70	42	11/29/2006	-76° 29.95'	174° 17.18'	12	25	0.18	x	x	
71	42	11/29/2006	-76° 29.95'	174° 17.18'	7	17	0.27	x		
72	43	11/30/2006	-76° 29.77'	171° 25.24'	10	21	0.22	x		

APPENDIX 3

Contour plots of latitudinal sections conducted in the Ross Sea Polynya within the “Controls on Ross Sea Algal Community Structure (CORSACS)” project during two cruises on the *RVIB N. B. Palmer* (Cruises NBP06-01, December 2005-January 2006 and NBP06-08, November-December 2006) and a short cruise as part of the “Interannual Variability in the Ross Sea (IVARS)” project at the end of January 2006.

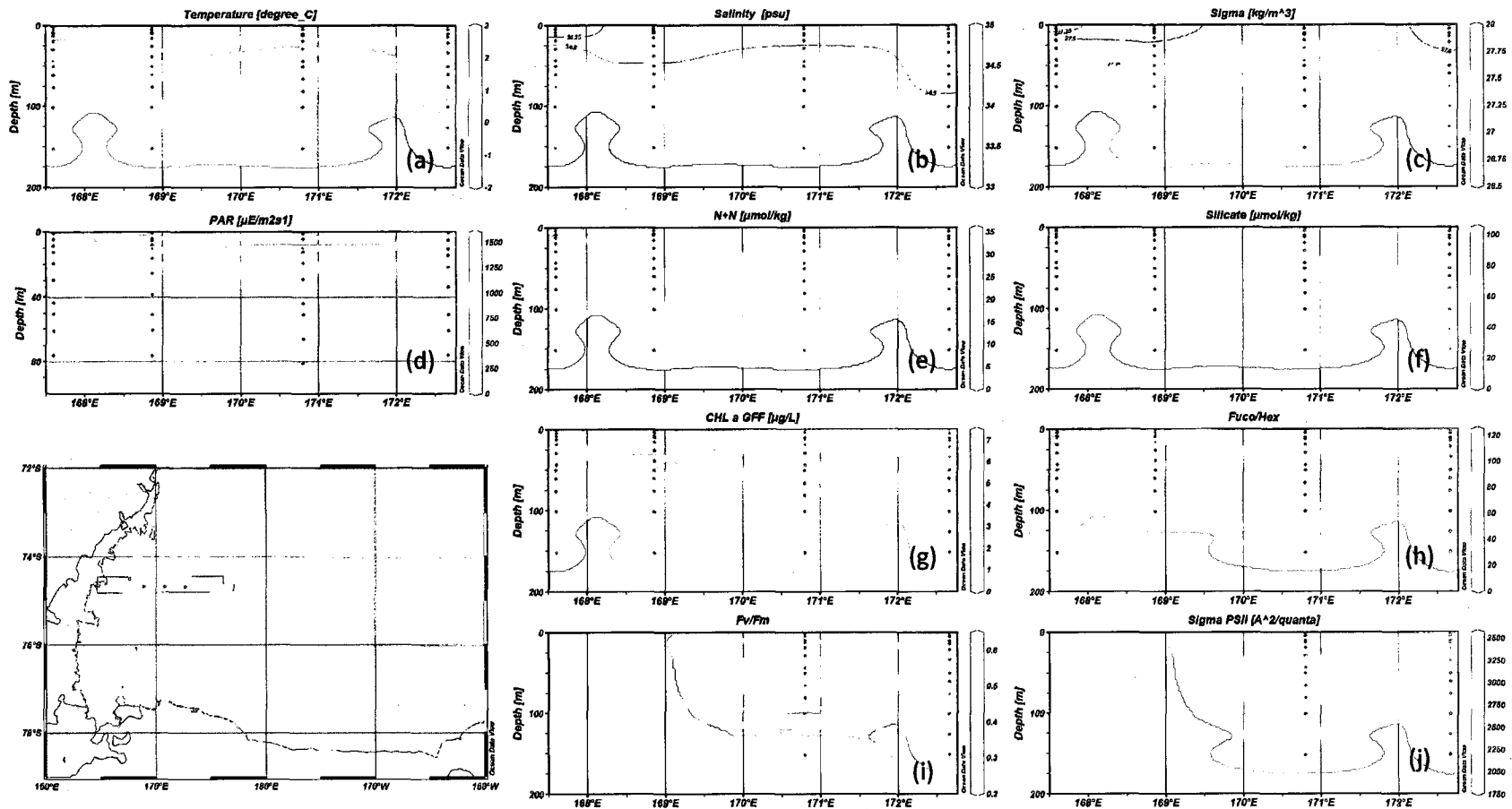


Figure 1. Vertical contours of temperature (a), salinity (b), water density (c), PAR (d), nitrate and nitrite concentration (e), silicate concentration (f), total chlorophyll *a* concentration (g), fucoxanthin to 19-hexanoloxyfucoxanthin ratio (h), photosynthetic quantum yield (i), absorption cross section of PSII (j) section at 74.5°S of NBP0601.

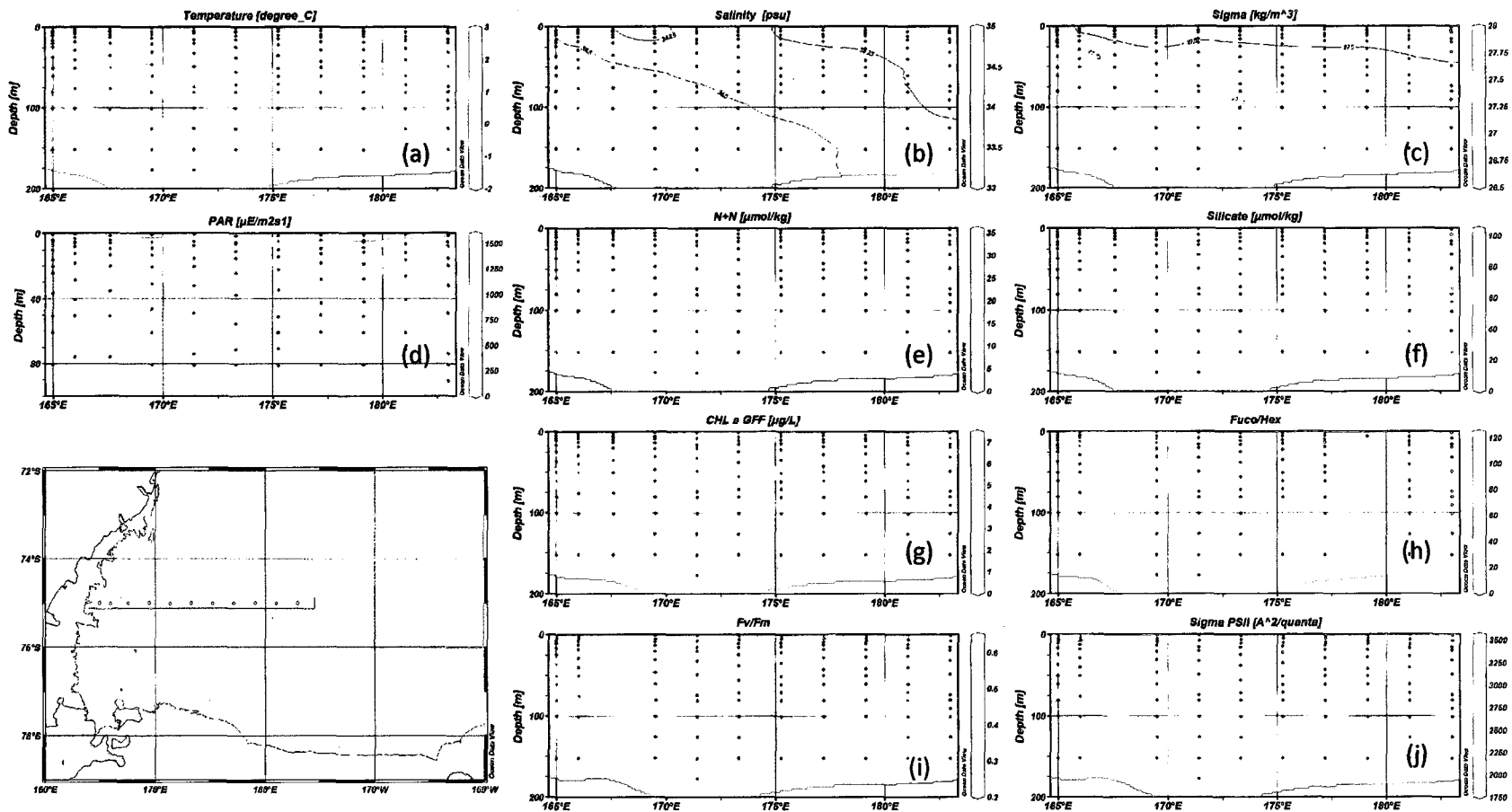


Figure 2. Vertical contours of temperature (a), salinity (b), water density (c), PAR (d), nitrate and nitrite concentration (e), silicate concentration (f), total chlorophyll *a* concentration (g), fucoxanthin to 19-hexanoloxyfucoxanthin ratio (h), photosynthetic quantum yield (i), absorption cross section of PSII (j) section at 75.0°S of NBP0601.

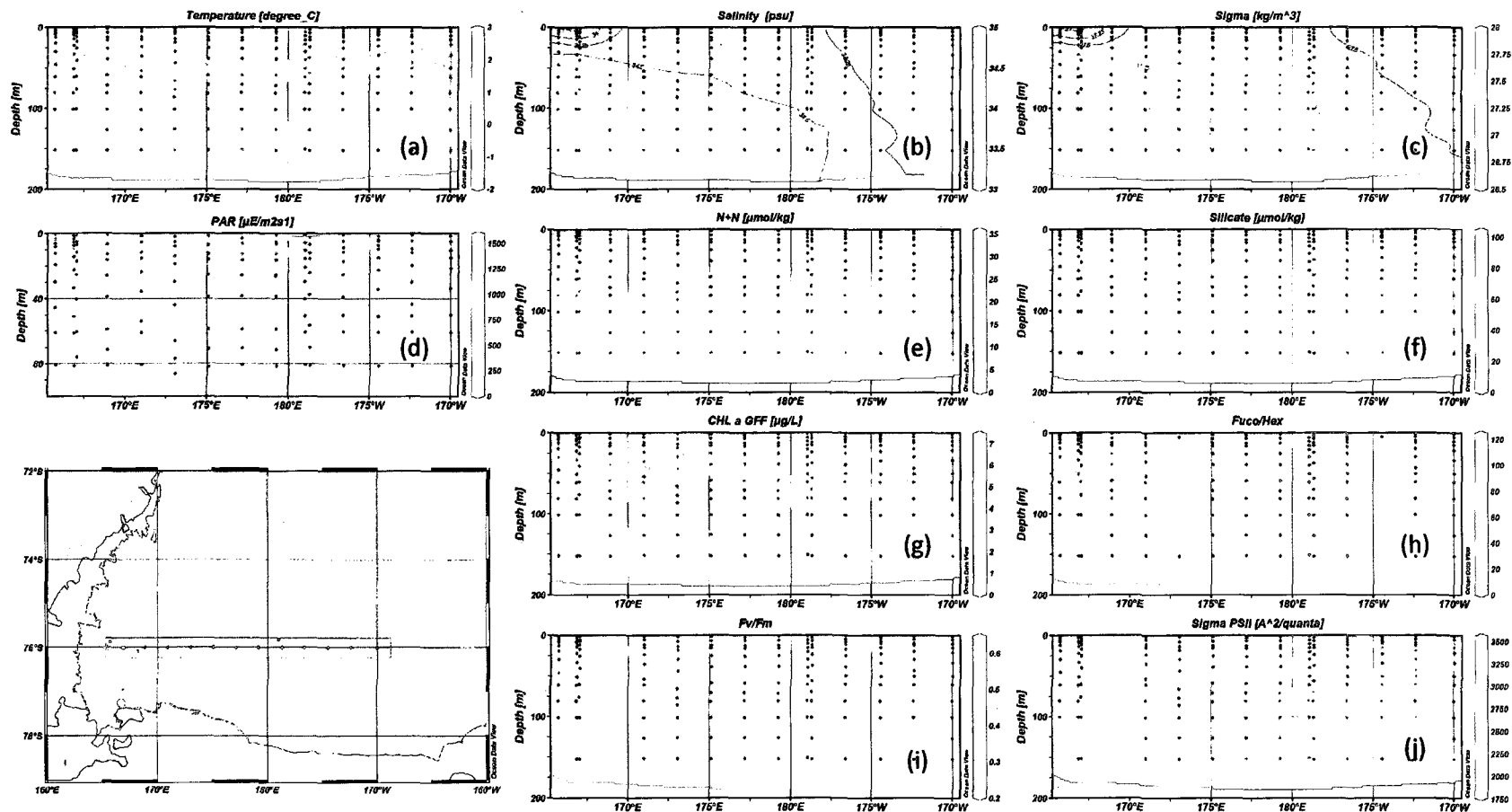


Figure 3. Vertical contours of temperature (a), salinity (b), water density (c), PAR (d), nitrate and nitrite concentration (e), silicate concentration (f), total chlorophyll *a* concentration (g), fucoxanthin to 19-hexanoxylfucoxanthin ratio (h), photosynthetic quantum yield (i), absorption cross section of PSII (j) section at 76.0°S of NBP0601.

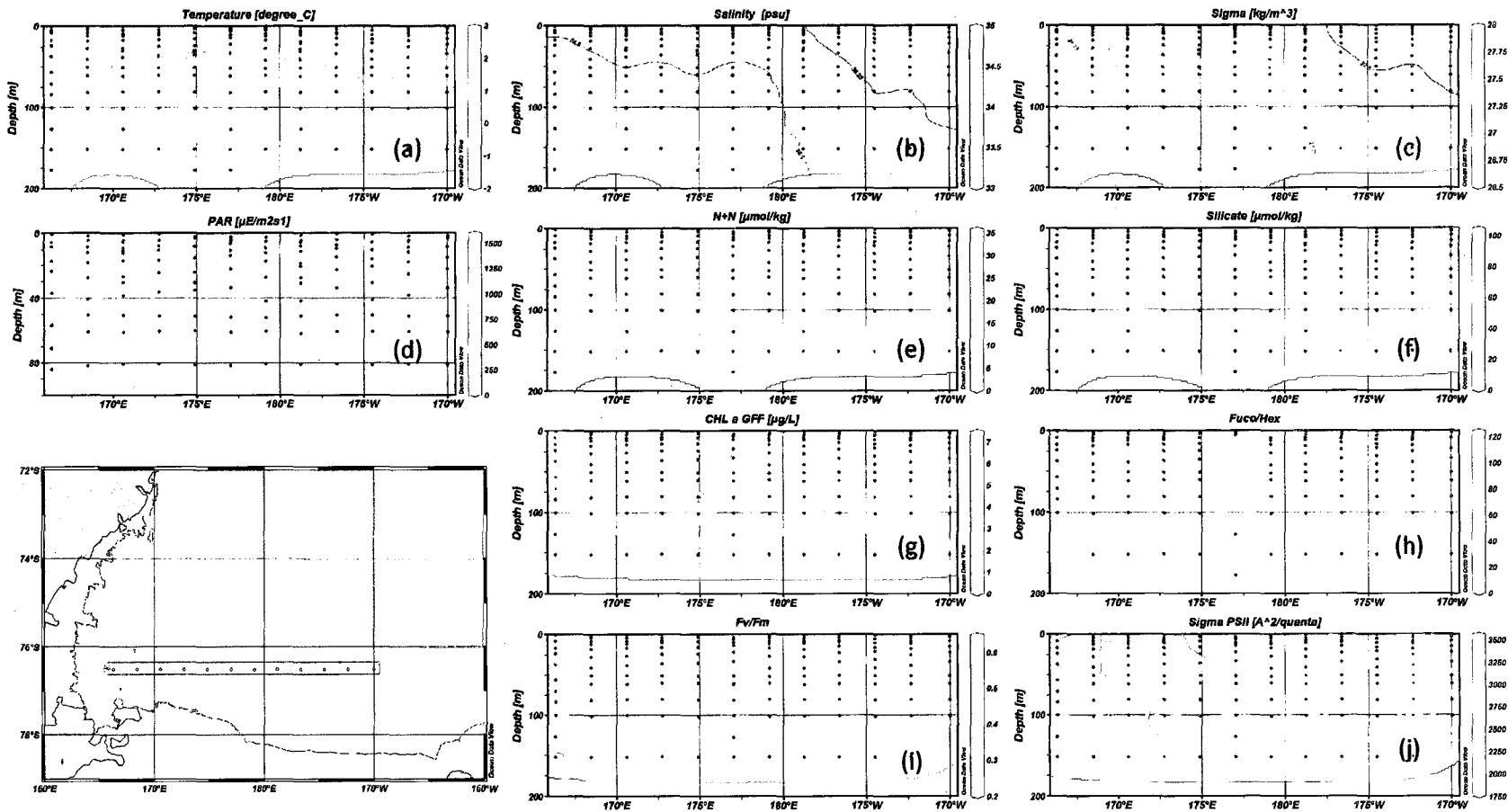


Figure 4. Vertical contours of temperature (a), salinity (b), water density (c), PAR (d), nitrate and nitrite concentration (e), silicate concentration (f), total chlorophyll *a* concentration (g), fucoxanthin to 19-hexanoloxyfucoxanthin ratio (h), photosynthetic quantum yield (i), absorption cross section of PSII (j) section at 76.5°S of NBPO601.

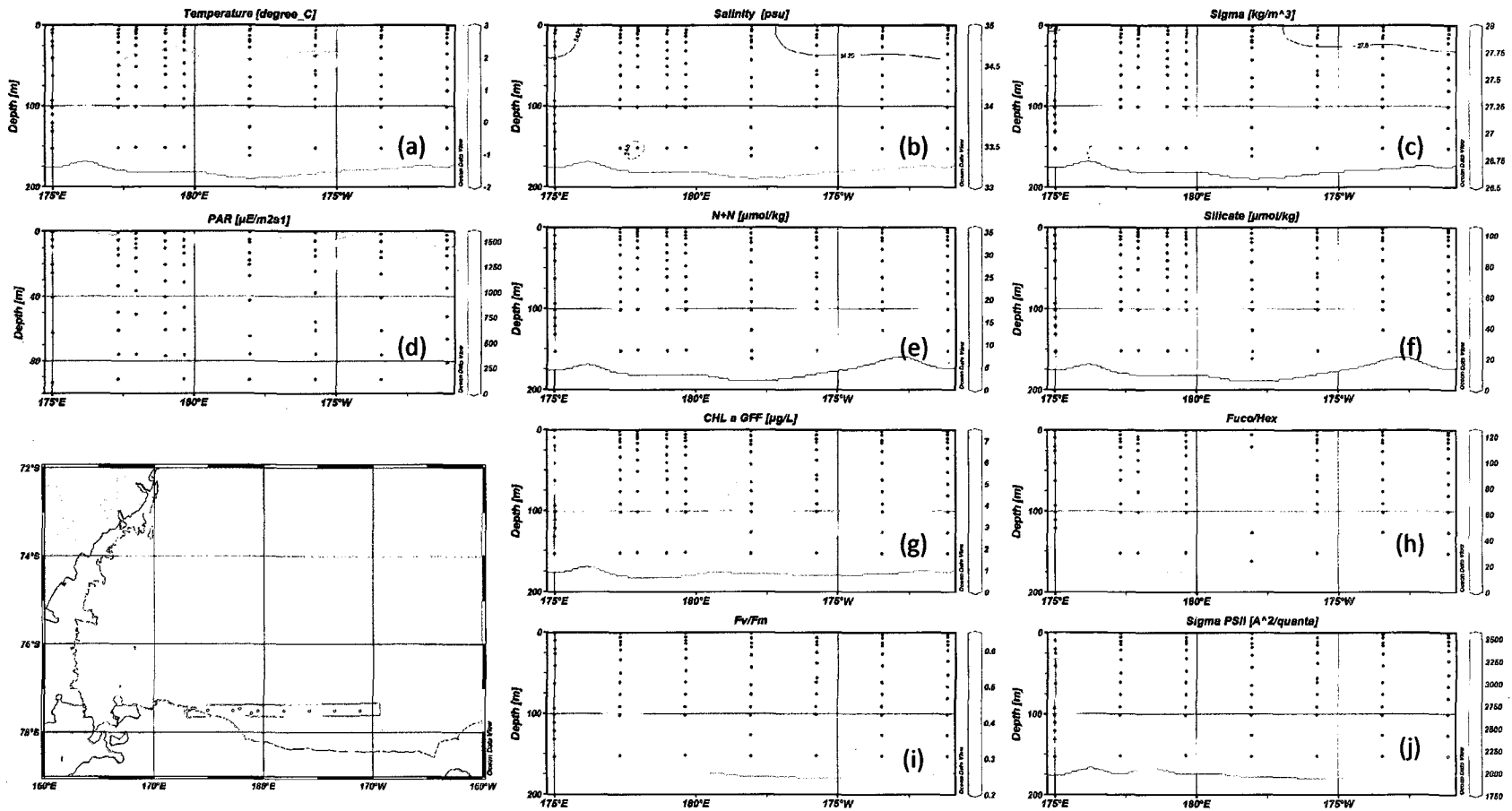


Figure 5. Vertical contour plots of temperature (a), salinity (b), water density (c), PAR (d), nitrate and nitrite concentration (e), silicate concentration (f), total chlorophyll *a* concentration (g), >20 μm fraction chlorophyll *a* concentration (h), photosynthetic quantum yield (i), absorption cross section of PSII (j) section at 77.5°S of NBP0601.

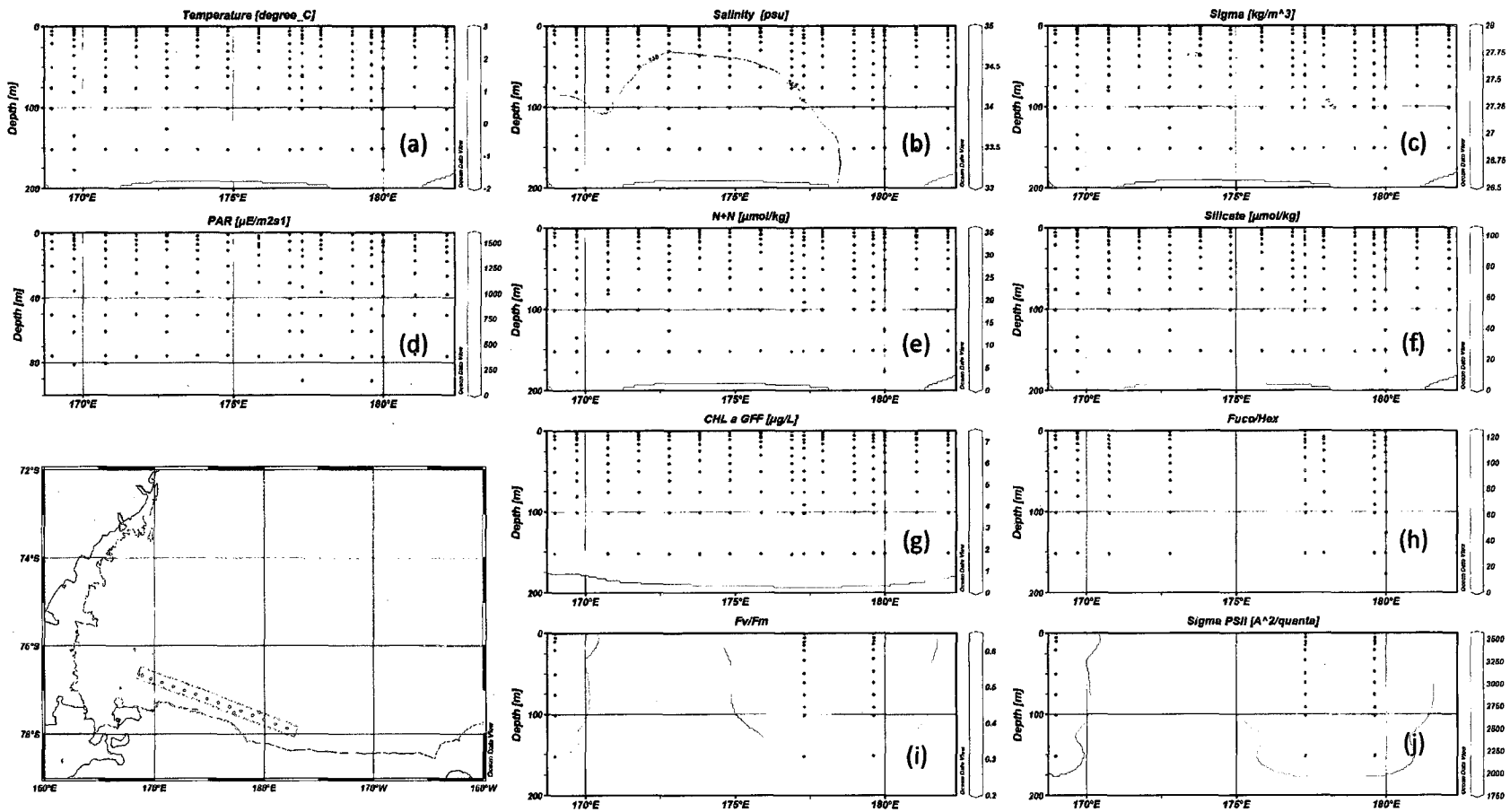


Figure 6. Vertical contour plots of temperature (a), salinity (b), water density (c), PAR (d), nitrate and nitrite concentration (e), silicate concentration (f), total chlorophyll *a* concentration (g), fucoxanthin to 19-hexanoloxyfucoxanthin ratio (h), photosynthetic quantum yield (i), absorption cross section of PSII (j) for IVARS section of NBP0601.

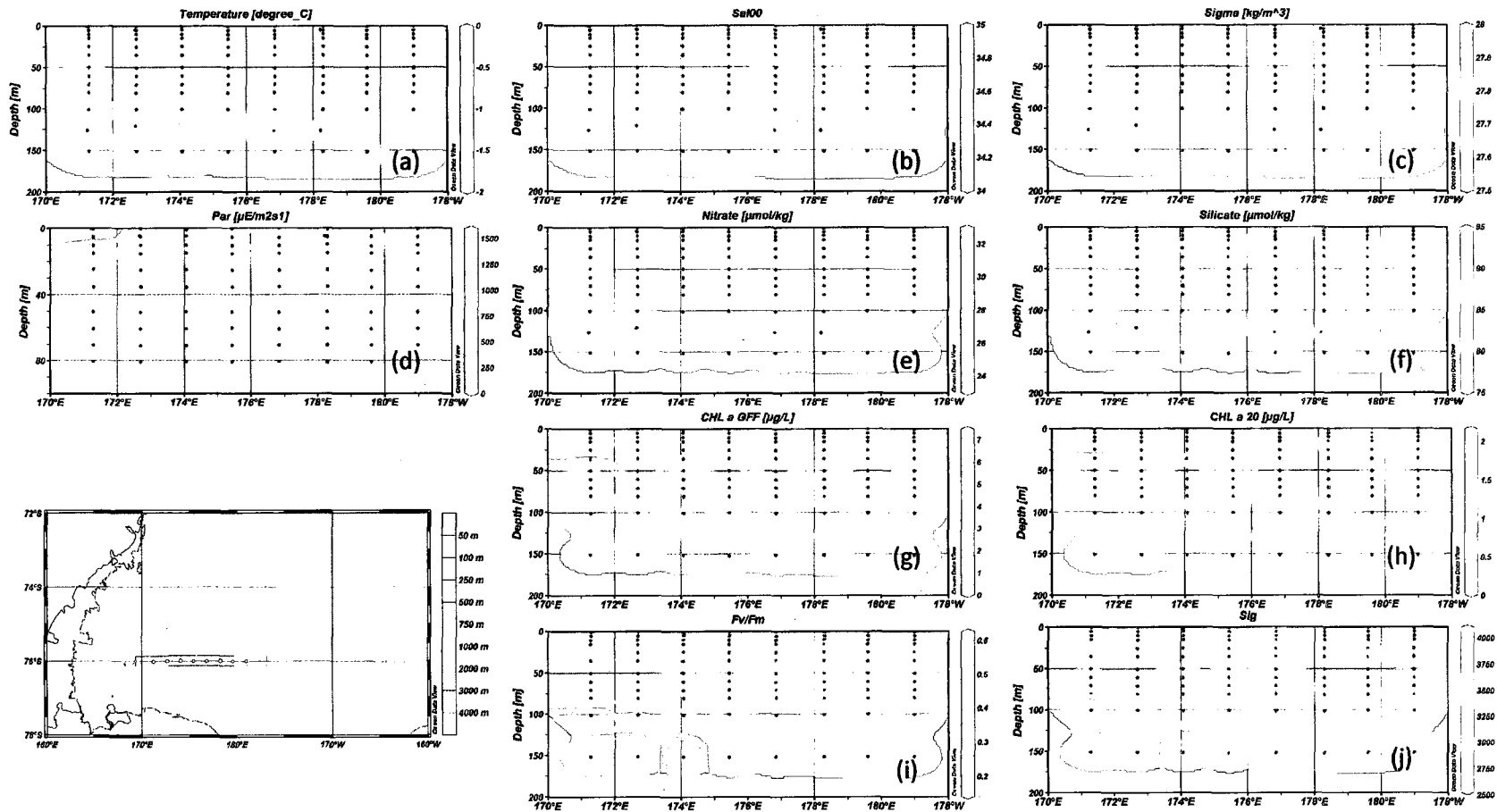


Figure 7. Vertical contour plots of temperature (a), salinity (b), water density (c), PAR (d), nitrate and nitrite concentration (e), silicate concentration (f), total chlorophyll *a* concentration (g), >20 μm fraction chlorophyll *a* concentration (h), photosynthetic quantum yield (i), absorption cross section of PSII (j) 76.0 °S section of NBP0608.

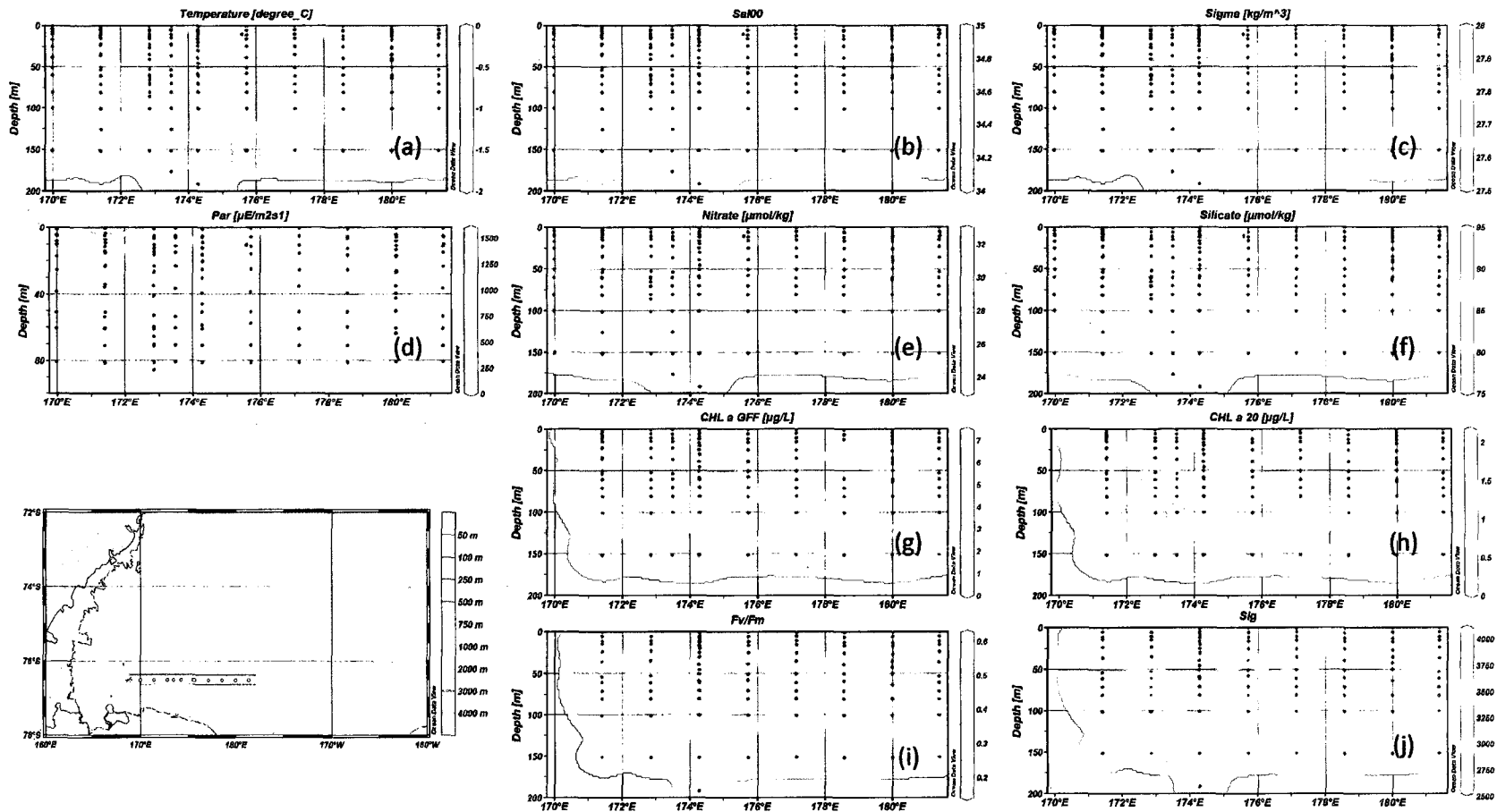


Figure 8. Vertical contour plots of temperature (a), salinity (b), water density (c), PAR (d), nitrate and nitrite concentration (e), silicate concentration (f), total chlorophyll *a* concentration (g), >20 μm fraction chlorophyll *a* concentration (h), photosynthetic quantum yield (i), absorption cross section of PSII (j) 76.5° S section of NBP0608.

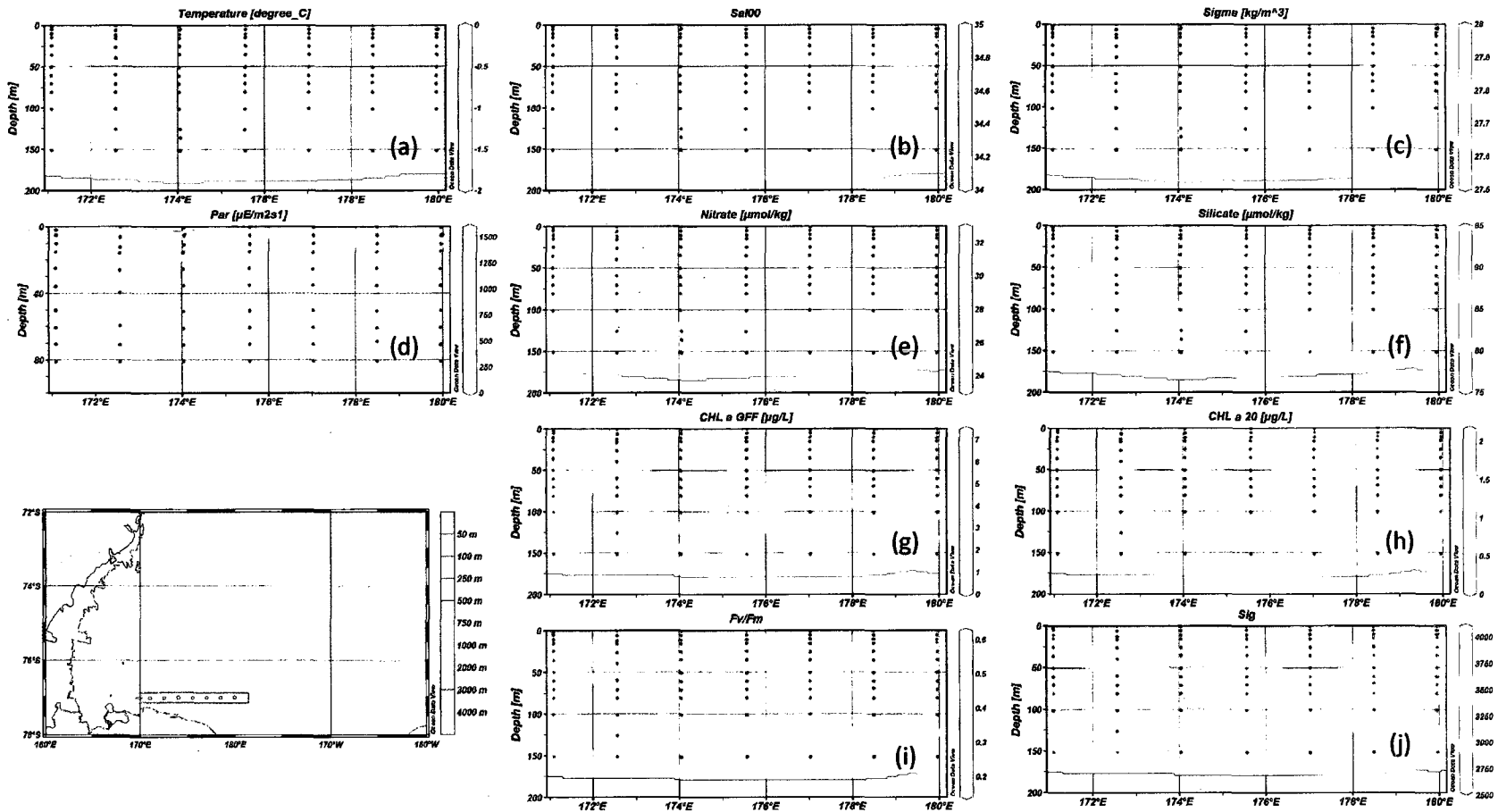


Figure 9. Vertical contour plots of temperature (a), salinity (b), water density (c), PAR (d), nitrate and nitrite concentration (e), silicate concentration (f), total chlorophyll *a* concentration (g), >20 μm fraction chlorophyll *a* concentration (h), photosynthetic quantum yield (i), absorption cross section of PSII (j) for 77.0 °S section of NBP0608.

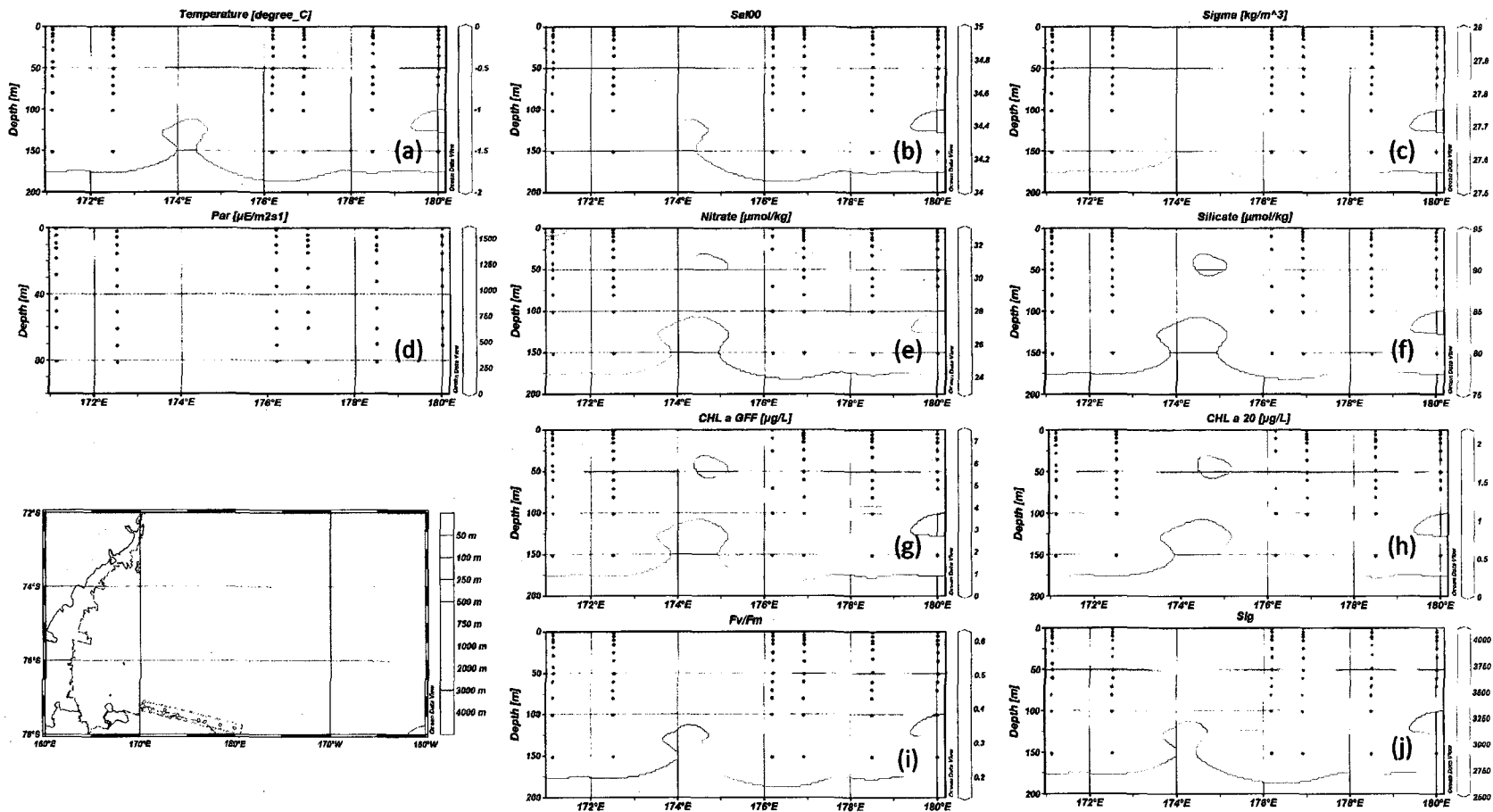


Figure 10. Vertical contour plots of temperature (a), salinity (b), water density (c), PAR (d), nitrate and nitrite concentration (e), silicate concentration (f), total chlorophyll *a* concentration (g), >20 μm fraction chlorophyll *a* concentration (h), photosynthetic quantum yield (i), absorption cross section of PSII (j) for IVARS section of NBP0608

VITA

Sasha Tozzi was born in Naples, Italy on July 23, 1971. He received a Bachelor of Science in 1997 graduating with a grade of 110/110 in Biological Sciences at the University of Naples, Italy "Federico II". In 1999 upon completion of his mandatory service for the Italian Army working as a civilian for the museum of the Royal Palace of Naples, he moved to the United States and to New Brunswick, NJ, where in 2001 under advisor Dr. Paul Falkowski he received a Master of Science in Oceanography at Rutgers University. In 2003 he entered the School of Marine Science at the College of William and Mary under advisor Dr. Walker O. Smith, Jr. While still a student at College of William and Mary he was employed by the Monterey Bay Aquarium Research Institute in Moss Landing, CA first in 2005 as a summer intern in Dr. Ken Johnson's Laboratory, and then again in July 2008 on a two-year NSF Fellowship working with Dr. Zbigniew Kolber. Sasha defended his Ph.D. in May 2009.